Coden: JPLPAY
Volume 9, Part A-2, No. 9, September 1971

Journal of Polymer Science

Part A-2: Polymer Physics

Contents

lished by INTERSCIENCE PUBLISHERS a division of John Wiley & Sons, Inc.

Journal of Polymer Science **Part A-2: Polymer Physics**

The Journal of Polymer Science is published in four sections as follows: Part A-1, Polymer Chemistry, monthly; Part A-2, Polymer Physics, monthly; Part B, Polymer Letters, monthly; Part C, Polymer Symposia, irregular.

Published monthly by Interscience Publishers, a Division of John Wiley & Sons, Inc., covering one volume annually. Publication, Executive, Editorial, and Circulation Offices at 605 Third Avenue, New York, N.Y. 10016. Second-class postage paid at New York, New York, and additional mailing offices. Subscription price, $325.00 per volume (including Parts A-1, B, and C). Foreign postage $15.00 per volume (including Parts A-1, B, and C).

JOURNAL OF POLYMER SCIENCE: PART A-2 VOL. 9, 1537–1551 (1971)

Salt Rejection by Polymer Membranes in Reverse Osmosis. I. Nonionic Polymers

H. YASUDA, and C. E. LAMAZE, *Camille Dreyfus Laboratory, Research Triangle Institute, Research Triangle Park, North Carolina 27709*

Synopsis

An attempt is made to analyze the relationship between salt rejection and water flux of nonionic polymer membranes in reverse osmosis on the basis of the movement of water in the membranes. The salt rejection R_S is a consequence of transport depletion of salt in relation to water flux. The transport depletion can be quantitatively expressed through knowledge of the mode of water transport and by application of free-volume theory to membrane transport phenomena. Water permeation can be characterized by a parameter $\omega = RTK_1/P_1v_1$, K_1 denoting hydraulic permeability, P_1 diffusive water permeability, v_1 the molar volume of water. Thus polymer membranes can be classified in three categories: $\omega = 1$ (diffusion membranes); $\omega > 1$ (diffusion-flow membranes); and $\omega \gg 1$ (flow membranes). Salt rejection R_S can be expressed in terms of P_1, the diffusive salt permeability P_2, and the effective pressure $(\Delta p - \Delta \pi)$:

$$R_S = \{\omega + [P_2RT/P_1v_1(\Delta p - \Delta \pi)]\}^{-1}$$

Experimental results obtained with various hydrophilic polymers are presented as the dependence of R_S on the logarithm of water flux. Good agreement was found between the experimental data and the calculated curve. Excessive swelling of membranes results in bulk flow of water (high ω) with coupled transport of salt. Hence the salt rejection decreases quickly as water flux increases beyond a threshold value above which water flux can be characterized as bulk flow.

INTRODUCTION

Study of water transport in various water-swollen polymer membranes has indicated that under applied hydraulic pressure both molecular diffusion and bulk flow can occur in polymer membranes, depending upon the water content or degree of swelling of the membranes.

For each type of transport, certain predictions of interaction between solute flux–and water flux are applicable. For instance, as long as water moves by a diffusion mechanism, it is very unlikely that coupling of water and solute flux would occur, and as long as water moves by bulk flow any postulation based upon the diffusion mechanism is bound to fail. Therefore, being able to determine the mode of transport of water should allow assignment of the most appropriate factors to explain the interaction between solute flux and water flux.

As a result, determining the mode of water transport would provide a practical means of classifying membranes in such a way that the mechanism of salt rejection could be analyzed on the basis of the underlying transport mechanisms.

This study is an attempt, on the basis of the above concepts, to explain the salt rejection of homogeneous polymer membranes in the process of reverse osmosis. The study is limited to homogeneous membranes so that characteristic properties of membranes of different thickness can be compared. In this respect, inhomogeneous (e.g., asymmetric) membranes, such as the Loeb-Sourirajan modified cellulose acetate membranes, cannot be compared unless the thickness of the effective layer can be accurately assigned.

The phrase "homogeneous membrane," as considered in this study, means a membrane that can be treated as a uniform matrix in the direction of the membrane thickness so that the flux multiplied by the thickness is constant independent of thickness; however, it does not necessarily require uniformity in the lateral directions as long as this nonuniformity does not change with thickness. For instance, grafted polymers and block-copolymer membranes in which considerable morphological inhomogeneity exists in the membrane phase, can be treated as homogeneous membranes if a proper correction factor is based on the volume fraction of permeable phase.

CLASSIFICATION OF POLYMER MEMBRANES BASED ON WATER PERMEABILITY AND THEIR SALT REJECTION

Water permeability K_1 of a membrane under an applied pressure gradient can be defined as

$$J_{1,f} = K_1(\Delta p/\Delta X) \tag{1}$$

where $J_{1,f}$ is the water flux per unit area of membrane subjected to a hydraulic pressure gradient; Δp is the hydraulic pressure difference across the membrane, and ΔX is the thickness of the membrane.

Thus defined, hydraulic permeability differs considerably from the diffusive permeability P_1 of water, which is defined by

$$J_{1,d} = P_1(\Delta C/\Delta X) \tag{2}$$

where $J_{1,d}$ is the diffusive water flux per unit area of membrane and ΔC is the external concentration difference of water across the membrane. The diffusive permeability can be obtained by the use of radioactive water to measure the diffusive flux of water in the absence of a hydraulic pressure gradient.

For the ideal case in which water moves in the membrane phase only by diffusion, K_1 and P_1 are related by[1]

$$K_1 = (v_1/RT)P_1 \tag{3}$$

where v_1 is the molar volume of water. Therefore, a parameter which describes the ratio of these two permeabilities of water can be defined as

$$\omega = K_1RT/P_1v_1 \tag{4}$$

It has been found that the value of ω is nearly unity for polymer membranes of low water content or so-called "tight" membranes[1,2] and increases in exponential fashion with the increase of water content.[1] The parameter ω for highly hydrated membranes can be expressed empirically by

$$\omega = m \exp \{-\Phi_w(1 - H)/H\} > 1 \tag{5}$$

where H is the volume fraction of water in a swollen membrane and m and Φ_w are constants (see Fig. 3).

Since $\omega = 1$ means that transport of water occurs by diffusion regardless of the applied driving force, a water-swollen membrane may be classified according to the value of ω, namely, (1) diffusion membranes, in which $\omega \approx 1$; (2) diffusion-flow membranes, transition from (1) to (3); and (3) flow membranes, in which ω can be given by eq. (5).

This kind of classification also describes the type of solute flux in the membrane. For instance, solute flux in a flow membrane is strongly coupled with water flux. However, this kind of classification does not necessarily describe the extent of salt rejection which would be observed in reverse osmosis. The salt rejection results from the transport depletion of the salt relative to the water flux, and the nature of the salt flux does not necessarily determine the extent of salt transport depletion. For instance, most ionic polymer membranes are flow membrane by this classification; however, the salt transport depletion due to the charge effect is sufficiently high to observe a variety of salt rejection with these flow membranes in which the salt flux is coupled with water flux. The details of this aspect will be discussed in a separate study (Paper II[3] of this series) for ionic polymer membranes.

The salt rejection is considered as the consequence of salt flux depletion relative to the water flux rather than exclusion of salt by membrane; therefore, regardless of the molecular mechanisms which cause the transport depletion, the salt rejection can be dealt with by using the following definitions:

$$R_S \equiv 1 - (C_2''/C_2') \tag{6}$$

where C_2' is the molar concentration of the salt in feed solution and C_2'' is the molar concentration of salt in effluent.

If the units of the water flux J_1 are taken as $l./cm^2$-sec and those of the salt flux J_2 mole/cm^2-sec, then C_2'' is

$$C_2'' = J_2/J_1 \tag{7}$$

Consequently, eq. (6) becomes

$$R_S \equiv 1 - (J_2/J_1C_2') \tag{8}$$

The mathematical expressions of J_1 and J_2 in relation to the driving force are dependent upon the mechanism of water and salt flux, and consequently differ in each of the three types of membranes. However, in order to analyze the permeability characteristics of a polymer membrane, the water permeability in reverse osmosis is defined in this paper as

$$J_1 = K_1(\Delta p - \Delta\pi)/\Delta X \tag{9}$$

where $\Delta\pi$ is the osmotic pressure of the feed solution. Consequently, K_1 does not refer to the true water permeability of membranes which have poor salt rejection; however, it does describe how much water (the quality of which is given by R_S and feed concentration) permeates through a membrane under given conditions. More rigorously, J_1 is given by

$$J_1 = K_1(\Delta p/\Delta X)(1 - aR_S) \tag{9'}$$

where a is the ratio $\Delta\pi/\Delta p$.

However, as long as a is maintained at a relatively small value (e.g., 0.25 under the experimental conditions used in this study), omission of the term aR_S seems to cause no more error in the overall accuracy of the experiment than the error of ambiguity involved in other factors, such as the value of ΔX and the effect of concentration polarization.

For the diffusion membrane, J_1 and J_2 can be described by the so-called solution-diffusion mechanism of transport.[4] The water flux in this case is explicitly given by eq. (9). Since $K_1 = P_1v_1/RT$ for these membranes,

$$J_1 = P_1v_1(\Delta p - \Delta\pi)/RT\Delta X \tag{10}$$

The salt flux J_2 is given by

$$J_2 = P_2(C_2' - C_2'')/\Delta X \tag{11}$$

Hence, for diffusion membranes,

$$R_S = \left(1 + \frac{P_2RT}{P_1v_1(\Delta p - \Delta\pi)}\right)^{-1} \tag{12}$$

Equation (12) has been shown to hold for various solutes in cellulose acetate membranes by Lonsdale et al.[5]

In the diffusion-flow membranes, water moves faster than the pure diffusive flux by the factor ω.

The word "flow" may need further clarification. According to the definition based on the permeability characteristic of water through the membranes, the permeation of water is faster in highly hydrated membranes than the diffusive flux of water created by the chemical potential increase resulting from the pressure increase. Whether this is due to a combination of diffusive flux and bulk flow (viscous flow under applied pressure) or due to the change of mode of water transport as a whole cannot be determined by the permeability study alone. However, regardless of the structure of the membrane, the diffusive water flux expressed by eq. (10) should occur if an effective pressure (Δp-$\Delta\pi$) is applied across the mem-

brane. This flux may be visualized by the similar situation of a diffusive flux superimposed on flow in a capillary. The use of eq. (10) in this case is an approximation as previously mentioned. The diffusive permeability P_1 for homogeneous polymer membranes is a function of the volume fraction of water in the membrane H.

In the homogeneous polymer membrane model, no fixed continuous passage like a capillary is assumed, and consequently the overall permeability is the statistical average of the fluctuating (both in location and time) permeable phases in the membane. Therefore, at a certain point within a membrane at a fixed time, the geometry of the polymer segments may be such that water movement is characterized as diffusion, but water may move more by flow when this portion of the membrane structure changes to a more loose geometric arrangement at some later moment. Whenever water moves by diffusion, the salt flux also should be characterized by diffusion, which is the basic assumption of this treatment. Therefore, it may be possible to set a mathematical model for water and salt fluxes in which the total water flux can be divided into two contributions

$$J_1 = J_1' + J_{1,d} \tag{13}$$

where J_1 is the total flux of water, J_1' is the water flux in excess of the diffusive flux $J_{1,d}$, which is given by

$$J_{1,d} = P_1 v_1 (\Delta p - \Delta\pi)/RT\Delta X \tag{14}$$

and it is assumed that in these nonionic membranes no salt rejection occurs whenever water moves by flow.

Then, J_2 can be given by the summation of the diffusive and the coupled flux as

$$J_2 = [K_1 - (P_1 v_1/RT)][(\Delta p - \Delta\pi)/\Delta X]C_2' + P_2[(C_2' - C_2'')/\Delta X] \tag{15}$$

The combination of eqs. (4), (8), (9), and (15) leads to

$$R_S = \{\omega + [P_2 RT/P_1 v_1 (\Delta p - \Delta\pi)]\}^{-1} \tag{16}$$

Since it is clear that eq. (12) is the special case of eq. (16) for $\omega = 1$, the transition from ideal diffusion membrane to flow membrane can be expressed by the parameter ω, and eq. (16) may be considered as the general expression applicable to nonionic polymer membranes.

For flow membranes, high salt rejection cannot be expected by nonionic membranes, since in this region P_1 and P_2 are nearly the same, and the value of ω is high enough to yield very low R_S as given by eq. (16). Therefore, for nonionic flow membranes, in which the main cause of salt transport depletion is due to lower diffusive flux of salt compared to water flux, only low salt rejection is expected.

EXPERIMENTAL

Membranes

Table I gives a description of the films used in this study. Most were prepared by casting a polymer solution on glass plates and air-dying slowly under a cover so as to avoid asymmetry in the film, and then equilibrating in water.

The preparation of the hydroxypropyl methacrylate (HPMA) homopolymer, the HPMA–glycidyl methacrylate (GdMA) copolymers, and the GdMA homopolymer (films 1–6), the HPMA–methyl methacrylate (MMA)

TABLE I
Description of Homogeneous Membranes Studied

Film	Polymer composition (monomer, mole-%)		Casting solvent system (Vol-%) or source or graft description
Cast Films			
1	HPMA	100	Dioxane/acetone, 50/50
2	HPMA[a]	100	Dioxane/acetone, 50/50
3	HPMA–GdMA	90/10	Dioxane
4		80/20	Dioxane
5		70/30	Dioxane
6	GdMA	100	Dioxane
7	HPMA–MMA	85/15	Dioxane/acetone, 40/60
8		80/20	Dioxane/acetone, 40/60
9		75/25	Dioxane/acetone, 40/60
10		65/35	Dioxane/acetone, 40/60
11	MMA–GMA	90/10	Dioxane/acetone, 40/60
12		80/20	Dioxane/acetone, 40/60
13		75/25	Dioxane/acetone, 40/60
14		70/30	Dioxane/acetone, 40/60
15	Avisco 215 PI		Commercial (Viscose Corp.)
16	E-398-3 Cellulose acetate		Ethyl acetate/acetone, 80/20
17	E-398-3 Cellulose acetate		Ethyl acetate
18	E-398-3 Cellulose acetate		Chloroform/methanol, 80/20
19	E-398-3 Cellulose acetate		Acetone
20	E-398-3 Cellulose acetate		Dioxane
21	E-398-3 Cellulose acetate		Acetone (Gulf General Aerojet)
22	Nylon 4		Hexafluoroisopropanol
23	Nylon 4–GMA		Formic acid/GMA monomer
Graft films			
24	Viscose–GMA		Mutual irradiation; 0.1 Mrad; 18.1 wt-% add-on
25	Viscose–GMA		Mutual irradiation; 2.5 Mrad; 16.3 wt-% add-on
26	Viscose–GMA		Mutual irradiation; 4.6 Mrad; 15.7 wt-% add-on

[a] After drying, the film was exposed to formic acid vapor for 16 hr.

copolymers (films 7–10) and the MMA–glycerol methacrylate (GMA) copolymers (films 11–14), have been described in detail previously.[6]

Film 15 was a commercial cellulose film from the American Viscose Corporation (Avisco 215 PI). Films 16–20 were Eastman cellulose acetate (39.8% acetyl content; falling ball viscosity, 3 sec) cast from the various listed solvent systems at 20% polymer by weight. The Alrac Corporation graciously supplied the nylon 4 (polypyrrolidone) used to prepare Film 22. The film was cast from a 10/90 (by weight) polymer–hexafluoroisopropanol solution.

Film 23 was prepared by polymerizing GMA in a solution of nylon 4 polymer dissolved in formic acid. The formic acid solution of nylon 4 was mixed with GMA monomer and an initiator, 2,2′-azobis(2-methylpropionitrile). The film was cast, air-dried to "set" the film slightly as the formic acid evaporated, then placed in a nitrogen atmosphere at 55°C to complete the polymerization of GMA in the nylon 4 polymer network.

Films 24–26 are termed "grafted" films. They were prepared by immersing porous nylon 4 films in GMA monomer solutions and irradiating the samples, by using a ^{60}Co γ source, at a dose rate of 0.1 Mrad/hr. The procedure resembles the grafting reaction of hydrophilic monomers in hydrophilic polymers, hence the term "grafted." The relative amounts of chemically grafted GMA and GMA polymer imbedded in the pores of the film are indistinguishable; therefore, the graft is described on the basis of total weight per cent added. The nylon 4 films used were cast from 10/90 polymer–formic acid solutions and were air-dried to produce opaque films. After irradiation in the presence of the GMA monomer solutions, the samples were removed from the solutions, washed, dried, and equilibrated in water for testing.

Measurements

The reverse osmosis measurements were made in a test loop consisting of four stirred cells pressurized by an air-driven pump. A schematic representation of the test loop is given in Figure 1.

The Amicon Model 420 high-pressure cells, accomodating an effective membrane area of 37.4 cm^2, were operated independently at relatively low feed solution flow rates and can be pressurized from 500 to 2000 psi. Concentration polarization buildup in each cell was minimized by use of an internal magnetic stirrer driven by an external horseshoe magnet operated with an ac motor, and by regulation of the feed flow rate (which must be maintained high compared to the effluent flow rate) using the outlet valve control for each cell.

Pressurization and circulation of the feed solution was maintained by a system consisting of a Sprague air-driven pump (S-440-CS35-55) used with a laboratory (100 psi) air line, a Greer bladder accumulator which eliminates pressure pulses due to pumping, and a Culligan Filter-gard which filters the feed before recirculating through the pump. The applied pressure was

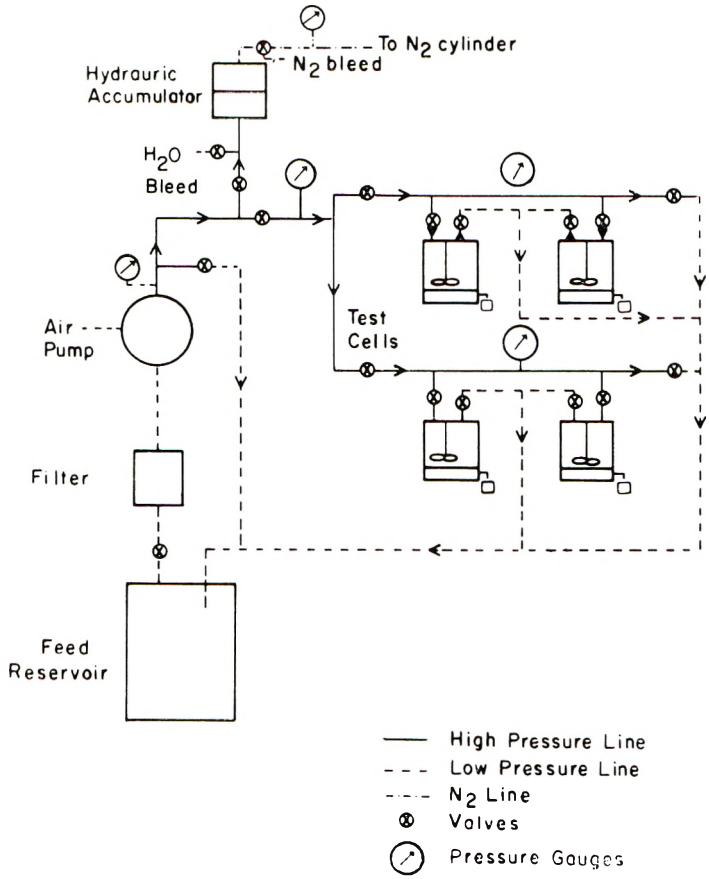

Fig. 1. Schematic drawing of the reverse osmosis test loop.

adjusted by the control valve of the pump and could be maintained within ±20 psi at 1500 psi.

All measurements were made at 1500 psi applied pressure, with a 3.5% NaCl solution by weight at 24–25°C. Water flux was calculated from the amount of effluent collected per unit time and the membrane area. Salt rejection was calculated on the basis of the relative conductivity of the feed solution in each cell to the effluent from each cell. The conductivity measurements were made with a Type CDM 2e conductivity meter manufactured by Radiometer of Copenhagen.

Water permeability was calculated from eq. (9). The thickness ΔX of the membrane sample was measured after reverse osmosis testing because some samples underwent noticeable compaction at high pressures. The use of the original thickness would have led to errors in the calculation of K_1.

The reverse osmosis measurements were continued on each film until values of water flux and salt rejection were stabilized, and these values were used in calculations and plots.

RESULTS AND DISCUSSION

The reverse osmosis results (shown in Table II) can be compared with separate sets of experimental results (i.e., P_1, ω, and P_2 as a function of the common parameter H) to examine the general dependence of R_S obtained with nonionic polymer membranes upon the water flux constant K_1.

The application of the free volume theory of diffusion to the homogeneous membrane model leads to the following expression.[1,7]

$$D = \nu \exp\{-V^*/V_f^0\} \exp\{-E/kT\} \tag{17}$$

Here, D is the diffusion constant of permeant in the membrane; ν is the translational oscillating frequency of the diffusing molecule, which is related to the diffusional jump distance d and Boltzmann's and Plank's constants as $\nu \approx d^2(kT/h)$; V^* is a characteristic volume parameter describing the diffusion of permeant molecules in the membrane (it is proportional to the sweeping volume of diffusing entity); V_f^0 is the total free volume in unit volume of the membrane; and E is the activation energy for diffusion. (The empirical activation energy includes the additional

TABLE II
Reverse Osmosis Data for Homogeneous Films

Film	Salt rejection R_S, %	Water permeability $K_1 \times 10^{10}$, cm²/sec atm
1	90	1.4
2	60	1.2
3	63	1.0
4	11	23.
5	57	4.6
6	4.8	48.
7	9.0	61.
8	20	8.6
9	26	2.6
10	7.0	27
11	16	1.9
12	56	1.1
13	64	1.4
14	44	3.8
15	12	5.5
16	83	2.7
17	93	2.3
18	91	1.9
19	95	.84
20	98	1.5
21	97	1.6
22	6.0	104
23	40	1.8
24	20	2.5
25	20	2.5
26	20	2.4

temperature dependence of the free volume.) On assuming additivity of free volume, the free volume in the membrane is given by

$$V_f^0 = HV_{f,1}^0 + (1 - H)V_{f,3}^0 \tag{18}$$

where $V_{f,1}^0$ is the free volume in unit volume of pure water, $V_{f,3}^0$ is the free volume in unit volume of the polymer, and H is the volume fraction of water in the membrane. Since the salt alone cannot permeate through dry polymer membranes (i.e., the salt cannot utilize $V_{f,3}^0$ for its transport), the effective free volume of membrane for salt transport can always be given by

$$V^0_{,\mathrm{eff(salt)f}} = HV_{f,1}^0. \tag{19}$$

The expression similar to eq. (19) for $V^0_{f,1\ \mathrm{eff}\ (H_2O)}$ applies only in the region $H \gg (1 - H)$ where the second term in eq. (18) can be neglected. Therefore the diffusion constant of water D_1 and of salt D_2 in the membrane can be given by

$$\ln(D_1/D_{1,0}) = -\beta_1 x(1 - \alpha)/(1 + \alpha x) \tag{20}$$

where $D_{1,0}$ is the self-diffusion constant of water:

$$x = (1 - \mathrm{H})/H$$
$$\alpha = V_{f,3}^0/V_{f,1}^0$$
$$\beta_1 = V_1^*/V_{f,1}^0$$

Similarly, we write

$$\ln(D_2/D_{2,0}) = -\beta_2(1 - \alpha)x \tag{21}$$

where $D_{2,0}$ is the diffusion constant of the salt in pure water and $\beta_2 = V_2^*/V_{f,1}^0$. How well eqs. (20) and (21) hold has been shown in the literature for water[1] and for NaCl[6-8] in various hydrophilic polymer membranes.

The diffusive permeability P which appears in eq. (16) is related to the diffusion constant D by

$$P = sD \tag{22}$$

where s is the partition coefficient, the ratio of concentration of permeant in the membrane to concentration in solution.

With introduction of a parameter which relates the partition coefficient to H

$$s = \gamma H \tag{23}$$

and recognition that $\gamma = 1$ for water, the diffusive permeability constant of water and salt in membrane can be derived as

$$P_1 = HD_{1,0}e^{-\beta_1(1-\alpha)x/(1+\alpha x)} \tag{24}$$

$$P_2 = \gamma HD_{2,0}e^{-\beta_2(1-\alpha)x} \tag{25}$$

From these equations, it is evident that log P_1 and log P_2 versus x are not strictly linear. However, due to the facts (1) that the pre-exponential

factor has much less effect on P than the exponential factors, (2) that $\beta(1 - \alpha)x/(1 + \alpha x)$ converges to $\beta(1 - \alpha).x$ in the region of small x, and (3) that γ generally decreases as x increases, then log P_1 and log P_2 decrease nearly linearly with x in the high hydration (small x) region.

The significant difference between P_1 and P_2 in the low H region can be explained by the difference between eqs. (24) and (25). Namely (1) water transport utilizes both $V_{f,1}^0$ $V_{f,3}^0$, whereas the salt transport occurs by

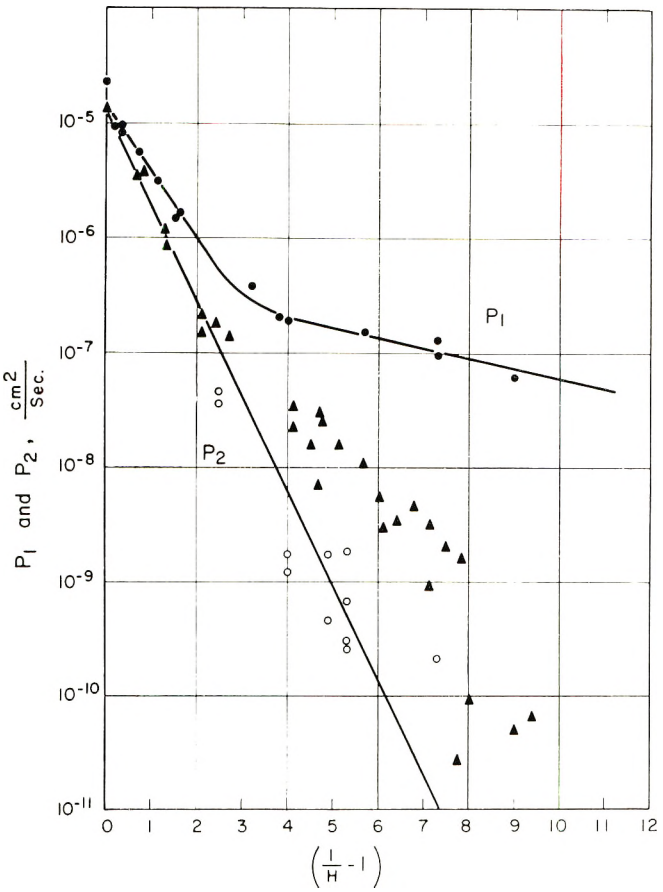

Fig. 2. Dependence of P_1 (diffusive permeability of water) and P_2 (diffusive permeability of NaCl) on $(1\text{-}H)/H$: (○) data of Lonsdale et al.;[9] (△) data of Yasuda et al.;[6] (●) data of Yasuda et al.[1]

utilizing only $V_{f,1}^0$. This characteristic distinction between diffusive permeabilities of water and NaCl is clearly evident, as can be seen in Figure 2 where log P_1 and log P_2 are plotted against x: log P_2 decreases nearly linearly with increasing x despite the obvious scatter due to the varying value of the parameter γ for the salt. (2) Another factor is the role of γ in eq. (25), i.e., $\gamma = 1$ for water, whereas γ for the salt generally decreases with

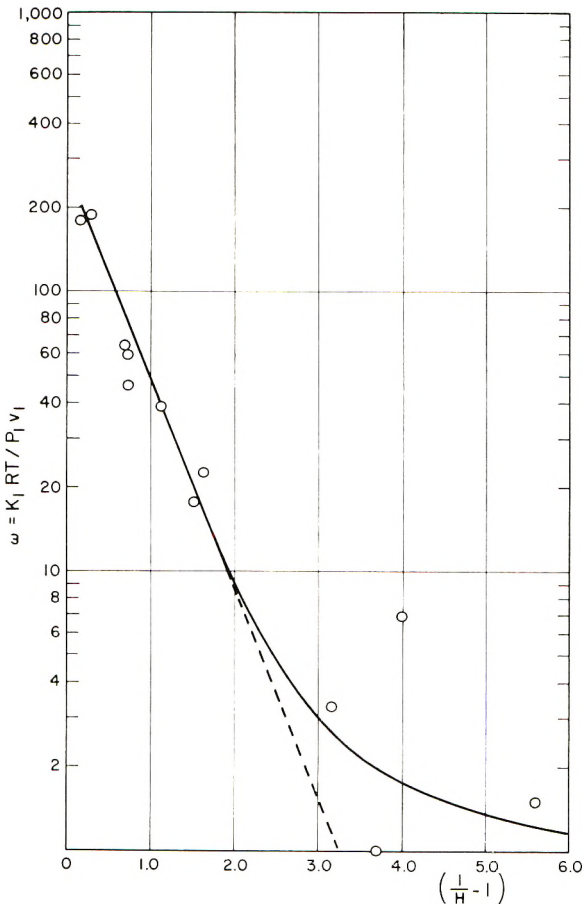

Fig. 3. Dependence of $\omega = K_1RT/v_1P_1$ on (1-H)/H.

increasing x. Therefore, in the low H region, log P_1 deviates more from the linear dependence on x which is found in high H region than does log P_2.

Since γ is not a constant but a parameter characteristic of a membrane, the value of P_2/P_1 as given in eq. (16) cannot be derived for the general case. However, the vast difference between P_1 and P_2 as functions of x can be expressed for a special case in which s_2 is given by $s_2 = e^{-bx}$, where b is a constant. This special case represents the solid straight line for P_2 in Figure 2. From this line, the ratio of P_2/P_1 (for the idealized case) as a function of x can be read, then a set of values for R_S and K_1 can be calculated by eqs. (4) and (16). For this calculation, $RT/v_1(\Delta p - \Delta\pi)$ is considered as a constant for the experimental conditions used. The value of ω is read from the linear portion of curve in the plots of log ω versus x shown in Figure 3. Although the experimental values of ω fluctuate in the diffusion region, ω is assumed to be unity for all cases above the value of x at which the linear portion of the log ω versus x plot intercepts the value of one.

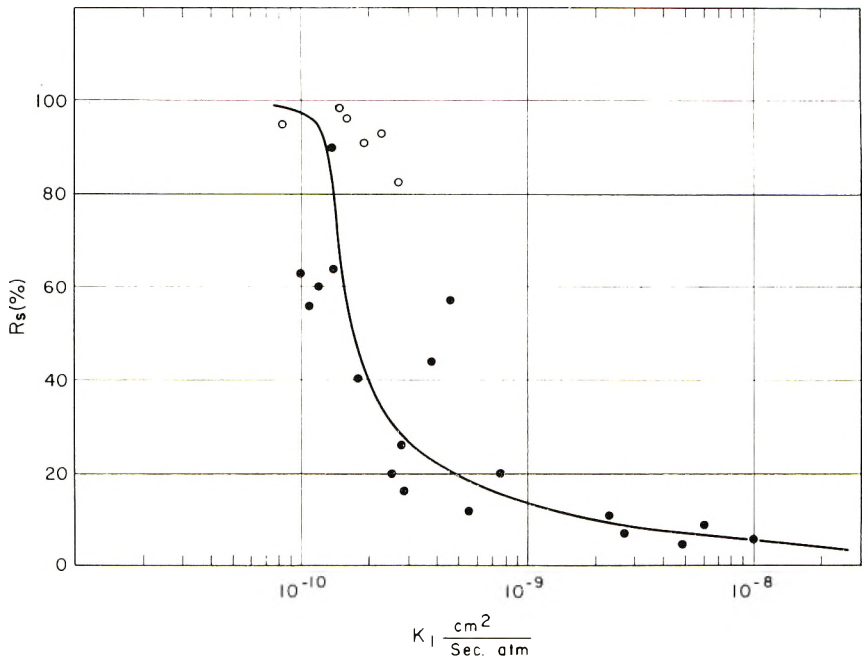

Fig. 4. Relationship between salt rejection R_s in reverse osmosis and log K_1 for nonionic polymer membranes: (○) cellulose acetate membranes, Eastman E-398-3, cast from various solvents; (——) values calculated from eq. (16) for the model case.

By using these generalized ω values for a given x, together with P_2/P_1 for the corresponding x value, the value of K_1 is calculated by eq. (4); i.e., $K_1 = \omega P_1 v_1/RT$.

It should be noted that values of H used in Figures 2 and 3 are measured under 1 atm pressure, and that ω is obtained with pure water. Therefore, this process is strictly for estimating corresponding parameters. Direct measurement of these parameters with actual membranes under reverse osmosis conditions is extremely difficult and impractical.

The general dependence of salt rejection on the water flux, which was obtained by a set of calculated values for the model case, is shown as a solid line in the plot of log K_1 versus R_S, and the results of Table II are plotted on the same graph in Figure 4.

In the plot in Figure 4, the value of R_S is quite straightforward; however, the value of K_1 may involve considerable uncertainty since K_1 is obtained by multiplying membrane thickness by the observed flux. The uncertainty of the calculation lies in the meaning of the thickness. Although all membranes studied were prepared with special caution to avoid skin formation or asymmetric structure, the complete elimination of this effect is nearly impossible. If, therefore, the actual flux and salt rejection are due to an effective layer which is smaller than the gross thickness, the calculated K_1 value will appear higher than the real value.

The same argument applies to the fluctuating ω values. The effect of uncertainty in the membrane thickness reflects more heavily on the hydraulic permeability than on the diffusive permeability, and, consequently, it tends to give a higher ω value. Therefore, only the mode of variation of ω (over three orders of magnitude) as a function of x should be emphasized, and the numerical values within an order of magnitude in the low H region should not be taken too literally.

In Figure 4, the results obtained with cellulose acetate membranes are shown by open circles and distinguished from the rest of the membranes. The scatter of these values may represent a measure of the order of magnitude of data scattering expected for this type of analysis, since all cellulose acetate membranes studied were cast from an identical polymer sample. The difference of solvent, in respect to conformation of polymer in the solutions and the ease of removal from the cast solution, would cause considerable variations in membrane properties.

The solvents used for preparation of membranes other than cellulose acetate may not be the best solvents for each polymer, and consequently performance may vary with different membrane preparations. Nevertheless, results analysed in this manner seem to reveal a consistent general trend between R_S and K_1 in nonionic polymer membranes.

The main intention of the model calculation is to find the general trend in the relationship between R_S and K_1, since these are only parameters which can be obtained under the exact conditions of reverse osmosis. The exact value of H in reverse osmosis is extremely difficult to obtain; however, it is not necessary to obtain it if a quantitative relation between K_1 and R_S can be established. In the qualitative sense, it is well known that the greater the water permeability, the lower is the salt rejection. This generally observed trend was expressed in a quantitative manner by this model calculation, which seems to offer the basis for comparing characteristic distinctions between nonionic membranes and ionic membranes without additional data but with K_1 and R_S directly obtained from the reverse osmosis experiments.

In order to have high salt rejection and high water flux constant, in a nonionic polymer, the membrane must have the maximum amount of water distributed evenly throughout the membrane without formation of large clusters (or aggregates) of water. Realistic polymer membranes are far from homogeneous in the molecular sense. For instance, a cellulose membrane which has a hydration value of approximately 0.45 allows permeation of solutes which have a characteristic diameter of 30 to 40 Å though their permeability is small.[7] This indicates that the membrane has intersegmental spaces of at least 30 to 40 Å, which is in good accord with the requirements to be fulfilled to explain P_1 and K_1 values, as previously mentioned.

On the other hand, if the amount of water which gives $H = 0.45$ is distributed evenly on the molecular level, approximately 18 water molecules are held by a cellobiose unit, which has 6 OH groups, i.e., only three water molecules per OH group. The cluster of three water molecules is too small to justify the assumption that water-soluble solutes permeate through free

volume occupied by water held in the membrane phase. Therefore, the even distribution of water should be interpreted in a morphological sense, but not in a molecular sense.

The effectiveness of a nonionic polymer as reverse osmosis membrane, therefore, depends exclusively on the equilibrium uptake of water and the morphological distribution of the water in membrane phase. Though the chemical nature of the polymers controls these factors, it is not directly related to the salt rejection or water flux constant. The extension of this approach to ionic polymer membranes will be discussed in detail in Paper II.[3]

This study was support by Office of Saline Water, U.S. Department of the Interior, Contract No. 14-01-0001-1452.

Authors are indebted to Mrs. D. K. Wood, Mrs. C. Foust, and Miss E. J. Higginbotham for their technical assistance.

The authors' special thanks are due to Dr. A. Peterlin, Director of Camille Dreyfus Laboratory for his thorough review and creative criticism.

References

1. H. Yasuda, C. E. Lamaze, and A. Peterlin, *J. Polym. Sci. A-2*, **9**, 1117 (1971).
2. G. Thau, R. Bloch, and O. Kedem, *Desalination*, **1**, 129 (1966).
3. H. Yasuda, C. E. Lamaze, and A. Schindler, *J. Polym. Sci. A-2*, **9**, 1579 (1971).
4. U. Merten and H. K. Lonsdale, in *Desalination by Reverse Osmosis*, U. Merten, Ed., The M.I.T. Press, Cambridge, Mass., 1966.
5. H. K. Lonsdale, B. P. Cross, F. M. Graber, and C. E. Milstead, paper presented at American Chemical Society Meeting, 1969; *Polym. Preprints*, **10**, No. 2, 1167 (1969).
6. H. Yasuda, C. E. Lamaze, and L. D. Ikenberry, *Makromol. Chem.*, **118**, 19 (1968).
7. H. Yasuda, A. Peterlin, C. K. Colton, K. A. Smith, and E. W. Merrill, *Makromol. Chem.*, **126**, 177 (1969).
8. H. Yasuda, L. D. Ikenberry, and C. E. Lamaze, *Makromol. Chem.*, **125**, 108 (1969).
9. H. K. Lonsdale, U. Merten, and R. L. Riley, *J. Appl. Polym. Sci.*, **9**, 1341 (1965).

Received June 17, 1970
Revised October 5, 1970

JOURNAL OF POLYMER SCIENCE: PART A-2 VOL. 9, 1553–1577 (1971)

Thermodynamic Parameters of Polymer-Solvent Systems from Light-Scattering Measurements Below the Theta Temperature

TH. G. SCHOLTE, *Central Laboratory DSM, Geleen, The Netherlands*

Synopsis

As is well known, the chemical potentials of polymer and solvent in solution and, hence, the Flory-Huggins interaction parameter χ can be determined from scattered light intensities from dilute and concentrated solutions of the polymer in the solvent concerned. Preferably, measurements should be performed at temperatures as low as possible, provided the temperature exceeds the cloudpoint for the concentration used. It is shown that the lower the temperature and, consequently the higher the scattered light intensity, the better is the accuracy of the parameters obtained. At each temperature the scattered light intensity shows a maximum at some concentration. Below the theta temperature the ratio of scattered light intensity and concentrations also shows a maximum at some concentration. The values and the concentrations of these maxima for various temperatures enable the maximum of the spinodal to be determined. The spinodal itself can be determined by an extrapolation procedure of the reciprocal scattered light intensities. Measurements have been performed with three narrow-distribution polystyrene samples in cyclohexane. On the basis of the results, χ and its dependence on concentration, temperature, and molecular weight can be determined to high accuracy.

INTRODUCTION

The intensity of light scattered by solutions is entirely determined by local fluctuations of the refractive index of the solution. The latter are due both to fluctuations in density and to fluctuations in concentration (see e.g., Coumou and Mackor[1]). The fluctuation theory of Smoluchowski[2] and Einstein[3] and its extension to solutions of polydisperse polymers given by Brinkman and Hermans,[4] Kirkwood and Goldberg,[5] and Stockmayer[6] show that there exists a definite relation between the intensity of the scattered light and the second derivatives of the free enthalpy (Gibbs free energy) of mixing with respect to the concentrations of the polymer components. This implies that light scattering intensity at various concentrations and temperatures may yield information on the thermodynamic parameters of the system.[1,7]

From the above theories it follows that in the vicinity of the spinodal the scattered light intensity will increase to very high values. In that region the theory becomes more complicated, *inter alia* because, as pointed out by Debye,[8] allowance must now be made for the additional energy associated with concentration gradients. However, this effect can be ruled out by extrapolating to zero scattering angle. It will be seen then that the above

relatively simple theory remains valid even in the vicinity of the spinodal; the only condition to be observed is that the measurements be carried out under circumstances where no phase separation occurs.

THEORY

Extrapolated to zero scattering angle, the intensity of light scattering due to concentration fluctuations is given by:[7]

$$[R_\theta^{(c)}]_{\theta=0} = (4\pi^2 n^2/\lambda^4)kT(dn/dw)^2\Big(\sum_i\sum_j B_{ij}/|b|\Big)\Delta V \qquad (1)$$

In this equation $R_\theta^{(c)}$ is the Rayleigh ratio of scattering arising from composition fluctuations, at an angle θ from the direction of the incident beam; λ the wavelength *in vacuo* of the light used, k is Boltzmann's constant; T is the absolute temperature; n is the refractive index; and w is the concentration (weight fraction) of the solution. The determinant $|b|$ has elements $\partial^2(\Delta G)/\partial w_k \partial w_l$, where ΔG is the free enthalpy of mixing in a volume element ΔV and w_k and w_l are the concentrations (weight fractions) of polymer components k and l, respectively. The cofactor of the element i, j of the determinant is denoted by B_{ij}.

Determination of the elements $\partial^2(\Delta G)/\partial w_k \partial w_l$ requires knowledge of ΔG as a function of concentration and composition of the polymer. Such a function is the Flory-Huggins equation[9–11] for the free enthalpy of mixing in a solution of a polydisperse polymer. There are some advantages to use of this equation with concentrations expressed in terms of weight fractions instead of volume fractions.[12] In terms of weight fractions w, the Flory-Huggins equation reads:

$$\Delta G/RT = \Big[w_0 \ln w_0 + \sum_i (M_0/M_i) w_i \ln w_i + g w_0 w\Big](\rho \Delta V/M_0) \qquad (2)$$

where ΔG is the free enthalpy of mixing of $\rho\Delta V$ grams of solution; R is the universal gas constant; ρ is the density of the solution; w_0 is the weight fraction of the solvent; M_0 is the molecular weight of the solvent; M_i is the molecular weight of component i of the polymer, and g is an interaction parameter. The summation has to be done over all polymer components.

In differential form, the Flory-Huggins equation is:[12,13]

$$\Delta\mu_0/RT = \ln(1 - w) + [1 - (M_0/\bar{M}_n)]\, w + \chi w^2 \qquad (3)$$

with $\Delta\mu_0$ the chemical potential of the solvent in solution minus the chemical potential of pure solvent; $\bar{M}_n$ is the number-average molecular weight of the polymer, and χ is the Flory-Huggins interaction parameter:*

$$\chi = g - (1 - w)(\partial g/\partial w)$$

Substitution of ΔG, according to eq. (2), in eq. (1) yields:

$$[R_\theta^{(c)}]_{\theta=0} = (4\pi^2 n^2/N_A\lambda^4)(dn/dw)^2(1/\rho)[w\bar{M}_w/(1 + Kw\bar{M}_w)] \qquad (4)$$

* In Tables I, II, and III and Figures 1, 2, and 3 we denote this quantity by χ_w, to indicate that it corresponds to the Flory-Huggins equation expressed in weight fractions.

where N_A is Avogadro's number, $\bar{M}_w$ is the weight-average molecular weight of the polymer, and

$$K = \frac{1}{M_0}\left(\frac{1}{1-w} + \frac{\partial^2\{w(1-w)g\}}{\partial w^2}\right) \tag{5a}$$

or

$$K = \frac{1}{M_0}\left[\frac{1}{1-w} - 2\chi - w\frac{\partial\chi}{\partial w}\right] \tag{5b}$$

Provided the distribution is relatively narrow, eqs. (4), (5a), and (5b) are also obtained when g is slightly dependent on the molecular weight; however, they then contain the molecular weight-dependent values of K, g, and χ. We can obtain $R_\theta^{(c)}$ from experiments by using the relation:

$$R_\theta^{(c)} = (n^2/n_B^2)R_B\Delta I \sin\theta \tag{6a}$$

or

$$[R_\theta^{(c)}]_{\theta=0} = (2n^2/n_B^2)R_B(\alpha\Delta I)_{\theta=0} \tag{6b}$$

In these equations ΔI denotes the difference in scattered light intensity between the solution and the pure solvent, relative to the scattering intensity of a standard liquid (e.g., pure benzene) measured perpendicular to the incident ray; n_B is the refractive index and R_B the Rayleigh factor of the standard; and α is the angle factor $(\sin\theta)/(1+\cos^2\theta)$ for unpolarized incident light. Since the scattering due to density fluctuations is only a small term in our series of experiments, it could be equated to the scattering of the pure solvent over the whole concentration range, without this causing any appreciable error. Otherwise, it would be necessary to determine the density scattering separately, e.g., from isothermal compressibility data as Coumou and Mackor[1] mention. Equation (4) then becomes:

$$(\alpha\Delta I)_{\theta=0} = \frac{2\pi^2 n_B^2}{N_A\lambda^4 R_B}\left(\frac{dn}{dw}\right)^2 \frac{1}{\rho}\frac{w\bar{M}_w}{1+Kw\bar{M}_w} \tag{7}$$

DIRECT DETERMINATION OF $\Delta\mu_0$ AND χ

Theoretical

One of the methods for determining the thermodynamic properties (chemical potential of polymer and solvent, interaction parameters) of a polymer–solvent system is based on measuring the intensity of light scattering at various concentrations. Such a series of measurements carried out at various temperatures also yields the temperature dependence of these parameters. If desired, the measurements may be performed on polymer samples differing in molecular weight to investigate the influence of the molecular weight on these parameters.

Combining eqs. (7) and (5b) with eq. (3), the Flory-Huggins relation, we get:

$$-\frac{\partial(\Delta\mu_0)}{\partial w} = RTM_0\left[\frac{2\pi^2 n_B^2}{N_A\lambda^4 R_B}\left(\frac{dn}{dw}\right)^2 \frac{w}{\rho(\alpha\Delta I)_{\theta=0}} + \frac{1}{\bar{M}_n} - \frac{1}{\bar{M}_w}\right] \tag{8}$$

The right-hand side of eq. (8) can be determined experimentally and yields $\partial(\Delta\mu_0)/\partial w$ at the concentration given. When this is done for a number of concentrations from very low values upwards, integration of $\partial(\Delta\mu_0)/\partial w$ gives $\Delta\mu_0$ for all desired values of w.* The interaction parameter χ can be determined from $\Delta\mu_0$.

From eq. (8) it is immediately evident that the higher the value of $(\alpha\Delta I)_{\theta=0}$, the greater will be the accuracy with which $(\partial\Delta\mu_0)/\partial w$ can be determined. Hence, values of $\Delta\mu_0$ and χ derived from it, can also be established with greater accuracy. It is clear, therefore, that as long as measurements can be made, it is advantageous to perform them at the lowest possible temperature, i.e., under conditions where the scattered light intensity is as high as possible.

Experimental

In a recent study[7] we performed measurements and ensuing calculations on solutions of three polystyrene samples ($\bar{M}_w$ = 51000, $\bar{M}_w$ = 163000 and $\bar{M}_w$ = 520000) in cyclohexane, covering the concentration ranges $0 < w < 0.3$, $0 < w < 0.2$ and $0 < w < 0.1$, respectively. The ranges were limited by the maximum concentrations at which the solutions could still be clarified by filtration. The temperatures used were 35, 45, and 65°C (the theta temperature of polystyrene in cyclohexane is approximately 34°C).

The measurements on solutions of the same polystyrene samples were now extended to lower temperatures. We used polystyrenes of narrow molecular weight distribution from the Pressure Chemical Co.: sample 7a, $\bar{M}_n$ = 49,000, $\bar{M}_w$ = 51,000; sample 1a, $\bar{M}_n$ = 154,000; $\bar{M}_w$ = 163,000, sample 5a, $\bar{M}_n$ = 435,000; $\bar{M}_w$ = 520,000.

The temperatures and concentrations used were as follows: sample 7a, 17.4–30°C; up to 20 wt-%; sample 1a, 25–35°C; up to 15 wt-%; sample 5a 28–35°C; up to 10 wt-%.

The measurements were performed by use of a Sofica 42000 M photogoniodiffusometer. The experimental procedure and method of calculation as well as the values used for dn/dw, ρ, R_B, and n_B have been given elsewhere.[7] Since in some cases the intensity of the scattered light was more than 1000 times the standard value (scattering in benzene through an angle of 90°), we had to fit some neutral absorption filters into the photogoniometer and to calibrate them in order to measure the intensity relative to that in benzene. The cyclohexane (Spectrosal, Hopkin and Williams, Ltd.) was previously dried by means of molecular sieves (Union Carbide, 1 Å). If no drying was carried out, the intensity of scattering was much higher, notably at lower temperatures.

* It is interesting to note that an analogous equation holds for the relation between $\partial(\Delta\mu_0/)\partial w$ and the concentration gradient in the case of sedimentation-diffusion equilibrium of a polydisperse polymer solution.[12]

Results

The principal results of the measurements, i.e., $\Delta\mu_0$, found by integration of $\partial(\Delta\mu_0)/\partial w$, and the value of χ calculated therefrom, are compiled in Tables I, II, and III.

TABLE I
Chemical Potential of Solvent and Interaction Parameter in Polystyrene–Cyclohexane Solutions (PS 7a, $\bar{M}_w$ = 51000)

w, g/g	Temp, °C	$-\Delta\mu_0 \times 10^{-6}$, erg/mole	χ_w
0.02	17.4	0.702	0.5201
	18.4	0.723	0.5182
	20.0	0.748	0.5160
	22.0	0.780	0.5133
	25.2	0.812	0.5108
	30.4	0.848	0.5086
0.04	17.4	1.187	0.5261
	18.4	1.253	0.5245
	20.0	1.333	0.5226
	22.0	1.432	0.5204
	25.2	1.551	0.5177
	30.4	1.694	0.5148
0.06	17.4	1.519	0.5322
	18.4	1.648	0.5308
	20.0	1.792	0.5292
	22.0	1.084	0.5272
	25.2	2.236	0.5246
	30.4	2.575	0.5214
0.08	17.4	1.752	0.5386
	18.4	1.962	0.5373
	20.0	2.183	0.5359
	22.0	2.479	0.5342
	25.2	2.911	0.5317
	30.4	3.535	0.5283
0.10	17.4	1.945	0.5453
	18.4	2.219	0.5442
	20.0	2.548	0.5429
	22.0	2.967	0.5412
	25.2	3.622	0.5387
	30.4	4.594	0.5353
0.15	17.4	2.383	0.5635
	18.4	2.861	0.5627
	20.0	3.521	0.5615
	22.0	4.354	0.5601
	25.2	5.762	0.5576
	30.4	7.884	0.5541
0.20	17.4	3.080	0.5840
	18.4	3.820	0.5832
	20.0	5.016	0.5821
	22.0	6.438	0.5807
	25.2	8.952	0.5782
	30.4	12.850	0.5745

TABLE II
Chemical Potential of Solvent and Interaction Parameter in Polystyrene–Cyclohexane Solutions (PS 1a, $\bar{M}_w$ = 163000)

w, g/g	Temp, °C	$-\Delta\mu_0 \times 10^{-6}$, erg/mole	χ_w
0.02	25.0	0.197	0.5142
	26.0	0.206	0.5134
	27.9	0.226	0.5115
	29.8	0.242	0.5101
	35.0	0.283	0.5065
0.04	25.0	0.327	0.5192
	26.0	0.355	0.5185
	27.9	0.415	0.5170
	29.8	0.465	0.5159
	35.0	0.610	0.5125
0.06	25.0	0.431	0.5252
	26.0	0.485	0.5246
	27.9	0.608	0.5232
	29.8	0.712	0.5222
	35.0	1.018	0.5190
0.08	25.0	0.531	0.5319
	26.0	0.617	0.5313
	27.9	0.818	0.5301
	29.8	0.994	0.5290
	35.0	1.527	0.5259
0.10	25.0	0.644	0.5390
	26.0	0.770	0.5385
	27.9	1.063	0.5374
	29.8	1.334	0.5363
	35.0	2.151	0.5332
0.15	25.0	1.093	0.5580
	26.0	1.400	0.5575
	27.9	2.040	0.5564
	29.8	2.640	0.5553
	35.0	4.513	0.5522

The accuracy of the results depends on the accuracy of the extrapolated values of $(\alpha\Delta I)_{\theta=0}$ and on that of the values used for dn/dw, $\bar{M}_n$, and $\bar{M}_w$. Estimating the accuracy of $(\alpha\Delta I)_{\theta=0}$ at $\pm 5\%$, that of dn/dw at $\pm 3\%$, and that of $\bar{M}_n$ and $\bar{M}_w$ at $\pm 3\%$, one finds the accuracy of $\partial(\Delta\mu_0)/\partial w$ to be approximately $\pm 10\%$. At the lowest concentrations the integrated value $\Delta\mu_0$ is highly dependent on $\bar{M}_n$, at higher concentrations rather on $\partial(\Delta\mu_0)/\partial w$. As a rule, the accuracy of $\Delta\mu_0$ may be taken equal to approximately $\pm 5\%$.

The accuracy of the calculated χ is more difficult to indicate. A rough estimate yields a maximum deviation of 0.0008 for sample 7a, of 0.0004 for sample 1a, and of 0.0002 for sample 5a at all temperatures and concentrations. Apart from this, there is the accuracy of the temperature at which the measurements have been performed. This is approximately 0.1°C.

TABLE III
Chemical Potential of Solvent and Interaction Parameter in Polystyrene–Cyclohexane Solutions (PS 5a, $\bar{M}_w = 520000$)

w, g/g	Temp, °C	$-\Delta\mu_0 \times 10^{-6}$, erg/mole	χ_w
0.02	28.2	0.070	0.5095
	29.2	0.078	0.5088
	30.2	0.082	0.5084
	31.2	0.090	0.5076
	32.4	0.098	0.5069
	35.0	0.111	0.5057
0.04	28.2	0.112	0.5157
	29.2	0.136	0.5151
	30.2	0.155	0.5147
	31.2	0.181	0.5140
	32.4	0.206	0.5134
	35.0	0.263	0.5121
0.06	28.2	0.150	0.5224
	29.2	0.198	0.5219
	30.2	0.242	0.5214
	31.2	0.294	0.5209
	32.4	0.348	0.5203
	35.0	0.476	0.5189
0.08	28.2	0.199	0.5296
	29.2	0.283	0.5290
	30.2	0.360	0.5286
	31.2	0.448	0.5280
	32.4	0.545	0.5275
	35.0	0.771	0.5261
0.10	28.2	0.285	0.5369
	29.2	0.413	0.5364
	30.2	0.536	0.5359
	31.2	0.674	0.5353
	32.4	0.832	0.5347
	35.0	1.195	0.5333

The Parameter χ as a Function of Temperature and Concentration

In Figures 1, 2, and 3, χ has been plotted versus $1/T$ for the various concentrations. The values at 35, 45, and 65°C[7] are also indicated.

These graphs show that χ is temperature-dependent, but also that χ cannot be described by means of a linear function of $1/T$ (nor, for that matter, by a linear function of T or ln T). In the range of temperatures concerned, one needs at least one more (quadratic) term for this purpose. In addition, the temperature dependence proves to vary with the concentration. This is particularly evident from Figure 12 in ref. 12, where χ has been plotted versus $1/T$ over the range of concentrations up to $w = 0.8$. An additional temperature dependence of χ is also seen in the lowest concentration and temperature ranges.

Restricting ourselves to the temperature region below 35°C and neglecting the lowest concentrations, we may, within the accuracy of measurement,

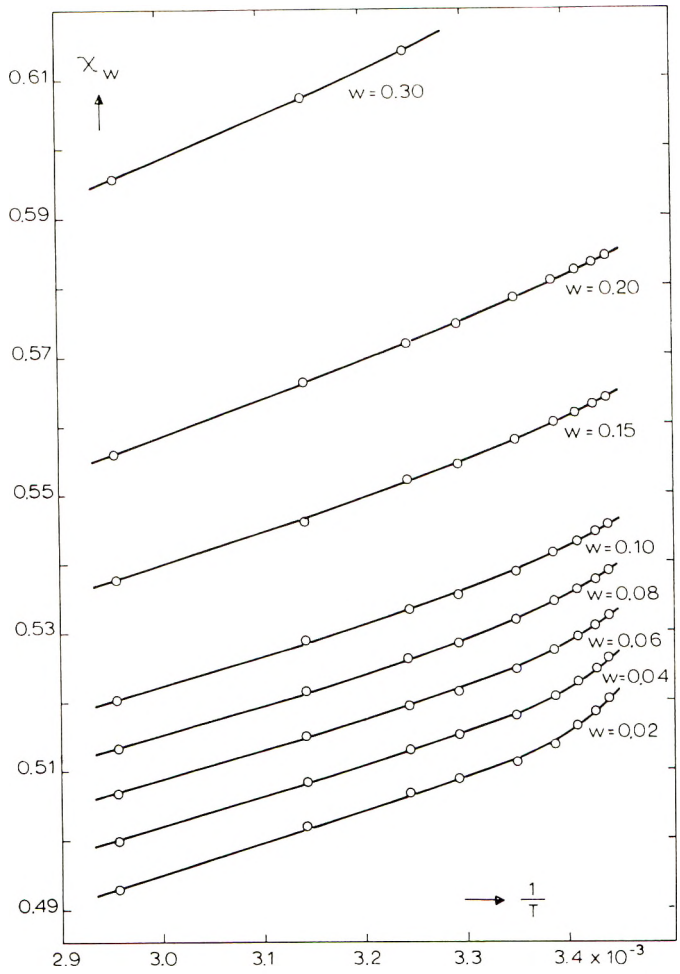

Fig. 1. Interaction parameter χ_w vs. reciprocal temperature $1/T$ for solutions of polystyrene 7a (M_w = 51000) in cyclohexane at various concentrations.

express χ as a linear function of $1/T$. In this limited region of concentration, the slope is scarcely dependent on concentration, but does depend on the molecular weight of the polymer. Approximating χ by

$$\chi = \chi_{00} + \chi_{01}/T + \chi_1 w + \chi_2 w^2 \tag{9}$$

we get the values shown in Table IV.

TABLE IV

PS sample	M_w	Concentration range, g/g	Temperature range, °C	χ_{00}	χ_{01}	χ_1	χ_2
7a	51000	0.10–0.20	17.4–35	0.2991	62	0.289	0.34
1a	163000	0.08–0.15	25–35	0.3304	52	0.317	0.25
5a	520000	0.04–0.10	28.2–35	0.3433	48	0.315	0.28

Within the deviation of 0.0002, χ can also be described by the same concentration dependence (χ_1 and χ_2) for the various molecular weights. This yields the functions:

PS 7a:

$$\chi = 0.2975 + 62/T + 0.306w + 0.30w^2 \tag{10a}$$

PS 1a:

$$\chi = 0.3310 + 52/T + 0.306w + 0.30w^2 \tag{10b}$$

PS 5a:

$$\chi = 0.3438 + 48/T + 0.306w + 0.30w^2 \tag{10c}$$

Summarizing these dependences we can draw the following conclusions. (1) χ is not linearly dependent on $1/T$. (2) The results obtained over a large range of concentrations show that the nonlinear term in $\chi = f(1/T)$ increases strongly at high concentrations. (3) At very low concentrations an additional temperature dependence appears in the lower temperature range. (4) In the range $0 < w < 0.20$ the concentration dependence can be represented by a quadratic function of w. The concentration dependence is

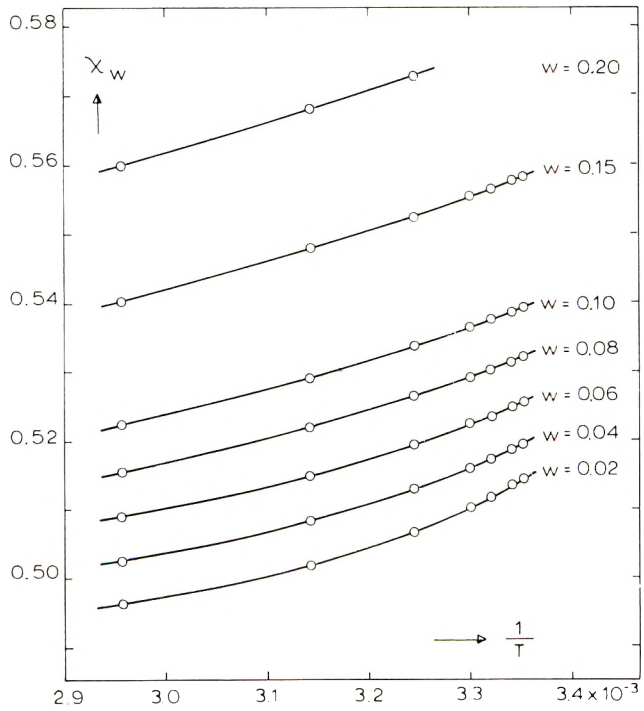

Fig. 2. Interaction parameter χ_w vs. $1/T$ for solutions of polystyrene 1a (M_w = 163000) in cyclohexane.

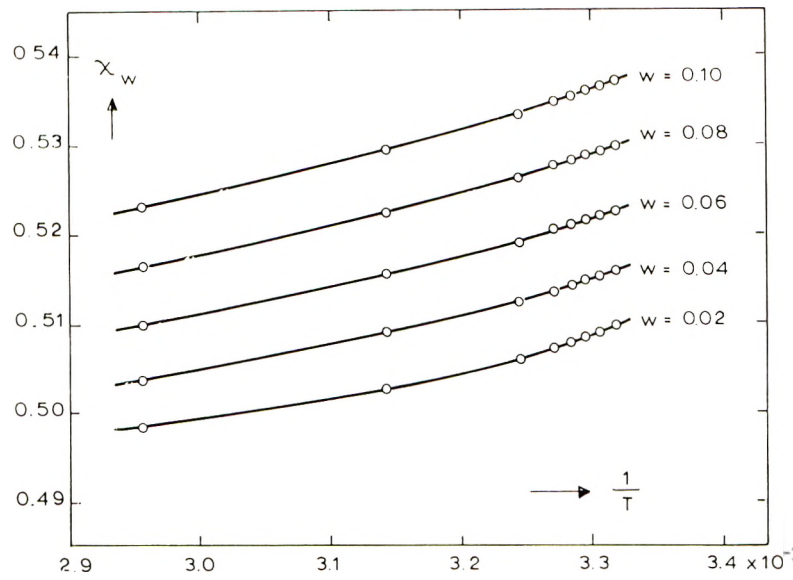

Fig. 3. Interaction parameter χ_w vs. $1/T$ for solutions of polystyrene 5a ($M_w = 520000$) in cyclohexane.

approximately the same for all molecular weights. (5) The temperature dependence (χ_{01}) varies with the molecular weight. Although χ_{00} depends on molecular weight, the combinations χ_{00}, χ_{01} for the three molecular weights studied lead to the same theta temperature (34°C), allowance being made for experimental uncertainty.

An explanation for the behavior mentioned under (3) may be that the Flory-Huggins equation is theoretically justified only in the region of higher concentrations. In dilute solutions, where the polymer molecules behave more or less as individual molecules, deviation from theory can manifest itself in a higher or lower value of the interaction parameter. Another possible cause is that at low concentrations and lower temperatures some phase separation of high molecular weight components has taken place. These trace amounts of precipitated polymer would increase the value of $(\alpha\Delta I)_{\theta=0}$, and thus lead to higher values of χ.

LOCI OF THE MAXIMA OF THE SCATTERED INTENSITY

Theoretical

In dilute polymer solutions, an increase in concentration is accompanied by an increase in the intensity of the scattered light. At higher concentrations, this increase is less sharp, and finally changes into a decrease. The concentration where $(\alpha\Delta I)_{\theta=0}$ is a maximum depends on the thermodynamic parameters of the system.

Let us now consider, instead of $(\alpha\Delta I)_{\theta=0}$, the slightly modified quantity:

$$A \equiv \rho(dn/dw)^{-2}(\alpha\Delta I)_{\theta=0} \tag{11}$$

At a given temperature, A will show a maximum at the concentration where $dA/dw = 0$. Using eq. (7), we thus get for this concentration:

$$w^2\bar{M}_w(dK/dw) = 1 \tag{12}$$

Substitution of K from eq. (5a) gives:

$$\frac{-1}{(1-w)^2} - \frac{\partial^2[w(1-w)g]}{\partial w^2} + \frac{M_0}{\bar{M}_w w^2} = 0 \tag{13a}$$

while substitution of K from eq. (5b), containing χ instead of g, leads to:

$$-\frac{1}{(1-w)^2} + 3\frac{\partial\chi}{\partial w} + w\frac{\partial^2\chi}{\partial w^2} + \frac{M_0}{\bar{M}_w w^2} = 0 \tag{13b}$$

If χ is concentration-independent, this equation can be transformed into:

$$w = 1/[1 + (\bar{M}_w/M_0)^{1/2}] \tag{14}$$

which is the equivalent of the equation Debye and Bueche[15] found in the case of a concentration-independent interaction parameter in the Flory-Huggins equation expressed in terms of volume fractions.

Applied to a given polymer–solvent system, eq. (13a) or eq. (13b) represents a line in the T, w plane, dependent on $\bar{M}_w$. This equation indicates, at every temperature, the concentration where A is a maximum.

If $\partial\chi/dw$ and $\partial^2\chi/\partial w^2$ are temperature-independent, i.e., if the entire temperature dependence of χ is accounted for in the concentration-independent term, eq. (13) represents a straight line at constant w (see Fig. 4).

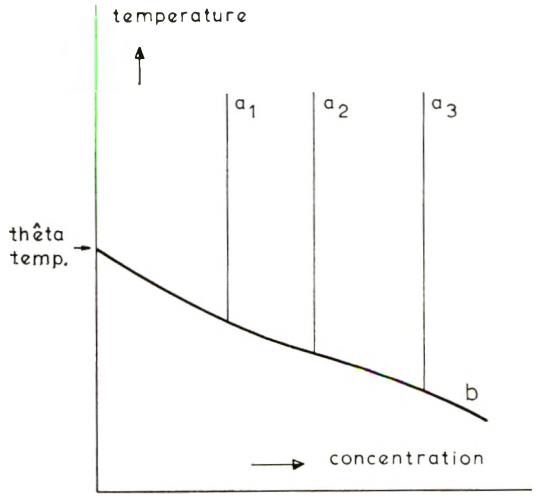

Fig. 4. Schematic plot showing concentrations where A and B pass through maxima as functions of temperature. Lines a_1, a_2, and a_3 correspond to maximum A for solutions of polymers with weight-average molecular weights increasing in order 1, 2, 3. Curve b locates maxima in B.

If either $\partial\chi/\partial w$ or $\partial^2\chi/\partial w^2$, or both, are temperature-dependent, the line will have a finite slope. This provides a direct means for determining whether and to what extent $3\partial\chi/\partial w + w\partial^2\chi/\partial w^2$ is temperature-dependent.

We can also consider the quotient of scattered light intensity and concentration. Generally, this quantity will decrease only with concentration, but at temperatures lower than the theta temperature it will at first increase to a maximum and then decrease. Let us consider the quantity:

$$B \equiv (\rho/w)(dn/dw)^{-2}(\alpha\Delta I)_{\theta=0} \tag{15}$$

By use of eq. (7), we see that the concentration w at which B is a maximum is given by:

$$K + w(dK/dw) = 0 \tag{16}$$

Upon substitution of K, from eq. (5a) and (5b), respectively, eq. (16) becomes:

$$-\frac{1}{(1-w)^2} - \frac{\partial^2[w(1-w)g]}{\partial w^2} - w\frac{\partial^3[w(1-w)g]}{\partial w^3} = 0 \tag{17a}$$

and

$$-[1/(1-w)^2] + 2\chi + 4w(\partial\chi/\partial w) + w^2(\partial^2\chi/\partial w^2) = 0 \tag{17b}$$

If the interaction parameter does not depend on the molecular weight of the polymer, eq. (17a) or eq. (17b) represents a line in the T,w plane, which is independent of the molecular weight. Since with $w = 0$, this equation yields $\chi = {}^1/_2$, the line meets the temperature axis at the theta temperature (see Fig. 4). Simultaneous validity of eqs. (13) and (17) leads to:

$$\frac{1}{1-w} + \frac{\partial^2[w(1-w)g]}{\partial w^2} + \frac{M_0}{\bar{M}_w w} = 0 \tag{18a}$$

and

$$[1/(1-w)] - 2\chi - w(\partial\chi/\partial w) + (M_0/\bar{M}_w w) = 0 \tag{18b}$$

This is the equation for the spinodal of the polymer–solvent system, expressed in terms of the weight fraction of the polymer.[13,14] In addition to satisfying eq. (18), the coordinates of the maximum of the spinodal must also conform to the relation obtained by differentiating the left-hand side of eqs. (18) with respect to w and equating to zero. This yields eqs. (13), implying that, at any value of $\bar{M}_w$, the lines defined by the maxima of A and B intersect in the maximum of the spinodal.

Results

Including the measurements reported previously,[7] results were available over the temperature range 17.4–65°C. Using the extrapolated values $(\alpha\Delta I)_{\theta=0}$ and those for ρ and dn/dw mentioned in the previous paper,[7] we

TABLE V
Loci of the Maxima and Maximum Values of A and B for Polystyrene–Cyclohexane Solutions

Polystyrene sample	Temp, °C	w for A_{max}, g/g	A_{max}, g/cm³	w for B_{max}, g/g	$B_{max} \times 10^{-4}$, (g/cm³)
PS 7a, $\bar{M}_w$ = 51000	17.4	0.137	19100	0.120	15.2
	18.4	0.138	11900	0.109	9.6
	20.0	0.131	7580	0.103	6.55
	22.0	0.130	5090	0.085	4.59
	25.2	0.130	3200	0.066	3.24
	30.4	0.124	2100	0.020	2.45
	35.0	0.114	1730		
	45.0	0.106	1230		
	65.0	0.098	780		
PS 1a, $\bar{M}_w$ = 163000	25.0	0.099	19900	0.065	24.6
	26.0	0.097	13900	0.058	18.5
	27.9	0.094	8480	0.036	12.3
	29.8	0.092	6200	0.024	10.3
	35.0	0.084	3320		
	45.0	0.087	1940		
	65.0	0.060	1230		
PS 5a, $\bar{M}_w$ = 520000	28.2	0.059	42100	0.042	96
	29.2	0.057	23600	0.035	54
	30.2	0.059	15250	0.028	39
	31.2	0.059	11350	0.023	29.5
	32.4	0.057	9000		
	35.0	0.053	5600		
	45.0	0.036	2890		
	65.0	0.035	1600		

calculated for every temperature the quantities A and B, and plotted them versus w. In Figure 5 the quantity A for solutions of polystyrene 7a is plotted versus w at nine temperatures.

Table V shows the values of w and A corresponding to the maxima of these curves. In Figure 6, B has been plotted as a function of the concentration. The loci and values of these maxima are also given in Table V.

The results of the measurements carried out on solutions of polystyrene 1a and 5a have been treated in a similar manner. Table V also shows the loci of the maxima, as well as the maximum values of A and B for solutions of these samples.

In Figure 7 the loci of the maxima of A and B are plotted versus the temperature. This graph corresponds roughly to that in Figure 4. On the whole, the accuracy is about 0.005 in the concentration and 0.1°C in the temperature. The three lines for the maxima of A are clearly not vertical. This suggests a temperature dependence of χ_1 and/or χ_2. The maxima of B for the three samples lie on slightly different lines, intersecting the axis with $w = 0$ at 33.5°C.

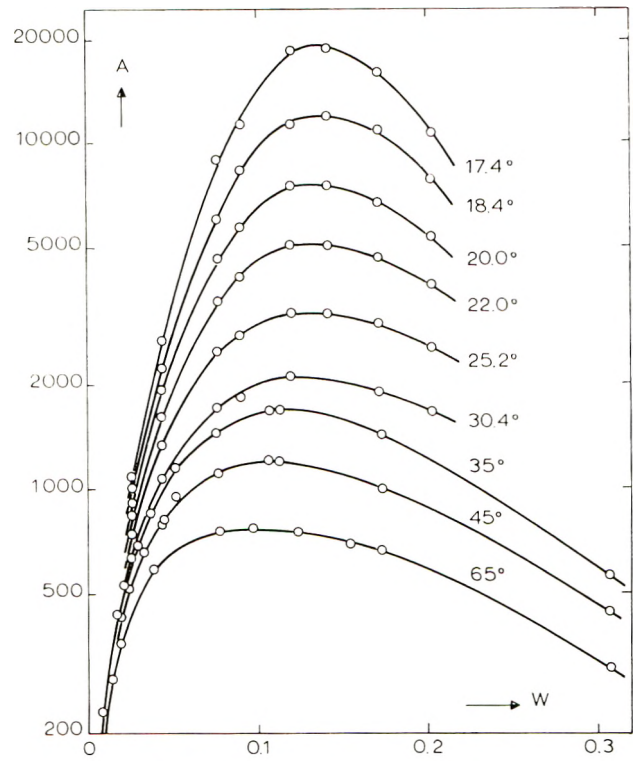

Fig. 5. Parameter A for sample 7a.

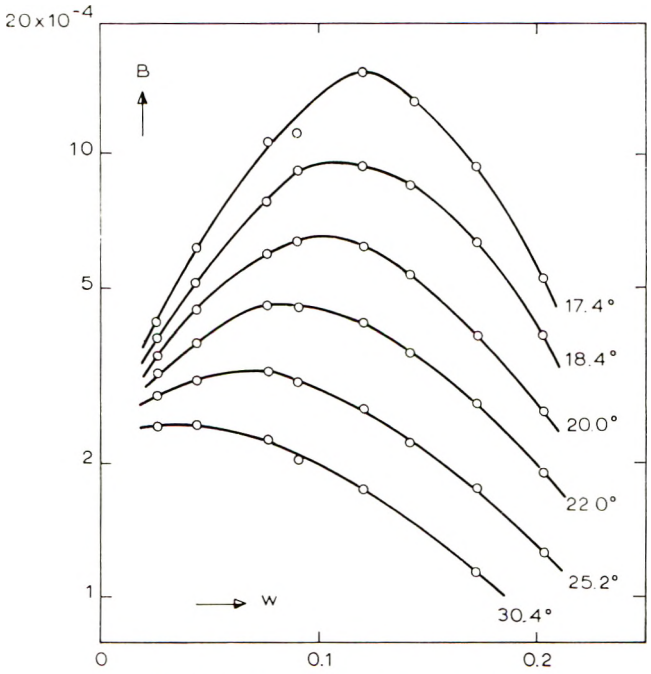

Fig. 6. Parameter B for sample 7a.

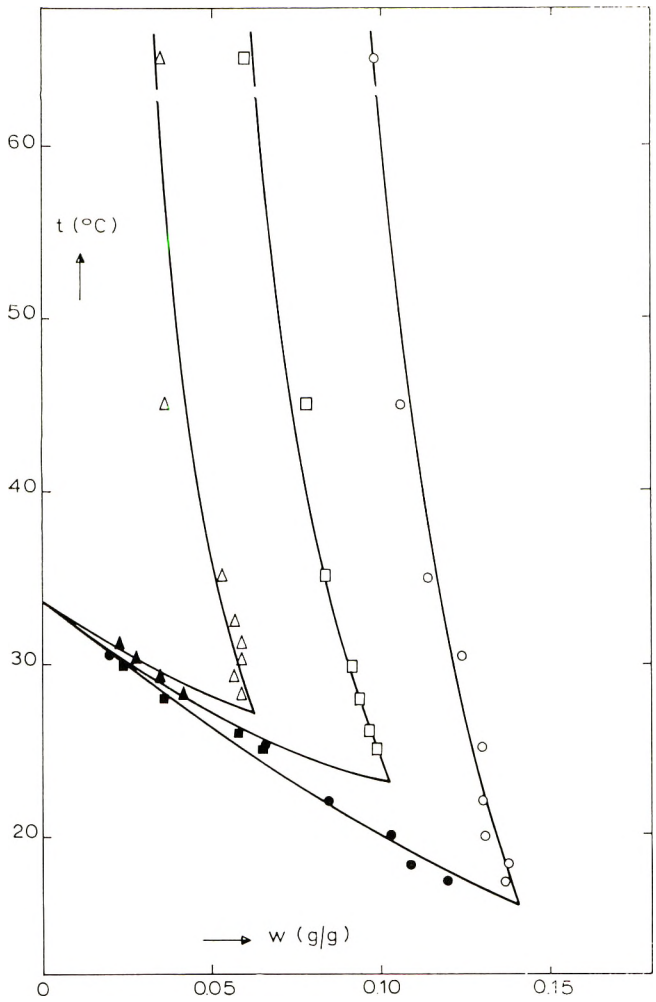

Fig. 7. Loci of the maxima of A and B for the three polystyrene samples in cyclohexane: (○) maximum of A, (●) maximum of B (sample 7a); (□) maximum of A, (■) maximum of B (sample 1a); (△) maximum of A, (▲) maximum of B (sample 5a).

Calculations from the Loci of the Maxima

The loci of the lines for the maxima of A and B enable us to estimate the concentration dependence of the interaction parameter. To this end, we represent χ as follows:

$$\chi = \chi_{00} + (\chi_{01}/T) + [\chi_{10} + (\chi_{11}/T)]w + \chi_2 w^2 \tag{19}$$

The parameters χ_1 $[=\chi_{10} + (\chi_{11}/T)]$ and χ_2 at a given temperature can then be calculated from the concentrations at which A and B pass through maxima. (In the equation for the B line we also use the χ values obtained by direct determination.) The results are shown in Table VI.

TABLE VI

PS sample	Temperature, °C	$w_{A_{max}}$	$w_{B_{max}}$	χ_2
7a	20	0.134	0.100	0.39
1a	26	0.097	0.060	0.43
5a	28.7	0.060	0.040	0.38

TABLE VII

PS sample	χ_1					
	20°C	26°C	28.7°C	30°C	40°C	50°C
7a	0.272			0.265	0.259	0.256
1a		0.287		0.285	0.281	0.276
5a			0.298	0.298	0.292	0.284

TABLE VIII

PS sample	Temp range, °C	Concentration range, g/g	χ_{00}	χ_{01}	χ_{10}	χ_{11}	χ_2
7a	17.4–30	0.10–0.20	0.3139	58	0.088	54	0.40
1a	25–35	0.06–0.15	0.3418	49	0.108	54	0.40
5a	28–35	0.04–0.08	0.3506	46	0.118	54	0.40

TABLE IX
Spinodal Concentrations and Temperatures

Polystyrene sample	w	$(1/T) \times 10^3$	Temp t, °C
PS 7a, $\bar{M}_w$ = 51000	0.0258	3.576	(6.4)
	0.0435	3.511	(11.6)
	0.0764	3.480	14.2
	0.0903	3.468	15.1
	0.1204	3.460	15.8
	0.1415	3.459	15.9
	0.1721	3.460	15.8
	0.2029	3.466	15.3
PS 1a, $\bar{M}_w$ = 163000	0.0186	3.448	(16.8)
	0.0407	3.398	21.1
	0.0620	3.377	22.9
	0.0821	3.374	23.2
	0.1012	3.373	23.3
	0.1243	3.375	23.1
	0.1496	3.383	22.4
PS 5a, $\bar{M}_w$ = 520000	0.0175	3.360	24.4
	0.0289	3.336	26.5
	0.0450	3.328	27.3
	0.0540	3.327	27.4
	0.0635	3.328	27.3
	0.0832	3.331	27.0
	0.1046	3.338	26.4

With $\chi_2 = 0.40$, the values of χ_1, found from the loci of the A lines are as given in Table VII.

The data of Table VII thus yield $\chi_{11} = 54$ and $\chi_{10} = 0.088$ (PS 7a), 0.108 (PS 1a) and 0.118 (PS 5a). By means of these coefficients the loci of the A

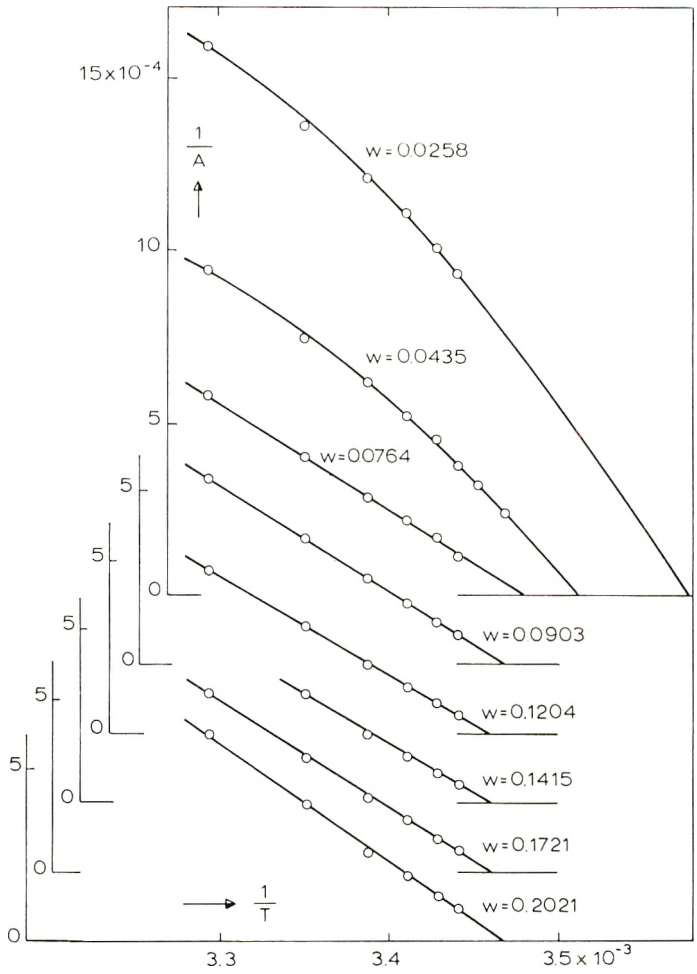

Fig. 8. Plots of $1/A$ vs. reciprocal temperature for sample 7a at various concentrations. Extrapolation to spinodal temperatures.

and B lines of polystyrene in cyclohexane can be described very satisfactorily.

Starting from this concentration dependence and the directly determined χ values, we find the sets of coefficients by means of which the χ values in the regions indicated in Table VIII can best be described.

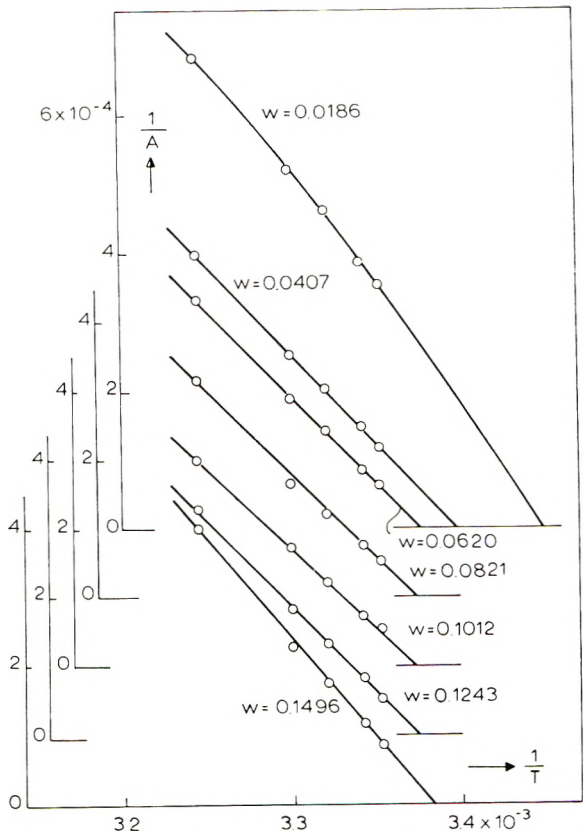

Fig. 9. Extrapolation of $1/A$ for sample 1a to spinodal temperatures.

DETERMINATION OF THE SPINODAL FROM $(\alpha\Delta I)_{\theta=0}$ VALUES

Method

The intensity of the scattered light increases with decreasing temperature, at an increasing rate as the distance from the spinodal becomes smaller. This provides a simple method for determining the spinodal directly from light scattering measurements. For, from the definition of A and eqs. (7) and (5b) it follows in a direct way that:

$$\frac{1}{A} = \frac{N_A \lambda^4 R_B}{2\pi^2 n_B^2} \frac{1}{M_0} \left[\frac{M_0}{w\bar{M}_w} + \frac{1}{(1-w)} - 2\chi - w\frac{\partial\chi}{\partial w} \right] \tag{20}$$

From eq. (18b) it is evident that $1/A = 0$ denotes the spinodal.

Plotting $1/A$ versus $1/T$ at a given concentration, we see that the resulting line intersects the axis $1/A = 0$ at the $1/T$ value of the spinodal corresponding to that particular concentration. The slope of the line (which is usually straight) indicates how $(2\chi + w\partial\chi/\partial w)$ depends on $1/T$. This is a direct and accurate method for determining the temperature correspond-

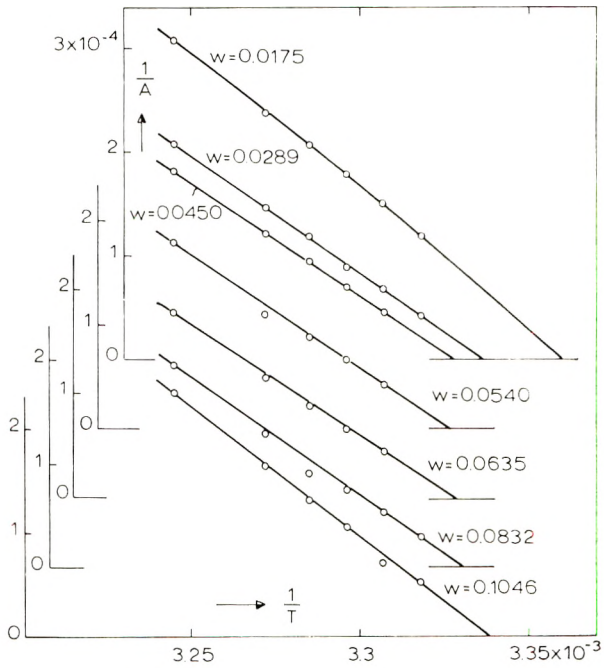

Fig. 10. Extrapolation of 1/A for sample 5a to spinodal temperatures.

ing to the spinodal at a given polymer concentration. It is evident that in the plotting procedure only points in the homogeneous region, i.e., outside the cloud point curve (binodal) can be used.

The spinodal temperature at a given concentration can be determined in a simpler way by plotting $1/(\alpha \Delta I)_{\theta=0}$ versus T and extrapolating to the intercept on the abscissa.

The spinodal temperatures of more complicated systems can be determined in exactly the same way. Plotting these temperatures versus concentration yields, e.g., the spinodal of a mixture of two polydisperse polymers or the spinodal surface of a ternary mixture (polymer + two solvents, two polymers + solvent, three polymers).

Plots

In Figure 8 we have plotted $1/A$ versus $1/T$ for polystyrene solutions (PS 7a) of various concentrations, and have determined the intercepts at $1/A = 0$. In conformity with our assumption that

$$\chi = \chi_{00} + (\chi_{01}/T) + [\chi_{10} + (\chi_{11}/T)]w + \chi_2 \tag{21}$$

the lines are straight, with the exception of those relating to the two lowest concentrations. This demonstrates that in the lowest range of concentrations the above assumption loses its validity (as can also be seen from Figs. 1, 2, and 3).

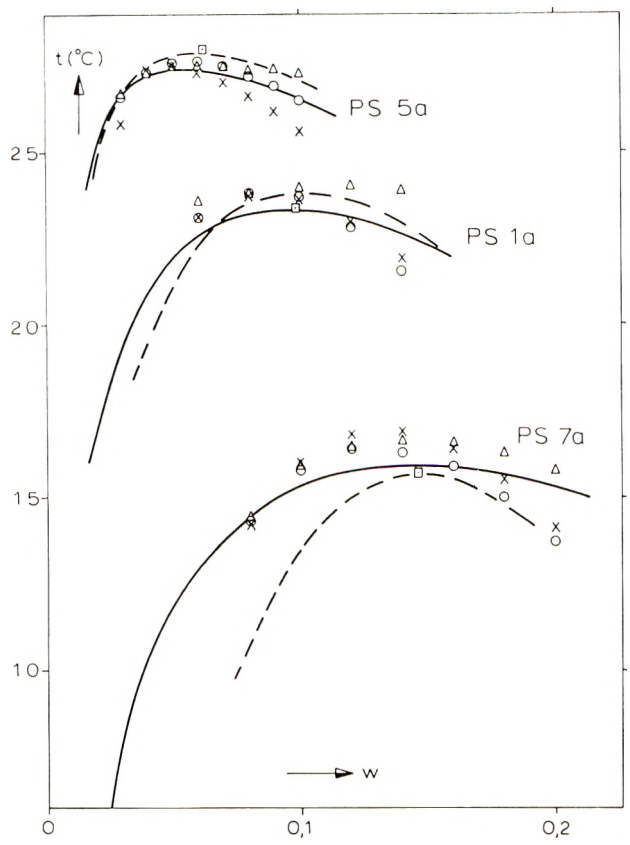

Fig. 11. Spinodals for the three polystyrene samples in cyclohexane: (——) spinodals determined directly (Table IX); (×) spinodals calculated from χ functions of eq. (9) and Table IV; (○) spinodals calculated from χ functions of eqs. (10); (△) spinodals calculated from χ functions of eq. (19) and Table VIII; (— —) spinodals calculated from Koningsveld's χ function;[16] (⊡) critical point, determined by Koningsveld, Kleintjens, and Shultz.[16]

From the intercepts we find the spinodal temperatures as shown in Table IX. The accuracy of these temperatures is a few tenths of a degree. The temperatures for the lowest two concentrations are less accurate, owing partly to the curvature of the lines and partly to the fact that the extrapolation has to be carried out over a larger interval.

Figures 9 and 10 show plots of $1/A$ versus $1/T$ for solutions of the polystyrene samples 1a and 5a. The results for these samples are also given in Table IX.

In Figure 11 we have plotted the spinodals so determined for the three polystyrene samples in cyclohexane. This figure also contains the spinodal values calculated from the χ functions previously determined in this paper, and the spinodal calculated from the function $\chi = 0.3455 + 47.36/T + 0.3136w + 0.3036w^2$ of Koningsveld et al.[16] (derived from g in his Table II).

Direct Determination of the Maximum of the Spinodal

A more direct method for determining the top of the spinodal is by plotting the reciprocal maximum values of A versus temperature (centigrade) t and concentration. The curves so found pass through zero at given values of t and w respectively, i.e., at the temperature and concentration corresponding to the maximum of the spinodal.

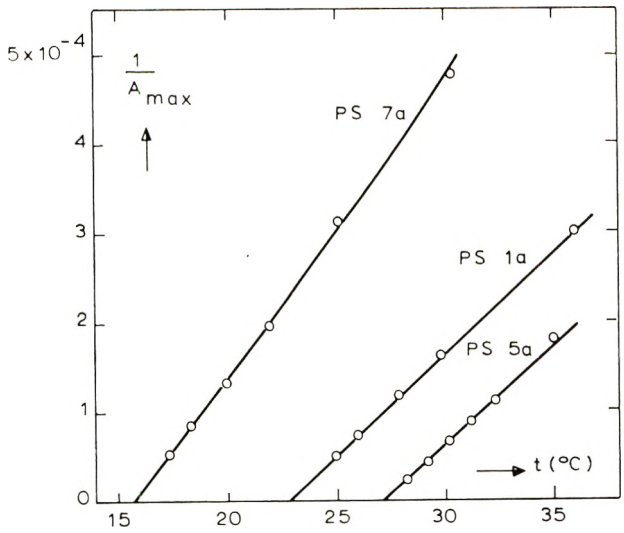

Fig. 12. $1/A_{max}$ vs. temperature for the three polystyrene samples. Extrapolation to the temperature of the maximum of the spinodal.

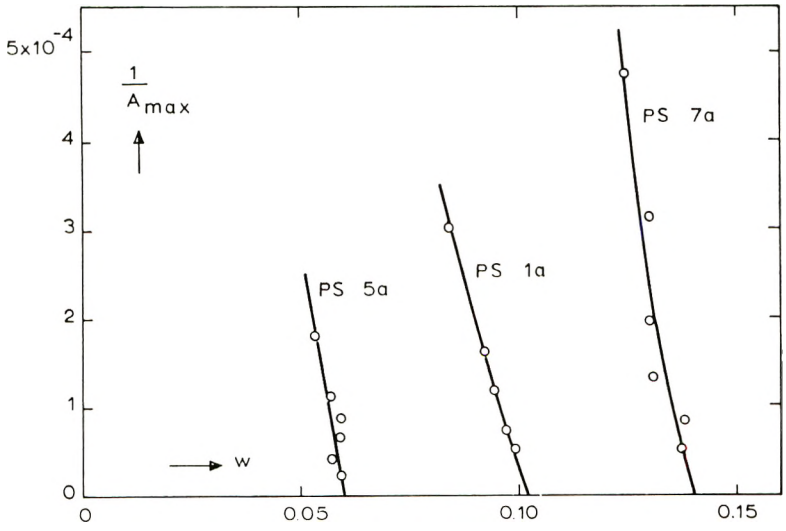

Fig. 13. $1/A_{max}$ vs. concentration for the three polystyrene samples. Extrapolation to the concentration of the maximum of the spinodal.

TABLE X

PS sample	$\bar{M}_w$	$w_{2,\,\max\,sp.}$, g/g	$t_{2,\,\max\,sp.}$, °C
7a	51000	0.149	15.8
1a	163000	0.102	23.0
5a	520000	0.060	27.2

TABLE XI

PS sample	w_{cr}, g/g	t_{cr}, °C
7a	0.146	15.7
1a	0.099	23.4
5a	0.064	28.0

In Figure 12, $1/A_{max}$ for the three samples has been plotted versus t. Figure 13 shows $1/A_{max}$ as a function of w. For the values of w and t, corresponding to the maxima of the spinodals we thus find the values given in Table X.

Simple calculation shows that the critical point in the solutions examined (polystyrenes with very narrow molecular weight distributions in cyclohexane) lies at a temperature less than 0.1°C below $t_{max\,sp.}$ and at a concentration of approximately $^1/_2\%$ above $w_{max\,sp.}$. Our values (Table X) are comparable to the critical points measured on the same polystyrene samples in cyclohexane by Koningsveld *et al.*[16] which are given in Table XI.

COMPARISON OF THE RESULTS WITH LITERATURE DATA

Our values found for the interaction parameter show a marked dependence on the concentration, a moderate dependence on the temperature, and, especially at low concentrations, a slight dependence on the molecular weight.

It is seen that the χ values for polystyrene sample 1a ($\bar{M}_w = 163000$) in cyclohexane, as found from light-scattering measurements and the data obtained from equilibrium ultracentrifugation[12] agree reasonably within experimental error (ca. 0.001) at all temperatures and concentrations at which the measurements were performed. Further, the concentration dependence proves to agree very well with that found by Krigbaum and Geymer[17] and by Koningsveld et al.[16]

In addition, our results extrapolated to zero concentration exhibit the same temperature and molecular weight dependence of the second virial coefficient as has been described in the literature. It is normally found that the absolute value of the second virial coefficient in dilute solutions decreases as the molecular weight of the polymer increases. For athermal solutions, Schulz et al.[18] report a linear dependence of the second virial coefficient A_2 on ln M. Sotobayashi and Ueberreiter[19] arrive at a dependence of the form $A_2 = a/M^{1/2} + b$. Our results can be compared best with the very accurate experimental results of Krigbaum.[20] Interpolation of the A_2

TABLE XII

	$10^5 \times A_2$			χ_0		
T, °K	$\bar{M}_n$ = 49000	$\bar{M}_n$ = 154000	$\bar{M}_n$ = 435000	$\bar{M}_n$ = 49000	$\bar{M}_n$ = 154000	$\bar{M}_n$ = 435000
303	−2.8	−2.2	−1.9	0.5018	0.5014	0.5012
313	6.4	5.8	5.3	0.4957	0.4963	0.4966
323	13.6	11.1	9.7	0.4914	0.4930	0.4939

TABLE XIII

	$\bar{M}_n$ = 49000	$\bar{M}_n$ = 154000	$\bar{M}_n$ = 435000
χ_{01} from Krigbaum's A_2 values	58	48	44
χ_{01} from χ vs. $1/T$	62	52	48
χ_{01} from χ from maxima of A and B	58	49	46

values in Krigbaum's Table I for the samples L5-6, HA-9, M2-2, and H1-4 yields the values given in Table XII.

The values for χ extrapolated to zero concentration (χ_0) obtained by the equation $\chi_0 = {}^1/_2 - M_0\rho_0 A_2$ are also given in Table XII.

From this temperature dependence of χ_0 it follows that χ_0 varies non-linearly with $1/T$ at all molecular weights. Between 303 and 313°K the temperature dependence is clearly greater than in the range 313–323°K, as is also evident from the curvature of the lines in Krigbaum's Figure 4 (A_2 versus T). This is in agreement with the dependence of χ on $1/T$ reported above (Figs. 1, 2, and 3).

Starting from the χ_0 values measured by Krigbaum at 303 and 313°K and putting $\chi_0 = \chi_{00} + \chi_{01}/T$, we see that the χ_{01} values derived for the three samples of different molecular weight, fall in the same range as our values (Table XIII).

The agreement, in particular that between the variations in χ_{01} with the molecular weight, is very good. Krigbaum's theta temperature for polystyrene in completely dry cyclohexane, 307.4°K, also shows good agreement with the value given above.

ANGULAR DISSYMMETRY OF SCATTERED LIGHT INTENSITY

A few years ago Debye[8,21] demonstrated the addition of an extra effect in the vicinity of the critical point. Since concentration gradients call for additional energy, very large concentration gradients are not likely to occur. Since, furthermore, fluctuations in concentration over small regions give rise to steeper gradients than similar fluctuations over larger regions, the former situation will be much less favored than the latter; this accounts for angular dissymmetry of the scattered light intensity.

It follows from Debye's theory, in which he assumes the polymer to be monodisperse, that in the vicinity of the critical temperature the dissym-

metry reaches a maximum at the critical concentration.[8,21,22] Borchard and Rehage,[23,24] however, found that the dissymmetry has its maximum at a much lower concentration, while Koningsveld demonstrated that in Debye's own experiments the maxima actually occur at concentrations lower than the critical one.[25] The explanation may be sought partially in the fact that for polydisperse polymers, it is not the critical concentration but the concentration corresponding to the maximum of the spinodal where the concentration fluctuations are maximal and, consequently, the gradient effect is strongest. Koningsveld and Rehage[26,27] demonstrated that in polydisperse polymer solutions, the maximum of the spinodal may lie at a concentration far below the critical concentration. In addition, nonregularity of the polymer solution may play a role.

In eq. (25′) of ref. 8 extrapolation of the scattered light intensity to zero scattering angle yields $s = 0$. It follows from this that the second term in the denominator of that equation, which represents the influence of the extra energy from the concentration gradients, then becomes equal to zero. This means that because only $\alpha\Delta I$ values extrapolated to zero scattering angle are used, the equations derived in the present article are valid, even in the vicinity of the spinodal; the effects due to the energy of the concentration gradients may then be disregarded.[28]

The author is greatly indebted to Mrs. E. M. L. Nijsten-Colaris for performing the light-scattering measurements and to Mr. N. L. J. Meyerink for determining the refractive index increments. He also thanks Dr. R. Koningsveld for his valuable comments.

References

1. D. J. Coumou and E. L. Mackor, *Trans. Faraday Soc.*, **60**, 1726 (1964).
2. M. Smoluchowski, *Ann. Physik.*, **25**, 205 (1908).
3. A. Einstein, *Ann. Physik.*, **33**, 1275 (1910).
4. H. C. Brinkman and J. J. Hermans, *J. Chem. Phys.*, **17**, 574 (1949).
5. J. G. Kirkwood and R. J. Goldberg, *J. Chem. Phys.*, **18**, 54 (1950).
6. W. H. Stockmayer, *J. Chem. Phys.*, **18**, 58 (1950).
7. Th. G. Scholte, *Europ. Polym. J.*, **6**, 1063 (1970).
8. P. Debye, *J. Chem. Phys.*, **31**, 680 (1959).
9. P. J. Flory, *J. Chem. Phys.*, **10**, 51 (1942).
10. M. L. Huggins, *Ann. N. Y. Acad. Sci.*, **43**, 1 (1942).
11. P. J. Flory, *Principles of Polymer Chemistry*, Cornell Univ. Press, Ithaca, N. Y., 1953.
12. Th. G. Scholte, *J. Polym. Sci. A-2*, **8**, 841 (1970).
13. R. Koningsveld and A. J. Staverman, *J. Polym. Sci. A-2*, **6**, 325 (1968).
14. R. Koningsveld, Advan. *Colloid Interface Sci.*, **2**, 151 (1968).
15. P. Debye and A. M. Bueche, *J. Chem. Phys.*, **18**, 1423 (1950).
16. R. Koningsveld, L. A. Kleintjens, and A. R. Shultz, *J. Polym. Sci. A-2*, **8**, 1261 (1970).
17. W. R. Krigbaum and D. O. Geymer, *J. Amer. Chem. Soc.*, **81**, 1859 (1959).
18. G. V. Schulz, H. Baumann, and R. Darskus, *J. Phys. Chem.*, **70**, 3647 (1966).
19. H. Sotobayashi and K. Ueberreiter, *J. Polym. Sci. A*, **2**, 1257 (1964).
20. W. R. Krigbaum, *J. Amer. Chem. Soc.*, **76**, 3758 (1954).
21. P. Debye, *Makromol. Chem.*, **35A**, 1 (1960).

22. P. Debye, H. Coll, and D. Woerman, *J. Chem. Phys.*, **32**, 939 (1960); *ibid.*, **33**, 1746 (1960).

23. W. Borchard and G. Rehage, paper presented at 6th IUPAC Microsymposium, Prague, 1969.

24. W. Borchard, paper presented at IUPAC International Symposium on Macromolecules, Leiden, 1970.

25. R. Koningsveld, *Discussions Faraday Soc.*, **49**, 144 (1970).

26. R. Koningsveld and A. J. Staverman, *J. Polym. Sci. A-2*, **6**, 349 (1968).

27. G. Rehage and R. Koningsveld, *J. Polym. Sci. B*, **6**, 421 (1968).

28. M. Kerker, *The Scattering of Light and Other Electromagnetic Radiation*. Academic Press, New York–London, 1969, p. 565.

Received October 12, 1970
Revised February 16, 1971

JOURNAL OF POLYMER SCIENCE: PART A-2 VOL. 9, 1579–1590 (1971)

Salt Rejection by Polymer Membranes in Reverse Osmosis. II. Ionic Polymers

H. YASUDA, C. E. LAMAZE, and A. SCHINDLER,
Camille Dreyfus Laboratory, Research Triangle Institute, Research Triangle Park, North Carolina 27709

Synopsis

The water permeability K_1 [which is related to water flux J_1 per unit membrane area by $J_1 = K_1(\Delta p - \Delta\Pi)/\Delta X$, where Δp is the pressure difference, $\Delta\Pi$ is the osmotic pressure of feed solution, and ΔX is the membrane thickness] of homogeneous ionic polymer membranes in reverse osmosis and their salt rejection R_S [which is given by $R_S \equiv 1 - (C_2''/C_2')$, where C_2' is the concentration of the salt in feed solution, and C_2'' is the concentration of salt in effluent] were examined with cationic and anionic membranes of block and graft copolymers. For ionic membranes, R_S and K_1 are related by $K_1 = A \exp\{-BR_S\}$, where A and B are constants. This equation was found to be independent of the ion charge, the chemical nature of the polymer, and film morphology. The principle of salt rejection by ionic membranes was explained by the difference in the transport volumes (volume elements available for transport) for mobile co-ions and water. The electric repulsive force between a fixed ion and a mobile co-ion decreases the transport volume of the latter, thus creating a transport depletion of salt flux relative to water transport. This transport depletion is governed by the amount of water sorbed by a fixed ionic site, which also determines the water flux. Consequently, R_S and K_1 for ionically charged membranes are related as described above. This relation significantly differs from that found between R_S and K_1 for nonionic polymer membranes, where the size and the solubility of ions in the membrane are mainly responsible for the transport depletion. The decline of R_S with increasing K_1 is much less in ionic membranes than in nonionic ones; however, in the high R_S region, K_1 for both ionic and nonionic membranes become similar as the dominant mode of water transport changes from flow to diffusion.

INTRODUCTION

The mode of water transport through water-swollen polymer membranes under a hydraulic pressure gradient, i.e., molecular diffusion or bulk flow, was shown in Part I[1] of this series to have a dominant effect on salt rejection by nonionic membranes. In nonionic polymer membranes, diffusive water flux under a pressure gradient is required for good salt rejection, and a membrane loses its salt rejecting character when water moves through the membrane by bulk flow, as a consequence of excessive swelling (at high water up-take).

From study of water transport in polymer membranes,[2] it became clear, however, that most ionic polymer membranes are "flow membranes" as defined in Part I, in which water transport occurs by bulk flow. Conse-

quently the solution-diffusion mechanism does not explain the salt rejection observed with most ionic membranes. The mechanism of solution-diffusion may play a role only in very tight ionic membranes which can be classified as diffusion membranes despite their ionic character.

It is quite obvious that interaction of fixed charges and mobile co-ions of salts, often referred to as Donnan exclusion, is largely responsible for the salt rejection of ionically charged polymer membranes.[3] However, the direct application of Donnan equilibrium to reverse osmosis encounters inherent difficulties and ambiguities of analysis. (1) An equilibrium between a two-component system (the solution phase) and a three-component system (the membrane phase) should be considered. Therefore, a rigorous treatment can be done only with activity coefficients based on molal concentration, particularly for membranes that have high polymer concentration. (2) The transport behavior of membranes (particularly water flux), however, is described by characteristic parameters per unit volume of the membrane. In other words, the transport property of membranes should be expressed in terms of molar concentration that can be considered nearly equal to molal concentration only in a dilute solution of two component systems. (3) A membrane under actual reverse osmosis condition is subjected to gradients of both pressure and concentration. Consequently, the activity coefficients involved in the Donnan equilibrium under the actual condition of reverse osmosis cannot explicitly be determined. It is therefore, necessary to use reverse osmosis data to explain the change of activity coefficients rather than attempt to explain the reverse osmosis data by the changes in activity coefficients.

With the approximation used in Part I of this series, the water permeability in reverse osmosis K_1 is given by

$$J_1 = K_1(\Delta p - \Delta\Pi)/\Delta X$$

where J_1 is the water flux per unit area of membranes, Δp is the pressure difference across the membrane, $\Delta\Pi$ is the osmotic pressure of the feed solution, and ΔX is the thickness of the membrane. The salt rejection R_S of a membrane in reverse osmosis is given by

$$R_S \equiv 1 - (C_2''/C_2')$$

where C_2' is the molar concentration of the salt in the feed solution and C_2'' is the molar concentration of salt in the effluent.

During the evaluation of block-copolymer polyelectrolyte membranes under reverse-osmosis conditions, a general relation between K_1 and R_S was found to exist in the range $0.1 < R_S < 0.9$

$$K_1 = A \exp\{-BR_S\} \tag{1}$$

where A and B are constants. Such a relation would be of great interest if it were of general validity irrespective of kind or structure of ionic membranes. The reverse osmosis experiments were, therefore, extended to include several other kinds of ionic membranes derived from polyethylene

(PE) by grafting with sodium polystyrene sulfonate (SPSS), quaternized poly-4-vinyl-pyridine (4VP), or sodium polyacrylate (SPA).

The dependence of R_S and K_1 for ionic membranes given by eq. (1) is considerably different from that for nonionic polymer membranes. This relation suggests that general but relatively simple parameters may exist which correlate K_1 and R_S, and that the salt rejection may be dealt with in a manner considerably simpler than the treatment based on Donnan equilibrium which does not yield a simple relationship. An attempt was made to explain the general trend represented by eq. (1) by the consideration of transport volumes (volume available for transport in the membrane) for water and for mobile ions.

EXPERIMENTAL

Membranes

Membranes used in this study were block and graft copolymers of combinations of ionic and hydrophobic units. Block copolymers consisted of styrene and 2-vinylpyridine units in various block sequences PS–PVP, PS–PVP–PS and $(PS–PVP)_n$ obtained by anionic polymerization. Membranes were cast from solutions, and the 2-vinyl-pyridine units were quaternized with methyl bromide or converted to salt with acid to form charged polymers. Graft copolymer membranes consisted of polyethylene (as the backbone chain) with grafted polystyrene, poly-4-vinylpyridine, or poly-

TABLE I
Block Copolymer Membranes

Membrane number	Polymer type	Polymer composition (before quaternization)	Casting solvent	Quaternization agent
		Styrene–2-vinylpyridine block copolymers		
1	VP–S–VP	1:2:1	THF	1,5-Dibromopentane
2	"	"	"	1,5-Dibromopentane
3	"	"	"	HCl
4	$(S-VP)_n$	1:1	"	Methyl bromide
5	"	"	"	1,5-Dibromopentane + HCl
6	"	"	"	Phosphoric acid
7	"	"	"	Methyl bromide
8	"	"	Benzene	Methyl bromide
9	"	0.4:1	THF	Methyl bromide
10	"	1.7:1	"	Methyl bromide
11	"	"	Benzene	Methyl bromide
12	"	3.8:1	THF	Methyl bromide
13	"	"	Benzene	Methyl bromide
		Styrene–4-vinylpyridine block copolymer		
14	S–VP	1:1	THF	HCl

TABLE II
Grafted Polyethylene Membranes

Membrane number	Grafted polymer	Grafting yield, g/g[a]	Ionization of grafted polymer
		Polyethylene–4-vinylpyridine	
15	4-vinylpyridine	1.82	Quaternized by H_2SO_4
16	4-vinylpyridine	1.82	Quaternized by MeBr
17	4-vinylpyridine	1.86	Quaternized by H_2SO_4
18	4-vinylpyridine	0.963	Quaternized by MeBr
19	4-vinylpyridine	1.35	Quaternized by H_2SO_4
20	4-vinylpyridine	1.55	Quaternized by MeBr
		Polyethylene–styrene	
21	Styrene	0.285	Sulfonation and Na salt formation
22	Styrene	0.371	Sulfonation and Na salt formation
23	Styrene	0.761	Sulfonation and Na salt formation
24	Styrene	0.344	Sulfonation and Na salt formation
25	Styrene	0.588	Sulfonation and Na salt formation
26	Styrene	0.494	Sulfonation and Na salt formation
27	Styrene	0.149	Sulfonation and Na salt formation
28	Styrene	0.134	Sulfonation and Na salt formation
29	Styrene	0.207	Sulfonation and Na salt formation
30	Styrene	0.245	Sulfonation and Na salt formation
31	Styrene	0.673	Sulfonation and Na salt formation

[a] Grafting yield: weight of vinyl polymer/weight of polyethylene.

TABLE III
Polyethylene Membranes Grafted with Acrylic Acid Polymer

Membrane number	Grafting method	Dose, Mrad	Reaction time or dose rate	Temp, °C	Salt formation
32	Peroxide	3	AA/EtOH 90 min	74	2% NaOH
33	Mutual[a]	1.0	0.01 Mrad/hr	Room temp	2% NaOH
34	Mutual[a]	2.0	"	Room temp	2% NaOH
35	Mutual[a]	3.4	"	Room temp	2% NaOH
36	Mutual[a]	4.3	"	Room temp	2% NaOH
37	Mutual[a]		"	Room temp	2% NaOH

[a] Mutual irradiation was carried out in a mixture of saturated $CuCl_2$ and the monomer in the ratio 1:1. Since grafting yield and hydration do not characterize the grafted membrane owing to the inhomogeneous nature of grafting, no grafting yields or hydrations were measured with these membranes. K_1 and R_S obtained in reverse osmosis were used to check the relation given by eq. (1).

(acrylic acid) side chains. The samples were sulfonated, quaternized, or treated with base to form the corresponding polyethylene–polyelectrolyte graft copolymers. Details of preparation and morphological properties of these membranes will be presented elsewhere but characteristic data to identify the membranes are given in Tables I, II, and III.

Reverse Osmosis Test

Measurements of salt rejection and water flux were carried out under the conditions described in Part I; i.e., 3.5% NaCl feed, 1500 psi applied pressure at 25°C. To determine the effect of the feed concentration, the salinity of the feed was reduced by adding deionized water and the applied pressure was reduced to maintain the effective pressure (total pressure less osmotic pressure) constant at 74.9 atm.

RESULTS AND DISCUSSION

Block copolymers composed of a hydrophobic polymer with a relatively high glass transition temperature, and a polymer that can be transformed easily into a polyelectrolyte are very useful as membrane materials for the study of the behavior of ionic membranes in reverse osmosis. The great advantage this kind of membrane has over other ionic membrane is facility and reproducibility of film formation. During film formation from solution, phase separation takes place, and the domains of the hydrophobic component provide the necessary crosslinks. Crosslink density and size of the polyelectrolyte domains can be easily varied by changing the block length ratio.

For all these ionic membranes, salt rejection and water flux are summarized in Table IV. The graphic representation of these data in Figure 1 strongly supports a generalization of eq. (1) for all kinds of ionic membranes. The scattering of data may be caused partly by the uncertainty of thickness measurements. Although membrane thicknesses were always measured immediately at the end of a reverse osmosis experiment, these values still might not correspond to the effective values during the experiment. Furthermore, very slight leakage will considerably decrease the salt rejection without affecting the permeability. Accordingly, experimental deviations from eq. (1) should mainly occur toward lower R_S values. Indeed, Figure 1 seems to indicate such a situation, the line representing a limit for the most perfect membranes.

The decrease of R_S with increase in K_1 is much less pronounced than for nonionic membranes where R_S decreases abruptly as K_1 exceeds a limiting value. With respect to the water transport, highly hydrated membranes belong to the flow type in which salt flux and water flux are strongly coupled. Consequently, only very low salt rejection is expected in highly hydrated nonionic membranes. In ionic membranes, salt rejection and water flux can be correlated best by an approach in which different transport volumes are assigned for salt and water.

The water up-take in the ionic domains will be governed by the number of fixed ions and by the film morphology since swelling will proceed until the swelling pressure equals the stress generated in the hydrophobic matrix. Because of Coulombic repulsion, the fixed ions on the polyelectrolyte will arrange into a diffuse ionic lattice without long-range order. Salt and water transport will proceed through this ionic lattice. For water transport the

TABLE IV
Salt Rejection and Water Flux of Ionic Polymer Membranes
(3.5% NaCl, 1500 psi, 25°C)[a]

Cationic polymers			Anionic polymers		
Membrane no.	R_S	$K_1 \times 10^{10}$, cm²/sec-atm	Membrane no.	R_S	$K_1 \times 10^{10}$, cm²/sec-atm
Block copolymer (St–2VP)			Graft copolymer (PE–SPSS)		
1	0.75	5.6	21	0.79	12
2	0.83	6.4	22	0.70	13
3	0.27	370	23	0.55	70
4	0.45	74	24	0.78	10
5	0.53	74	25	0.60	72
6	0.50	99	26	0.70	18
7	0.51	86	27	0.82	5.0
8	0.45	85	28	0.80	6.7
9	0.05	4300	29	0.50	43
10	0.70	16	30	0.54	40
11	0.63	34	31	0.30	146
12	0.42	140	Graft Copolymer (PE–SPA)		
13	0.39	260	32	0.60	19
14	0.72	14	33	0.68	6.6
Graft copolymer (PE–4VP)			34	0.67	5.1
15	0.68	2.1	35	0.70	6.8
16	0.38	160	36	0.60	7.5
17	0.85	3.2	37	0.65	8.6
18	0.38	130			
19	0.90	2.2			
20	0.47	83			

[a] 4VP, 4-vinylpyridine; SPSS, sodium polystyrene sulfonate; SPA, sodium polyacrylate.

total volume of the hydration water may be available, whereas for the salt transport the available water volume will be smaller because Coulombic repulsion between the fixed ions on the polymer and the co-ions of the salt will restrict their mutual approach to a minimum distance. Outside this salt-excluding water shell surrounding each fixed ion, the salt solution will invade the membrane at feed concentration.

For the mathematical description of this model the following volumes have to be defined, all referring to one fixed ionic site: V_0 the total volume of the hydrated membrane per ionic site; V_1 the volume impermeable to water; and V_2 the volume impermeable to salt.

If we assume that the volume $(V_2 - V_1)$ will allow transport of pure water, that $(V_0 - V_2)$ will allow transport of unmodified feed solution, and that the rates of volume flow in both elements are identical, the total water flux can be represented by

$$J_1 = \Phi_1 + \Phi_2 \tag{2}$$

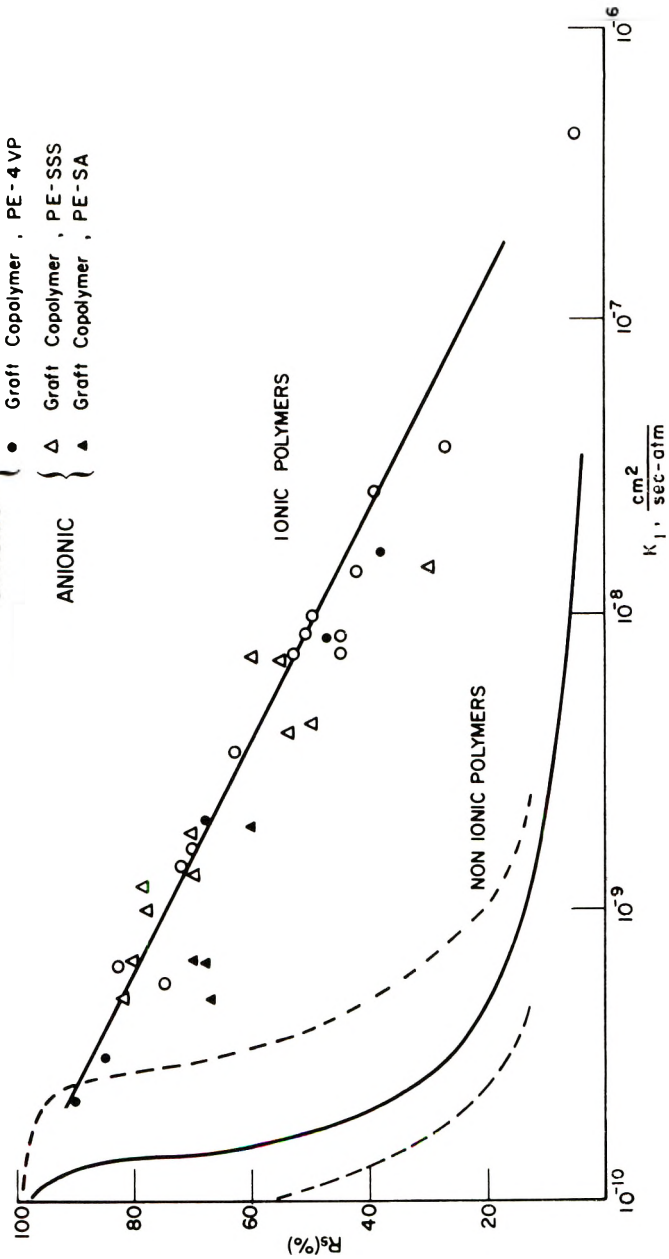

Fig. 1. Dependence of the salt rejection R_s on the water permeability K_1 for ionic membranes.

where

$$\Phi_1 = [(V_2 - V_1)/(V_0 - V_1)]J_1 \quad (3)$$

$$\Phi_2 = [(V_0 - V_2)/(V_0 - V_1)]J_1 \quad (4)$$

The salt flux, J_2 is then given by

$$J_2 = \Phi_2 C_2' \quad (5)$$

where C_2' is the feed concentration of the salt.

In the notation used in Part I, the effluent concentration C_2'' is given by

$$C_2'' = J_2/J_1 \quad (6)$$

and salt rejection R_S is given by

$$R_S = 1 - (J_2/J_1C_2') \quad (7)$$

Consequently, in this situation, R_S is related to V_0, V_1, and V_2, as

$$R_S = (V_2 - V_1)/(V_0 - V_1) \quad (8)$$

The fixed-ion concentration C^*, in moles/kg water, is given by

$$C^* = 1/[(V_0 - V_1)N] \quad (9)$$

where N is Avogadro's number.

Equations (8) and (9) lead to the shell volume

$$V_2 - V_1 = 10^{27}R_S/C^*N \quad (10)$$

The difference in impermeable volumes $(V_2 - V_1)$ corresponds to the volume of the salt-excluding water shell surrounding each fixed ionic site. Because the shell thickness represents the minimum approach distance of two similarly charged ions, the shell volume has to be constant irrespective of the kind or the concentration of the fixed ions in the membrane, though it might depend somewhat on the feed concentration as will be discussed later. Table V lists $V_2 - V_1$ values for several polyvinylpyridine block copolymer membranes quaternized with methyl bromide, where C^* was determined by conductometric titration with silver nitrate. It can be seen that the shell volumes are fairly constant. In the last column of Table V the radii of equivalent spheres of volume $V_2 - V_1$ correspond closely to the minimum approach distance between a fixed ion of the polymer and the co-ion of the salt. In this case both ions are assumed to be dimensionless point charges.

Since $(V_2 - V_1)$ is reasonably constant, eq. (10) suggests that the salt rejection of ionic membranes is directly proportional to the fixed-ion concentration C^*. This relation was substantiated by measurements of C^* in membranes, as is shown in Figure 2. Equation (8) can be expressed in terms of the volume fraction $H = (V_0 - V_1)/V_0$ of water in the swollen membrane:

$$R_S = [(V_2 - V_1)/V_1][(1 - H)/H] \quad (11)$$

TABLE V
Volume of Salt-Excluding Water Shells $V_2 - V_1$ and Radius r of Equivalent Sphere of Volume $V_2 - V_1$[a]

Membrane number	Salt rejection	Fixed ion concentration, mole/kg water	$V_2 - V_1$, Å^3	r, Å
10	0.70	2.73	426	4.7
11	0.63	2.81	372	4.5
7	0.51	2.25	376	4.5
4	0.45	1.90	394	4.5
12	0.42	1.35	515	5.0
13	0.39	1.07	605	5.2
13	0.33	1.44	381	4.5
9	0.05	0.35	238	3.8

[a] Feed concentration, 3.5%; applied pressure, 1500 psi.

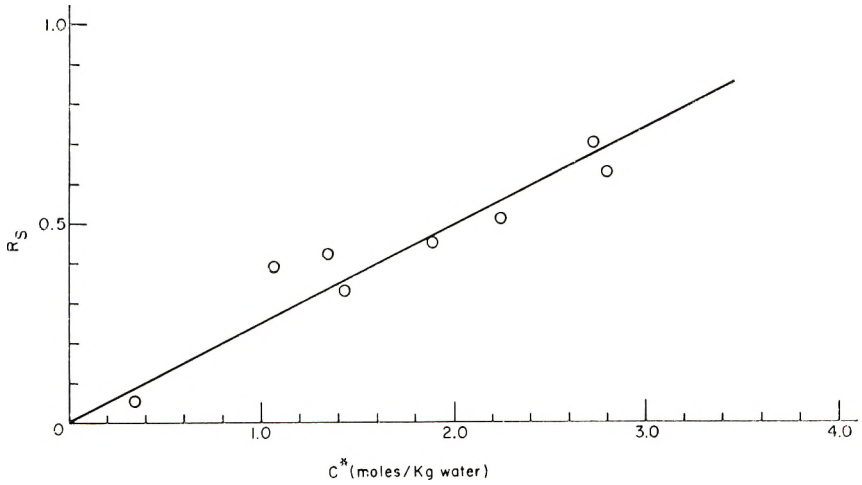

Fig. 2. Relationship between the salt rejection R_S and the fixed ion concentration C^* of the polystyrene–poly(2-vinylpyridine methyl bromide) block copolymer membranes.

The value of V_1 in strict sense is closely related to the molecular volume of the repeating unit of the polymer. However, the water uptake in the actual ionic polymer membrane is governed not only by the number of fixed ions but also by the film morphology and/or molecular crosslinks. The ideal situation in which V_1 is close to the molecular volume of the repeating unit may be obtainable only in polymer solution of ionic polymers which are polymerized from ionic monomers.

The introduction of ionic sites by chemical reaction of polymers hardly proceeds to 100%, and V_1 is the average of ionized and nonionized repeating units. The repeating units near the crosslinks may have higher V_1 than the rest of repeating units. Therefore, V_1 in realistic membranes may not be directly proportional to the molecular volume of the repeating unit.

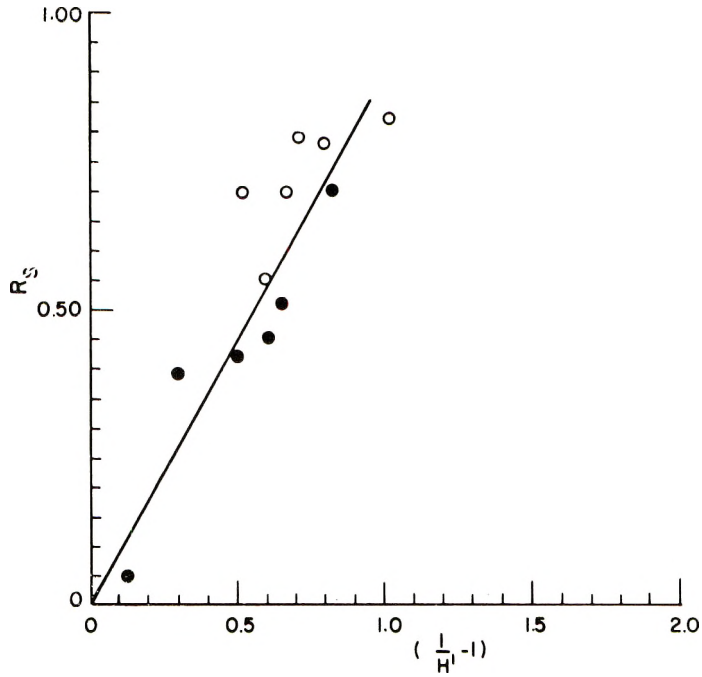

Fig. 3. Relationship between the salt rejection R_S and the parameter $(1/H') - 1$ for ionic polymer membranes: (○) graft copolymer (PE–SSS), anionic; (●) block copolymer (ST–2VP), cationic. H' is the volume fraction of water in hydrophilic domain of membranes.

Under these conditions, it may be assumed in first approximation, that V_1 does not vary much in practical ionic membranes. If we can assume that $(V_2 - V_1)/V_1$ is a constant, a direct proportionality between R_S and $(1 - H)/H$ is suggested by eq. (10). This relation is examined in Figure 3 for membranes of block copolymer and graft copolymer. In Figure 3, H' is used to represent the water content of hydrophilic domains since these membranes contain a considerable portion of impermeable hydrophobic domains. This correction may cause some scattering of points, particularly for graft-copolymer membranes in which some portion of hydrophilic domains may not be contributing to the overall transport property of the membrane. Nevertheless, Figure 3 shows that the relations given by eq. (11) with approximation of $(V_2 - V_1)/V_1$ being a constant are indeed found in ionic membranes.

The hydraulic permeability constant of water for highly hydrated membranes can be approximated by an expression of the form[2]

$$K_1 = K_0 \exp\left\{-B'(1 - H)/H\right\} \tag{12}$$

where K_0 and B' are constants (see Fig. 4). It should be noted that eq. (12) is empirical and only approximate for a certain range of small values of $(1 - H)/H$, though most ionic polymer membranes fall in this region.

TABLE VI
Calculated Radius r of Equivalent Impermeable Sphere

Feed concentration C_2', mole/kg water	r, Å		
	Membrane 8	Membrane 10	Membrane 13
0.616	4.5	4.7	5.2
0.320	4.8	5.0	5.5
0.188	5.1	5.0	5.8
0.099	5.3	5.1	6.2
0.045	5.4	5.2	—

With the assumption of a constant $(V_2 - V_1)/V_1$, eqs. (11) and (12) can be combined to give eq. (1). This relation has an important practical value in characterizing reverse osmosis performance of ionic membranes, since K_1 and R_S are ordinarily the only parameters observable in reverse osmosis. As was stated above, V_1 in a strict sense is not a universal constant and should vary with different polymers. However, this variation in V_1 does not alter the dependence of R_S on log K_1 and will be reflected in the slope of a plot of R_S versus log K_1. Therefore, if we allow a certain range in values of R_S and log K_1, R_S and K_1 for most ionic membranes can generally be represented by eq. (1).

In general, for a given membrane, the salt rejection increases with decreasing feed concentration. This increase demands an increase in the salt-excluding shell volume $(V_2 - V_1)$, provided that C^* can be assumed to remain constant. The measurement of C^* was done with membranes equilibrated with pure water and the values were assumed to remain unaffected by changing feed concentration. However, for more rigorous treatment, the effect of feed concentration and pressure on the membrane hydration had to be considered.

Such an increase in the shell volume becomes reasonable if one considers that the closest average approach distance of two ions of similar charge is determined by the concentration of all ions present. The calculated equivalent radii of the salt-rejecting shell are shown in Table VI. The results indicate a general increase of r with decrease of feed concentration.

It is worth noting that reverse osmosis data[4-6] reported by many investigators for various charged membranes fit the general trend shown in Figure 1 and also that the time-dependent changes observed with some membranes also follow the general quantitative relation, i.e., the increase of flux with decrease of salt rejection and vice-versa. This behavior may reflect changes in membranes under the conditions of testing. Namely, membranes may swell or contract in the salt solution under higher pressure; however, this change will be reflected in H, and consequently in C^*, in such a way that all the relations given by eqs. (10), (11), and (12), are followed; hence the results observed as R_S and K_1 are expected to follow the general relations described by eq. (1).

As was shown in Part I dealing with nonionic polymers, the present work demonstrates salt rejection can be treated as a consequence of transport depletion of salt relative to the water flux rather than as the result of blocking of salt transport. The transport depletion can be explained by consideration of volumes available for transport of water and salt in homogeneous polymer membranes in the membrane phase of both ionic and nonionic polymers. It is worth noting that throughout this analysis the derivations are based on one model of membrane, i.e., the homogeneous polymer membrane as described in the literature,[1,7] and it is only necessary to characterize the movement of water (solvent) in the membrane to explain the phenomena observed with different types of membranes. It is also interesting to note that the relation shown in Figure 1 for ionic polymer membranes converges to the same point as nonionic membranes when R_S increases, or K_1 decreases, indicating that very high salt rejection by ionic polymer membranes no longer can be attributed to rejection by an ionic mechanism. As the water permeability approaches the diffusion region, salt rejection by tight ionic membranes may be best explained by a solution-diffusion mechanism, in which the partition coefficient may be explained by the Donnan equilibrium.

It may be concluded that the salt transport depletion relative to water transport is caused by the difference in characteristic volume or size of hydrated ions and water molecules. In nonionic membranes, it depends on the size of hydrated solute molecules and water. In ionic membranes, the impenetrable ionic field (for similarly charged ions) overrides the effects of the size of hydrated ions. In both cases, salt rejection and water flux seem to be best understood by the concept of "transport volume" described in this paper.

This study was supported by the U. S. Department of Interior, Office of Saline Water, Contract No. 14-01-0001-1785. The authors' special thanks are due Dr. Anton Peterlin, Director, Camille Dreyfus Laboratory, Research Triangle Institute, for stimulating discussion and creative criticism.

References

1. H. Yasuda and C. E. Lamaze, *J. Polym. Sci. A-2*, **9**, 1537 (1971).
2. H. Yasuda, C. E. Lamaze, and A. Peterlin, *J. Polym. Sci. A-2*, **9**, 1117 (1971).
3. J. S. Johnson, Jr., L. Dresner, and K. S. Kraus, in *Principles of Desalination*, K. S. Spiegler, Ed., Academic Press, New York, 1966.
4. A. S. Hoffman and M. Modell, *Saline Water Conversion Report 1968*, U. S. Department of Interior, Office of Saline Water, 1968, p. 128.
5. E. T. Bishop, G. Lopatin, and W. P. O'Neill, *Saline Water Conversion Report 1969–1970*, U. S. Department of Interior, Office of Saline Water, 1970, p. 6.
6. V. Stannett, private communication.
7. H. Yasuda, A. Peterlin, C. K. Colton, K. A. Smith, and E. W. Merrill, *Makromol. Chem.*, **126**, 177 (1969).

Received October 12, 1970
Revised February 17, 1971

JOURNAL OF POLYMER SCIENCE: PART A-2 VOL. 9, 1591–1601 (1971)

Characterization of Moisture-Cured Polyurethane Films

A. M. HASSAN and L. N. RAY, JR.,
Research and Development Center, Armstrong Cork Center, Lancaster, Pennsylvania 17604

Synopsis

A series of polyurethanes (PU) prepolymers with NCO/OH ratios of 2.1:1 and 1.9:1 were prepared by reacting hydrogenated methylene di-*p*-phenyl diisocyanate (HMDI) with triol mixtures of TP740 (molecular weight 740) and TP1540 (molecular weight 1540). Stress–strain (S/S) and swelling equilibrium measurements were performed using thin-film samples prepared by moisture-curing the prepolymer at room temperature. The swollen PU networks gave an S/S curve which is fully described by rubber elasticity theory. The Mooney-Rivlin constant C_1 (swollen) was found to increase directly while the molecular weight between crosslinks M_c decreases as the number of branches per cubic centimeter is increased. The solvent–polymer interaction parameter χ determined in benzene was $0.077 + 0.97v_r$, where v_r is the volume fraction of rubber in the swollen network. The crosslink density ν', and M_c were calculated from the relations $\nu' = \rho NB$ and $M_c = 0.667\,B^{-1}$, where B denotes moles of branches per gram, and were found to be in good agreement with ν' and M_c established from S/S and swelling-equilibrium measurements. In calculating ν' and M_c, the water–PU crosslinking reaction at room temperature was assumed to occur mainly through the formation of a urea linkage.

INTRODUCTION

Stress–strain measurements and rubber elasticity theory have been used to characterize polyurethane elastomers.[1–5] This type of measurement, however, has not been applied to the characterization of polyurethane networks in thin films because: (1) it is difficult to make the measurement on a thin film and, (2) more significantly, at room temperature, polyurethane films are not in the rubbery state (i.e., T_g is higher than 25°C) and hence rubber elasticity theory cannot be applied in the characteristization.[6] When sufficiently swollen in a solvent, however, these polyurethane networks behave much as crosslinked rubbers, and the study of stress–strain and swelling-equilibrium behavior can be used to establish the crosslink density and the average molecular weights between crosslinks M_c. In this investigation we examined the S/S and the swelling equilibrium behavior of a series of polyurethane thin films with widely differing chemical compositions. The results, which are discussed in terms of rubbery elasticity and swelling-equilibrium theories, are used to establish the effect of PU composition on network structure.

EXPERIMENTAL

Samples

The various samples examined and their compositions are shown in Table I. The polyurethane prepolymers were prepared at 70°C as 40% solids in xylene by reacting hydrogenated methylene di-*p*-phenyl diisocyanate (HMDI) (Allied Chemical Co.) with mixtures of polyether-based triols in the presence of 0.1% dibutyltin dilaurate. The NCO:OH ratio was kept at 2.1:1 for series A, and 1.9:1 for series B. The triol mixtures were made by mixing triol TP740 (molecular weight 740) and triol TP1540 (molecular weight 1540) at the molor ratios shown in Table I. Both triols are commercial (Wyandotte Chemical Co.) poly(propylene oxide) adducts of trimethylolpropane. After addition of 1% dibutyltin dilaurate (based on solids weight) to the prepolymer solution, polyurethane films were solvent-cast on glass plates with an 8-mil Bird applicator. The films were left to moisture-cure at room temperature for several weeks. It was assumed that they were completely cured after this time interval after which the tests were made. All samples examined were selected from films of uniform thickness in which no imperfection due to air or gas foaming was observed.

TABLE I
Compositions of Moisture-Cured Polyurethane Networks

	Sample	HMDI, %	NCO:OH ratio	Polyol mixture TP740:TP1540, molar ratio
Series A				
	1	34.9	2.1:1	0:100
	2	42.0	2.1:1	50:50
	3	43.8	2.1:1	60:40
	4	45.7	2.1:1	70:30
	5	49.9	2.1:1	90:10
	6	52.7	2.1:1	100:0
Series B				
	7	32.7	1.9:1	0:100
	8	39.6	1.9:1	50:50
	9	41.3	1.9:1	60:40
	10	43.2	1.9:1	70:30

Method

Stress–strain (S/S) and swelling-equilibrium measurements were made on the samples by the procedures described in an earlier paper.[7] Special clamps were made to keep the film sample from slipping during S/S measurements. A standard die (0.635 × 7.62 cm) was used to cut the samples. Densities were determined in a density-gradient column. The cross-sectional area A_0 was determined from the weight of the sample W through the relation $A_0 = W/\rho L$, in which ρ is the sample density and L is the length.

RESULTS AND DISCUSSION

Stress/Strain Data on Dry (Unswollen) Polyurethane Films

Typical stress/strain results obtained from unswollen samples are shown in Figures 1 and 2. Polyurethane samples 1, 2, 3, and 4 with 70% or less of the triol in the form of TP740 and containing less than 45% HMDI give a rubberlike stress–strain curve with a barely noticeable yield point. The yield point becomes more distinct as the amount of HMDI in the formula is increased and as the ratio of TP740 to the total triol in the formula is increased beyond 70%. Sample 6 prepared with TP740 as the only triol has a distinct yield point and an S/S curve characteristic of cold-drawn polymeric materials. The stress at an elongation ratio α of 1.5 also increases as the proportion of TP740 in the formula is increased, as is shown in Figure 1. These conclusions are also true for series B, for which stress–strain curves are shown in Figure 2. In this study, an increase in TP740 involves a concomitant increase in the percentage of HMDI in the formula (see Table I). The observed increases in the modulus and in the ultimate strength of the samples are due to the increase in the HMDI which is the "hard" segment in the polymer, and to the increase in the TP740:TP1540

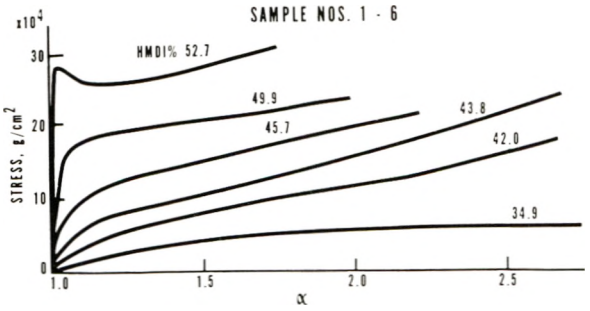

Fig. 1. Stress vs. extension ratio α in dry (unswollen) polyurethane (series A) films, NCO:OH = 2.1:1.

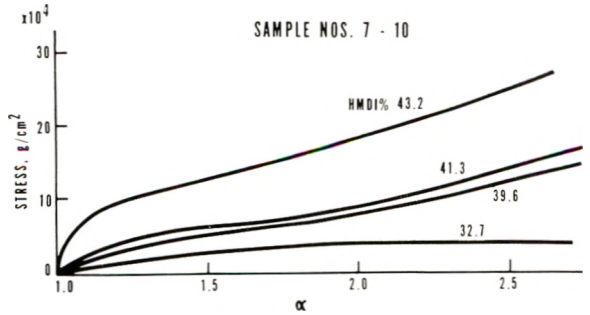

Fig. 2. Stress vs. extension ratio in dry (unswollen) polyurethane (series B) films, NCO:OH = 1.9:1.

ratio in the formula, which as shown later, leads to an increase in crosslink density. The S/S measurements in the dry state cannot distinguish between the two effects. If sufficient molecular motion is introduced in the network chains through swelling, making the polyurethane film a truly crosslinked rubber network, then, according to rubber elasticity theory, the S/S curve of such networks is determined only by their degree of crosslinking.

Network Characterization from S/S of Swolen Networks

A typical S/S curve for a PU thin film swollen in benzene, sample 6, is shown in Figure 3 together with the S/S curve for the dry unswollen sample. Swelling reduced considerably the strength of the sample by destroying most, if not all of the physical bonds (van der Waals and hydrogen

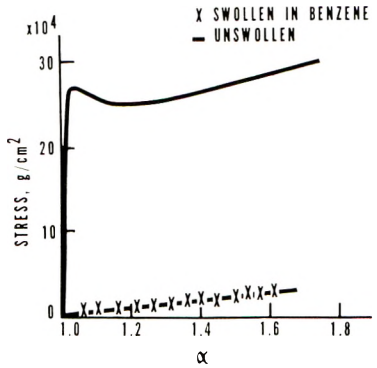

Fig. 3. Stress vs. extension ratio in dry and swollen polyurethane (sample 6).

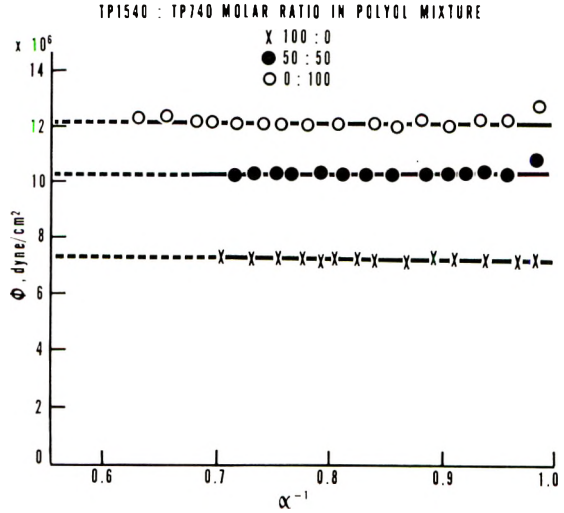

Fig. 4. Plots of ϕ vs. α^{-1} for polyurethane thin films swollen in benzene.

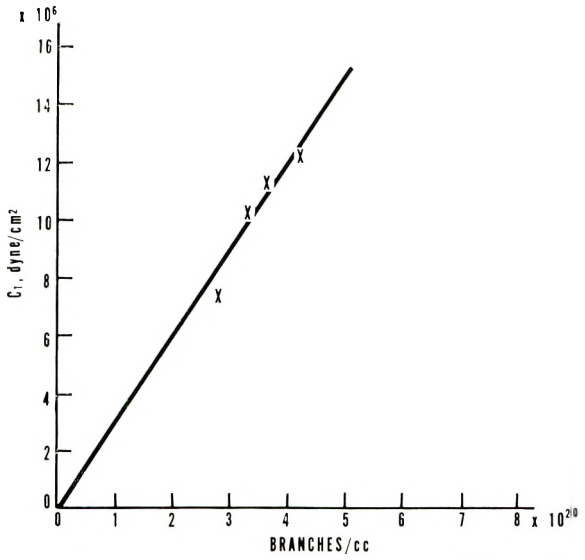

Fig. 5. Plot of C_1 vs. branches/cc in polyurethane (series A).

bonds). The difference in areas under the two curves is probably related to a great extent to these physical interactions. The S/S behavior of the swollen sample is typical of that of a rubbery polymeric network. It is possible to use such S/S results in conjunction with rubber elasticity theory to characterize the swollen PU films.

According to the Mooney-Rivlin equation,[8,9]

$$\phi \equiv (f/2A_0)v_r^{1/3}(\alpha - \alpha^{-2})^{-1} = C_1 + C_2\alpha^{-1} \tag{1}$$

a plot of ϕ versus α^{-1} should give a straight line, as Figure 4 shows for the present series, with an intercept

$$C_1 = {}^1/_2\nu kT = {}^1/_2\rho RTM_c^{-1} \tag{2}$$

and a slope of C_2. In the above equations, f is the force, A_0 is the cross-sectional area of the sample, v_r is the volume fraction of rubber in the swollen sample, ν is the number of chains between crosslinks per unit volume (cubic centimeter), M_c is the average molecular weight between crosslinks, ρ is the density, and k and R are the Boltzmann and gas constants, respectively. As can be seen in Figure 4, the slope C_2 is zero; therefore, the polyurethane networks resemble other swollen elastomer networks in behavior.[10]

Values of C_1 for swollen polymers obtained by this method are shown in Table II and plotted versus concentration of branches in Figure 5 for the various polyurethanes examined. As is expected, C_1 increases linearly when the concentration of branches, which is controlled by the TP740:TP1540 ratio, is increased in the formula. The number of branches per cubic centimeter is $(m_1 + m_2)N\rho$, where N is Avogadro's number, m_1 and m_2 are moles of TP740 and TP1540, respectively, per gram. The triol branch point

TABLE II
Effect of Polyurethane Composition on χ, v_r, C_1, ν, and M_c

Sample	NCO/OH ratio	TP740:-TP1540, molar ratio	v_r	χ[a] From v_r	χ[a] From w_f	C_1, dynes/cm² × 10^{-6}	Branches/cc × 10^{-20}	$\nu \times 10^{-20}$, chains/cc[b]	M_c
1	2.1	0:100	0.441	0.512	0.523	7.78	2.77	3.78	1730
2	2.1	50:50	0.507	0.570	0.583	9.45	3.32	4.59	1430
3	2.1	60:40	0.521	0.581	0.598	9.85	3.47	4.79	1370
4	2.1	70:00	0.571	0.634	0.614	11.60	3.62	5.66	1160
6	2.1	100:0	0.618	0.694	0.672	13.1	4.18	6.37	1030
7	1.9	0:100	0.415	0.480	0.505	7.21	2.86	3.50	1870
8	1.9	50:50	0.525	0.587	0.563	10.05	3.47	4.88	1350
9	1.9	60:40	0.530	0.591	0.577	10.18	3.62	4.95	1330
10	1.9	70:30	0.547	0.608	0.593	10.75	3.79	5.22	1260

[a] Determined from $\chi = .077 + 0.97v_r$ and $\chi = 0.23 + 84w_f$.
[b] Determined from C_1 (swollen) $= 0.5\nu kt$.

becomes a crosslink point upon curing of the sample. For example, C_1 is only 7.3×10^6 dyne/cm^2 for sample 1 having 2.77×10^{20} branches/cc, compared with C_1 of 10.2×10^6 and 12.1×10^6 dyne/cm^2 for samples 2 and 6 having 3.32×10^{20} and 4.18×10^{20} branches/cc, respectively.

Characterization of Polyurethane from Swelling-Equilibrium Measurements

Characterization of polyurethanes from swelling-equilibrium measurements can be made through the Flory-Rehner equation[11,12]

$$\ln(1 - v_r) - v_r - \chi v_r^2 = (2C_1V_0/RT)[v_r^{1/3} - (v_r/2)] \quad (3)$$

where χ is the solvent–polymer interaction parameter and V_0 is the molar volume of the solvent. Equation (3) relates three variables (v_r, C_1, and χ), two of which (v_r and C_1) can be obtained experimentally, and hence, allows calculation of χ. In this work, v_r was determined from swelling-equilibrium measurements, carried out as described in earlier work,[7] while C_1 was taken from the results of S/S measurement made on the benzene-swollen PU networks discussed in the preceding section. Values of χ obtained by this procedure are plotted versus v_r in Figure 6. By extrapolating the straight line in Figure 6 to $v_r = 0$, χ can be expressed by:

$$\chi = 0.077 + 0.97v_r \quad (4a)$$

The solvent–polymer interaction parameter χ, which increases with v_r according to eq. (4a), was also found to increase linearly with an increase in the amount of HMDI in the polyurethane polymer. The dependence of χ on polymer composition was established by plotting χ versus weight fraction w_f of HMDI in the polymer. As Figure 6 shows, χ can be expressed in terms of w_f by the following relation:

$$\chi = 0.23 + 0.84w_f \quad (4b)$$

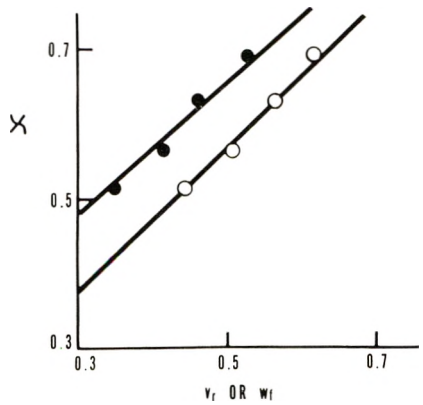

Fig. 6. Variation of interaction parameter with (○) volume fraction of polymer in swollen polyurethane and with (●) weight fraction of HMDI in polyurethane (series A).

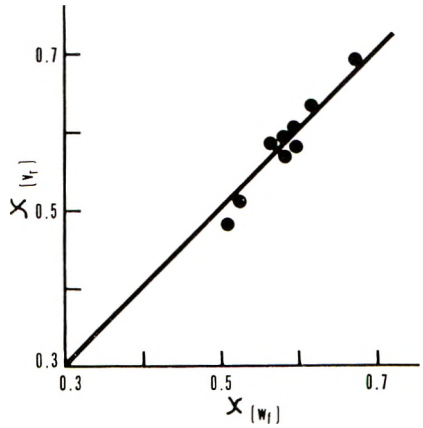

Fig. 7. Solvent–polymer interaction parameters derived from $\chi = 0.077 + 0.97\ v_r$, [eq. (4a)] vs. solvent polymer–interaction parameters derived from $\chi = 0.23 + 0.84\ w_f$ [eq. (4b)].

In the present series the changes in HMDI were made by changing the ratio of TP740:TP1540 in the polyol mixture while maintaining the NCO:OH ratio constant. As Table II shows, this leads to changes in number of branches per cubic centimeter (ca. 0.08×10^{20} branches/cc for 1% change in HMDI) which in turn cause the observed changes in crosslink density and v_r. Because of this change in v_r which accompanies the changes in sample composition, the present experiment cannot distinguish the separate effects of sample composition and v_r on χ. In spite of this, both eqs. (4a) and (4b) are useful functions for predicting χ from v_r or from w_f for polyurethane networks within the composition ranges shown in Table I. Volumes of the polymer interaction parameter determined according to these equations are shown in Table II and plotted against each other in Figure 7. As is shown in Figure 7, the two χ values are in good agreement and, therefore, χ can be determined either from eq. (4a) or from eq. (4b). In this investigation, however, χ was determined from eq. (4a).

Table II shows values of χ, v_r, C_1, M_c, and ν obtained from the swelling-equilibrium measurements through eqs. (3) and (2) by using the χ values given by eq. (4). Values shown for samples 1, 2, 4, and 6 are the average results derived from both the S/S and the swelling-equilibrium measurement. As the number of branches per unit volume in the sample is increased, v_r increases. This is also true of C_1 and ν, which increases directly as the number of branches per unit volume is increased.

Calculation of Crosslink Density and M_c

In the formation of the PU prepolymer the NCO group in the HMDI reacts with the OH of the triol to give a urethane linkage. Use of excess HMDI leads to branched NCO-terminated prepolymer chains. Curing of the prepolymer and formation of a network occur when the prepolymer is exposed to moisture. A terminal NCO group first reacts with water to give

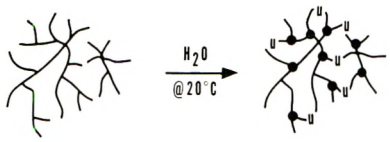

Fig. 8. Formation of polyurethane network.

a carbamic acid which rapidly decomposes to give an amine. The amine then reacts quickly with another NCO to give a urea linkage.[13] If this reaction occurs intermolecularly, two molecules become linked through a urea linkage u. Repetition of this reaction leads finally to the formation of a network in which all the NCO-terminated branches and chain ends are presumably linked together, as shown schematically in Figure 8.

In this model the urea group links the chains, but it does not constitute a crosslink point. The branch point which becomes a junction point in the cured system constitutes the crosslink point. In moisture-cured polyurethanes the crosslinking reaction is largely limited to the above reaction—the formation of urea-crosslink bonds. The formation of allophanate and biuret linkages is reported to occur only when the system is heated at temperatures above 100°C or when a catalyst is added.[13] In these polyurethanes moisture-cured at room temperature, we have assumed that although biuret and allophanate formation may occur to some extent, the main crosslinking reaction is accomplished through the formation of a urea bond. For the present polyurethane networks which are based on the trifunctional triols, the above model tells us that ν', the concentration of crosslinks, is

$$\nu' = \rho NB \tag{5a}$$

where B is the number of moles of branches per gram and N is Avogardo's number. Since three chains terminate at a branch point, the concentration ν of crosslinked chains, is given by

$$\nu = {}^1/_2(3\rho NB) \tag{6}$$

The factor one-half is introduced to avoid counting each chain twice. The crosslink density ν' is given by

$$\nu' = 0.667\nu \tag{5b}$$

Crosslink densities ν' can be determined according to eq. (5b) from the measured values ν shown in Table II by multiplying the latter values by ${}^2/_3$. Observed values of ν' determined by this method are of the same magnitude as the number of branches per cubic centimeter shown in Table II, which was determined from the sample composition shown in Table I.

Comparison of eqs. (6) and (2) leads to

$$G_1 = 0.5(1.5)\rho RTB \tag{7}$$

where R is in erg/deg-mole. A plot of ν or G_1 versus branches per cubic centimeter should give a straight line passing through the origin with a slope

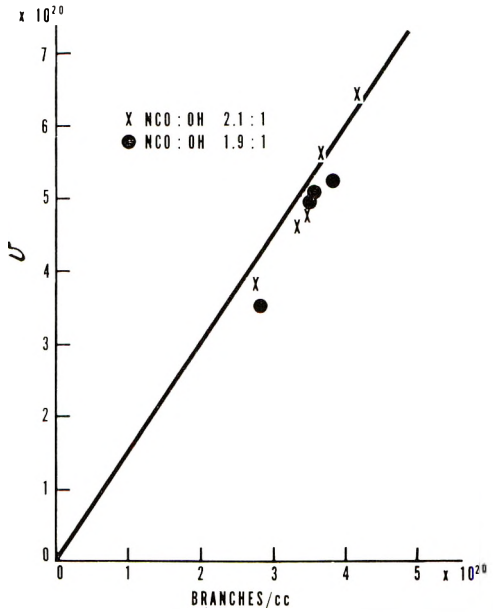

Fig. 9. Plots of chains/cc. vs. branches/cc in polyurethane.

of $1.5kT$ for the first case and a slope of $0.75kT$ for the second case. This is shown for ν (from Table III) in Figure 9, in which the solid line is the theoretical line drawn according to eq. (6) with a slope of 1.5. The experimental results, although showing some scattering, seem to fall on this line. The model, however, tends to predict a larger degree of crosslinking than is observed. The discrepancy could arise because not all the NCO-terminated chains enter into the crosslinking reactions shown above, which are all assumed to occur intermolecularly.

The average molecular weight of chain elements between crosslinks is represented by $M_c = 0.667B^{-1}$, with B in units of moles/g. Values of M_c calculated from this relation are compared with observed values in Table III and plotted in Figure 10. Again, for the reasons given above, the calculated M_c tends to be smaller than the observed value. In spite of this, we

TABLE III
M_c (Calculated) vs. M_c (Observed) in Polyurethanes

Sample	M_c (observed)	M_c (calculated)
1	1730	1580
2	1430	1310
3	1370	1260
4	1160	1210
6	1030	1050
7	1870	1540
8	1350	1260
9	1330	1200
10	1260	1150

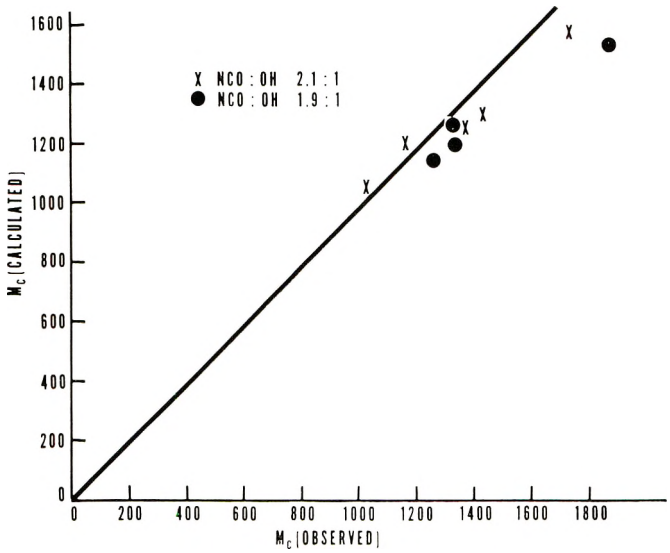

Fig. 10. Calculated and observed average molecular weight of chains between crosslinks.

feel that the data show a reasonably good agreement and suggest the formation of approximately one crosslink per branch in the present system.

The authors thank Dr. J. F. Remar for preparing the samples.

References

1. R. Blokland, *Elasticity and Structure of Polyurethane Networks*, Rotterdam Univ. Press, Rotterdam, (Gordon and Breach, New York), 1968.

2. R. Blokland and W. Prins, *J. Polym. Sci. A-2*, **7**, 1595 (1969).

3. T. Tanaka and T. Yokoyama, *Rubber Chem. Technol.*, **35**, 970 (1962).

4. L. D. Loan, *Techniques of Polymer Science*, Paper Symposium Plastics and Polymer Group, London, 1963, p. 24.

5. A. J. Havlik, T. L. Smith, Jet Propulsion Laboratory, Pasadena, Calif. Technical Report No. 32-180.

6. P. J. Flory, *Principles of Polymer Chemistry*, Cornell Univ. Press, Ithaca, N. Y., 1953, Chap. XI.

7. A. M. Hassan and L. N. Ray, paper presented at 3rd Middle Atlantic Regional Meeting, American Chemical Society, Philadelphia, Pa., February 1968; *J. Applied Polymn. Sci.*, in press.

8. M. Mooney, *J. Appl. Phys.*, **11**, 582 (1940).

9. R. S. Rivlin and D. W. Saunders, *Phil. Trans. Roy. Soc.* (London), **Ser. A**, 243, 251 (1951).

10. S. M. Gumbrell, L. Mullins, and R. S. Rivlin, *Trans. Faraday Soc.*, **49**, 1945 (1953).

11. P. J. Flory and J. Rehner, *J. Chem. Phys.*, **11**, 521, (1943).

12. P. J. Flory, *J. Chem. Phys.*, **18**, 108 (1950).

13. J. H. Saunders and K. C. Frisch, *Polyurethane Chemistry and Technology*, Part II, Interscience, New York, 1964, p. 456.

Received June 29, 1970
Revised March 5, 1971

JOURNAL OF POLYMER SCIENCE: PART A-2 VOL. 9, 1603–1627 (1971)

Transitions and Relaxations in Aromatic Polymers

WOLFGANG WRASIDLO, *Materials Sciences Laboratory, Boeing Scientific Research Laboratories, Seattle, Washington 98124*

Synopsis

Transition and relaxation phenomena in 26 structurally related polyquinoxalines and other aromatic polymers were studied over a temperature range from 70 to 770°K by means of calorimetric, dilatometric, dynamic mechanical, and dielectric techniques. Differential thermal analysis and x-ray data showed these polymers to be essentially amorphous. The lack of crystallinity is attributed to geometric isomerism, resulting in conformational as well as configurational disorder. Calorimetric measurements gave discontinuities in heat capacities ranging from 12 to 54 cal/°C per mole of repeat-unit structures and provided unambiguous assignments of glass transition temperatures of these polymers. Depending upon structure, T_g varied from 489 to 668°K. Thermal expansion curves of annealed bulk polymer samples between 70 and 770°K exhibited only one discontinuity over the entire temperature range, namely at T_g, thus indicating the absence of any motion leading to transitions in the solid state of these polymers. Viscoelastic properties were obtained by means of torsional braid analysis and a longitudinal vibrational apparatus. In a typical case, the dynamic mechanical relaxation spectrum contained three loss maxima. A peak of low amplitude occurring at 483°K was attributed to impurity effects, resulting from endgroups and species of low molecular weight. The second and only major relaxation process occurred at 579°K, in the glass transition interval. A third, weak loss peak of unknown origin was found in the liquid state at 683°K. On the other hand, the dielectric loss curves of various polymers exhibited only one broad and strong absorption maximum at temperatures 30 to 100°K higher (depending upon a particular polymer) than equivalent major mechanical loss peaks. These differences are interpreted from a mechanistic point of view. Major mechanical relaxations occurring in the glass transition interval of these polymers are proposed to result from translational motions.

INTRODUCTION

Completely aromatic polymers offer a unique opportunity for studying molecular motions, in particular, motions responsible for transition and relaxation effects. In ordinary linear aliphatic polymers, relaxation processes are believed to originate in rotations of whole chains, chain segments, or individual moieties within a molecular unit.[1,2] In fully aromatic polymers, rotational mobility is greatly restricted due to resonance and steric effects (i.e., high barriers to rotation arising from *ortho* substituents). Consequently we expect primary motions such as are affected by the glass or melt transitions to be manifested in other than rotational interactions.

To the author's knowledge no detailed investigations have been reported which attempt to identify mechanisms of motion in aromatic polymers,

although several papers on dynamic mechanical properties of these polymers have appeared in the literature.[3–6]

The objective of this continuing effort is to obtain experimental evidence for the existence of transitions and relaxations in aromatic polymers by employing dynamic mechanical, dielectric, dilatometric, and calorimetric techniques. This will hopefully lead to at least a conceptual view on mechanisms of molecular motion in these polymers.

EXPERIMENTAL

Polymer Synthesis and Sample Preparation

Polyquinoxalines and polyphenylquinoxalines were synthesized according to procedures described elsewhere.[7–11] Clear, yellow, pinhole-free film specimens were prepared by casting 15% polymer solutions on glass plates and evaporating the solvent (*m*-cresol) at 80°C for 2 hr followed by heating for 2 hr at 200°C under reduced pressure. Bulk specimens were made by pressing powders at 300°C at 15,000 psi. All specimens were annealed at 20°C above T_g in a nitrogen atmosphere for 15 min.

Apparatus and Measurements

Specific heat measurements were carried out on a DuPont differential thermal analysis unit (900 DSC-cell) according to a procedure described by Wunderlich.[12] First, an empty aluminum capsule was run against another empty capsule of known weight to establish the asymmetry of the system as a function of temperature. Minor deflections of about 0.1 in. at the highest instrument sensitivity (0.004 mV/in.) were recorded. The temperature axis of the recorder was calibrated by using A. H. Thomas organic calibration standards. The melting points obtained agreed within ±0.5°C of the recorder readout. Heat-capacity calibration curves were obtained on sapphire by using Ginnings and Furukawa's values on specific heats of aluminum oxide.[13] Finally, a series of runs was made on polymers at a heating rate of 20°C/min in a helium atmosphere (flow 0.1 l./min). The standard deviation of averages of four runs from a smooth curve was ±3%. The internal precision of the instrument is believed to be ±2%.[12]

Dynamic mechanical properties were measured on a direct reading viscoelastometer and by means of torsional braid analysis (TBA). The commercial apparatus described by Takayanagi[14] is limited in temperature to 250°C and was modified for high-temperature operation. The heating chamber was replaced by a high-temperature tube furnace provided with atmosphere control, capable of controlled heating to 700°C. Spring-action sample holders and aluminum connecting rods were replaced by screw-action clamps and hollow stainless-steel rods. Copper fins were placed in series on the connecting rods near the stress and strain transducers to prevent excessive heat buildup. TBA data were obtained in an apparatus described by Gillham.[15]

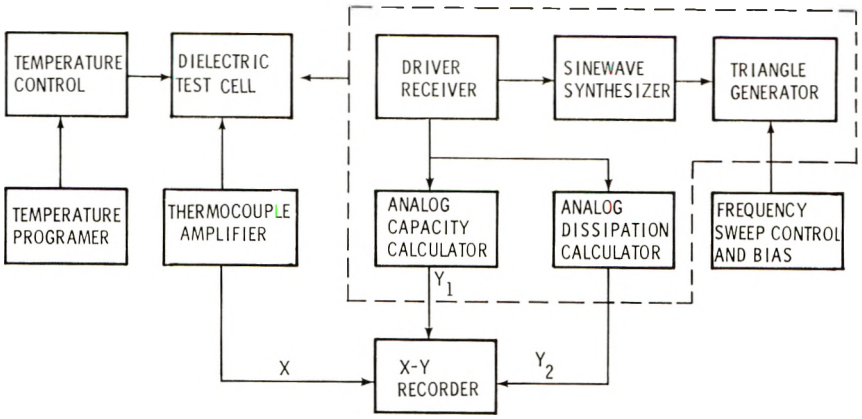

Fig. 1. Block diagram of dynamic scanning dielectrometer (Audrey II with high-temperature test cell).

The apparatus employed for dielectric measurements was developed in our laboratory. A block diagram of the dynamic scanning dielectrometer (Audrey II, manufactured by Tetrahedron Associates, San Diego) is shown in Figure 1. A dielectric test cell was constructed with internal heaters for operation up to 500°C at linear heating rates ranging from 0.5 to 30°C/min. Measurements were made by placing film samples (ca. 2 mil thick) into a three-terminal electrode assembly under light spring pressure. Since the cell clamps exert a moderate pressure on the disk samples some sample distortions occurred (ca. 5% of original thickness), particularly at the higher temperatures, and an equivalent air capacity for the deformed samples had to be calculated. The thermocouple for sample temperature readout was placed in one of the electrodes, electrically insulated by a boron nitride sleeve, and adequately shielded.

In dilatometric work the DuPont thermomechanical analyzer, Model 940 was employed. The apparatus was modified for high temperature measurements. Calibration was done by determining the expanison profile of an aluminum cylinder at a heating rate of 5°C/min and by using the literature[16] values for the coefficients of linear thermal expansion of pure aluminum.

RESULTS

In the interest of brevity, detailed experimental results are given for only one of the 26 polyquinoxalines investigated. Numerical results for the other polymers are listed in Tables I–III. The polyquinoxaline chosen for detailed discussion has the repeat-unit structure I.

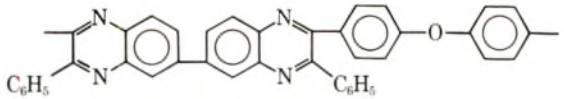

I

(Polymer 14)

TABLE I
ΔC_p for Polyquinoxalines at the Glass Transition Temperature

No.	Structure	T_g, °C	No. bonds[a]	ΔC_p Cal/°C-mole	ΔC_p Cal/°C-unit
1	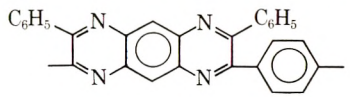	668	4	25.9	6.48
2	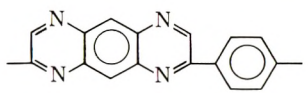	665	2	12.7	6.32
3	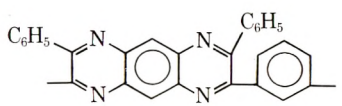	638	4	26.7	6.67
4	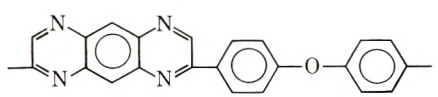	626	4	20.6	5.18
5	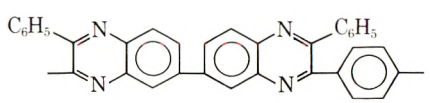	645	5	28.4	5.78
6	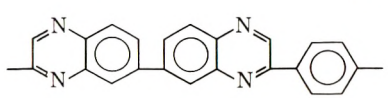	649	3	18.5	6.15
7	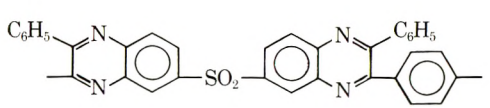	618	6	31.8	5.33

[a] Number of bonds between the phenyl groups.

8	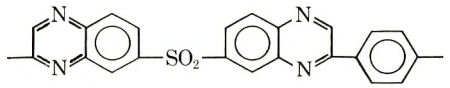	615	4	22.1	5.52
9	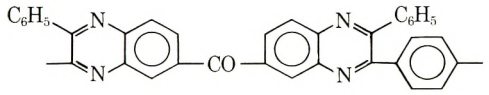	598	6	32.1	5.37
10	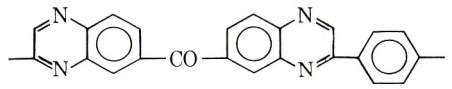	591	4	23.9	6.00
11	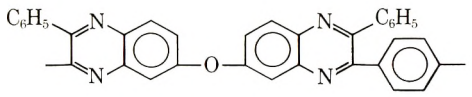	577	6	33.3	5.56
12	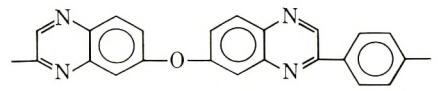	579	4	39.8	5.43
13	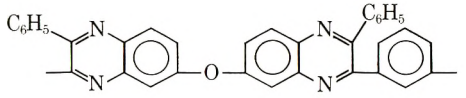	543	6	33.6	5.56
14	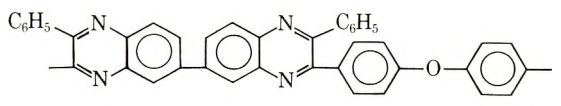	573	7	42.7	6.11
15	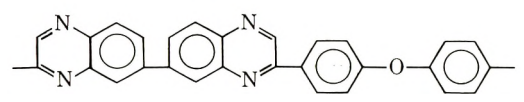	578	5	29.6 M	5.94

(*continued*)

TABLE I (*continued*)

No.	Structure	T_g, °C	No. bonds[a]	ΔC_p Cal/°C-mole	ΔC_p Cal/°C-unit
16	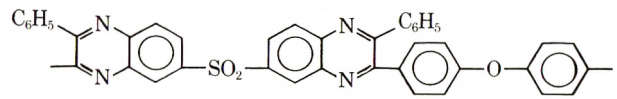	563	8	45.0	5.63
17	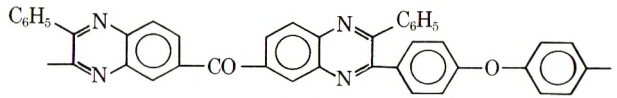	544	8	46.5	5.85
18	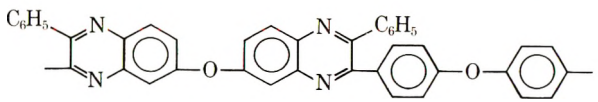	531	8	41.6	5.23
19	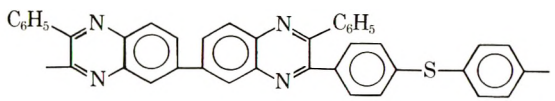	561	7	39.4	5.67
20	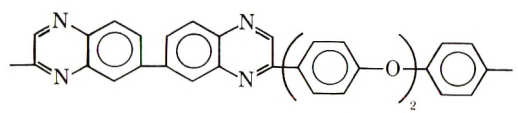	508	7	42.0	6.00
21	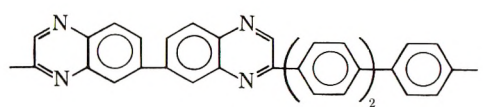	578	5	29.1	5.80
22	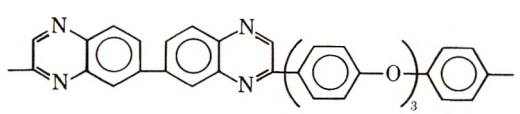	489	9	54.4	6.00

[a] A flexible bond is any bond connected to aromatic rings.

TABLE II

Heat Capacity of Poly[2,2′-(*p*,*p*′-oxydiphenyl)-6,6′-bis(3-phenylquinoxaline)]

Temp, °C	C_p, cal/deg-g	Temp, °C	C_p, cal/deg-g
20	0.286	260	0.459
30	0.301	270	0.465
40	0.308	280	0.470
50	0.315	290	0.488
60	0.324	300	0.540
70	0.329	310	0.556
80	0.336	320	0.564
90	0.343	330	0.570
100	0.351	340	0.574
110	0.357	350	0.578
120	0.365	360	0.582
130	0.373	370	0.587
140	0.380	380	0.592
150	0.386	390	0.596
160	0.393	400	0.600
170	0.400	410	0.605
180	0.407	420	0.609
190	0.414	430	0.614
200	0.420	440	0.618
210	0.426	450	0.623
220	0.434	460	0.627
230	0.440	470	0.631
240	0.447	480	0.635
250	0.453	490	0.639
		500	0.642

TABLE III

Effect of Copolymerization on Transitions and Relaxation Maxima

Polymer	Composition	$(\Delta C_p)_{1/2}$, °K	E''_{max}, °K	ϵ''_{max}, °K
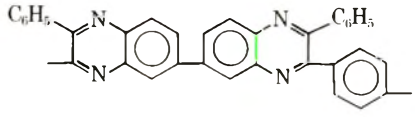	100/0	645	658	708
Block copolymer[a]	75/25	626	642	688
Block copolymer[a]	50/50	617	625	681
Block copolymer[a]	25/75	603	619	664
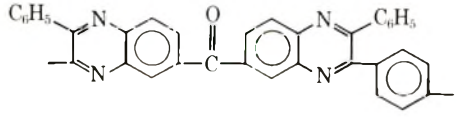	0/100	598	613	651

[a] The average length of a block, estimated from viscosity data, was about 10–20 repeat units.

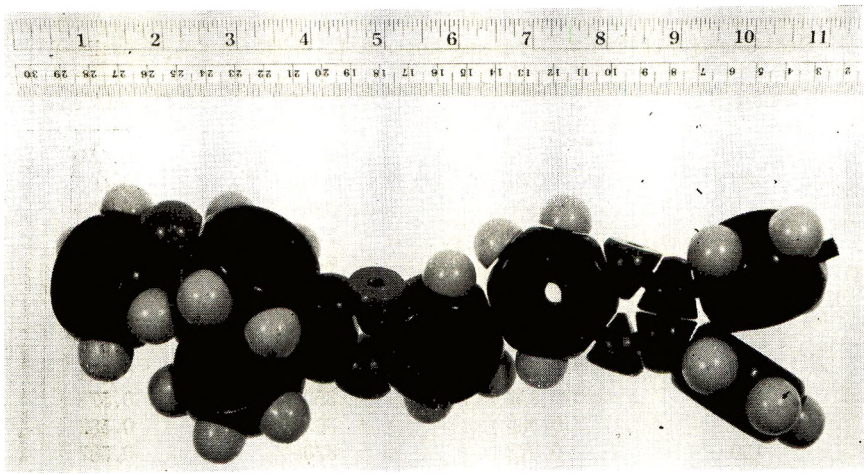

Fig. 2. Model of poly[2,2′-(*p*,*p*′-oxydiphenyl)-6,6′-bis(3-phenylquinoxaline)].

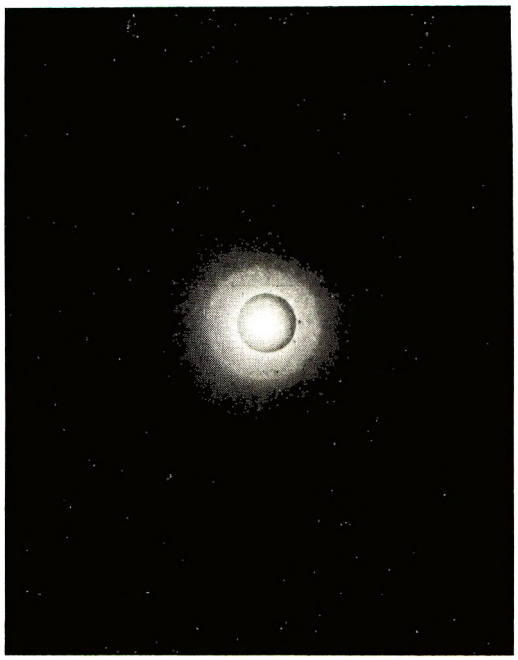

Fig. 3. Flat-plate x-ray photograph of polymer 14 at 25°C. Nickel-filtered CuK α radiation, specimen-to-film distance 5 cm.

It was, as were all the other polymers, thoroughly characterized by elemental analysis, infrared, ultraviolet, and mass spectroscopy, and by model compound synthesis. The weight-average and number-average molecular weights determined by gel-permeation chromatography were 255,000 and 72,000 respectively, and the repeat unit length was about 24 Å (Fig. 2). The polymer was completely soluble in chloroform (η_{inh} = 2.4) and phenolic

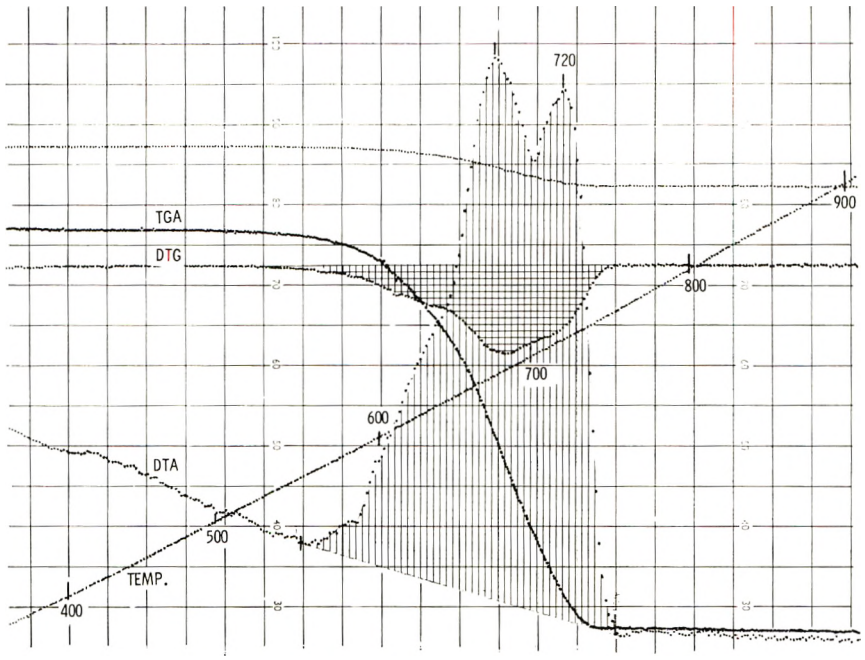

Fig. 4. Recorder trace of simultaneous TGA–DTA of 10 mg sample of polymer 14 (heating rate 5°C/min, TGA sensitivity 1.0 mg/in.; DTA sensitivity 10 μV/in.; Pt–Pt 10 rd).

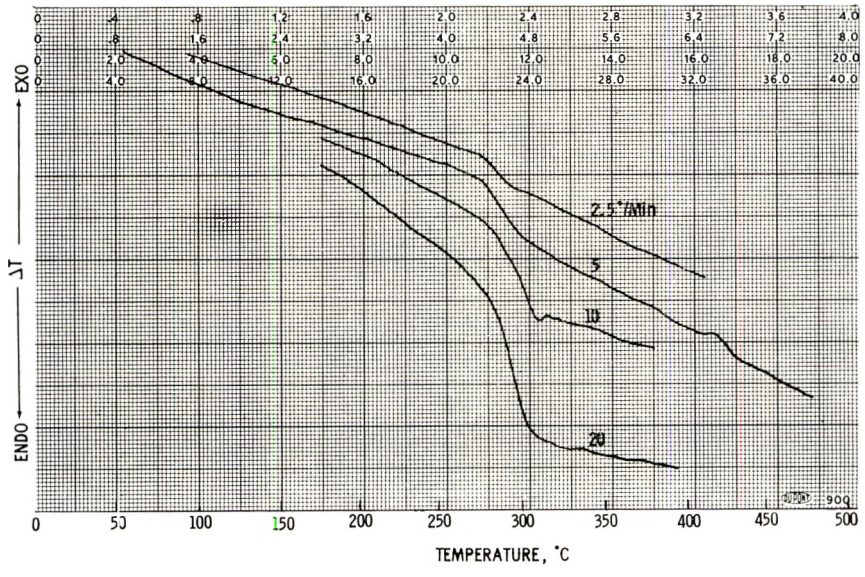

Fig. 5. Recorder trace of differential temperature vs. temperature.

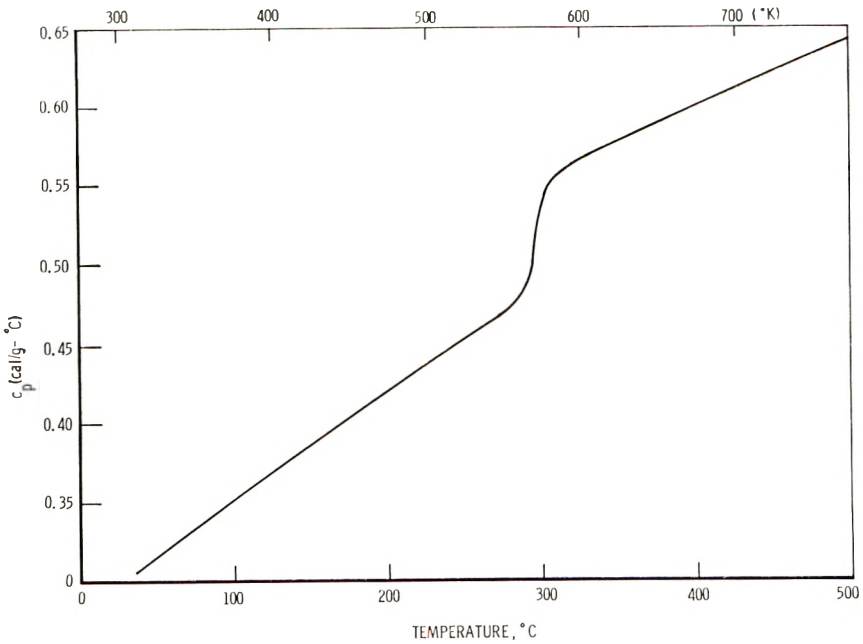

Fig. 6. Plot of heat capacity vs. temperature for polymer 14.

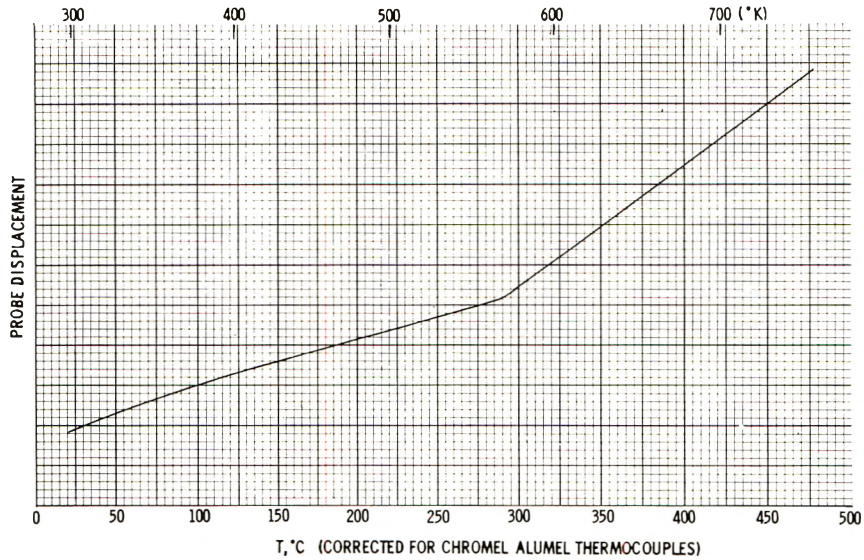

Fig. 7. Recorder trace of thermal expansion vs. temperature (heating rate 5°C/min, He atmosphere, displacement sensitivity 1.35×10^{-3} in./in. of chart paper).

solvents and therefore considered to be completely linear. A flat-plate x-ray diffraction pattern of a film specimen (Fig. 3) was diffuse, indicating the absence of an X-ray crystallinity. Differential thermal analysis gave no melting peaks, and thus indicated no thermodynamic crystallinity. Prior to transition and relaxation measurements, the chemical stability was

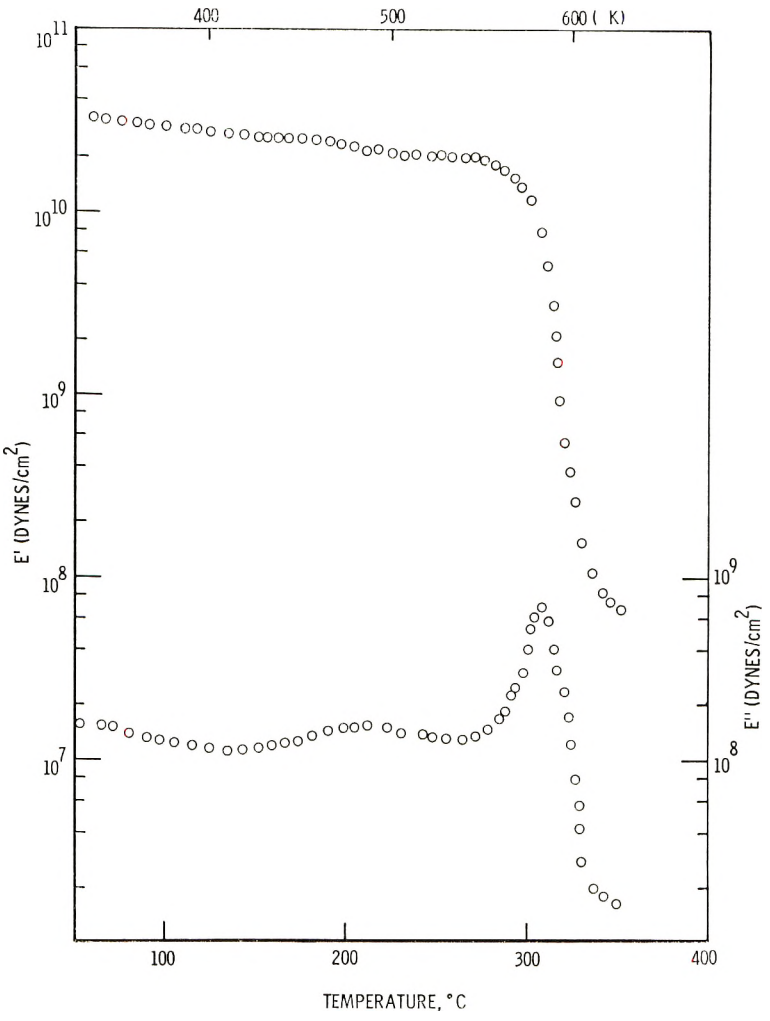

Fig. 8. Plot of dynamic tensile modulus E' and storage modulus E'' vs. temperature (measurements made at a heating rate of 5°C/min in a helium atmosphere, frequency 110 cps).

tested by means of simultaneous TGA-DTA measurements in the Mettler thermal analyzer. Under the conditions indicated in Figure 4, exothermic decomposition starts at 555°C and is accompanied by simultaneous weight loss. All other polymers listed in Table I gave thermal decomposition

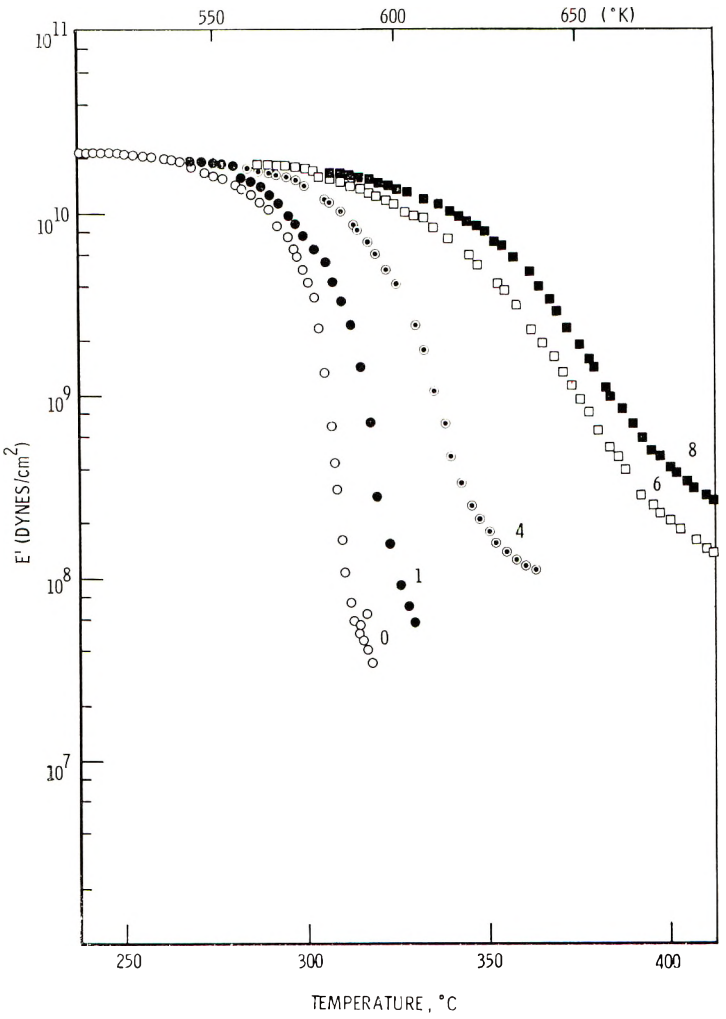

Fig. 9. Plot of dynamic storage modulus vs. temperature. Effect of thermal history on E′ (thermal cycling for 1, 4, 6, and 8 hr in a helium atmosphere).

temperatures above 500°C. On the basis of these data, the possibility of degradation during measurements up to 500°C was excluded.

Results of relaxation and transition measurements for polymer 14 are illustrated in Figures 5–13 and in Table II. Figure 5 is a differential thermogram at various heating rates. The glass transition interval occurring between 537°K and 578°K was readily apparent from these curves, exhibiting endothermic sigmoid character through T_g. Only a minor shift of these curves towards higher temperatures occurred on increasing the heating rate from 2.5 to 20°C/min. Therefore, the effect of heating rate on T_g within these limits could be neglected. The information contained in Figure 5 served as a basis for heat capacity measurements. In Table II

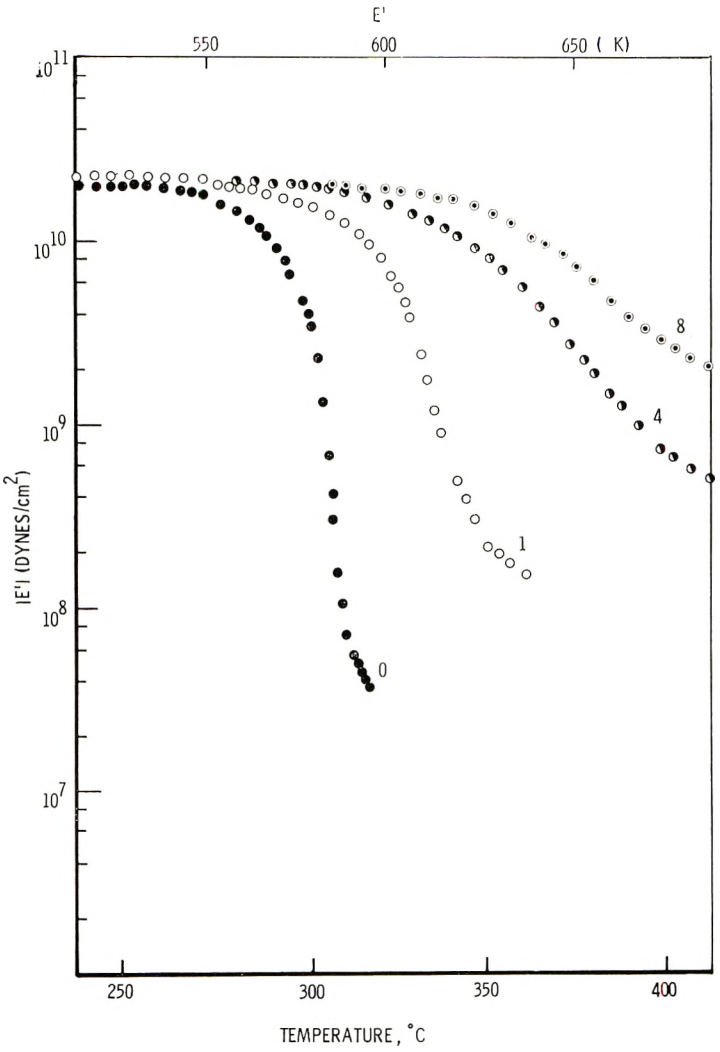

Fig. 10. Plot of dynamic storage modulus vs. temperature. Effect of thermal history on E′ (thermal aging for 1, 4, and 8 hr in dry air).

the heat capacity of polymer 14 is listed at 10°C intervals between 20 and 500°C, and the data are plotted in Figure 6. Below and above the glass transition interval the specific heat is a smooth monotonic function of temperature and around T_g becomes S-shaped. The change in heat capacity was obtained from the amplitude of the sigmoidal curve and the numerical results for this and other polyquinoxalines are listed in Table I. Since C_p values were measured by DTA, a nonequilibrium technique, in some cases small peaks were observed in apparent C_p. As Reilly and Karasz[17] pointed out, such peaks are due to the time lag for internal equilibrium to occur and should not be confused with first-order phenomena. The glass transition

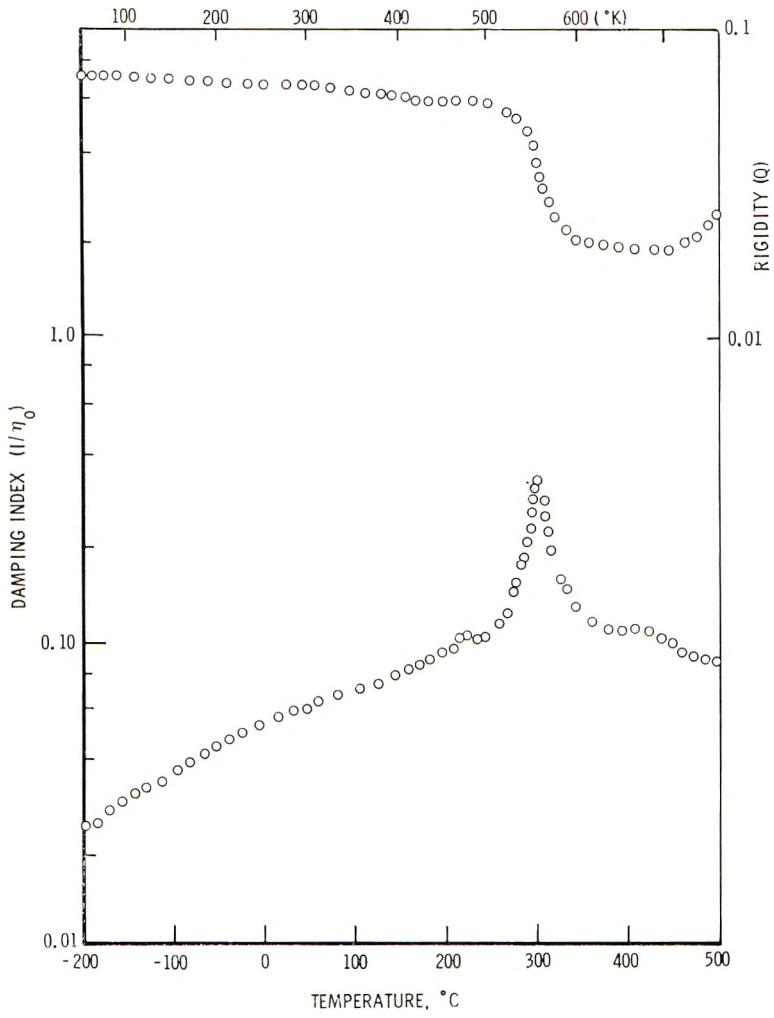

Fig. 11. Plot of damping and rigidity index vs. temperature (measurement made at a heating rate of 5°C/min in a helium atmosphere).

temperature, defined as the "temperature of half-freezing of holes,"[21] was taken at 568°K the midpoint of the ΔC_p versus T curves. Table I lists the number of flexible bonds in the polymer repeat-unit structures by which the change in molar heat capacity was divided to yield ΔC_p per unit. A hypothetical unit was defined as the smallest molecular segment connected to the chain by flexible bonds. A flexible bond was defined as any primary bond connecting aromatic rings. The following units were identified from repeat-unit structures: pyrazyl, quinoxalyl, phenyl, phenylene, sulfonyl, carbonyl, oxy, and thio. Heat capacities computed in Table I were relatively constant with an average value of 5.5 ± 0.7 cal/°C per unit. The linear thermal expansion of bulk sample annealed at 315°C in a nitrogen

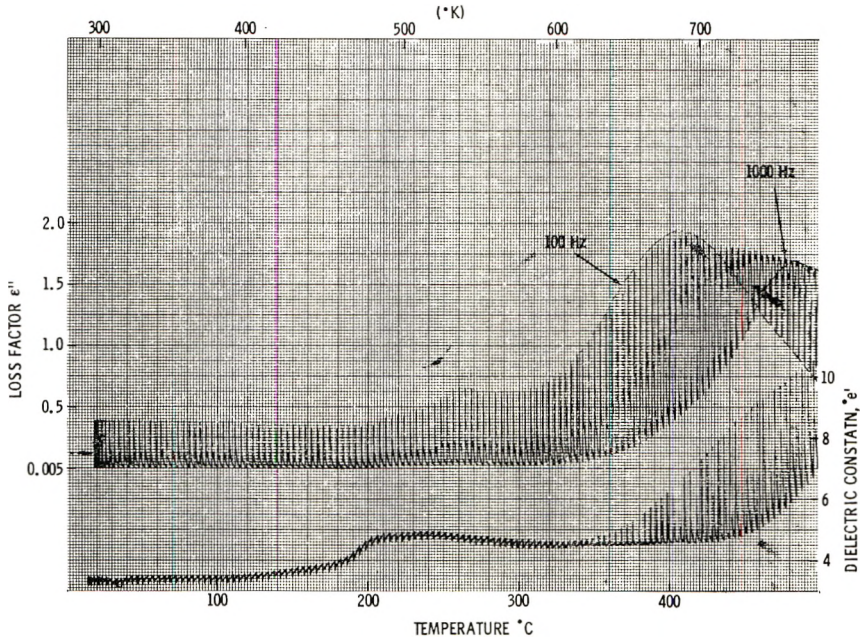

Fig. 12. Recorder trace of dissipation factor and capacitance vs. temperature (heating rate 5°C/min, He atmosphere, frequency sweeps 100 to 1000 Hz).

atmosphere is shown in Figure 7. Between 70°K and 568°K, the expansitivity α is an almost linear function of temperature. At 568°K, the glass transition temperature, α exhibits a sharp discontinuity resulting in a threefold increase in slope. The linear expansion coefficients below and above T_g were 59.4×10^{-6} and 184×10^{-6}°C^{-1}, respectively.

Next, the dynamic mechanical properties were measured in a variety of ways. The dynamic tensile storage E' and loss E'' moduli of a film specimen, plotted as a function of temperature, is shown in Figure 8. The measurement was made at a heating rate of 5°C/min in a helium atmosphere at a frequency of 110 cps. An almost linear, small decrease of E' up to 473°K is attributed to thermal expansion of the film. At 483°K a small but distinct change in slope of E' and corresponding maximum in E'' occurs. On thermal cycling of this specimen up to 670°K, the peak persists. Therefore, the possibility of a plasticizing effect due to solvent coupling of chain segments was excluded. Polymer 15, the nonphenylated analog of polymer 14, also exhibited a small dispersion peak at 475°K. Therefore, it is unlikely that phenyl side-group motion is the cause of this relaxation. At this time, we feel that the absorption is due to impurity effects (i.e., low molecular weight species and endgroups).

A major relaxation occurs in the glass transition interval between 547°K and 600°K, resulting in a decrease of E' from 3×10^{10} to 6×10^{7} dyne/cm^2. The loss modulus exhibits a maximum at 579°K, 11°K above T_g. This difference is to be expected, since the mechanical method measures a

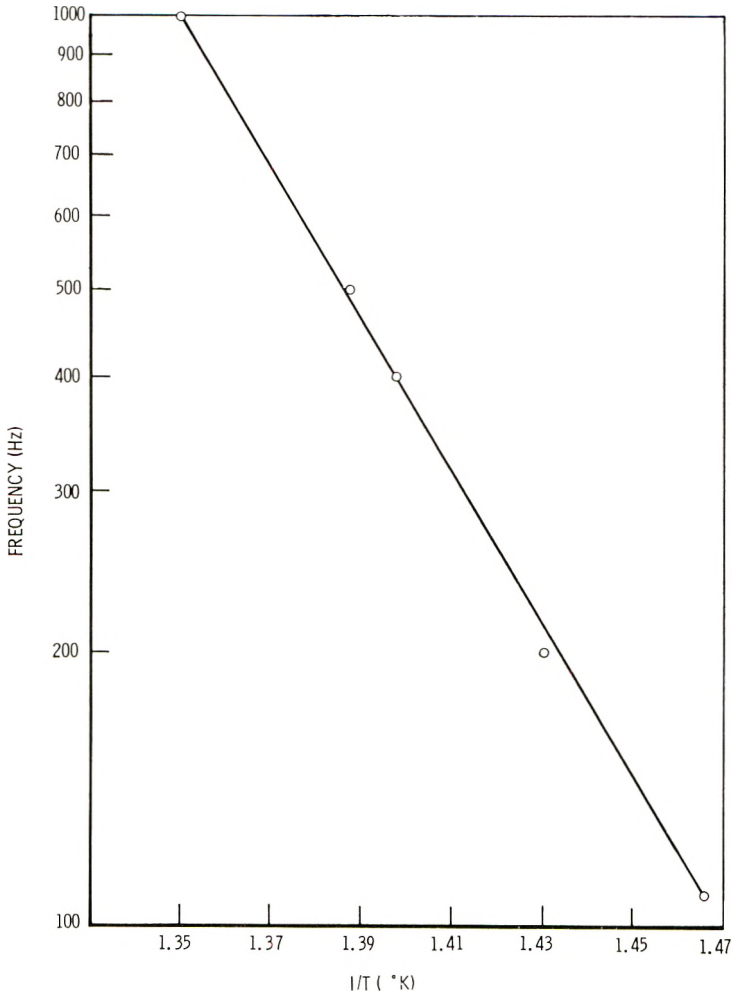

Fig. 13. Arrhenius plot for dielectric relaxation of polymer 14.

time-dependent relaxation effect (i.e., the kinetic component of T_g), while calorimetrically a thermodynamic transition at essentially zero frequency is measured. The effect of thermal history on the dynamic modulus is shown in Figures 9 and 10. On heating of film specimens for 1, 4, 6, and 8 hr at 400°C in a helium atmosphere, the modulus curves progressively shift towards higher temperatures with inflection points at 589, 620, 648, and 660°K, respectively. Cycling in air (Fig. 10) produces similar results but in much shorter times. We attribute the effects of thermal cycling in an inert atmosphere to pyrolytic crosslinking and in air to oxidative coupling.

Torsional braid analysis (Fig. 11) between 70 and 770°K was performed in a helium atmosphere at a heating rate of 5°C/min (frequency ca. 0.5 cps). No relaxation effects were noted from 70 to 480°K. The damping-

index curve exhibits three maxima at 484, 573, and 689°K, respectively. Loss maxima at 484 and 573°K agree well with the data obtained with the longitudinal apparatus, considering the differences in frequencies applied in the two methods.

Dielectric measurements were carried out on polymer films (ca. 2 mils thick). The general dependence of dissipation factor (tan δ) and capacitance on temperature and frequency is illustrated in Figure 12. A small loss maximum at 535°K disappeared on thermal cycling of the specimen up to 600°K and is probably due to trace amounts of solvent present in the original film specimen. Between 575 and 770°K a major relaxation occurs, reaching dissipation maxima at 677 and 754°K at 110 Hz and 1000 Hz, respectively, with a flat frequency envelope in between. Correspondingly, the capacitance undergoes a sigmoid increase with inflection points at the maximum dissipation. The ac dynamic dielectric constants ϵ' and loss factors ϵ'' calculated from these curves are indicated on the y-axis scale of Figure 12.

In Figure 13, the logarithm of frequency of the loss maxima is plotted against temperature. From the slope of the line an activation energy of 41 kcal was calculated, which is of the order of an energy of activation for viscosity.

DISCUSSION

Mechanism of Motion

Superficially a study of motion in polyquinoxalines may seem difficult. To start with, repeat-unit structures of these polymers are complex by comparison with ordinary polymers. Then, there exists the possibility of geometric isomerism. For example, three "repeat-unit isomeric forms" IA, IB, and IC exist for polymer 14.

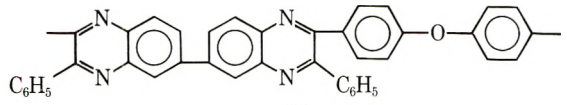

IA

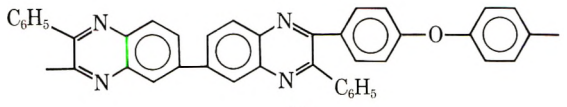

IB

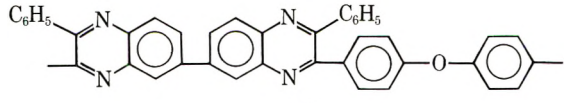

IC

While the probability of forming these isomers decreases from IA to IC and is dictated by the reactivity of reactants (i.e., inductive and electromeric effects), all isomers are distributed statistically along the polymer chain.

Consequently, we expect configurational as well as conformational disorder, and therefore lack of crystallinity. The introduction of flexibilizing groups (i.e., oxy, carbonyl, sulfone) will further contribute to produce conformationally disordered portions of the chain. Therefore it is not surprising that the polymers listed in Table I, when synthesized by ordinary chemical routes, are essentially amorphous, in the sense that no heat of melting or sharp x-ray diffraction patterns are observed.

This simplifies matters considerably. First we need not be concerned with dynamic processes associated with crystallinity, such as melting, dislocations, local motions within crystallites, interaction of amorphous–crystal interfaces, etc. Secondly, thermal expansion and dynamic mechanical measurements do not indicate transitions or relaxations (except for impurity effects) from 70°K up to the glass transition temperatures of these polymers. Thus, secondary main chain processes often found in amorphous polymers (e.g., loose folds or motion of short chain segments) and side-group motions such as phenyl group rotations are apparently not active (i.e., are frozen in) at temperatures below T_g. Thus we need to consider only large-scale main chain motion beginning at the glass transition. Discontinuities in the heat capacity in the glass transition intervals (Fig. 6) led to unambiguous assignments of T_g. In all cases, expansivity–temperature curves also showed sharp increases in slope at T_g. The jump in heat capacity per mobile aromatic unit (Table I) ranged from 5.2 to 6.5 cal/°C, with an average value of 5.5 ± 0.7 cal/°C. These values are about twice what one finds for other polymers.[18] A possible explanation for these differences may be found by considering the following.

According to the hole theory of liquids as developed by Frenkel[19] and Eyring[20] the total heat capacity of a liquid is proportional to the sum of heat capacities of the molecules and holes:

$$C_l = f(C_m + C_h).$$

The process of hole formation is assumed to require a hole energy E to overcome the cohesive forces and form a mean hole-volume v_h. Wunderlich[21] applied this theory to glasses and arrived at the following expression, representing the change in heat capacity at T_g due to hole formation:

$$\Delta C_p = (\partial H/\partial T)_p = \epsilon(dN/dt)_q$$

where dN/dt is the rate of hole formation and $q = dT/dt$ is the heating rate. At equilibrium, the number of holes N^* at temperature T are related to their volume v_h by the Boltzmann expression

$$N^*(T)\, v_h = N_0 v_0 \exp\left\{-\epsilon/RT\right\}$$

The change in heat capacity at T_g is thus related to the cohesive energy of the system through ϵ, and to chain mobility through the quantities N and v. The hole volume can be intuitively associated with the size of a rigid chain segment; the number of holes N is attributed to the ability of segments to undergo cooperative motions (e.g., internal rotations and/or intermolecular

segmental motions). In aromatic polymers it is reasonable to expect rigid chain segments to be considerably larger (20–30 Å) than in ordinary polymers and therefore to be associated with a larger hole volume. On the other hand, by the same argument, less flexible chains should produce a correspondingly smaller number of holes; consequently we expect the product Nv and therefore the change in free volume in the glass transition interval to remain relatively constant for different polymers. This implies that the observed increase in ΔC_p can be attributed to ϵ, a quantity related to the cohesive energy of the system. Consistent with this argument is the observation that ΔC_p remains relatively constant for the 22 polymers listed in Table I for which one would expect the cohesive energy to be approximately equivalent.

A comparison of heat capacities with the dynamic mechanical data (Figs. 6–8 and Tables III and IV) showed that the only major mechanical relaxation process occurs in the glass transition interval. However, comparison of the dielectric with the mechanical relaxation spectrum (Figs. 6 and 11 and Tables III and IV) showed the dielectric loss maxima to occur at significantly higher temperatures. For example, in the case of polymer 14 the 110-cycle ϵ''_{max} was found at 677°K, 98°K higher than the 110-cycle E''_{max}. These results suggest that rotations of whole chains or chain segments—or even single quinoxaline moieties—that have to dominate dielectric losses are apparently only weakly active, if at all, in the glass transition interval (i.e., in polymer 14, the onset of a dielectric relaxation actually occurs at 580°K, in the T_g range). What then is a plausible mechanism of motion in the glass transition region of polyquinoxalines and probably many other aromatic polymers? As previously pointed out, extremely high barriers to internal rotation in aromatic polymers due to *ortho* substituents and resonance effects are expected. These barriers will vary of course, depending upon a particular flexibilizing group in the chain, a particular *ortho* substituent (e.g., phenyl, hydrogen, etc.), also upon the mass and size of a group or segment to be rotated (i.e., the reduced moment of inertia). While oscillations of quinoxaline rings are possible, such motions apparently do not give rise to dielectric relaxations. (Torsional oscillations of the quinoxaline groups are apparently confined to vibrations or librations). We propose that dominant motions responsible for the glass transition in polyquinoxalines correspond to main chain translations.

A wholly aromatic, long-chain molecule is envisioned to take on the shape of a flexible ribbon rather than of a stiff rod or string of beads The elasticity of the ribbon depends upon the number and kind of flexibilizing components (i.e., oxy, thio, carbonyl sulfone, etc.). Deformation or reorientation in a ribbon segment may occur in the following modes: (1) stretching; (2) out-of-place bending; (3) in-plane bending; (4) twisting (Fig. 14). The first mode, symmetric or asymmetric stretching, is an internal deformation and involves either local vibrations at lower energies or bond breaking at high energies; therefore it is of no particular interest here. The second deformation, designated out-of-plane bending or buckling, depending upon

TABLE IV
Transition Temperatures and Temperatures of Maximum Relaxations for Various Polymers
(A comparison of Various Methods)

Polymer	Calorimetry $(\Delta C_p)_{1/2}$, °K	Dilatometry $\Delta\alpha$, °K	Dynamic mechanical E''_{max}, °K[a]	Dynamic dielectric ϵ''_{max}, °K[a]
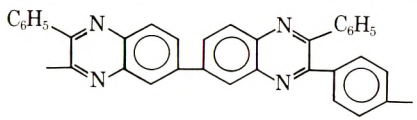	645	638	658	708
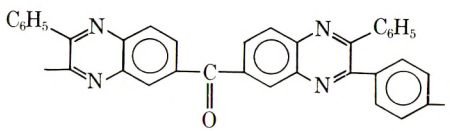	598	595	613	651
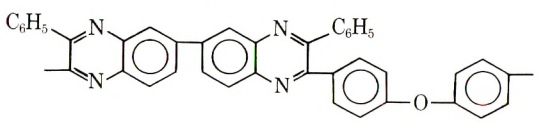	568	567	579	677
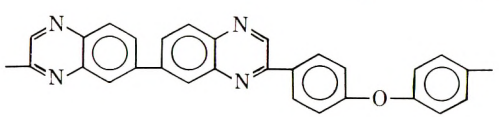	578	580	577	695

[a] Applied frequencies 110 cps.

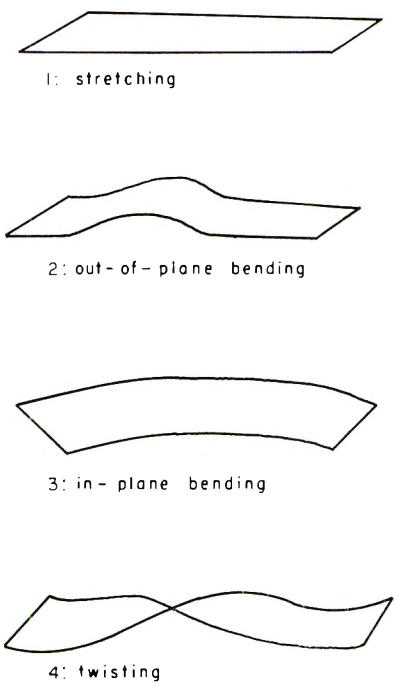

Fig. 14. Deformation in a ribbon segment.

the amplitude, results in longitudinal translations. This type of motion would be strongly mechanically active and give rise to free volume effects. Some hindered rotations in the more flexible portion of the ribbon could take place to cause a dielectric relaxation of low strength and long relaxation times, (i.e., not observable under our experimental conditions). The third motion, in-plane bending (or wagging) involves translations perpendicular to the ribbon axis. The extent to which such a deformation is at all possible would depend upon the inhomogeneity of the ribbon (i.e., number, kind and distribution of flexbilizing components). It could contribute strongly to motion in a highly flexibilized system such as in polymer 22 and wound be only weakly mechanically active in the rigid structure of polymer 1. The fourth motion, twisting, is an out-of-plane deformation involving bond rotations. Depending, among other things, on the time scale (i.e., experimental frequency), the length of the ribbon, and on the number of available equilibrium conformations we can expect relaxations, or multiple relaxations. In any event this motion would be strongly dielectrically active.

Either one or a combination of all transformational motions could occur in the T_g interval; the temperatures of these deformations would depend upon the stiffness and homogeneity of the ribbon. Glass transitions in polyquinoxalines occur as low as 489°K for polymer 22 and as high as 668°K for polymer 1. On the basis of the above model, this behavior can be ex-

plained. The nature of dielectric relaxations, occurring 30 to 100°K above T_g, is less clear. Torsional braid analysis of polymer 14 showed that these strong dielectric losses are also weakly mechanically active. On the other hand, within the limits of our measurements, neither heat capacity nor thermal expansion data reveals the presence of a transition in this region. Nevertheless, the dielectric data shows that this relaxation region is strongly time (frequency)-dependent, and involves relatively high activation energies (ca. 40 kcal). Work is underway to elucidate the nature of this dispersion.

Structure–Property Relationships

The proposed translational mechanism was strongly supported by comparing T_g of phenyl-substituted polyquinoxalines with their unsubstituted analog. If hindered rotations would indeed constitute the underlying mode of motion at T_g, we expect the phenyl-substituted polymers to exhibit higher T_g values, since rotation involving the phenyl side groups is governed by high steric hindrances and the high moment of inertia of this group ($I_r = 20 \times 10^{-40}$ g-cm^2). In the 22 polymers examined, this was not found to be the case. A comparison of polymer 1 with 2 is particularly convincing. Both structures are analogous, containing three fused rings connected by a *p*-phenylene moiety, with the exception that polymer 1 contains phenyl side groups in place of hydrogen atoms. Since the only possible way to achieve bond rotation in polymer 1 is to involve the bulky phenyl side group, this polymer should exhibit a higher T_g for a rotational mechanism to prevail; yet structures 1 and 2 exhibit practically the same T_g.

Other structural effects, of particular interest to the organic chemist were noted. For example, a comparison of polymers 1, 5, 7, 9, and 11 shows that the relative order of flexibilizing groups decreasing T_g (and relaxation temperatures) is diphenyl ether > benzophenone > diphenyl sulfone > biphenyl > phenyl. A comparison of polymers 6, 15, 20, and 22 shows the effect of phenoxy groups on the glass transition temperature (Table V).

TABLE V
Effect of Flexibilizing Groups on T_g

Polymer	Structure	T_g, °K
6	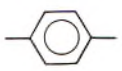	649
15	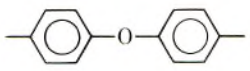	518
20	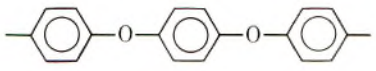	508
22	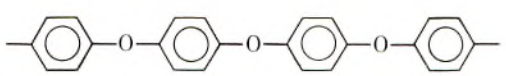	489

Introducing one, two and three successive phenoxy groups into the repeat unit structures produced a pronounced lowering in T_g.

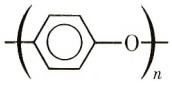

PPO

The glass transition of poly(1,4-phenylene oxide) (PPO) measured under similar conditions occurred at 607°K. We attribute the lower T_g in structures 15, 20, and 22 to greater conformational disorder, (e.g., the presence of quinoxaline rings interrupt chain periodicity).

The effects of copolymerization on T_g and dynamic mechanical and dielectric properties were demonstrated for the biphenyl–benzophenone system. From the results in Table III, the role of the chain flexibilizing benzophenone moiety in decreasing T_g and temperatures of maximum dielectric and mechanical absorptions of copolymers becomes evident.

The influence of different heterorings on the thermal properties of aromatic properties was demonstrated for three polymers:

Polyimide (No T_g)

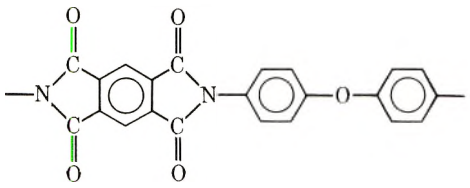

Polyquinoxaline (T_g, 626°K)

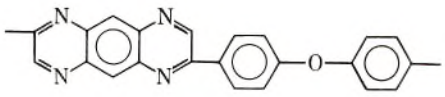

Polyquinoxaline

Poly-*as*-triazine (T_g, 496°K)

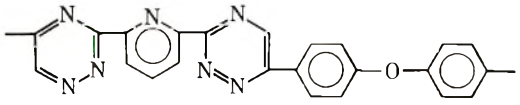

Poly-*as*-triazine

For brevity only the T_g results will be discussed here. (A detailed study of these polymers will be published in the near future.) The polyimide (H-film), has no glass transition temperature up to 800°K and decomposes shortly thereafter. Its structural analog, the polyquinoxaline (which was specifically synthesized for comparative purposes) exhibits a T_g at 626°K. While the polyimide is insoluble, the polyquinoxaline is very soluble in many organic solvents. Although the repeat unit structure of both poly-

mers are very similar, they differ in several important aspects. First, structural isomerism exists in the polyquinoxaline giving rise to two isomeric forms:

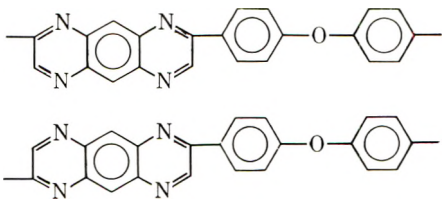

On the other hand, structural isomerism is not possible in the polyimide. Consequently the polyimide is configurationally ordered while the polyquinoxaline is not. Both polymers gave the diffuse x-ray pattern characteristic of amorphous materials and indicating conformational disorder. The fact that the polyimide exhibits no T_g below its decomposition temperature may be attributed in part to configurational regularity. In this connection it is to be noted that even in the absence of conformational periodicity, configurationally ordered chains could cause particularly high barriers to translational motion.

Secondly, the carbonyl groups of the imide ring are more polarizable than the nitrogen atoms in the quinoxaline rings. This leads to stronger dipole interactions, giving rise to stronger interchain association in the polyimide. This effect would induce restrained translational motion and therefore, increase T_g.

Third, the possibility of mild crosslinking exists in the polyimide structure, resulting in some amide crosslinks during the imidization reaction, and again increasing the T_g of this polymer.

At this time it is not clear to what extent each of the three factors mentioned contributed to the absence of a glass transition in polyimide.

The poly-*as*-triazine differs from the polyimide and polyquinoxaline, in that its heterorings are linked to the chain by single bonds rather than fused to benzene rings, and therefore enhance chain mobility and produce an expected decrease in T_g.

Finally we note that properties such as heat capacity, coefficient of linear thermal expansion, dynamic modulus, and T_g of these polymers cannot always be treated as materials constants. As exemplified by the modulus–temperature data in Figures 9 and 10, such properties are variable, depending, among other things, upon sample environment and thermal history.

When nonequilibrium techniques are employed, it is important to establish a range of heating rates (as was done in Fig. 5) in which reproducible results can be obtained. Since transitions and relaxations in aromatic polymers take place at relatively high temperatures, experimental time scales must be kept short, and samples must be protected by inert atmospheres to avoid side effects such as thermal and oxidative crosslinking or degradation during measurements.

References

1. R. F. Boyer, in *Transitions and Relaxations in Polymers* (*J. Polym. Sci., C*, **14**), R. F. Boyer, Ed., Interscience, New York, 1966, p. 3.
2. D. U. McCall, (*Nat. Bur. Stand. Spec. Publ.*), Nat. Bur. Stand., Washington D.C., 1969, pp. 301, 475.
3. E. Butta, S. DePetris, and M. Pasquini, *J. Appl. Polym. Sci.*, **13**, 1073 (1969).
4. R. Matles and E. G. Rochow, *J. Polym. Sci. A-1*, **4**, 375 (1966).
5. S. L. Copper, A. D. Mair, and A. V. Tobolsky, *Text. Res. J.*, **35**, 1110 (1965).
6. M. Baccaredda, E. Butta, V. Frosini, and S. DePetris, *Mat. Sci. Eng.*, **3**, 157 (1968).
7. P. M. Hergenrother and H. H. Levine, *J. Polym. Sci. A-1*, **5**, 1453 (1967).
8. W. Wrasidlo and J. M. Augl, *J. Polym. Sci. A-1*, **7**, 3393 (1969).
9. W. Wrasidlo and J. M. Augl, *J. Polym. Sci. B*, **8**, 69 (1970).
10. W. Wrasidlo and J. M. Augl, *Macromolecules*, **3**, 544 (1970).
11. P. M. Hergenrother and D. E. Kiyohara, *Macromolecules*, **3**, 387 (1970).
12. B. Wunderlich, in *Differential Thermal Analysis, Part IV*, A. Weissberger, Ed., in press, Chap. 17.
13. D. C. Ginnings and G. T. Furukawa, *J. Amer. Chem. Soc.*, **75**, 522 (1963).
14. M. Takayanagi and M. Yoshino, *J. Japan Soc. Text. Mat.*, **8**, 308 (1959).
15. J. K. Gillham, *Polym. Eng. Sci.*, **7**, 225 (1967).
16. *American Institute of Physics Handbook*, 2nd ed. McGraw-Hill, New York, 1963, pp. 4–66.
17. J. M. O'Reilly and F. E. Karasz, *J. Polym. Sci.*, **4**, 54 (1966).
18. B. Wunderlich, *J. Phys. Chem.*, **64**, 1052 (1960).
19. J. Frenkel, *Kinetic Theory of Liquids*, Oxford Univ. Press, London, 1946.
20. H. Eyring, *J. Chem. Phys.*, **4**, 283 (1936).
21. B. Wunderlich, *Adv. Polym. Sci.*, **7**, 282 (1970).

Received January 14, 1971

JOURNAL OF POLYMER SCIENCE: PART A-2 VOL. 9, 1629–1640 (1971)

Sorption Properties of Polypropylene

HIROSHI OCHIAI, KUNIHIKO GEKKO,* and
HITOSHI YAMAMURA, *Department of Chemistry, Faculty of Science, Hiroshima University, Hiroshima 730, Japan*

Synopsis

The sorption properties of atactic polypropylene (APP) and isotactic polypropylene (IPP) were studied by equilibrium sorption of various organic solvents. The variation of the Flory-Huggins interaction parameter χ for the APP-CCl_4 system at 25°C was expressed as a function of the volume fraction v_2 of polymer by the relation: $\chi = 0.113 \exp\{1.879\, v_2\}$. The average molecular weight $\bar{M}_c$ of the polymer chains between successive crystallites for IPP subjected to different thermal treatments was calculated to be 250 to 350 by the equation of Flory and Rehner. From the variation of $\bar{M}_c$ with solvent concentration, we estimated the number fraction of polymer chains actually contributing to elastic deformation. The clustering function for solvent in the polymer calculated by the method of Zimm and Lundberg decreased linearly from a positive value to -1 with increasing solvent concentration. Clustering of solvent molecules was found to occur more easily in APP than in IPP.

INTRODUCTION

It has long been known that useful information about the physical properties of polymeric materials can be derived from measurement of equilibrium swelling and of the vapor pressure of solvent over polymer solutions.[1–4] The theory of polymer solutions is well established for such relatively simple polymer solutions as rubber–benzene[1,2] and polystyrene–benzene[3,4] but not yet for such complicated systems as crystalline polymers and polyelectrolytes. In particular, the thermal and mechanical history and solvent treatment influence considerably the permeability of a crystalline polymer, so that there exist many unsolved problems in the treatment of experimental data. Therefore studies of these polymers have been carried out by many investigators.[5–8] In this work, measurements of vapor sorption and equilibrium swelling were made on atactic and isotactic polypropylene in order to clarify the relation between the sorption properties of such a highly crystalline polymer and the state of aggregation of the polymer chains.

The activity a_1 of solvent in a solution of amorphous (uncrosslinked) polymer is expressed by an equation due to Flory and Huggins:[9,10]

$$\ln a_1 = \ln v_1 + v_2 + \chi v_2^2 \tag{1}$$

* Present address: Department of Food Science and Technology, Faculty of Agriculture, Nagoya University, Nagoya, Japan.

Here, v_1 and v_2 are the volume fractions of solvent and polymer, respectively, and χ is an interaction parameter. For crosslinked polymer systems, however, a term for the free energy corresponding to elastic deformation of chain segments should be added to eq. (1). If the swelling process occurs with no heat change other than the heat of mixing and if mixing occurs without significant change in the total volume of the system, the activity can be represented by the equation of Flory and Rehner:[11,12]

$$\ln a_1 = \ln v_1 + v_2 + \chi v_2^2 + (\rho_2 V_1/\bar{M}_c)[\langle\alpha\rangle_0^2 v_2^{1/3} - (2v_2/f)] \qquad (2)$$

where $\bar{M}_c$ is the average molecular weight of the elastically effective chains, ρ_2 is the density of the polymer, V_1 is the molar volume of the solvent, $\langle\alpha\rangle_0$ is the ratio r/r_0 of the mean end-to-end distances for the swollen and unswollen polymer, and f is the functionality of crosslinking junctions. In dealing with data for a crystalline polymer, we assume that it is composed of crystalline and amorphous regions, and that the crystalline regions are not accessible to solvent molecules. Since the crystallites are considered to constitute effective crosslinking junctions of large functionality f, the term $2v_2/f$ can be neglected, as f is much greater than $2v_2$. Thus, if the values of χ and $\langle\alpha\rangle_0$ are known, the value of $\bar{M}_c$, i.e., the average molecular weight of amorphous chains between successive crystallites, may be estimated. For such a highly crystalline polymer as polypropylene with an especially large modulus, the polymer chains in the amorphous regions are expected to be constrained by the surrounding crystallites to some extent, and the degree of this constraint characterizes the physical properties of crystalline polymers. From this point of view, it seems to be interesting and important to study the internal constraint of these crystalline polymers through sorption measurements.

EXPERIMENTAL

Samples

Atactic polypropylene (APP), furnished by Sumitomo Chemical Industries, Ltd., was extracted with ether to remove stereoregular polymer completely. The extracted sample was purified by reprecipitation with acetone as a poor solvent, and was freeze-dried to remove solvent completely. The viscosity-average molecular weight of the APP was estimated to be 1.50×10^4 from viscosity measurements in benzene at 30°C.[13] The density of APP was determined by flotation in various concentrations of aqueous methanol at various temperatures: values were 0.854 g/cc at 25°C, 0.847 at 35°C, and 0.841 at 45°C.

Isotactic polypropylene samples were obtained by the following procedure. About 10 g of Sumitomo sample S-101 was dissolved under a nitrogen atmosphere at 140°C in 500 ml of tetralin containing 0.1 g/100 ml Ionol antioxidant, and the solution was then poured into acetone to reprecipitate the polymer. The residue (94.5%) obtained by *n*-heptane extraction was

used as isotactic polypropylene (IPP). The average molecular weight of the sample from the intrinsic viscosity in tetralin at 135°C was found to be 2.05×10^5 according to the relation derived by Parrini.[14] For swelling measurements, this polymer was used in the form of a film 0.1 mm thick, which was molded by hot-pressing and annealing at 125°C *in vacuo* for 3 hr. The density of this film was 0.907 g/cc at 25°C. To study the relation between the thermal history and swelling, six samples were subjected to different thermal treatments as follows. A small quantity of polymer was confined in a glass tube under vacuum, heated to 180°C, and then cooled to room temperature. The slowly cooled sample (I) was prepared by lowering the temperature from the melting temperature to room temperature over a period of 4 days. The quenched sample (VI) was prepared by putting the glass tube containing the molten polymer into a liquid nitrogen bath. The annealed samples (II–V) were prepared by maintaining the previously quenched samples at a given temperature for 3 hr and then cooling slowly to room temperature. The crystallinity of these samples was estimated from Natta's formula:[15]

$$\text{Per cent crystallinity} = \frac{0.983 + 9(t + 180) \times 10^{-4} - (1/d)}{4.8(t + 180) \times 10^{-6}} \quad (3)$$

where d is the density at t°C.

Methods

Apparatus identical to that used by Nakajima et al.[16] was used for measuring the equilibrium sorption of the vapor. A polymer sample was suspended from a calibrated quartz-spring balance in the saturated vapor of the organic solvent. The equilibrium pressure and the weight of the sorbed vapor were determined from the point at which the extension, as measured by a cathetometer, remained constant for 12 hr. The volume fractions v_2 and v_1 of polymer and sorbed solvent, respectively, in the amorphous regions at equilibrium were calculated from the experimentally determined weight fractions by assuming that the solvent volume and the polymer volume are additive on mixing, that sorption occurs only in the amorphous regions of the polymer, and also that the degree of crystallinity is not changed by swelling. The density of the amorphous region in IPP was assumed to be equal to that of the completely amorphous sample, i.e., 0.854 g/cc at 25°C.[17] The organic solvents used in this work were special grade reagents (without further purification). Heat-degassed dioctyl phthalate, a substance of negligible vapor pressure, was mixed with solvent to obtain the desired vapor pressure. The activity of the vapor was assumed to be p_1/p_1°, where p_1° and p_1 are the vapor pressures of pure solvent and polymer solution respectively at a given temperature. Equilibrium sorption measurements were performed with a bulk sample of APP and a film (thickness of 0.1 mm, $d = 0.907$ g/cc) of IPP.

For the equilibrium swelling measurements, the surface of the sample was cleaned with methanol, and the sample was dried to constant weight *in*

vacuo. Samples were then immersed in 20 ml of liquid solvent at a given temperature. At 24-hr intervals the samples were quickly removed, excess liquid was wiped from their surfaces with filter paper, and they were weighed. This procedure was repeated to determine equilibrium swelling.

RESULTS AND DISCUSSION

Concentration Dependence of Polymer–Solvent Interaction Parameter

The experimental results of equilibrium sorption for the APP–CCl_4 system at 25°C are shown in Table I and Figure 1. Figure 1 also shows the results for the IPP–CCl_4 system at 25°C, which will be discussed in the following section. The values of χ calculated by using eq. (1) are listed in the third column of Table I and shown in Figure 2 as a function of the volume fraction of polymer. It is evident that χ increases as v_2 is increased. The relation between these values of χ and v_2 can be expressed by

$$\chi = 0.113 \exp\{1.879\, v_2\} \tag{4}$$

for the APP–CCl_4 system at 25°C.

Expansion of eq. (4) in series leads to

$$\chi = 0.113 + 0.0212 v_2 + 0.200 v_2^2 + \ldots \tag{5}$$

This expanded form agrees with Huggin's theory[18,19] of the concentration dependence of χ. This agreement is probably due to the fact that the interaction between molecules of APP and CCl_4 is very weak and hence such solutions exhibit relatively simple structures. The interaction parameter χ can be expressed theoretically as a function of temperature alone according

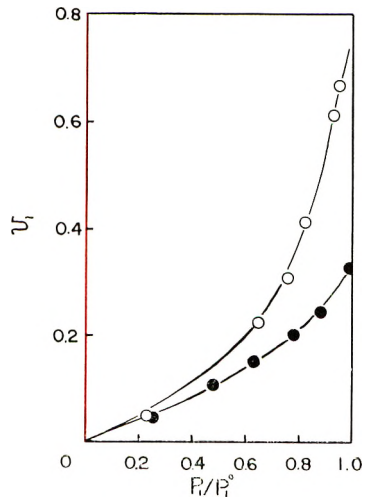

Fig. 1. Sorption isotherms of carbon tetrachloride in polypropylene at 25°C: (○) atactic polypropylene; (●) isotactic polypropylene.

TABLE I
Vapor Sorption Data for the System Atactic Polypropylene–CCl_4 at 25°C

a_1	v_2	χ	$a_1/1-v_2$
0.950	0.334	0.221	1.448
0.935	0.392	0.250	1.538
0.819	0.588	0.287	1.988
0.756	0.694	0.438	2.471
0.646	0.778	0.480	2.910
0.228	0.954	0.704	4.957

to Flory's theory,[20] while in fact this parameter has been found to depend on the concentration for many polymer solutions.[21–24] At present, it is difficult to explain the numerical factors in eq. (4) or (5) in terms of the molecular parameters.

Limited Sorption in Crystalline IPP and Equilibrium Swelling of Thermally Treated IPP

Results of measurements of equilibrium sorption are listed in Table II for the IPP–CCl_4 system at 25°C. Typical plots of a_1 versus v_1 for the IPP–CCl_4 system at 25°C have already been shown together with those for the APP–CCl_4 system in Figure 1. In calculating $\bar{M}_c$ from eq. (2), we assumed that χ for the amorphous regions of IPP has the same value as for APP at the same concentration and that the relation $\langle\alpha\rangle_0^2 = 1$ holds approximately both before and after swelling.

Furthermore, we also plotted the sorption data in Figure 3 according to a rearranged form of eq. (2):[6,7]

$$(\ln a_1 - \ln v_1 - v_2)/v_2^2 = \chi + (\rho_2 V_1/\bar{M}_c)v_2^{-5/3} \qquad (6)$$

in which the concentration dependence of χ is neglected. The values of χ and $\bar{M}_c$ calculated from the intercept with the ordinate and the slope by use of eq. (6) were $\chi = 0.297$ and $\bar{M}_c = 225$. Values of $\bar{M}_c$ of similar magnitude were found for polypropylene[7] and polyethylene.[6]

TABLE II
Vapor Sorption Data for Isotactic Polypropylene–CCl_4 at 25°C

a_1	v_2	χ	$\bar{M}_c$	g^a
1.000	0.680	0.39	253	1.000
0.971	0.682	0.40	294	0.860
0.879	0.757	0.47	290	0.871
0.774	0.801	0.51	343	0.737
0.624	0.845	0.56	528	0.479
0.475	0.891	0.62	774	0.340
0.245	0.948	0.68	1977	0.128

[a] The quantity g denotes the ratio of each value of $\bar{M}_c$ at $a_1 < 1$ to the value of $\bar{M}_c$ (= 253) at $a_1 = 1$.

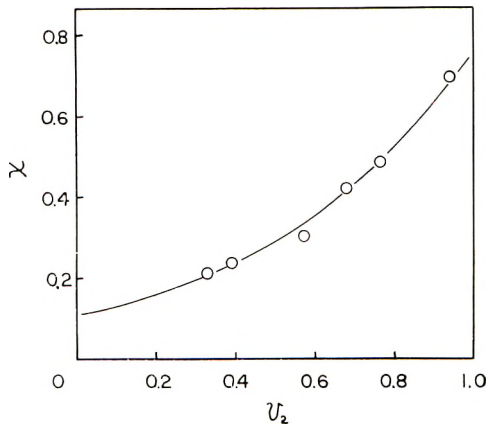

Fig. 2. Interaction parameter χ vs. v_2 for the system atactic polypropylene–CCl_4 at 25°C: (——) $\chi = 0.113 \exp\{1.879\, v_2\}$.

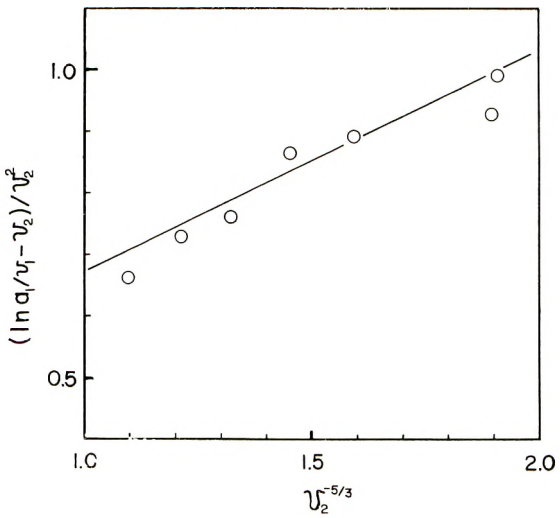

Fig. 3. Plot of $(\ln a_1/v_1 - v_2)/v_2^2$ vs. $v_2^{5/3}$ for the IPP–CCl_4 system.

At fixed activity, the value of v_1 for IPP is smaller than that of v_1 for IPP. That is, the amount of absorbed vapor on IPP is considerably less than that predicted on the assumption that the crystallites act merely as dispersed particles. In other words, for crystalline IPP (crystallinity 67%) the polymeric chains in the amorphous region can be considered to be spatially constrained and elastically deformed by the crystallites so that the penetration of solvent molecules is depressed. It should be noted from Table II that the molecular weight ($\bar{M}_c$) of the amorphous chain segments of IPP calculated by eq. (2) decreased with increasing solvent activity. This may indicate that the amorphous segments of highly crystalline polymers are in a very different situation from those of the usual amorphous

network polymer. The difference between the activities for APP and IPP at the fixed concentration corresponds to the last term in eq. (2). Since constancy of internal energy can be assumed in the deformation of polymer chains by swelling, the last term in eq. (2) must be ascribed to the variation of elastic entropy, and this variation naturally affects the value of $\bar{M}_c$. In the range of negligibly small variation of elastic entropy ($v_1 < 0.05$), the value of $\bar{M}_c$ will apparently approach infinity. In such a case, the amorphous region of IPP will not be influenced by crystallites as crosslinking junctions. Therefore it is reasonable to presume that the penetration of solvent molecules into the amorphous regions of IPP is similar to that of APP at least in equilibrium swelling at low solvent activity. This behavior can be explained by considering the distribution of elastic potential energy in the amorphous regions of IPP. In other words, in equilibrium swelling at a lower solvent activity, the solvent molecules initially penetrate into the polymer and absorb at the sites of lowest elastic potential, namely, at those subjected to the least constraint.

Next, let us consider the dependence of $\bar{M}_c$ on solvent concentration or activity. If no change occurs in the network during swelling, the value of $\bar{M}_c$ should be relatively constant. In the equilibrium swollen state, the network chains are expanded until the osmotic pressure generated by the mixing of solvent with polymer is balanced by the elastic retractive force of the network, and $\bar{M}_c$ is related to the effective number ν_e of chains in the network, by $\nu_e = \rho N_a/\bar{M}_c$. Therefore, the observed variation of $\bar{M}_c$ can be interpreted in terms of ν_e. At $a_1 = 1$, the osmotic pressure generated has its maximum value, all the network chains take part in the swelling deformation, and each network exhibits the maximum expansion, where the networks are in the critical elastic state. Then the values of $\bar{M}_c$ or ν_c at $a_1 < 1$ are only apparent values and will be designated $\bar{M}_c^*$ or ν_e^*. Hence, the observed increase of $\bar{M}_c$ with decreasing solvent concentration implies a decrease of the number of elastically effective chains actually contributing to the elastic deformation. Denoting the ratio ν_e^*/ν_e or $\bar{M}_c/\bar{M}_c^*$ by g (here $\bar{M}_c = 253$), we modify eq. (2) as follows:

$$\ln a_1 = \ln v_1 + v_2 + \chi v_2^2 + (g\rho_2 v_1/\bar{M}_c)v_2^{1/3} \qquad (2')$$

Then the parameter g must express the number fraction of the elastically effective chains actually contributing to the elastic deformation in the equilibrium swollen state at the given solvent activity, and also must express the degree of deformation of the polymer chain in relation to the maximum expanded state. As can be seen in Figure 4, the value of g approaches unity with increasing v_1. It is an interesting fact that g is proportional to v_1 in the initial stage of swelling, which supports our previous report[25] that the activation energy for the molecular motion of the backbone chain of IPP decreases inversely with increasing degree of swelling in the range $0 < v_1 < 0.1$. The variation of g probably gives a measure of the mobility of the polymer chains, which is enhanced by the penetration of solvent molecules.

For the six samples of IPP subjected to different thermal treatments, the

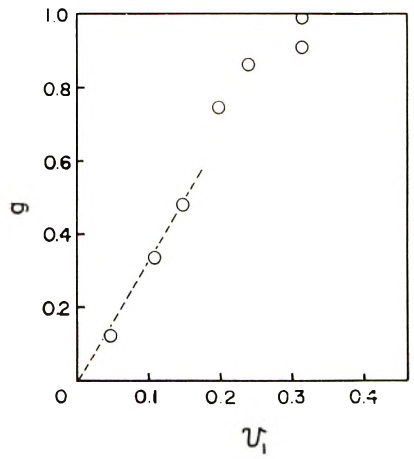

Fig. 4. Values of g vs. v_1 in isotactic polypropylene–CCl_4 at 25°C.

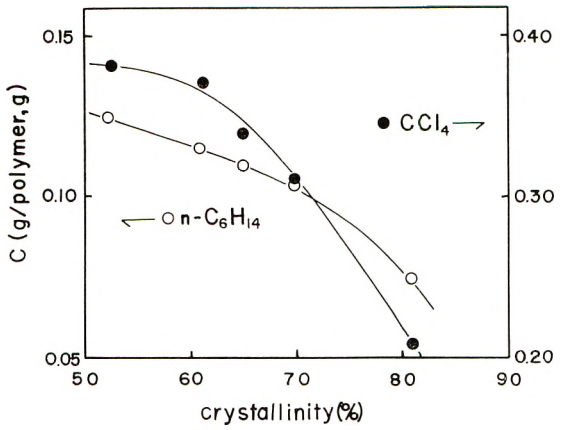

Fig. 5. Concentration of sorbed solvent vs. crystallinity in isotactic polypropylene at 25°C.

results of equilibrium swelling in CCl_4 and in n-hexane at 25°C are shown in Figure 5 and Table III. In the calculation of $\bar{M}_c$ from the swelling data on n-hexane, χ was taken at 0.27, since χ for n-hexane was found to be independent of concentration.[7]

As expected, the degree of swelling decreased with increased annealing temperature. In general, one might also expect that $\bar{M}_c$ should decrease as crystallites grow during annealing of the polymer at temperatures above the glass transition.[26] Also, from x-ray measurements it is observed that crystalline regions become more perfect as the annealing temperature is increased. In the present work, however, it was found that the higher the annealing temperature, the larger the value of $\bar{M}_c$. This result can be explained through the kinetic theory[27] of partial melting and recrystallization involving a relatively large amount of paracrystallite, as reported from

TABLE III
Effect of Thermal Treatment on the Swelling of Isotactic Polypropylene at 25°C

Sample	Condition of treatment	Density, g/cc	Crystallinity, %	*n*-Hexane			Carbon tetrachloride		
				Solvent, g / Polymer, g	v_2	$\bar{M}_c$	Solvent, g / Polymer, g	v_2	$\bar{M}_c$
I	Slow cooled from melt	0.919	81	0.074	0.666	369	0.208	0.632	316
II	Annealed at 150°C	0.910	70	0.103	0.693	321	0.309	0.646	300
III	Annealed at 120°C	0.906	65	0.109	0.713	290	0.339	0.658	287
IV	Annealed at 100°C	0.903	61	0.115	0.721	278	0.372	0.660	284
V	Annealed at 60°C	0.895	51	0.124	0.747	242	0.382	0.698	245
VI	Quenched	0.896	53	0.121	0.752	236	0.376	0.702	239

x-ray diffraction[28] and viscoelastic[29] studies. That is to say, during swelling deformation these paracrystalline parts can act as crosslinking junctions similar to the usual crystalline regions, whereas after thermal treatment they reorient or melt out, depending on whether the size of a paracrystallite is larger or smaller than some critical size governed by the temperature. Consequently, the extent of interlamellar linking and entanglement which would be of major importance in sorption was decreased by thermal treatment. The lower density of sample V, as compared to sample VI, may be explained by the fact that the smectic crystalline form existing in large quantity in a quenched sample melts out at about 60°C.[29] Thus, it seems that the characteristic swelling properties of thermally treated IPP can best be explained by the kinetic theory of melting and recrystallization of paracrystallites. However, it should be noted that substantial changes in crystalline structure, such as recrystallization by solvent and fragmentation of crystalline domains by the osmotic pressure generated by mixing with solvent, may occur during the sorption and swelling measurements, and that such changes will increase the value of $\bar{M}_c$.

Solvent Clustering Function

For the clarification of the difference of sorption properties between APP and IPP in the range of small v_1, estimation of the magnitude of the intermolecular interactions from the effect of solvent clustering has been shown to be useful. An appropriate relation is obtained from an expression derived by Zimm and Lundberg[30]

$$\frac{G_{11}}{\bar{V}_1} = -v_2 \frac{\partial}{\partial a_1}\left(\frac{a_1}{1 - v_2}\right) - 1$$

where G_{11} is the cluster integral and $\bar{V}_1$ is the partial molecular volume of the solvent. When the activity coefficient does not vary with the concentration, as in the case of an ideal solution, G_{11} is $-\bar{V}_1$. This means that a particular molecule of type 1 (solvent) in such a polymer–solvent system excludes its own volume to the other molecules without affecting their random distribution. If the solvent molecules are inclined to aggregate or to avoid one another, G_{11} correspondingly assumes a large positive or a negative value, respectively.

Values of the clustering function, $G_{11}/\bar{V}_1$, were calculated for the sorption of CCl_4 in polypropylene at 25°C by assuming volume additivity. These are plotted against volume fraction v_1 in Figure 6.

In both the APP–CCl_4 and IPP–CCl_4 systems, it can be seen that a linear relation exists between $G_{11}/\bar{V}_1$ and v_1. Furthermore, in the initial stage of swelling the solvent molecules have a strong tendency to form clusters. The initially high value of $G_{11}/\bar{V}_1$ implies that after the first solvent molecule has penetrated into the polymer and loosened the structure, subsequent solvent molecules are able to enter more easily in the neighborhood of the first solvent molecule than elsewhere. Furthermore the smaller values of $G_{11}/\bar{V}_1$ for IPP than for APP can be explained as follows. Although the

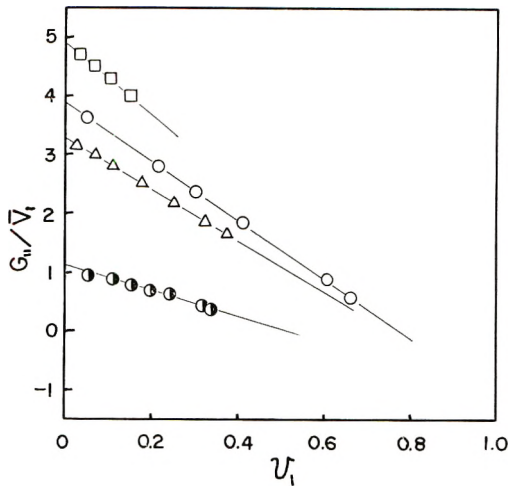

Fig. 6. Clustering function $G_{11}/\bar{V}_1$ vs. v_1 in the system polypropylene–CCl_4 at 25°C: (○) atactic polypropylene; (◑) isotactic polypropylene; (□) polyethylene–methyl bromide;[6] (△) polyethylene–ethyl bromide.[6]

molecular chains of APP are easily loosened by the penetration of solvent molecules, the mobility of amorphous molecular chains of IPP is restricted by the crystallites. The site including the first penetrant molecule will be in a state of higher elastic potential than the other vacant sites. Therefore, in IPP, subsequent solvent molecules penetrate selectively into other amorphous regions of lower potential, rather than into amorphous regions already containing penetrant molecules. Hence the clustering probability of solvent molecules will be decreased. These situations can be better explained by considering the random distribution of elastic potential in the amorphous regions of IPP, as mentioned previously.

References

1. G. Gee and L. R. G. Treloar, *Trans. Faraday Soc.*, **38**, 147 (1942).
2. G. Gee and W. J. C. Orr, *Trans. Faraday Soc.*, **42**, 507 (1946).
3. C. E. Baughan, *Trans. Faraday Soc.*, **44**, 495 (1948).
4. H. Tompa, *J. Polym. Sci.*, **8**, 51 (1952).
5. R. F. Baddour, A. S. Michaels, H. J. Bixler, R. P. De Filippi, and J. A. Barrie, *J. Appl. Polym. Sci.*, **8**, 897 (1964).
6. C. E. Rogers, V. Stannett, and M. Szwarc, *J. Phys. Chem.*, **63**, 1406 (1959).
7. K. P. Kwei and T. K. Kwei, *J. Phys. Chem.*, **66**, 2146 (1962).
8. A. S. Michaels and R. W. Hausslein, in *Transport Phenomena in Polymeric Films* (*J. Polym. Sci. C*, 10), C. A. Kumins, Ed., Interscience, New York, 1965, p. 61.
9. P. J. Flory, *J. Chem. Phys.*, **9**, 660 (1941); *ibid.*, **10**, 51 (1942).
10. M. L. Huggins, *J. Chem. Phys.*, **9**, 440 (1941).
11. P. J. Flory and J. Rehner, Jr., *J. Chem. Phys.*, **11**, 512, 521 (1943).
12. P. J. Flory, *J. Chem. Phys.*, **18**, 108 (1950).
13. F. Danusso and G. Moraglio, *Atti. Accad. Lincei, Rend. Sci. Fis Mat. Nat.*, **25**, 509 (1959).
14. P. Parrini, F. Sebastiano, and G. Messina, *Makromol. Chem.*, **38**, 27 (1960).

15. F. Danusso, G. Moraglio, and G. Natta, *Ind. Plast. Mod.*, **10**, 40 (1958).
16. A. Nakajima, H. Yamakawa, and I. Sakurada, *Kobunshi Kagaku*, **14**, 333 (1957).
17. R. G. Quynn, J. L. Riley, D. A. Young, and H. D. Noether, *J. Appl. Polym. Sci.*, **2**, 166 (1959).
18. M. L. Huggins, *J. Polym. Sci.*, **16**, 209 (1955).
19. M. L. Huggins, *J. Amer. Chem. Soc.*, **86**, 3535 (1964).
20. P. J. Flory, *Principles of Polymer Chemistry* Cornell Univ. Press, Ithaca, N. Y., 1953, Chaps. 11–13.
21. M. Senez and H. Daoust, *Can. J. Chem.*, **40**, 734 (1962).
22. P. J. Flory and H. Daoust, *J. Polym. Sci.*, **25**, 429 (1957).
23. W. R. Krigbaum and D. A. Geymer, *J. Amer. Chem. Soc.*, **81**, 1859 (1959).
24. D. Patterson and S. N. Bhattacharya, *Polymer*, **6**, 466 (1965).
25. K. Gekko, H. Ochiai, and H. Yamamura, *J. Sci. Hiroshima Univ., A-II*, **31**, 111 (1967).
26. L. Manderkern, *Crystallization of Polymers*, McGraw-Hill, New York, 1964.
27. K. Kamide and M. Sanada, *Kobunshi Kagaku*, **24**, 662 (1967).
28. G. W Schael, *J. Appl. Polym. Sci.*, **10**, 901 (1966).
29. M. Takayanagi, *Kogyo Kagaku Zasshi*, **63**, 1492 (1960).
30. B. H. Zimm and J. L. Lundberg, *J. Phys. Chem.*, **60**, 425 (1956).

Received December 4, 1968
Revised December 21, 1970

JOURNAL OF POLYMER SCIENCE: PART A-2 VOL. 9, 1641–1655 (1971)

Morphology of Polyethylene Crystallized Under the Simultaneous Influence of Pressure and Orientation in a Capillary Viscometer

RICHARD G. CRYSTAL, *Rochester Research Laboratories, Xerox Corporation, Rochester, New York 14603, and* JOHN H. SOUTHERN,* *Polymer Science and Engineering, University of Massachusetts, Amherst, Massachusetts 01002*

Synopsis

The morphology of high-density polyethylene crystallized under simultaneous pressure and shear in an Instron capillary viscometer has been examined by scanning electron microscopy, electron microscopy, and selected-area electron diffraction. Two distinct fibrous morphologies were observed in these unusually transparent strands. The outer sheath was composed of fibers, 3000 Å in diameter, aligned parallel to the extrusion direction and apparently interconnected by a lamellar cross texture. A highly crystalline ribbon texture composed of fine fibers, 200–250 Å in diameter, dominated the inner core. Sharp-spot electron diffraction patterns obtained from these central ribbons indicated a high degree of *c*-axis orientation parallel to the fibers and an extended-chain crystal structure. The melting behavior of both irradiated and unirradiated strands examined by differential scanning calorimetry was consistent with the formation of two distinct crystalline morphological units.

INTRODUCTION

The morphologies of linear polyethylene crystallized from the melt under high pressure and crystallized under shear from both the melt and dilute solution have been reported previously. Wunderlich and others[1–6] have described the extended-chain structure crystallized under static pressures of at least 300 atm. The morphology so produced is characterized by striated, extended-chain crystals in which the molecular axis is oriented parallel to the striations. Pennings and others[7–9] have demonstrated that a fibrous morphology is generated when, for example, a dilute solution of polyethylene (1% in xylene) is stirred during crystallization. Electron microscopy has shown that the individual fibers crystallized under these shearing conditions contain chain-folded lamellae attached to an extended chain central backbone, resulting in a "shishkabob" arrangement. Furthermore, Keller and Hill[10,11] have shown that an analogous, fibrous crystalline structure can be generated when a lightly cross-linked polyethylene is

* Present address: Technical Center, Monsanto Company, Pensacola, Florida 32502.

cooled from the melt under stress. They reported extensive evidence that that resulting morphology is a consequence of extended-chain backbones acting as sites for nucleation of chain-folded growth in directions perpendicular to the extended-chain crystal structure.

This paper describes the crystalline morphology induced in linear polyethylene when it is crystallized under the simultaneous influence of flow orientation and high pressure realized in the Instron capillary rheometer. The pressure and orientation effects resulted in an unusually transparent high density polyethylene having a significant content of highly oriented crystallites.[12–14] The resulting highly ordered, fibrous texture was observed to have many similarities to morphologies generated in shear-crystallized, high-pressure-crystallized, and cold-drawn polyethylene.

EXPERIMENTAL

The polymer used in this study was commercially available high-density polyethylene, Dupont Alathon 7050, having number- and weight-average molecular weights of 18,400 and 52,500, respectively. Samples were prepared in the Instron rheometer operated at a constant plunger velocity by using a capillary 0.0508 cm in diameter and 1.55 cm long with a 90° entrance angle. Crystallization was induced under the combined orientation and pressure effects produced at a 0.5 cm/min plunger velocity and a rheometer temperature of 136°C.

After the plunger was activated, a sustained pressure rise was observed (see Fig. 1), together with abnormal extrudate swelling. Both factors were evidence of crystallite formation. Crystallite nucleation and growth were expected, since the equation of state developed by Wunderlich[1] for high-density polyethylene indicated that the melt was definitely in a supercooled state under the existing pressure and temperature. An observed decrease in the linear extrusion velocity, attributed to crystallization, was accompanied by a rapid increase in the pressure to the 1920 atm upper limit available in the Instron rheometer. The pressure trace (Fig. 1) showed a distinct discontinuity at 575 atm which occurred after crystallization had begun. This inflection point implied that crystallization had resulted in a significant contraction of the polyethylene in the reservoir. Plunger motion was halted at 1920 atm, but extrusion was continued at 0.02 cm/min by adjusting pressure.[13] The distinctive sample morphology discussed herein resulted from the intense orientation effects that occurred as the crystallizing polyethylene was forced under 1920 atm from the cylindrical reservoir of 0.9530 cm diameter into the 0.0508 cm capillary. The partially crystalline mass was subjected to high shear as well as pressure, leading to crystal reorganization as well as additional crystallization. The higher crystalline content was confirmed by the increased heat of fusion of the transparent strands obtained from the capillary relative to that of the polyethylene obtained from the reservoir.[12] The specimens were removed from the rheometer after cooling to 114°C under 1920 atm. This cooling cycle

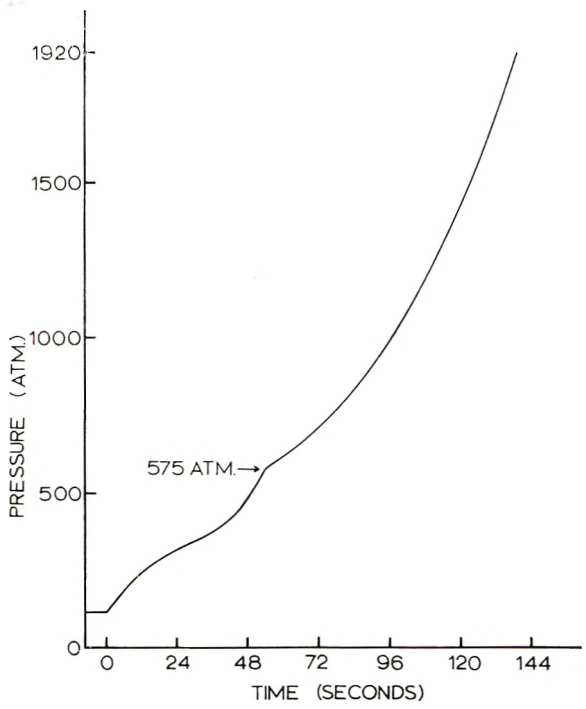

Fig. 1. Instron pressure trace at 136°C under a plunger velocity of 0.5 cm/min with a capillary of 0.0508 cm diameter, 1.55 cm length, and 90° entrance angle.

circumvented the melting that would have occurred at 136°C and atmospheric pressure.

Specimens were examined by scanning electron microscopy (SEM) as well as by direct transmission and replication electron microscopy (TEM). SEM specimens were prepared by fracturing the transparent strands longitudinally, vacuum-coating with 50 Å gold film, and then observing with a Cambridge Ultrascan instrument. TEM specimens were prepared using such techniques as one-step and two-step replication methods, ultramicrotomy with Br_2 staining, and selected-area electron diffraction. A Phillips EM 200 electron microscope equipped with a tilting stage and a Jeolco T7 electron microscope were used to observe the TEM specimens. Preparation and observational procedures will be further discussed as necessary in conjunction with specific micrographs.

RESULTS

Sample Appearance

The transparent strands were formed by a procedure that was similar to a drawing operation. In light of Peterlin's observation that extensive drawing causes localized melting during deformation,[15] it was anticipated that the restructured extruded strands would have a morphology different

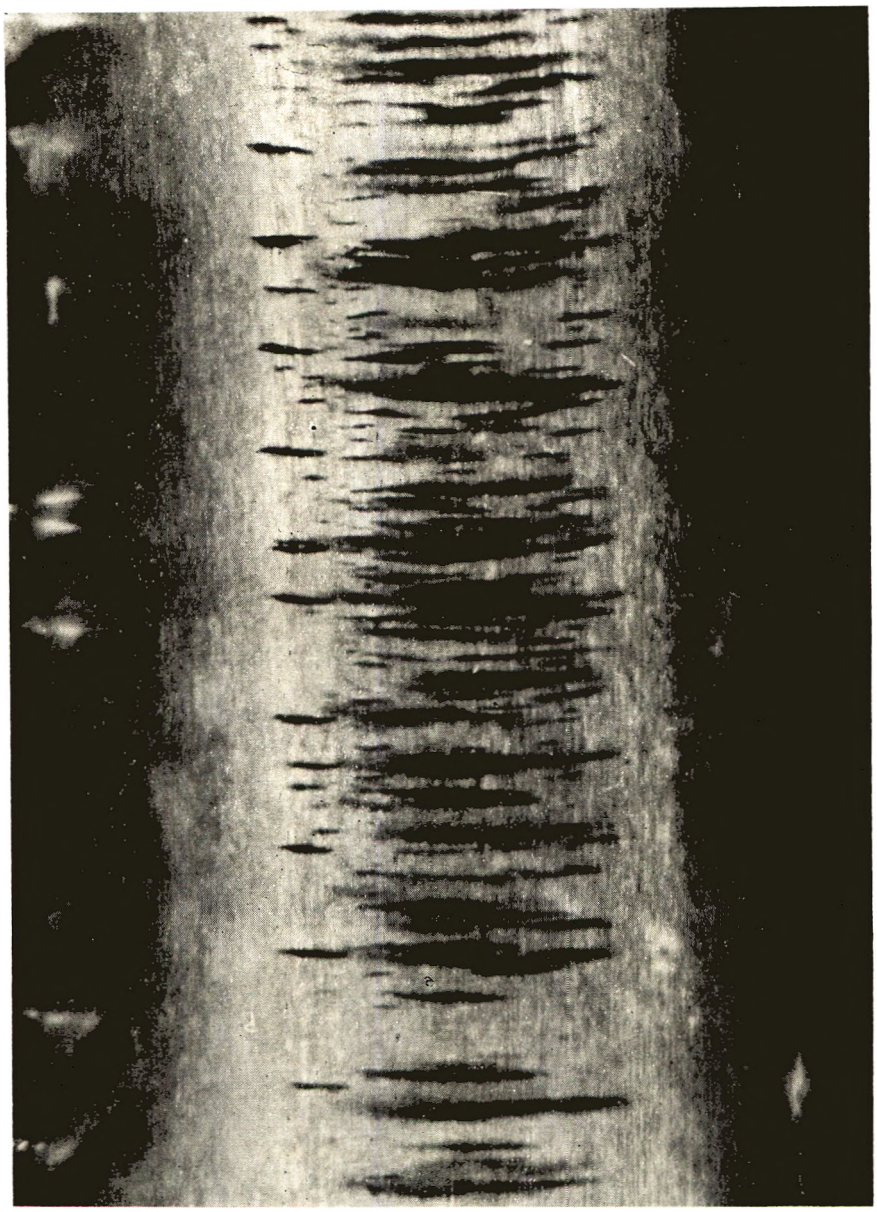

Fig. 2. Microcracks in a strand crystallized in the Instron rheometer at 131°C (optical micrograph).

than that of the polyethylene obtained from the reservoir. Furthermore, the transparent strands were not simply the result of crystallization directly from the flowing melt in the capillary. Indeed, transparent strands were also formed at 60°C by simply applying 1920 atm to a solid plug of polyethylene in the reservoir, forcing it into the capillary to form the unusual structure of the strand. However, the lower-temperature procedure often resulted

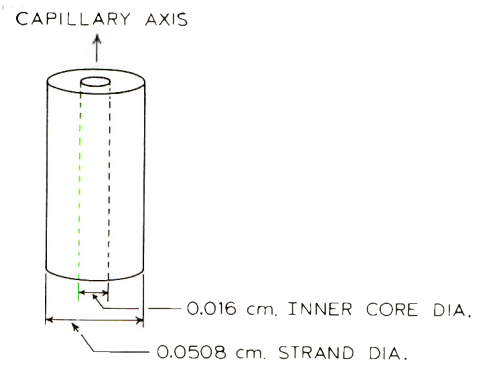

Fig. 3. Schematic diagram of strand indicating inner and outer sheaths discussed in the text.

in microcracks located mainly in the central core of the strands (see Fig. 2). The fusion curve for the sample shown in Figure 2 was both lower and broader in melting temperatures than curves for samples crystallized at 136°C.[13] The existence of microcracks running both perpendicular to the strand length and at 45°, together with the observed lower melting point, were consistent with the disruption of the crystalline structure due to excessive stress. The central core structure failed under tensile stress, as is indicated by the cracks in the region perpendicular to the strand length; the structure failed in shear near the outer radius, as is indicated by cracks oriented at 45° to the tensile force (the maximum-shear plane). This was consistent with a previous observation that the maximum longitudinal velocity gradient responsible for drawing occurs along the central axis of the strand, while the maximum radial velocity gradient, a shearing effect, occurs near the outer radius.[12] Morphological observations described in this paper indicate basic structural differences between the inner core and the outer sheath of the strand which are defined schematically in Figure 3. In all probability, these differences arise from the different orientation effects attributed to the different velocity gradients existing in the central core and the outer sheath regions during the crystallization process.

Scanning Electron Microscopy

In spite of the 200 Å resolution limit of the SEM, its large depth of field proved to be invaluable in defining the structure. Two distinct fibrous textures were observed. One of these, shown in Figure 4, was found only in the outer sheath of the strand. These 3000 Å diameter fibers, oriented parallel to the flow direction, formed the dominant structure for radius values 0.008–0.025 cm delineating the outer sheath (see Fig. 3). A cross texture running perpendicular to the 3000 Å diameter fiber axes was observed upon close inspection of Figure 4. This texture appeared to be spaced more or less periodically along the main fibers at 500 Å intervals and often spanned several adjacent fibers. The cross texture appeared to be

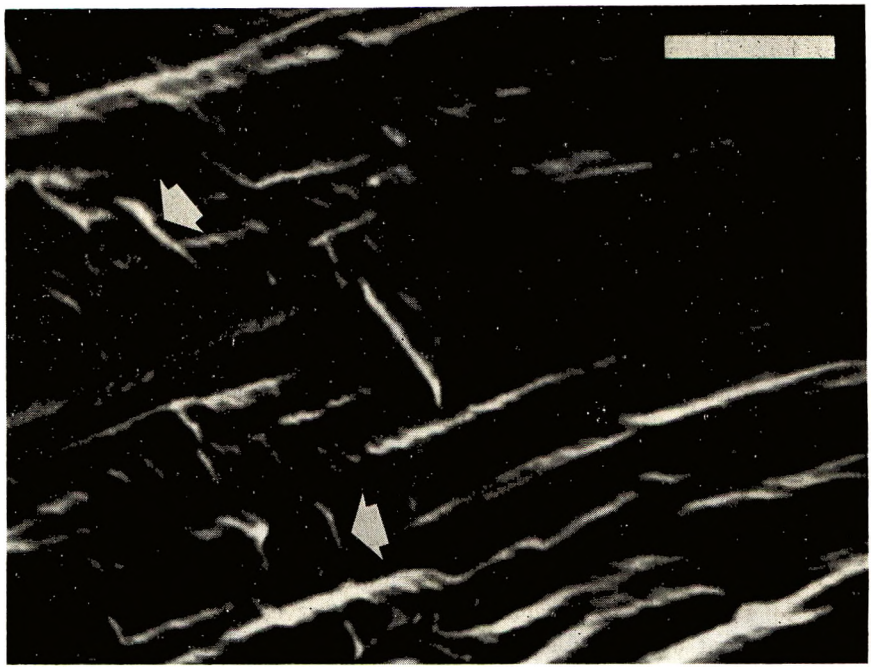

Fig. 4. Outer-sheath texture. Scanning electron micrograph; bar, 1 μ.

basically lamellar; however, the SEM resolution limit was approached in attempting to further define the texture. In many cases, this lamellar texture was observed to twist around the central fiber thread in a helical fashion. Both the size and orientation of the fibers were consistent with the previously published observations[12] concerning the scanning electron micrograph of a sample fractured by the bending at liquid nitrogen temperatures.

The inner core of the strand consisted of fine, flat, ribbonlike structures, rather than the 3000 Å diameter fibers comprising the outer sheath. When freshly cleaved samples were first introduced into the SEM, the ribbons appeared to be flat and aligned parallel to one another as well as to the capillary axis (Fig. 5*a*). After approximately 30 min, these ribbons began to move apart and coil into a twisted array. This effect is illustrated by comparing the structures (note arrows) in Figures 5*a* and 5*b*, two photomicrographs taken at 10-min intervals. The coiling is not caused by localized heating induced by the electron beam of the SEM because beam energy is far lower than in the conventional electron microscope. Indeed, coiling of fibers exposed by fracture was noted in samples "aged" outside the instrument at room temperature. The higher magnification photomicrograph in Figure 6 shows the separate ribbons curling away from larger ribbon bundles (note arrows). Regular cross striations were also observed on the inner core ribbons; however, this particular cross texture appeared to resemble a crystallographic pleating rather than a lamellar overgrowth. The individual ribbons varied in approximate width between 1000 and 5000 Å and were estimated to be approximately 200–400 Å thick. The

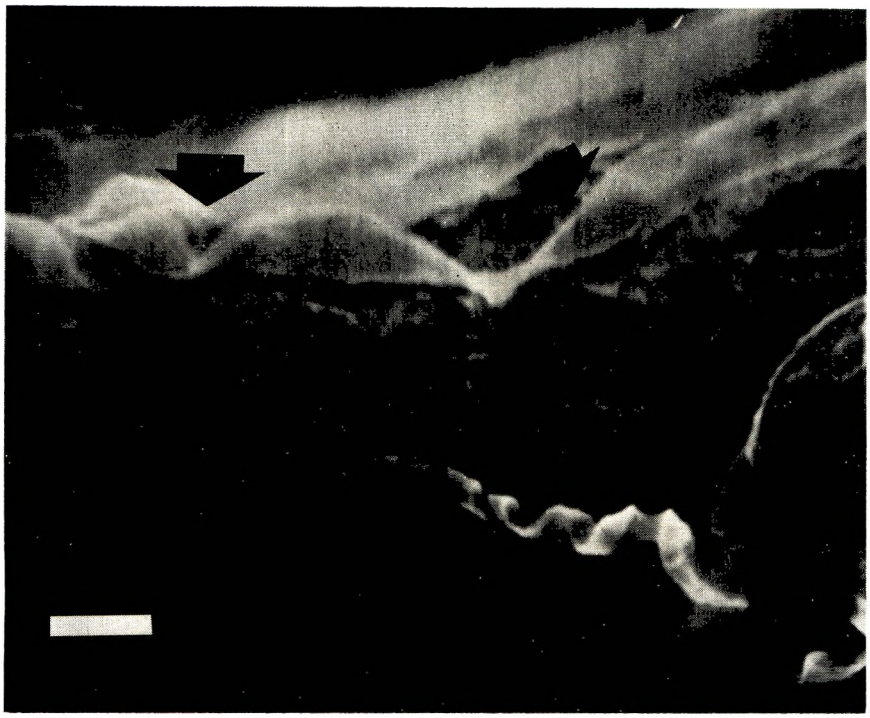

(*a*)

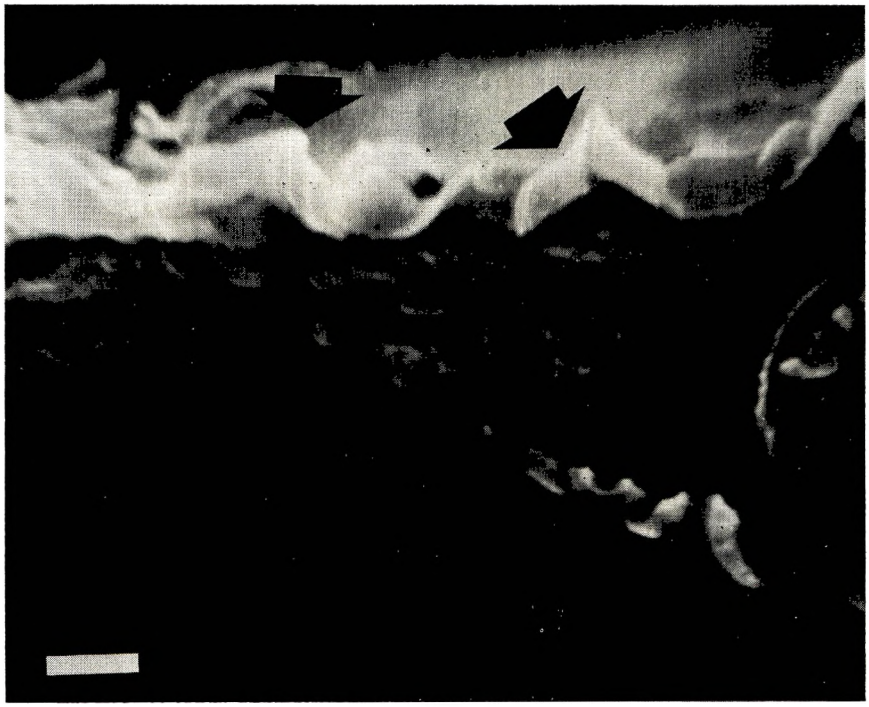

(*b*)

Fig. 5. Inner-core texture: (*a*) upon insertion into the microscope; (*b*) 10 min after insertion. Scanning electron micrographs: bar, 1μ.

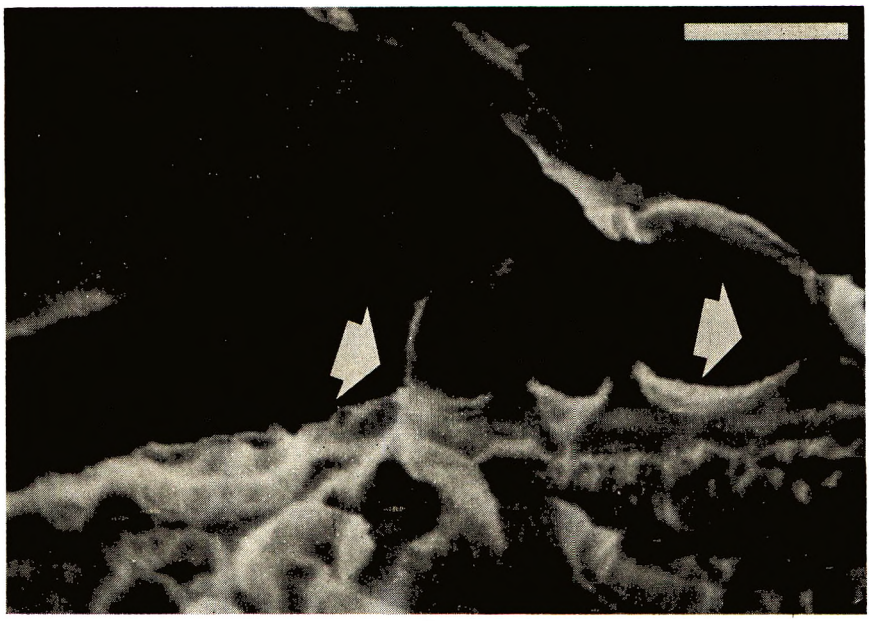

Fig. 6. Ribbons in the inner core. Scanning electron micrograph; bar, 1μ.

ribbon substructure will be described in connection with TEM since the thickness measurements approach the SEM resolution limit.

It should be mentioned that the ribbon coiling implies two important features of this particular morphology. First, inter-ribbon bonding is significantly lower than that of the outer sheath. The cross texture observed with the latter structure apparently imparts a three dimensional cohesiveness to the fibers, suggesting the presence of interfibrillar linkages. Indeed, no fiber coiling or separation was observed after extended periods in the SEM. Second, the ribbons in the bulk-crystallized state undoubtedly contained a significant residual strain which is apparently relieved by the coiling mechanism. Such residual strain may have had inherent crystallographic as well as shear-induced origins similar to those causing periodic twisting in polyethylene spherulites.[16]

Transmission Electron Microscopy

Specimens were examined in the conventional electron microscope using both fracture replication and direct transmission techniques. Fracture-surface replication proved somewhat difficult because of surface roughness. However, good quality replicas were obtained by shadowing the surface directly with Pt–C, evaporating a thin carbon layer, and finally stripping the layers with acetone–swollen acetate strips. The acetate was then removed by dissolving in amyl acetate, to leave a negative Pt–C shadowed carbon replica. Selected-area electron diffraction was performed on several polyethylene fiber fragments which fortunately adhered to such replicas.

Fig. 7. Carbon replica showing inner core fiber bundles. Electron micrograph.

The ribbonlike fibrous texture of the inner core seen in the SEM photomicrographs was also observed in the shadowed carbon replicas. Electron micrographs showed that the ribbons extended for tens of microns and contained fine fiber bundles oriented parallel to the long axis of the strand. Figure 7 is a replication electron micrograph of these fiber bundles, in which parting of the individual fibers from the bundles during fracture replication is visible (see arrows). Note both the fiber lengths and apparently weak interfiber bonding. Individual fiber bundles in microtomed sections were examined by staining with Br_2 vapor, which preferentially attacks the less ordered regions between the component fibers. Specimens were mounted in an epoxy embedding material (Cargille NYSEM) and sectioned on a Sorvall Porter-Blum MT-2 ultramicrotome by use of a Dupont 43° diamond knife. Sectioning across a strand proved impractical since the fiber bundles readily splayed apart owing to the weak bonding between the fiber bundles. Sectioning parallel to the strand axis proved to be more feasible, but stringy, rather than smooth, sections were obtained with this procedure. Figure 8 is a transmission electron micrograph of microtomed fibers from the strand inner core stained with Br_2. The fibrous, stringy texture was quite visible; however, fiber splaying due to the action of the knife was also obvious. The ultimate subunit of the ribbon structure was found to be a 200–250 Å diameter fiber (see arrows in Fig. 8). Since individual fibers adhered to several of their neighbors after splaying apart, some type of interfiber bonding may have existed within a fiber bundle. A nodular structure superimposed on the ultimate fibers was also observed; however, this was probably an artifact of the Br_2 vapor staining process.

Fig. 8. Microtomed, Br_2-stained section from the inner core. Transmission electron micrograph.

Electron Diffraction

Unstained sectioned fibers and, in a few cases, shadowed fibers adhering to the carbon replicas were examined by electron diffraction using electron microscope stage tilting techniques. Exceptionally well-developed spot patterns were obtained from the strand inner core where the ribbon like structure was observed. Proper stage rotation revealed a highly ordered and oriented crystal structure within the ultimate fibers. Figures 9 and 10 show sharp electron diffraction patterns and the corresponding reciprocal lattice diagrams obtained from the inner core material. Note that the shorter exposure time of Figure 9 permitted observation of lower-order reflections, whereas the longer exposure time of Figure 10 provided the higher-order reflections. In both cases, $(0kl)$ reflections were observed while $(h0l)$ reflections were undetectable with further stage rotation. No explanation was found for the failure to detect the $(h0l)$ reflections, other than thickness effects associated with difficulty in passing electrons through the thick dimension of the ribbon. This would suggest that interfiber bonding in ribbons occurs primarily along $(0k0)$ planes.

The polyethylene crystal structure is based on an orthorhombic unit cell, requiring that the reciprocal and true lattice directions be parallel. Furthermore, polyethylene belongs to the D_{2h}^{16} space group. Such symmetry conditions require that permissible $(0kl)$ reflections satisfy the equation: $k + l = 2n$. Each of the twenty-six distinct reflections observable in

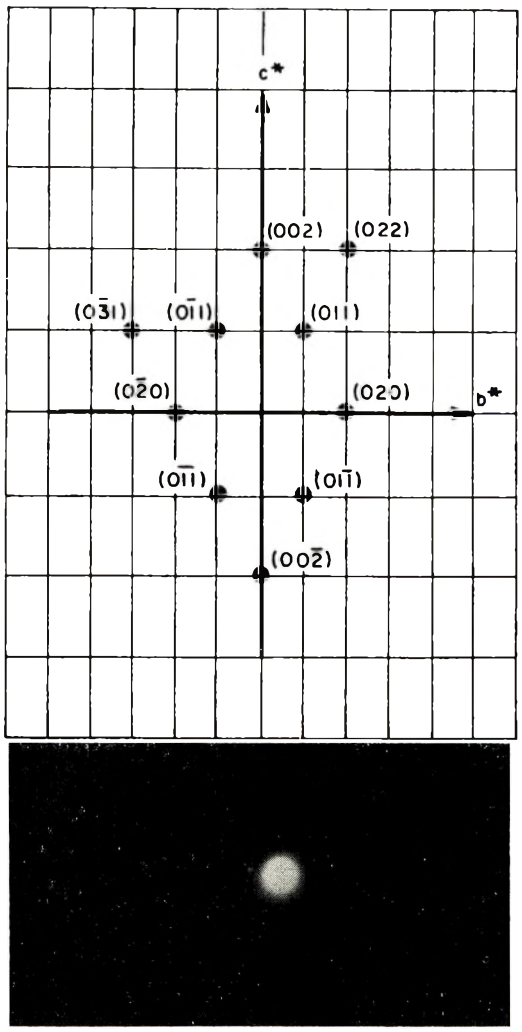

Fig.9. Electron diffraction pattern and reciprocal lattice diagram of inner-core material.

Figures 9 and 10 comply with this restriction. The electron diffraction data show that an unusually high degree of crystalline order (for polyethylene) exists in the inner core of the strand. The crystallographic c axis, the axis parallel to the polyethylene chain backbone, was found to be oriented parallel to the long axis (within $\pm 5°$) of the strand. This high degree of chain orientation is consistent with the c-axis orientation function $+0.996$ determined previously with wide-angle x-ray measurements.[14] In contrast, electron diffraction studies of the 3000 Å diameter, fibrous morphology of the outer sheath produced only typical oriented fiber patterns similar to those obtained by Keller[10,11] from stress-crystallized polyethylene. The resulting diffuse arcs may have been produced by the polycrystalline lamellar cross texture observed on the 3000 Å fibers.

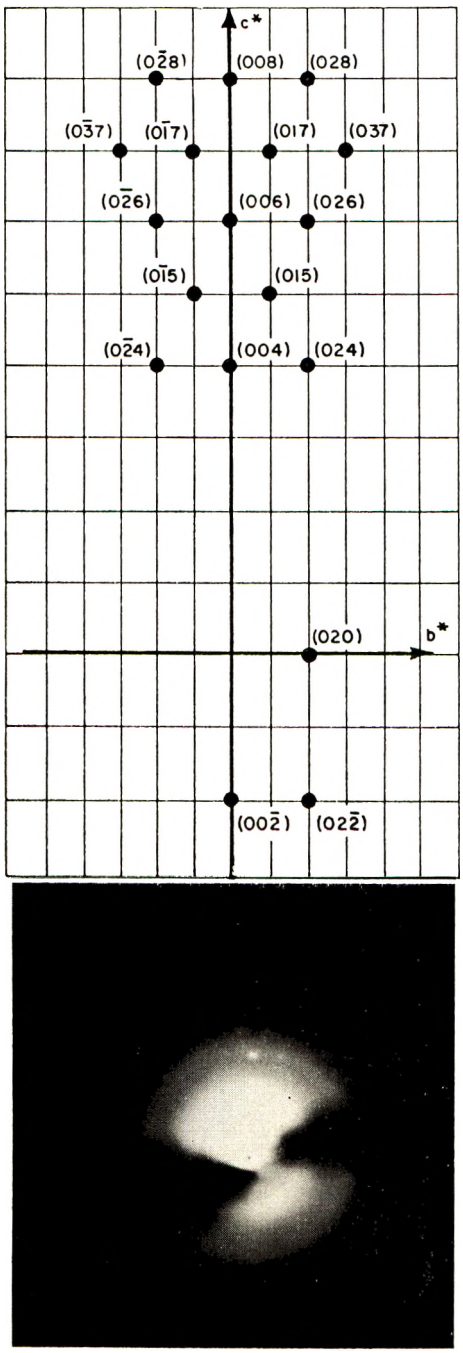

Fig. 10. Electron diffraction pattern and reciprocal lattice diagram of inner-core material (long exposure time).

DISCUSSION AND CONCLUSIONS

Two distinct morphological units are produced in the Instron strands: the highly crystalline ribbons in the inner core and the less ordered 3000 Å diameter fibers of the outer sheath. Similar units have been observed by Pennings and Kiel[7] in the fibrous structures crystallized under the influence of shear in a dilute solution. They, too, described the morphological entities as being either ribbons or fibers having a lamellar overgrowth. The 3000 Å fibers may well be the melt-crystallized analog of the fibers grown from dilute solution by Pennings and Kiel.

Fibrous morphologies are not uncommon in crystalline polymers, especially if the polymer chain backbone is too stiff to accommodate chain folding. O'Leary and Geil[17] have described the fibrous textures in crystalline polytetrafluoroethylene in a manner similar to that used to define the polyethylene structure of this work. Crystal[18] has also described a fibrous morphology for crystalline poly-*N*-vinyl-carbazole, an apparently stiff molecule containing bulky pendant groups which inhibit free rotation about the polymer backbone. Because chain folding cannot be accommodated in poly-*N*-vinylcarbazole, this polymer apparently crystallizes into a fibrous structure containing weak interfiber bonds. While *c*-axis orientations were noted in these references, sharp-spot electron diffraction patterns were not reported.

Additional evidence for the existence of two distinct morphological units in the Instron strands was found in the fusion curves obtained from the melting of the strands in the Perkin–Elmer differential scanning calorimeter (DSC), Model 1-b. The DSC traces for two strands crystallized with the Instron procedure at 132°C are shown in Figure 11. It was noted that these strands appeared to be similar in structure to those examined in the above micrographs (crystallization at 136°C). One of the strands was exposed to 25 Mrad of irradiation in order to suppress reorganization during melting.[19,20] Both strands were found to have relatively high peak-value melting points, consistent with the presence of extended-chain crystals.[4] Furthermore, the irradiated strand showed a multipeak fusion curve indicative of two crystalline forms. A possible explanation for such behavior would be that the more perfect inner-core ribbon structure melted at the higher peak temperature, and the less ordered outer-sheath structure, containing chain-folded lamellae and defects, melted at the lower peak temperature. The primary effect of the radiation has been to resolve the single fusion curve, corresponding to the unirradiated sample, into low and high melting peaks for the irradiated sample. These observations are consistent with the hypothesis that the structure in the inner core of the strand appears to be dominated by an extended-chain crystalline structure, while that of the outer sheath is dominated by epitaxial chain-folded lamellae.

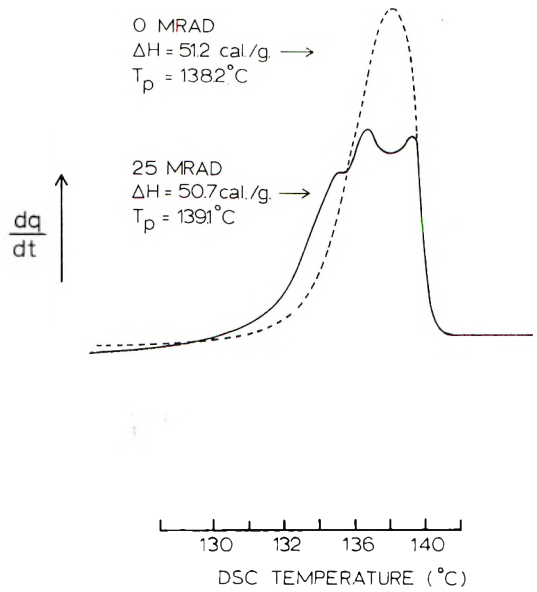

Fig. 11. Differential scanning calorimeter trace showing the effect of irradiation on the melting behavior of a transparent strand, produced at 132°C with a capillary of diameter 0.0762 cm and 1.0 cm/min plunger velocity.

The inner-core ribbon structure was the most perfect of the two crystalline units defined in this study. Well developed single-crystal electron diffraction patterns obtained from ribbons indicate that they are made up of extended-chain crystals. The eighth-order reflection along the *c* axis has been detected (see Fig. 10) by using a very small aperture achieved with the Phillips EM200 knife-type diffraction aperture. In order to obtain such an electron diffraction pattern, the crystalline order must have been in register over a considerable portion of the aperture opening. Otherwise, a more polycrystalline pattern would be expected. Note that a lamellar structure connected by tie molecules, such as the model proposed by Peterlin for drawn polyethylene,[15] would not result in sharp diffraction spots for the (0*kl*) planes over a 5000 Å length of the fiber. In the Peterlin model, the lamellae that stack together to form a fibril would be free to rotate around the *c* axis, thereby prohibiting the formation of coherent sets of diffraction planes for all except the (00*l*) planes. Figures 9 and 10 show the presence of other sets of diffraction planes. Only a well developed extended-chain crystal model which maintains a high degree of order and register across the aperture opening could account for the observed diffraction spots from the inner-core fibers.

The formation of an extended-chain structure by crystallizing from the bulk polyethylene is particularly significant from the aspect of improved mechanical properties. In addition to the transparency of the strands, the modulus of the central core containing the extended-chain crystal structure may well be extremely high in the direction of the strand length. If defect-

free extended-chain ribbons could be produced in a commercial process analogous to the Instron procedure, significant improvement in mechanical properties would be realized.

The authors wish to thank F. J. Walton and R. Fernquist of the Xerox Corporation for their invaluable technical assistance throughout this project. The authors are also indebted to P. Goldstein of the Xerox Corporation and R. S. Porter, R. S. Stein, F. P. Price, and R. D. Ulrich of the University of Massachusetts for helpful discussions.

References

1. B. Wunderlich and T. Arakawa, *J. Polym. Sci. A*, **2**, 3697 (1964).
2. E. Hellmuth and B. Wunderlich, *J. Appl. Phys.*, **36**, 3039 (1965).
3. B. Wunderlich and C. Cormier, *J. Polym. Sci. A-2*, **5**, 987 (1967).
4. D. Rees and D. Bassett, *J. Polym. Sci. B*, **7**, 273 (1969).
5. L. Mandelkern, M. Gopalan, and J. Jackson, *J. Polym. Sci. B*, **5**, 1 (1967).
6. B. Wunderlich, *J. Polym. Sci. B*, **5**, 7 (1967).
7. A. Pennings and A. Kiel, *Kolloid-Z. Z. Polym.*, **205**, 160 (1965).
8. T. Kawai, T. Matsumoto, M. Kato, and H. Maeda, *Kolloid-Z. Z. Polym.*, **222**, 1 (1969).
9. R. Williamson and R. Novak, *J. Polym. Sci. B*, **5**, 147 (1967).
10. M. Hill and A. Keller, *J. Macromol. Sci.-Phys.*, **B3**, 153 (1969).
11. A. Keller, *Repts. Progr. Phys.*, **31**, 623 (1968).
12. J. H. Southern and R. S. Porter, *J. Macromol. Sci.-Phys.*, **B4**, 541 (1970).
13. J. H. Southern and R. S. Porter, *J. Appl. Polym. Sci.*, **14**, 2305 (1970).
14. C. R. Desper, J. H. Southern, R. D. Ulrich, and R. S. Porter, *J. Appl. Phys.*, **41**, 4284 (1970).
15. A. Peterlin, *Polym. Eng. Sci.*, **9**, 172 (1969).
16. J. R. Burns, *J. Polym. Sci. A-2*, **7**, 593 (1969).
17. K. O'Leary and P. H. Geil, *J. Appl. Phys.*, **38**, 4169 (1967).
18. R. G. Crystal, paper presented to the Division of High Polymer Physics, American Physical Society Meeting, Dallas, Texas, March 1970; *Macromolecules*, in press.
19. H. E. Bair and R. Salovey, *J. Macromol. Sci.-Phys.*, **B3**, 3 (1969).
20. T. W. Huseby and H. E. Bair, *J. Polym. Sci. B*, **5**, 265 (1967).

Received October 27, 1970
Revised March 15, 1971

JOURNAL OF POLYMER SCIENCE: PART A-2 VOL. 9, 1657–1668 (1971)

Reaction Kinetics in Dilute Solutions of Chain Molecules Carrying Randomly Spaced Reactive and Catalytic Chain Substituents. II. Dependence of the Ring Closure Probability on the Solvent Medium and the Nature of the Chain Backbone

NEIL GOODMAN and HERBERT MORAWETZ,
Polymer Research Institute, Polytechnic Institute of Brooklyn, Brooklyn, New York, 11201

Synopsis

Ternary copolymers of acrylamide or methacrylamide with small proportions of comonomers carrying reactive *p*-nitrophenyl ester and catalytic pyridine groups in the side chains were prepared. The kinetics of the ester solvolysis was followed in highly dilute solutions, so that the rate was controlled by interaction of groups carried by the same chain backbone. Data were obtained in water and aqueous methanol and were interpreted by a computer simulation procedure in terms of the dependence of the probability of encounter between two chain substituents on their spacing along the chain backbone. This probability decreased more slowly with increasing separation of the interacting groups when the solvation of the polymer was reduced, but even in solvents approaching Θ conditions the results deviated from theoretical predictions for chains without excluded volume. The formation of cyclic conformations is considerably more difficult in methacrylic than in acrylic chains, although the chain flexibility, as characterized by unperturbed chain dimensions, is very similar in the two systems.

INTRODUCTION

It is customary to characterize the flexibility of polymer chains by the extension of the molecular coils in solution, i.e., by the root-mean-square radius of gyration derived from light scattering data or estimated from the intrinsic viscosity. In principle, one could use for the same purpose the rate of cyclization of polymer chains terminated with suitable reactive groups, but the preparation of monodisperse polymers with the two interacting groups attached to the chain ends is technically not feasible.

In a previous investigation[1] we have shown that it is possible to study by an indirect method the dependence of the ring closure probability on the spacing of two interacting groups along a polymer chain. We prepared copolymers carrying a small number of reactive nitrophenyl ester groups and catalytic pyridine residues attached at random to the polymer backbone. By studying the kinetics of the ester solvolysis at high dilution of the copoly-

mer, we ensured that the catalytic effect of a pyridine group was only significant if it was attached to the same polymer as a given ester group. Since the ester groups were located at different spacings from the catalytic groups, the kinetics of the process had to be described by a distribution function $W(k_1)$ of first-order rate constants k_1. Thus, the fraction y of unreacted ester decayed with time t as

$$y = \int W(k_1) \exp\{-k_1 t\} dk_1$$

It was found that the experimental data could be fitted by a computer simulation procedure which allowed the results to be interpreted in terms of the dependence of the ring closure probability on the spacing of the interacting groups along the polymer chain.

In this paper the previous study is expanded to illustrate the dependence of the ring closure probability on the nature of the solvent medium and to compare the behavior of polyacrylamide and polymethacrylamide chains.

THEORETICAL CONSIDERATIONS

The probability distribution function of the end-to-end displacement h of long, freely jointed chains is given[2] by

$$W(h)dh = (3/2\pi\langle h^2\rangle)^{3/2} \exp\{-3h^2/2\langle h^2\rangle\} 4\pi h^2 dh \quad (1)$$

where $\langle h^2\rangle$ is the mean-square value of h. The effective concentration of the second chain end in the neighborhood of the first chain end is defined by the limiting value of $W(h)/4\pi h^2$ as $h \to 0$ which becomes, by using eq. (1)

$$c_{\text{eff}}^0 = (1000/\bar{N})(3/2\pi\langle h^2\rangle)^{3/2} \quad (2)$$

where c_{eff}^0 is specified as a molarity (with h in cm) and $\bar{N}$ is Avogadro's number. If the chain ends carry groups which can react with one another and if the reaction of two small molecules carrying such groups is characterized by a second-order rate constant k_2, then the first-order rate constant of the intramolecular reaction will be $k_1 = k_2 c_{\text{eff}}^0$, or,

$$k_1 = k_2(1000/\bar{N})(3/2\pi\langle h^2\rangle)^{3/2} \quad (3)$$

For idealized chains consisting of Z infinitely thin links of length, b, $\langle h^2\rangle = Zb^2$. For real chains, the ratio $\langle h^2\rangle/Zb^2$ approaches for long chains and in theta solvents a limiting value C_∞ (which lies in the range 6–10 for vinyl polymers,[3a] each skeletal bond being considered as a link) reflecting the bond angles and restrictions on the internal angles of rotation along the chain backbone. The value of C_∞ may be obtained from the dependence of $[\eta]_\Theta$, the intrinsic viscosity in theta-solvent media, on the molecular weight M by using[3b] the equations

$$C_\infty = (K_\Theta/\Phi)^{2/3} M_0/2b^2 \quad (4)$$

$$K_\Theta = [\eta]_\Theta/M^{1/2}$$

where $\Phi = 2.6 \times 10^{21}$ is the Flory constant and M_0 the molecular weight of the monomer residue. It should be stressed that all the relations given above hold only for chains for which $\langle h^2 \rangle^{1/2}$ is small compared to the contour length of the chain.

Let us now consider the value of k_1 for a reactive group attached to the nth monomer residue of a vinyl polymer chain which carries catalytic groups on a number of other monomer residues. Assuming that the mean square displacement of the nth and jth monomer residues $\langle h_{jn}^2 \rangle$ depends only on $|j - n|$, i.e., $\langle h_{jn}^2 \rangle = 2C_\infty |j - n| b^2$ (since there are two bonds in the chain backbone for each monomer residue) and that the statistical treatment is applicable if $x \equiv |j - n|$ is equal or larger than a critical value x', we obtain from eqs. (3) and (4)

$$k_1 = k_2(1000\Phi/\bar{N}K_\Theta)(3/2\pi M_0)^{3/2}\left[\sum_{x=x'}^{x=n}(p_j x)^{-3/2} + \sum_{x=x'}^{x=P-n}(p_j x)^{-3/2}\right] + k_1' \tag{5}$$

where P is the degree of polymerization, $p_j = 1$ or $p_j = 0$ depending on whether the jth monomer does or does not carry a catalytic group, and k_1' accounts for the contribution to k_1 from interactions of groups for which $x < x'$.

If a polymer carries only a small number of reactive groups and all other monomer residues carry catalytic substituents, k_1 will assume a value k_1^{max} given by eq. (5) with $p_j = 1$ for all values of j. When only a fraction ω of monomer residues carry catalytic groups, the initial apparent first-order rate constant (corrected for any process taking place in the absence of intramolecular catalysis) will be

$$(k_1^{init})_{corr} = \omega k_1^{max} = \omega k_2 c_{eff}^{max} \tag{6}$$

where c_{eff}^{max} represents the effective concentration in the neighborhood of a small number of reactive chain residues if all the other residues carry catalytic substituents. Setting $p_j = 1$ in eq. (5), substituting integrals for the summations, and neglecting k_1' in the evaluation of k_1^{max}, we obtain, provided $x' \ll n$, $x' \ll P - n$

$$(k_1^{init})_{corr} = \omega k_2(4000\Phi/\bar{N}K_\Theta)(3/2\pi M_0)^{3/2}(x')^{-1/2} \tag{7}$$

For any separation x of the interacting groups along a polymer chain, the ring closure probability should decrease in good solvent media, where the excluded volume effect has to be taken into account. A number of investigators have tried to estimate the magnitude of this effect by computer simulation[4-9] and concluded that for large values of x the ring closure probability is proportional to x^{-a}, where the ring closure exponent a lies between 1.8 and 2.0.

On the other hand, for relatively short chains, $\langle h^2 \rangle$ has been found to have the same value in good solvent, as in theta media.[10,11] The ring closure probability might, therefore, also be insensitive, for small values of x, to the nature of the solvent. We have used in our previous study[1] an approximate

treatment where the ring closure probability was considered solvent-independent for $x = x'$, decaying as x^{-a} for $x > x'$. This treatment leads to a replacement of eqs. (5) and (7) by

$$k_1 = k_2(1000\Phi/\bar{N}K_0)(3/2\pi M_0)^{3/2}(x')^{a-3/2} \times \left[\sum_{x=x'}^{x=n}(p_j x)^{-a} + \sum_{x=P-n}^{x=P-x'}\right](p_j x)^{-a} + k_1' \quad (8)$$

$$(k_1^{\text{init}})_{\text{corr}} = \omega k_2[2000\Phi/\bar{N}K_0(a-1)](3/2\pi M_0)^{3/2}(x')^{-1/2} \quad (9)$$

EXPERIMENTAL

Copolymers used in this study were prepared from acrylamide or methacrylamide with small proportions of the reactive comonomer I and the catalytic comonomer II. Chemical compositions (determined spectro-

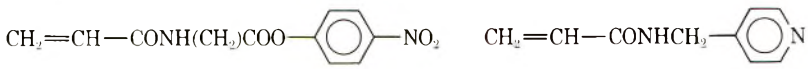

I II

scopically[1]) and intrinsic viscosities are listed in Table I. The molecular weights of the acrylamide copolymers were estimated from $[\eta]_{H_2O}^{25} = 6.31 \times 10^{-5}M^{0.80}$ found by Scholtan[12] for polyacrylamide.

TABLE I
Copolymers Used in This Study

Copolymer designation	Main monomer[a]	Mole fraction of reactive comonomer × 10^2	Mole fraction II (ω) × 10^2	$[\eta]$ (25°C, H_2O), dl/g
A	AA	1.1[b]	—	0.37
B	AA	1.0[c]	—	0.53
C	AA	—	1.20	1.00
D	AA	1.0[c]	0.33	0.88
E	AA	1.2[c]	1.20	1.63
F	AA	0.9[c]	1.18	0.67
G	AA	1.2[d]	1.00	1.57
H	MA	1.1[c]	—	0.29
J	MA	—	1.16	0.32
K	MA	1.0[c]	1.15	0.36

[a] AA = acrylamide; MA = methacrylamide.
[b] *p*-Nitrophenyl methacrylate.
[c] Comonomer I.
[d] *p*-Nitrophenyl ester of *N*-acrylyl 6-aminocaproic acid.

All kinetic runs were carried out in pH 6 phosphate buffers at 25°C. The progress of the ester solvolysis was followed spectrophotometrically at 320 nm. The fraction α of the pyridine residues in the catalytically active basic form was estimated by comparison of the optical density at 260 nm at a given pH with the value for the protonated form at pH 2 and the basic form at pH 10. In studies involving terpolymers containing both nitrophenyl

ester and pyridine substituents, the kinetic runs were carried out at a polymer concentration of 2.0 g/l. It was verified by an experiment with a mixture of the reactive copolymer B and the catalytic copolymer C that intermolecular catalysis is not significant under these conditions.

RESULTS

To study the influence of the excluded volume effect on the intramolecular group interactions, kinetic measurements were carried out in water-methanol mixtures. The intrinsic viscosity data given in Table II show that the solvation of the acrylamide copolymers is decreased on addition of methanol. The exponent in the Mark-Houwink relation $[\eta] = KM^{\gamma}$ drops from 0.80 for water solutions to 0.67 in 20% methanol and to 0.53 for 40% aqueous methanol which may, therefore, be taken as approaching a theta solvent ($\gamma = 0.5$).

TABLE II
Dependence of the Intrinsic Viscosity of Acrylamide Copolymers on the Solvent Medium

Copolymer designation	M_w[a]	$[\eta]$, dl/g		
		H_2O	20% Methanol	40% Methanol
A	52,000	0.37	0.51	0.25
B	80,000	0.53	0.41	0.30
D	150,000	0.88	0.67	0.46
G	310,000	1.57	1.09	0.67

[a] The viscosity-average molecular weight of the copolymers was estimated from the data given by Scholtan[12] for polyacrylamide.

Reactivity of Monomers and Binary Copolymers

Table III lists the spontaneous first-order rate constant k_s and the second-order rate constant k_2 of the reaction catalyzed by the pyridine residues of compound II for the monomer I and the copolymer B or H in pH phosphate buffer and in buffer solutions containing 14%, 20%, or 40% methanol. The second-order rate constants are based on the stoichiometric concentration of II, and Table III lists also the fraction α of the pyridine residues which have been found spectroscopically to be in the basic form. In aqueous solutions, α was found to be very similar for the monomer II and for the catalytic copolymers C and H.

The data show that k_2 decreases on methanol addition, although α increases with an increasing methanol concentration. This effect is more pronounced for copolymer B than for monomer I, presumably because the catalytic monomer II would tend to be at a lower local concentration in the domain of the hydrophilic acrylamide copolymer than in the system as a whole. This partial exclusion of the catalytic species apparently more than compensates for the fact that the higher water concentration in the polymer domain tends to favor the ester solvolysis.

TABLE III
Hydrolysis of *p*-Nitrophenyl Ester Residues in Monomer I and Its Copolymers

Medium	$k_s \times 10^3$, min^{-1}			k_2, l./mole-min			Fraction of pyridine residues in basic form		
	Monomer I	Copolymer B	Copolymer H	Monomer I	Copolymer B	Copolymer H	Monomer II	Copolymer C	Copolymer J
H_2O	3.6	3.4	3.4	2.7	2.6	2.6	0.66	0.67	0.66
14% MeOH	4.9	—	4.5	2.0	—	—	0.79	—	0.75
20% MeOH	6.0	5.4	—	1.7	1.4	—	0.83	0.79	—
40% MeOH	9.7	8.3	—	1.15	0.67	—	0.94	0.89	—

Reactivity of Ternary Copolymers of Acrylamide

The ester solvolysis of the ternary copolymer E (containing a mole fraction $\omega = 0.012$ of catalytic monomer II residues) showed, as expected, a strong deviation from first-order kinetics, reflecting a dispersion of the rate constant k_1. To obtain the contribution to the initial apparent value of this rate constant due to intramolecular catalysis, the rate constant k_s for the spontaneous reaction has to be subtracted from the observed value of k_1^{init} to obtain a corrected value $(k_1^{init})_{corr}$. This quantity was interpreted by eq. (6) to yield c_{eff}^{max}, on using for k_2 the values obtained for the solvolysis of monomer I when catalyzed by monomer II.

The results listed in Table IV show that c_{eff}^{max} increases by 18% and by 60% when the solvent medium is changed from water to one containing 20% and 40% methanol, respectively. This is in agreement with eq. (9), which predicts that $c_{eff}^{max} = (k_1^{init})_{corr}/k_2$ should increase as the ring closure exponent a decreases in poorer solvent media. However, the interpretation of this change of c_{eff}^{max} is uncertain, since the k_2 for the reaction of the two monomeric species does not take into account the increased concentration of water in the polymer domain when a mixed solvent system is used. On the other hand, we cannot use for k_2 the value obtained with systems containing a binary copolymer carrying reactive substituents and a catalytic monomer, since the catalytic monomer will tend to be excluded, as noted above, from the polymer domain.

The solvolysis kinetics of the ternary copolymers E and F, which had a similar chemical composition but differed by a factor of 3 in their chain length, were found to be indistinguishable. This is in accordance with the expected behavior since the contribution to k_1 decreases rapidly with an increasing separation x of thr interacting groups [eqs. (5) and (8)] and the rate constant approaches, for chains of infinite length, a limiting value depending on x' [eqs. (7) and (9)]. The result shows clearly the inadequacy of the treatment of Loucheux and Banderet,[13] who assumed that reaction rates involving the chemical interaction of two groups attached to a flexible polymer chain could be estimated from the average concentration of such groups in a hydrodynamically equivalent sphere. If this model is applied to a series of copolymers with the same chemical composition but varying chain length, it leads to the faulty prediction that k_1, at any given degree of conversion, is inversely proportional to the intrinsic viscosity.

In interpreting c_{eff}^{max} by eqs. (6) and (9), we used $K_\Theta = 9.0 \times 10^{-4}$, estimated from a Stockmayer-Fixman extrapolation[14] of our intrinsic viscosity

TABLE IV
Reactivity of Ternary Copolymer E in Aqueous Methanol

	Water	20% methanol	40% methanol
$(k_1^{init})_{corr}$	0.091	0.067	0.052
k_2	2.7	1.7	1.15
c_{eff}^{max}	2.8	3.3	4.5

data in 40% methanol. We found previously[1] that the chain-closure exponent for polyacrylamide chains in water solution is close to $a = 2$. With these data, we obtain a c_{eff}^{max} value of 1.7 for $x' = 10$, as compared to $c_{eff}^{max} = 2.8$ obtained from the kinetic data in water solution.

An increasing breadth of the distribution function $W(k_1)$ is reflected in an increasing deviation from first-order kinetics. Since $W(k_1)$ will be broadened by an increase in the chain-closure exponent, we may use the deviation from first-order kinetics as a measure of a. A computer simulation procedure[1] was used for this purpose. A sample of 100 chains of 1000 units was generated by a conventional Monte Carlo method by using a probability $\omega = 0.012$ that any jth unit carries a catalytic residue. If it is assumed that the reactive group is carried by the central chain segment and that no interaction is possible between units separated by fewer than $x' = 10$ units, the contribution to the first-order rate constant of the ith chain due to intramolecular catalysis is

$$k_{1i} = C \left(\sum_{x=-500}^{x=-10} |p_{ij}x|^{-a} + \sum_{x=10}^{x=500} |p_{ij}x|^{-a} \right) \tag{10}$$

where $x = j$-500 and C is evaluated from the requirements that $\langle k_{1i} \rangle$, the average value of k_{1i}, be equal to the apparent initial first-order rate constant

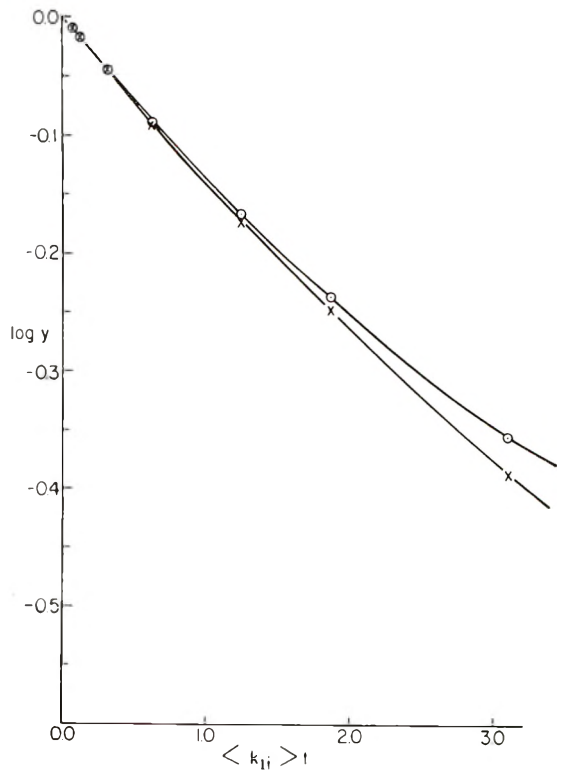

Fig. 1. Dependence of the deviation from first-order kinetics on the choice of x' (computed curves for $a = 3/2$ and $\omega = 0.012$): (O) $x' = 10$; (×) $x' = 20$.

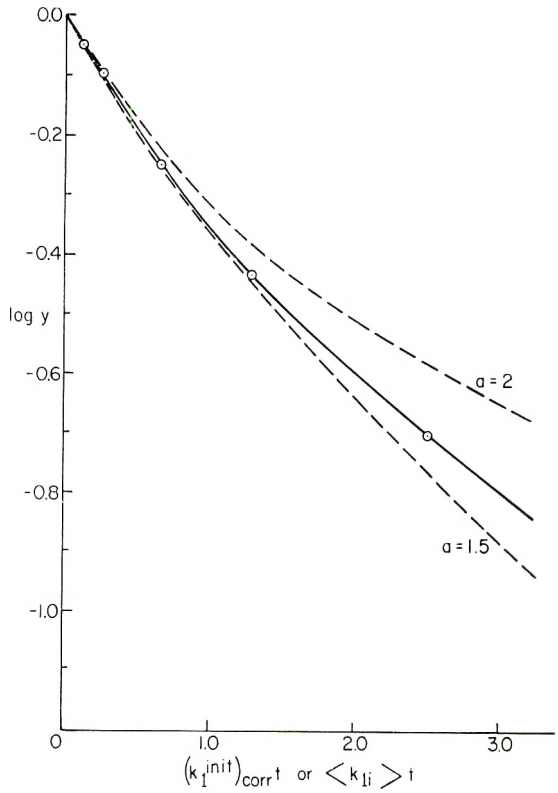

Fig. 2. Comparison of the kinetic pattern for copolymer E with kinetic curves computed for $a = 3/2$ and $a = 2$.

corrected for spontaneous solvolysis.[1] From the distribution of the k_{1i} values, kinetic curves can then be generated by the computer by using eq. (11)

$$y = \frac{1}{100} \sum_{i=1}^{i=100} \exp\{-(k_{1i} + k_s)t\} \tag{11}$$

for comparison with experimental data.

Before using this procedure to estimate a, we must satisfy ourselves that the results will not be unduly influenced by the arbitrary choice of x'. Figure 1 shows a plot of $\log y$ as a function of $\langle k_{1i} \rangle t$ computed for $x' = 10$ and $x' = 20$ (with $k_s = 0$ and $a = 3/2$). It may be seen that a doubling of the value of x' has an extremely small effect on the extent of the deviation from first-order kinetics. Using then $x' = 10$, we find the experimental curve in Figure 2 to be intermediate between the computed curves for $a = 3/2$ and $a = 2$. The decrease in the value of the ring-closure exponent as compared with that observed in the more highly solvating water solution (corresponding to $a = 2$)[1] is in accord with expectation. On the other hand, the data show that a exceeds significantly the theoretical value of 3/2 for random chains without excluded volume even in a medium approaching theta condi-

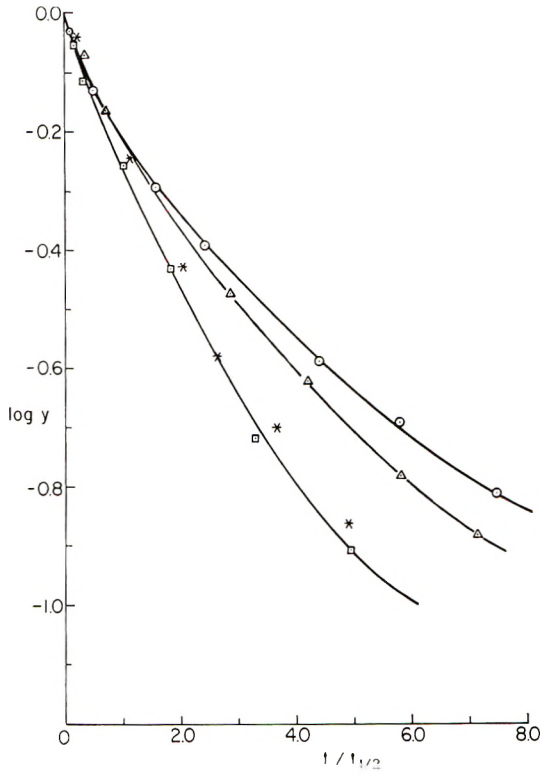

Fig. 3. Dependence of the kinetic pattern on the nature of the polymer backbone and and the solvent medium: (○) acrylamide copolymer in water; (□) acrylamide copolymer in 40% methanol; (△) methacrylamide copolymer in water; (*) methacrylamide copolymer in 14% methanol.

tions. The increase in the $c_{\text{eff}}^{\max}$ value by a factor of 1.6 when water is substituted by 40% methanol as the solvent medium (Table IV) corresponds, according to eqs. (6) and (9), to a reduction of a from 2 to 1.63, a value which corresponds reasonably well to the curvature of the plot shown in Figure 2.

Reactivity of Ternary Methylacrylamide Copolymers

The ternary methacrylamide copolymer K was studied in water and in 14% aqueous methanol. The solution containing this methanol concentration was close to the polymer precipitation point and was assumed, therefore, to approximate a theta solvent. Figure 3 shows plots of log y against $t/t_{1/2}$, where $t_{1/2}$ is the time required for 50% conversion, to demonstrate the dependence of the deviation from first-order kinetics on the nature of the chain backbone and the solvent power of the medium. The deviation from first-order kinetics is found to be very similar for the acrylamide copolymer in 40% methanol and the methacrylamide copolymer in 14% methanol, i.e., in media approaching the theta condition. When the two copolymers

TABLE V
Comparison of c_{eff}^{max} for Different Types of Chains

Copolymer designation	Type of chain	Volume fraction methanol	$(k_1^{init})_{corr}$	c_{eff}^{max}
E	Acrylamide	0	0.091	2.8
K	Methacrylamide	0	0.069	2.2
E	Acrylamide	40	0.062	4.5
K	Methacrylamide	14	0.068	3.0

are compared in water solution, the reaction of the more highly solvated acrylamide copolymer deviates more strongly from a first-order process.

Table V lists the values of $(k_1^{init})_{corr}$ for the ternary copolymers of acrylamide and methacrylamide in water and in solvent media approximating theta conditions. From these data, c_{eff}^{max} as defined in eq. (6) are derived by using the values of ω from Table I and k_2 from Table III. We may note that c_{eff}^{max} for the acrylamide copolymer is about 50% higher than for the methacrylamide copolymer when they are compared in theta media. From eqs. (6) and (7), we should expect c_{eff}^{max} to be inversely proportional to $K_\Theta M_0^{3/2}(x')^{1/2}$. Data listed by Kurata and Stockmayer for poly(methyl acrylate) and poly(methyl methacrylate)[15] suggest that the K_Θ values of acrylic and methacrylic chains lie within experimental error of one another. The data may then be interpreted by assigning to the polymethacrylamide chain an x' value about 50% larger than that characterizing the polyacrylamide chain. This conclusion is not unreasonable, since conformational analyses have shown that medium-size cyclic compounds have severe restrictions on geminal substitution of the atoms in the ring.[16] We should, expect, therefore, that in spite of the similar flexibility of polyacrylic and polymethacrylic chains, as characterized by the extension of their molecules, substantially longer chains would be required in the latter to produce cyclic structures free of significant strain.

This paper is abstracted from a Ph.D. thesis submitted by Neil Goodman to the Graduate School of the Polytechnic Institute of Brooklyn, June 1971.

References

1. N. Goodman and H. Morawetz, in *Polymers and Polymerization* (*J. Polym. Sci.*, *C*, **31**), C. G. Overberger and T. G Fox, Eds., Interscience, New York, 1971, p. 177.
2. W. Kuhn, *Kolloid-Z.*, **68**, 2 (1934).
3. P. J. Flory, *Statistical Mechanics of Chain Molecules*, Interscience, New York, 1969, (a) pp. 40–43; (b) p. 38.
4. F. T. Wall, L. A. Hiller, Jr., and W. F. Addison, *J. Chem. Phys.*, **23**, 2314 (1955).
5. B. J. Hiley and D. M. Sykes, *J. Chem. Phys.*, **34**, 1531 (1961).
6. C. Domb, *J. Chem. Phys.*, **38**, 2957 (1963).
7. C. Domb, J. Gillis, and G. Wilmers, *Proc. Phys. Soc.*, **85**, 625 (1965).
8. M. E. Fischer, *J. Chem. Phys.*, **45**, 1469 (1966).
9. M. Kumbar and S. Windwer, *J. Chem. Phys.*, **49**, 4057 (1968).

10. C. Rossi, U. Bianchi, and E. Bianchi, *Makromol. Chem.*, **41**, 31 (1960).
11. R. Okada, Y. Toyoshima, and H. Fujita, *Makromol. Chem.*, **59**, 137 (1965).
12. W. Scholtan, *Makromol. Chem.*, **14**, 169 (1954).
13. M. H. Loucheux and A. Banderet, *J. Polym. Sci.*, **48**, 405 (1960); *Bull. Soc. Chim. France*, **1964**, 1220.
14. W. H. Stockmayer and M. Fixman, in *First Biannual American Chemical Society Polymer Symposium* (*J. Polym. Sci. C*, **1**), H. W. Starkweather, Jr., Ed., Interscience New York, 1963, p. 137.
15. M. Kurata and W. H. Stockmayer, *Fortschr. Hochpolym. Forsch.*, **3**, 196 (1963).
16. C. Cordes, V. Prelog, E. Troxler, and H. H. Westen, *Helv. Chim. Acta*, **51**, 1663, (1968).

Received February 25, 1971

JOURNAL OF POLYMER SCIENCE: PART A-2 VOL. 9, 1669–1679 (1971)

Catalysis of Ionic Reactions by Polyelectrolytes. IV. Quenching of the Quinine Cation Fluorescence by Fe^{++}, Ag^{+}, and Br^{-} in Solutions of Poly(vinylsulfonic Acid)

ISSAM A. TAHA and HERBERT MORAWETZ, *Polymer Research Institute, Polytechnic Institute of Brooklyn, Brooklyn, New York 11201*

Synopsis

The fluorescence quenching of the doubly charged quinine cation by Fe^{++}, Ag^{+}, and Br^{-} was studied in the presence and absence of polyvinylsulfonate (PVS). The quenching by cationic species was greatly enhanced by PVS at low polyion concentrations; at higher concentrations of PVS, the fluorescence intensity increased owing to displacement of the quinine cations from the polyion domain. Quenching of quinine fluorescence by Br^{-} was repressed by PVS. Interpretation of the data with the use of Fe^{++} as the quenching agent led to "effective concentrations" of counterions in the polyion domain similar to those calculated from the catalysis of the redox reaction of $Co(NH_3)_5Cl^{++}$ with Fe^{++}. This may indicate that the reagent ions are not rigidly bound to the polyion chain, since such binding would affect differently processes with high and low activation energies. The Stern-Volmer constant for self-quenching of the quinine fluorescence can also be obtained from fluorescence intensity data in PVS solution.

INTRODUCTION

Low concentrations of polyions have been shown to have very large effects on the rates of ionic reactions. If the reaction involves two counterions, the reactants are concentrated in the polyion domain and the polyion acts, therefore, as a powerful catalyst.[1–9] On the other hand, if the reaction involves ions of opposite charge, one of the reagents is attracted and the other is repelled by the polyion, and the polyion acts then as an effective inhibitor.[10] The same principles would be expected to apply to the effect of polyions on the efficiency with which the fluorescence of ionic species is reduced by ionic quenching agents. We have reported previously a case of this type, involving the quenching of the fluorescence of the uranyl ion by the ferrous ion in poly(vinylsulfonic acid) (PVS) solution.[11] In the present investigation we have used as the fluorescing species the doubly protonated quinine cation, which has two important advantages compared to the uranyl ion. (1) The uranyl ion UO_2^{++} is in equilibrium with condensed species such as $U_2O_5^{++}$, $U_3O_8^{++}$, etc., and the equilibrium between these species is perturbed by the polyion. No such complication arises in the case of the quinine cation. (2) The fluorescence of quinine is much more intense than

that of the uranyl ion. This allows us to use much lower concentrations of the fluorescing species, so that the binding sites of the polyion may be in large excess over the quinine cations without requiring polymer concentrations at which the polymer molecules would be heavily intertwined. Data obtained under such conditions may be interpreted in terms of an "effective concentration in the polyion domain," which yields an insight into the nature of counterion binding.

EXPERIMENTAL

Inorganic Reagents

Fresh ferrous perchlorate solutions (in $10^{-3}M$ perchloric acid) were prepared from analytical reagent-grade ferrous perchlorate hexahydrate. The analysis for Fe^{++} was carried out by measuring the optical density of the *o*-phenanthroline complex at 512 nm. Oxygen-free nitrogen was bubbled through the solution until used. Sodium bromide was used as a source for bromide ions. Solutions were prepared gravimetrically from reagent grade sodium bromide. Silver perchlorate solutions were prepared from purified anhydrous silver perchlorate. Sodium perchlorate solutions were prepared gravimetrically from purified sodium perchlorate and were used to keep constant ionic strength of $2.5 \times 10^{-3}M$ for fluorescence quenching studies using sodium bromide.

Organic Reagents

Quinine sulfate solutions in $10^{-3}M$ $HClO_4$ were prepared from purified quinine sulfate (Matheson, Coleman & Bell) (MW 746.90). The molar extinction coefficient of the quinine ions at pH 1 were 85 at 400 nm and 5175 at 346 nm (reported,[12] 5200 at 346 nm in $0.1N$ H_2SO_4). Solutions of $10^{-5}M$ quinine sulfate in $10^{-3}M$ perchloric acid were used throughout this investigation unless otherwise stated.

The sodium salt of poly(vinylsulfonic acid) (PVS), was prepared from the monomer (Columbia Organic Chemicals Co.) as described previously.[11] Solutions of PVS were made up gravimetrically.

Spectroscopy

Both the ultraviolet absorption spectrum and the fluorescence measurements were made in a 1-cm cell. The absorption spectra were determined by using a Beckman DU-2 spectrophotometer, and the fluorescence spectra were obtained with a Hitachi MPF-2A spectrophotometer equipped with excitation and emission monochromators. For fluorescence measurements, the quinine sulfate solutions were excited at 346 nm unless otherwise stated and the emission spectrum was scanned between 360 and 600 nm. Slit openings corresponding to 6 nm were used for excitation and emission. A spectrofluorimeter filter was used to eliminate light of wavelength below 350 nm due to scattering of the excitation light.

Fluorescence quenching was followed by measurement of the relative intensities in solutions containing increasing concentrations of the quenching agent. When the reaction was carried out in the presence of PVS, an aliquot of stock solution of PVS was added to a solution containing all other electrolytes. However, the order of mixing the reactants was found to have no measurable effect on the results.

The ferrous ion was found to be a rather weak quencher for the quinine ion fluorescence in the absence of PVS. Therefore, in order to produce a measurable quenching effect, Fe^{++} was used in concentrations at which the absorption of light by Fe^{++} became significant. It was therefore necessary, for an accurate evaluation of the quenching efficiency of Fe^{++}, to correct for light attenuation due to absorption. The factor by which the fluorescence intensity is reduced owing to light absorption has been shown[11] to be given by

$$(I/I_0)_{abs} = D_0(1 - 10^{-D})/D(1 - 10^{-D_0}) \quad (1)$$

where D and D_0 are the optical densities of the solution in the presence and in the absence of the quenching agent. In the presence of PVS, attenuation of light by absorption was negligible, since lower concentrations of Fe^{++} were needed to produce a measurable quenching effect, as will be discussed later. No corrections were made for light absorption by the other electrolytes used in this study since it was negligible in comparison with their quenching effect.

RESULTS AND DISCUSSION

Quinine fluorescence has been widely studied and quinine solutions are frequently employed as standards in fluorescence analysis. Melhuish[13] determined the fluorescence quantum yield for the quinine ion and found it to be 0.55 at 366 nm in 0.1N H_2SO_4. This value has been used frequently to determine the quantum yields of fluorescence of other compounds. Recently, other values for the quantum yield of the quinine ion fluorescence have been reported.[14]

However, the value of 0.55 remains in use and reasonable quantum yield values were obtained for other substances using Melhuish's value as a standard of comparison.[15]

The reported pK values of quinine are 8.4 (for the tertiary amine) and 4.7 for the quinoline nucleus.[16]

We have conducted our experiments in $10^{-3}M$ perchloric acid where the ground state is almost entirely in the doubly ionized form. In order to evaluate the pK of the excited state, the relative fluorescence intensities at 452 nm were measured at pH values of 1 to 7. Perchloric acid solutions were used for pH 1 to 3 and commercial buffers for higher pH values. Any quenching due to the use of the buffer was accounted for by measuring the relative fluorescence intensities at increasing buffer concentrations and the use of the relation[17]

$$I_0/I = 1 + K_{sv}[Q] \quad (2)$$

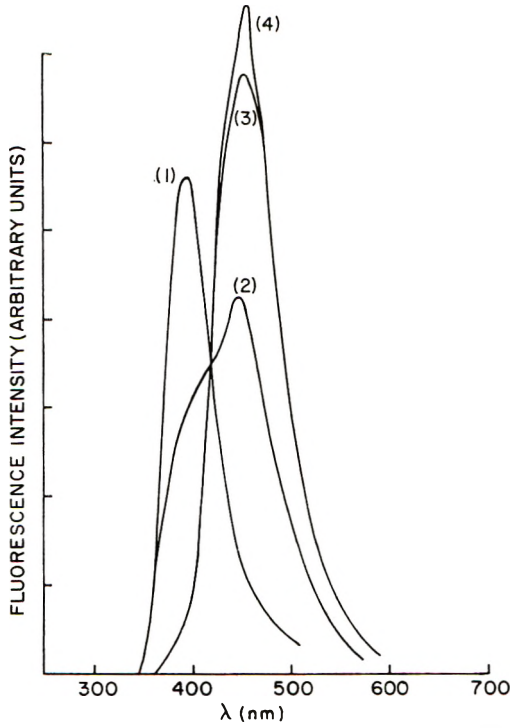

Fig. 1. Fluorescence of 2×10^{-5} M quinine solutions: (*1*) aqueous solutions; (*2*) 10^{-4} M $HClO_4$; (*3*) 10^{-3} M $HClO_4$; (*4*) 10^{-1} M $HClO_4$.

where I_0 and I are the fluorescence intensities in the absence and in the presence of the quenching agent, K_{sv} is the Stern-Volmer constant and $[Q]$ is the concentration of the quencher.

The appearance of an isosbestic point in the fluorescence spectra at 415 nm in the presence of different concentrations of perchloric acid confirms that the singly and doubly charged quinine cations are the only fluorescent species in the system. The spectra obtained with excitation at 346 nm are shown in Figure 1. A maximum fluorescence at 390 nm is observed in the spectrum of the water solutions of the quinine sulfate. A second maximum appears at 452 nm when $10^{-4}M$ perchloric acid is added and increases at higher $HClO_4$ concentrations at the expense of the 390 nm peak which eventually disappears. Presumably, the peak at 390 nm corresponds to the fluorescence of the singly charged quinine ion, while the 452 nm peak corresponds to that of the doubly charged ion. This maximum is red-shifted to 462 nm with a considerable reduction in intensity when light with a wavelength of 400 nm is used for excitation. The relative fluorescence intensities at 452 nm and the molar extinction coefficients at 346 nm are given in Table I. From these, values of 4.3 and 3.9 can be derived for ionization constants for quinine in the ground state and the excited state (the quinoline nitrogen). Thus, 95% of the quinine ions are doubly charged in the ground state at pH 3.

TABLE I
Variation of the Relative Fluorescence Intensities and Extinction Coefficients of Quinine Solutions with pH

pH	ϵ_{346}	Relative fluorescence intensity I_{452}	$100\ I_{452}/\epsilon_{346}$
7	1515	15.2	1.0
6	1642	16.0	0.975
5	2400	—	—
4.63	2685	31.5	1.170
4	3940	52.1	1.320
3	3950	92.0	1.854
2	5200	96.3	1.852
1.3	5350	100.0	1.870
1	5350	100.0	1.870

Effect of PVS on Quinine Fluorescence

The effect of PVS addition on the fluorescence of quinine in the presence of $10^{-3}M$ $HClO_4$ is shown in Figure 2 for excitation at 346 nm and at 400 nm. With small additions of PVS, the fluorescence intensity I drops sharply. However, as the PVS concentration is increased, I increases and approaches the value observed in the absence of polymer (I_0) if the quinine cations is excited at 346 nm. If excitation at 400 nm is used, I exceeds I_0 in the presence of a large excess of PVS.

These findings may be interpreted as follows. When the quinine cation is bound to the polyion, its local concentration in the polymer domain is so high that self-quenching, unobservable in the dilute solutions in the absence of PVS, becomes an important factor. When the amount of PVS added is small, the fraction of the quinine bound to the polymer increases with increasing PVS concentration and the self-quenching becomes more pronounced. However, when the binding sites of the polymer are in large excess over the quinine, the quinine will be essentially completely bound, and its local concentration in the polymer domains will be inversely proportional to the PVS concentration. Thus, the extent of self-quenching will be gradually reduced and eventually eliminated in the limit of a very large excess of PVS. This interpretation is analogous to that proposed by Bradley[18] to account for the effect of varying DNA concentrations on the fluorescence of acridine orange. The dependence of the quinine fluorescence behavior on the wavelength used for excitation has been noted by previous investigators,[19-21] and Chen has suggested[21] that two different excited singlet states are involved. Our data indicate that the fluorescence intensity of the species produced by irradiation at 346 nm is not altered by association with the polymer if there is no self-quenching. The species produced by irradiation at 400 nm fluoresces more intensely when bound to a large excess of PVS. This is analogous to the behavior of some dyes (e.g., crystal violet) which have been shown to fluoresce only when associated with polyanions.[22]

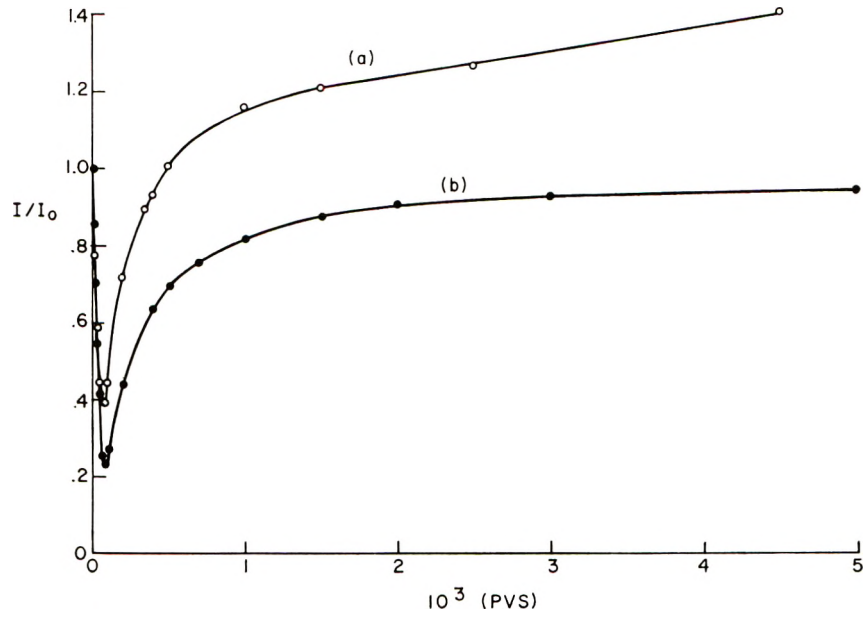

Fig. 2. Effect of poly(sodium vinylsulfonate) on the fluorescence intensities of quinine sulfate solutions: (*a*) fluorescence intensities at 462 nm, excitation at 400 nm; (*b*) fluorescence intensities at 452 nm, excitation at 346 nm.

Effect of PVS on the Quenching of Quinine Fluorescence

Quenching of the fluorescence of the quinine ion in the presence and the absence of PVS was studied at pH 3. Three ions were used, i.e., the divalent cation Fe^{++}, the monovalent cation Ag^{+}, and the monovalent anion, Br^{-}. The results are shown in Figures 3, 4, and 5. In the absence of PVIS, the quenching was found to depend upon the concentration of the quenching agent as indicated by thr Stern-Volmer equation (2). The values of K_{sv} were found to be 15.6 l./mole for Fe^{++}, 6.5 l./mole for Ag^{+}, and 462 l./mole for Br^{-}.

In the presence of PVS, however, the fluorescence intensity for the quinine ion shows a more complicated dependence on the quenching ion concentration. In the case of Fe^{++}, this dependence was qualitatively similar to that observed previously[11] for the quenching of the uranyl ion by Fe^{++}. However, enhancement of the quenching efficiency produced by the PVS was higher in the present case.

At very low concentrations of the quenching agent, the fluorescence intensity decreased sharply with increasing Fe^{++} or Ag^{+} concentrations reflecting a greatly increased quenching efficiency due to the concentration of the counterions in the polyion domain. At higher concentrations of the quenching ions, the quinine ions are displaced from the polymer binding sites and consequently are removed from the region where the quenching agents are at high concentrations. We have pointed out previously[11] that

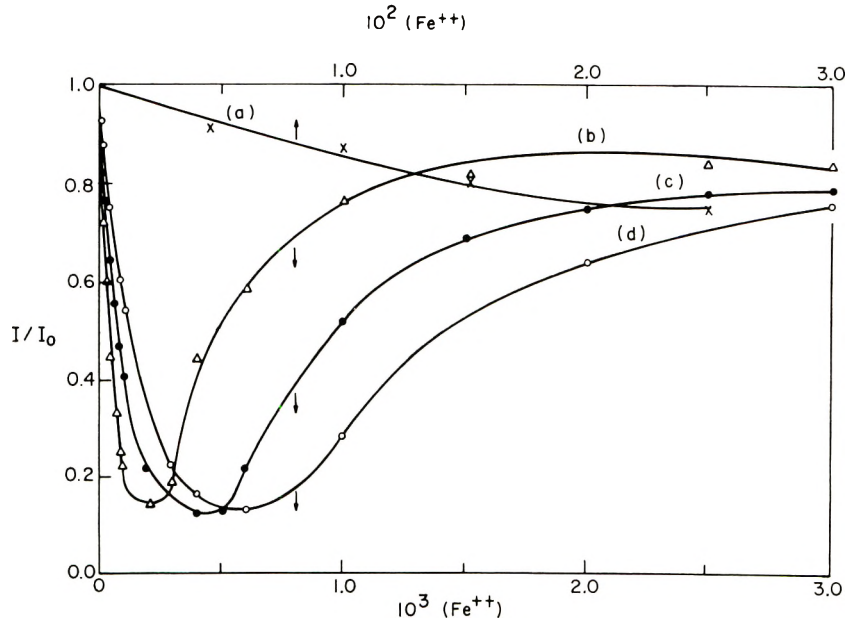

Fig. 3. Effect of PVS on the quenching of quinine fluorescence by Fe^{++} in the presence of 10^{-3} *M* $HClO_4$: (*a*) no PVS; (*b*) 10^{-3} *N* PVS; (*c*) 2×10^{-3} *N* PVS; (*d*) 3×10^{-3} *N* PVS.

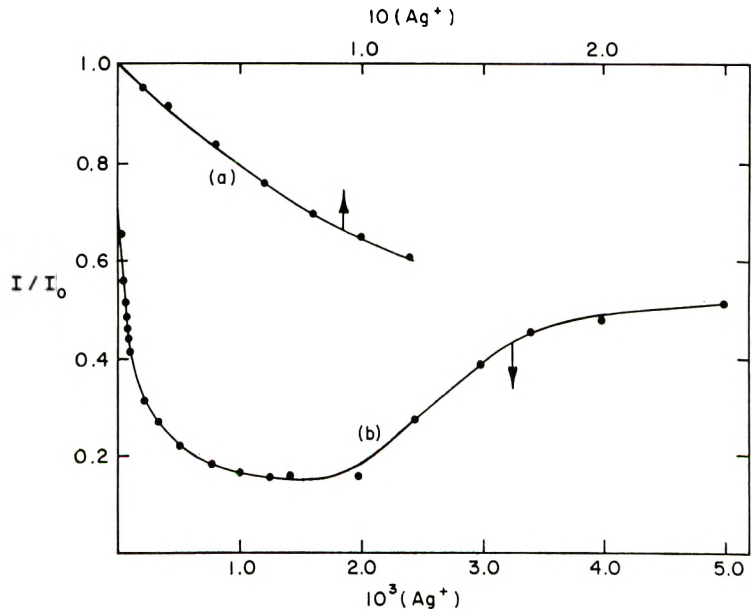

Fig. 4. Effect of PVS on the quenching of quinine fluorescence by Ag^+: (*a*) no PVS; (*b*) 3×10^{-4} *N* PVS.

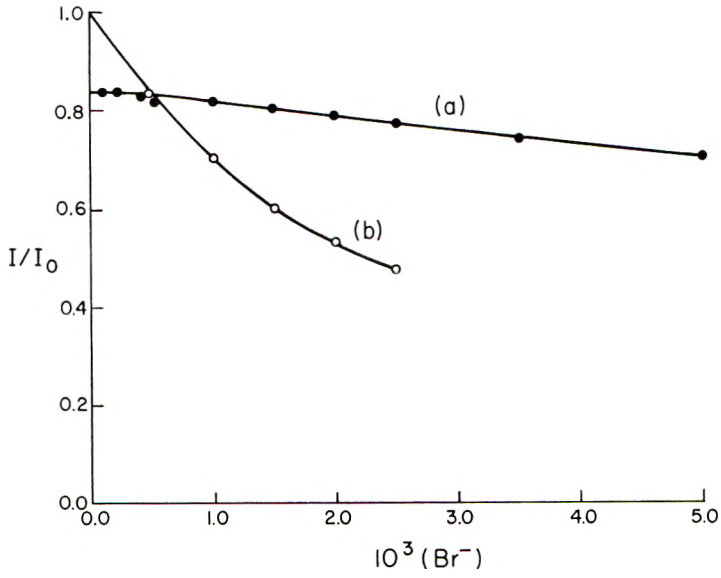

Fig. 5. Effect of PVS in the quenching of quinine fluorescence by Br^-: (*a*) 10^{-4} *N* PVS; (*b*) no PVS.

such a displacement will result in a strongly enhanced fluorescence intensity, provided that the exchange of the bound and free fluorescent species is slow compared to the lifetime of the excited state. This was the case with the fluorescence of the uranyl ion with an excited lifetime $\tau = 1.5 \times 10^{-6}$ sec and should hold, therefore, even more for the fluorescence of quinine with $\tau = 19.4 \times 10^{-9}$ sec.[23] It should be noted here that, while the fluorescence intensity more than doubled when the concentration of the Fe^{++} ion increased from $2 \times 10^{-4}M$ to $4 \times 10^{-4}M$, it remained virtually unchanged when the Ag^+ concentration was increased from $5 \times 10^{-4}M$ to $20 \times 10^{-4}M$. This indicates that it is more difficult for the singly charged silver ion to displace the doubly charged quinine ion from the polymer domain. At still higher concentrations of Fe^{++}, the fluorescence shows a slowly decreasing intensity, presumably due to quenching outside of the polymer domain.

As would be expected, PVS is effective in suppressing the quenching of quinine fluorescence by bromide ions, since the anionic quenching agent is repelled from the polymer domains to which the quinine is bound.

In previous studies in this laboratory concerned with the catalysis of ionic reactions by polyions,[7,8] it was pointed out that an interpretation of the data is particularly simple when the polyion binding sites are in substantial excess over doubly charged counterion reagents. In that case, we may assume that practically all of the reagent ions are bound to the polyions and the "effective local concentration" of any species $[M_L^{++}]$ in the polyion domain may be related to its stoichiometric concentration $[M^{++}]$ by the relation $[M_L^{++}] = (2[M^{++}]/P)\, C_{eff}^{max}$ where P is the normality of the polyion and C_{eff}^{max} is the "maximum effective local concentration" of the doubly

charged counterions which would correspond to a complete saturation of the polyion binding sites. Assuming then that the Stern-Volmer constant has the same value for quinine cations and Fe^{++} bound to PVS as it has in the absence of the polyion, we have, in analogy to eq. (2),

$$I_0/I = 1 + 2K_{sv}[Fe^{++}]C_{eff}^{max}/P] \quad (3)$$

This relation holds if the binding of the quinine cation to the polymer does not lead to a change in the fluorescence efficiency, a condition which is satisfied when using excitation at 346 nm, and if the polyion is in large excess over the quinine, so that the effect of self-quenching may be neglected. The plot suggested by eq. (3) is shown in Figure 6 and leads to a C_{eff}^{max} value of 1.0 mole/l.

The significance of C_{eff}^{max} is, unfortunately, not as clear as one might wish. Originally, it was believed that it depends only on the spatial distribution of counterions in the polyion domain.[7] However, the effect of a large excess of PVS on the reaction of $Co(NH_3)_5Cl^{++}$ with Hg^{++} and with Fe^{++} at 5°C leads to different C_{eff}^{max} values, i.e., 14*M* and 1*M*[8], respectively. This shows that the nature of the medium in the polyion domain introduces effects specific to a given reaction which are superimposed on the effect produced by the concentration of the reagent ions.

In spite of this uncertainty, the fact that PVS has a similar effect on the redox reaction of $Co(NH_3)_5Cl^{++}$ with Fe^{++} and on the quenching of the quinine cation by Fe^{++} may have some interesting implications on the nature of the binding of the reagent ions to the polyion. If the counterions are free to diffuse within the polyion domain, the acceleration of any chemical process involving two counterions would be expected to be mostly due to the concentration of the interacting species in this region, with specific effects, depending on the nature of the process playing a relatively minor role. However, if the counterion reagents are "site-bound" to the polyion[24,25] two of these counterions could only interact with one another if the polyion chain assumes a conformation to bring them into juxtaposition. (It is here assumed that the motion of a "site-bound" ion from one binding

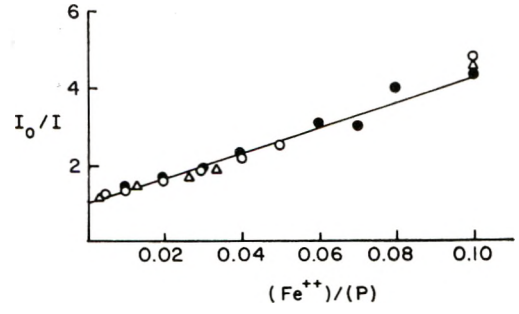

Fig. 6. Determination of C_{eff}^{max} from the dependence of the quinine fluorescence quenching on the $[Fe^{++}]/[P]$ ratio at various PVS concentrations: (●) 10^{-3} *N* PVS; (○) 2×10^{-3} *N* PVS; (△) 3×10^{-3} *N* PVS.

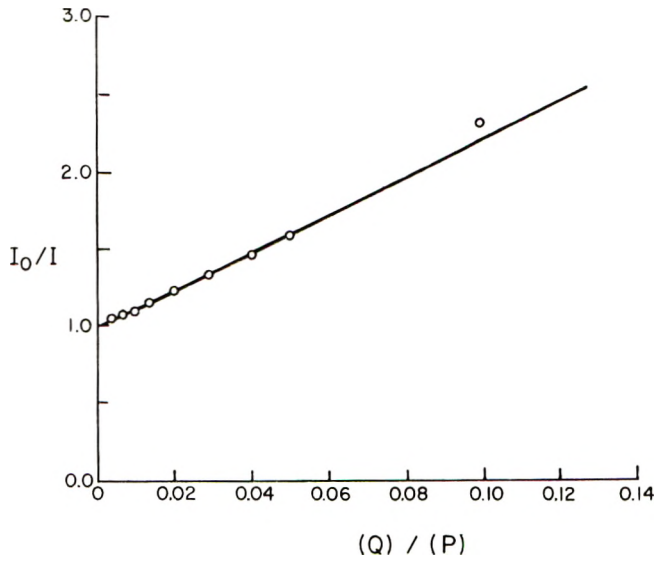

Fig. 7. Determination of the Stern-Volmer constant for the self-quenching of quinine from data in PVS solution.

site to another is a slow process). In this case, the factors governing the reaction rate will depend on the magnitude of the activation energy involved in the process. If this activation energy is high, so that the interacting species have to diffuse towards each other and separate many times before a chemical process occurs, the reaction rate will depend on the population of cyclic chain conformations, i.e., on the chain flexibility.[26] However, if the activation energy is low, the reaction will be diffusion-controlled, i.e., it will depend on the rate of conformational transitions of the polyion. The observation that C_{eff}^{max} is similar for the reaction of $Co(NH_3)Cl^{++}$ with Fe^{++} (a process with a high activation energy) and for the quenching of the excited quinine cation by Fe^{++} (a process with a very low activation energy) can be interpreted as indicating that the reagent ions are not likely to be rigidly held on the polyion.

Finally, we may utilize the value of C_{eff}^{max} to estimate the Stern-Volmer constant for the self-quenching of the quinine cation. This quantity cannot be determined in the absence of polyions, since the optical density of the solution would become prohibitively large before self-quenching becomes significant. However, we can use fluorescence intensities in the presence of a large excess of PVS (I) and in the absence of PVS (I_0) at the same quinine concentration [Q] and interpret the data by a relation analogous to eq. (3) (with [Q] substituted for $[Fe^{++}]$ to yield the self-quenching constant K_{sv}'. The plot shown in Figure 7 is linear for small values of 2[Q]/[P], yielding $K_{sv}' = 5.8$ l./mole.

We are grateful for support of this work by Grant GM-05811 of the National Institutes of Health.

References

1. C. L. Arcus, T. L. Howard, and D. S. South, *Chem. Ind.* (London), **1964**, 1756.
2. C. L. Arcus and B. A. Jackson, *Chem. Ind.* (London), **1964**, 2022.
3. W. Kern, W. Herold, and B. Scherlag, *Makromol. Chem.*, **17**, 231 (1956).
4. T. J. Painter, *J. Chem. Soc.*, **1962**, 3032.
5. I. Sakurada, Y. Sakagnali, T. Ono, and T. Ueda, *Makromol. Chem.*, **91**, 243 (1966).
6. N. Ise and F. Matsui, *J. Amer. Chem. Soc.*, **90**, 4242 (1968).
7. H. Morawetz and B. Vogel, *J. Amer. Chem. Soc.*, **91**, 563 (1969).
8. H. Morawetz and G. Gordimer, *J. Amer. Chem. Soc.*, **92**, 7332 (1970).
9. S. Brückner, V. Crescenzi, and F. Quadrifoglio, *J. Chem. Soc. A*, **1970**, 1158.
10. H. Morawetz and J. A. Shafer, *J. Phys. Chem.*, **67**, 1293 (1963).
11. I. A. Taha and H. Morawetz, *J. Amer. Chem. Soc.*, **93**, 829 (1971).
12. R. Rusakowicz and A. C. Testa, *J. Phys. Chem.*, **72**, 793 (1968).
13. W. H. Melhuish, *J. Phys. Chem.*, **65**, 229 (1967).
14. J. Drobnik and E. Yearghers, *J. Mol. Spectry.*, **19**, 154 (1965).
15. C. A. Parker and W. T. Rees, *Analyst*, **85**, 587 (1960).
16. A. Albert, *Heterocyclic Chemistry*, Oxford Univ. Press, London, 1959, p. 362.
17. O. Stern and M. Volmer, *Physik. Z.*, **20**, 183 (1919).
18. D. F. Bradley, *Trans. N.Y. Acad. Sci.*, [2], **24**, 64 (1961).
19. D. W. Moss, *Clin. Chem. Acta*, **5**, 283 (1960).
20. H. C. Borrensen, *Acta Chim. Scand.*, **19**, 2089 (1965).
21. R. F. Chen, *Anal. Biochem.*, **19**, 374 (1967).
22. G. Oster and J. Bellin, *J. Amer. Chem. Soc.*, **79**, 294 (1957).
23. W. R. Ware and B. A. Baldwin, *J. Chem. Phys.*, **40**, 1703 (1964).
24. H. Morawetz, *Macromolecules in Solution*, Interscience, New York, 1965, pp. 369–377.
25. G. S. Manning, *J. Chem. Phys.*, **51**, 924 (1969).
26. N. Goodman and H. Morawetz, *J. Polym. Sci. C*, **31**, 177 (1970).

Received January 29, 1971
Revised March 23, 1971

JOURNAL OF POLYMER SCIENCE: PART A-2 VOL. 9, 1681–1691 (1971)

Polymerization of Monolayers. VI. Influence of the Nature of the Exchangeable Ion on the Tacticity of Insertion Poly(Methyl Methacrylate)

ALEXANDRE BLUMSTEIN, KIRIT K. PARIKH, and SHADI L. MALHOTRA, *Department of Chemistry, Lowell Technological Institute*, and RITA BLUMSTEIN, *Lowell Technological Institute Research Foundation, Lowell, Massachusetts 01854*

Synopsis

The influence of the nature of exchangeable cations on the tacticity of poly(methyl methacrylate) (PMMA) prepared from montmorillonite–MMA adsorption complexes was investigated. The strength of ion-dipole interactions was estimated either by the value of the electrostatic interaction potential or by the value of the carbonyl-stretching frequency shift. It was shown that P_i, the percentage of isotactic triads in the polymer, increases with increasing strength of the ion–dipole interactions, while the persistence ratio and the mean length of closed isotactic (or syndiotactic) sequences remain essentially unchanged regardless of the nature of the cation. It was shown that values of P_i may vary from 0.15 for weakly interacting ions to 0.5 for strongly interacting ones, reaching at the upper limit the value calculated from the model proposed in a previous paper, thus confirming its validity.

INTRODUCTION

In a series of preceding papers it was shown that, in the free-radical polymerization of polar monomers adsorbed as mono-molecular layers between the lamellae of sodium montmorillonite, the organization of monomer molecules within the monolayer influences the structure[1] and the stereostructure[2] of the polymers.

The poly(methyl methacrylate) (PMMA) prepared from MMA–montmorillonite complexes was found to be composed of short stereosequences with a predominantly isotactic component.[2] The statistics of stereosequence distribution was found to be neither Bernoullian nor Markoffian;[3] the percentage of isotactic component increased with increasing exchangeable ion population on the surface of the mineral and was essentially independent of temperature in the interval between 20 and 160°C. The experimental results were interpreted by assuming that a fraction of the polar monomer molecules within the monolayer are associated with the exchangeable cations through dipole-ion associations. The monomer molecules engaged in MMA–ion complexes join the growing chain only as part of an isotactic "dyad." The fraction of isotactic "dyads" is determined by the

number of exchangeable ions per unit surface, that is, by the exchange capacity of the mineral. The molecules which do not belong to the MMA–ion complexes are assumed to be free "monads" which add to the growing chain as they would in free-radical solution polymerization. The tacticity of the insertion polymer was explained by assuming that free monomer adds to the chain with a single parameter controlling the stereospecificity σ, and the dyads add to the chain with another placement parameter σ'. The population of isotactic triads as defined by Bovey and Tiers[4] was found to agree qualitatively with the values of P_i, the percentage of isotactic triads, calculated with the help of equations derived from the model for a given value of the exchange capacity.[2]

In this paper the influence of the nature of the ion, particularly of the strength of the dipole ion association, is discussed. The exchangeable ions studied were from groups IA and IIA of the periodic table as well as Ag^+, Cu^{2+}, Ni^{2+}, Zn^{2+}, Al^{3+}, and Ti^{4+}.

In deriving the equation based on our polymerization model with sodium montmorillonite, it was assumed that each sodium ion enters in stable association with two monomer molecules forming an isotactic "dyad." The value of P_i is given by:

$$P_i = [1/(1 + \alpha)][\alpha\sigma(2\alpha\sigma + \beta\sigma' + \beta) + \beta\sigma'] \quad (1)$$

and

$$P_s = [1/(1 + \alpha)]\alpha(1 - \sigma)[2\alpha(1 - \sigma) + \beta(1 - \sigma')] \quad (2)$$

where σ and σ' represent the probability that monads and dyads, respectively, will add to the growing chain in an isotactic sequence; α and β are the mole fractions of "free" and associated molecules, respectively, and for a monolayer coverage, are related to the exchange capacity by $\beta = 0.0087qM_{MMA}$ and $\alpha = 1 - 0.0087qM_{MMA}$ where M_{MMA} denotes the molecular weight of the monomer–methyl methacrylate and q is the exchange capacity in equivalents/gram.

For a montmorillonite with an exchange capacity $q = 0.85$ meq/g, eq. (1) predicts for $0.22 \leq \sigma(25°C) \leq 0.23$ and $\sigma' = 0.75$[2] a value of P_i of 0.48 ± 0.03.

Experimentally P_i was found to be 0.38. We expect to find that the stronger the dipole–ion interaction, the higher the value of P_i and the closer it will be to the value predicted by eq. (1), for $q = 0.85$ meq/g. Similarly, we would expect the values of P_s, the percentage of syndiotactic triads in the polymer, to be close to those calculated from eq. (2) for strongly interacting ions. On the other hand, if the dipole–ion partnership is loose, the value of P_i should be smaller than that found for Na montmorillonite. According to our model, the stereosequence length should be essentially independent of the nature of the ion. The strength of the interactions was qualitatively estimated by infrared spectroscopy. Complexes with approximately monomolecular coverage were prepared from vapor phase at room temperature and their spectra recorded close to equilibrium conditions.

A detailed study of various complexes of different homoionic montmorillonites with a model, nonomonomeric compound, methyl acetate (MA) was made. Spectra of monomer–montmorillonite complexes were also recorded.

EXPERIMENTAL

Materials

All materials used, including the montmorillonite, were identical to those described in the preceding papers of this series.[1,2]

Polymerization and Characterization of Polymer

Complexes of nearly monolayer coverage of MMA were prepared with various homoionic montmorillonites. The complexes were prepared by vapor-phase adsorption at 70 or 30°C. In the former case, a free radical initiator was deposited on the mineral from a mixture of hexane and benzene prior to complex formation (azobisisobutyronitrile at 1 wt-% with respect to the dried montmorillonite); the polymerization was carried out at 70 or 90°C for 24 hr. In the latter case, polymerization was at room temperature and initiated by γ-rays (total irradiation dose 6 Mrad, dose rate 0.3 Mrad/hr).

Techniques

The techniques for preparation of homoionic minerals, preparation of complexes, determination of coverage, initiator deposition, polymerization, polymer extraction, and purification are described elsewhere.[1,2] The tacticity of polymers was determined by means of NMR spectroscopy as previously described.[2]

Adsorption Isotherms

Adsorption from vapor phase was carried out as follows. After deposition of the initiator, the dry, finely divided, and accurately weighed mineral was exposed in a thermostatted vacuum desiccator to a given relative pressure of monomer. After equilibration (3 hr), the mineral was reweighed and the equilibrium uptake calculated. The relative vapor pressure of monomer was varied by use of binary mixtures of MMA with an inert, nonvolatile compound such as castor oil. A calibration curve was obtained, giving the equilibrium vapor pressure of MMA as a function of the composition of the mixture. The adsorption yield of the complex could then be adjusted at will by equilibrating the mineral with a large excess of a castor oil–MMA mixture of appropriate composition.

Infrared Spectra

Montmorillonite–MA complexes were prepared at room temperature by vapor-phase adsorption on a dehydrated mineral which had been passed through a 200-mesh sieve. The complexes were dispersed in Nujol at a con-

centration of 15 wt-% and the viscous Nujol paste was evenly spread between two rock salt plates. The infrared spectra were taken at room temperature with a Beckman IR-10 instrument. The polystyrene band at 1601 cm^{-1} was used as standard.

The same technique was employed for montmorillonite–MMA complexes.

Care was taken to avoid as much as possible loss of organic material and hydration of the complexes during handling.

RESULTS AND DISCUSSION

Figures 1 and 2 show two typical adsorption isotherms of MMA, for a Na^+ and a Ca^{2+} montmorillonite, respectively. The percentage of adsorption τ (weight of monomer, g/100 g of clay) is plotted against the relative pressure of monomer at several temperatures between 50 and 70°C. Sodium montmorillonite adsorbs in a one-step process with an adsorption

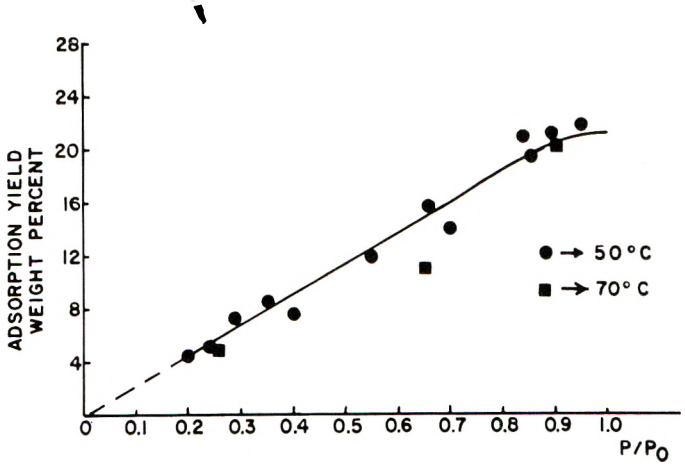

Fig. 1. Adsorption isotherm for Na^+ montmorillonite: (●) 50°C; (■) 70°C.

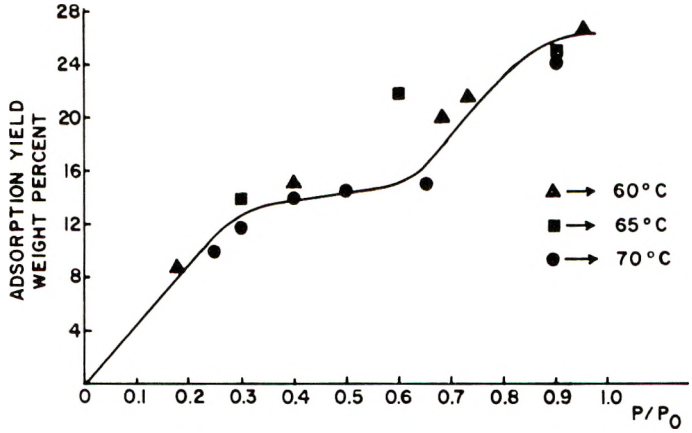

Fig. 2. Adsorption isotherm for Ca^{2+} montmorillonite: (▲) 60°C; (■) 65°C; (●) 70°C.

plateau at approximately 23% of monomer. Calcium montmorillonite displays a two-step process, with the first plateau at $\tau = 15\%$ and the second at $\tau = 25\%$, approximately. An equilibrium uptake $\tau = 23\%$ corresponds to a tight monolayer of MMA molecules covering the totality of the mineral surface.[2]

The equilibrium uptake fluctuates depending on the nature of the exchangeable cation. The complexes discussed below have a monomer coverage $\tau = 23 \pm 4\%$ and are referred to as "monolayer" complexes. The infrared spectra of monomer complexes are independent of the exact degree of coverage within the above range.

Figure 3 shows some representative infrared spectra. The carbonyl stretching absorption is located at 1745 cm^{-1} for MA and at 1732 cm^{-1} for MMA. Figure 3*a* which gives the spectrum of a Zn montmorillonite shows that there is no interference by the mineral in the carbonyl absorption region. A band at 1635 cm^{-1}, which is due to the presence of residual hydration water, varies somewhat in width and intensity, depending on the nature of the exchangeable ion.

Figures 3*b*–3*e* show the carbonyl absorption region of some complexes of approximately monomolecular coverage. It is obvious that the carbonyl group assumes several different states of bonding to the mineral surface. A sharp peak or a shoulder is always present at, or very close to, the stretching frequency of the free carbonyl. This is considered as belonging to the "free" monad molecules. Displaced towards a lower frequency is a considerably broader and more intense band, often displaying a secondary peak or shoulder. This reflects the absorption by carbonyls associated with the exchangeable ions. The stronger the electrostatic ion–dipole interaction, the greater the contribution of a single-bonded resonant form $C^+—O^- \ldots M^{n+}$ and the lower the carbonyl absorption frequency.

We have taken the shift $\Delta\bar{\nu}$ with respect to the free carbonyl position to be an indication of the strength of the ion–dipole interaction in the molecules belonging to the dyads. With ions belonging to groups IA and IIA, the carbonyl peak is relatively narrow, With the other ions, the band broadens, and in the case of Al^{3+} and Ti^{4+}, the shift can be estimated to no better than ± 4 cm^{-1} with the available instrument.

Table I gives the infrared shifts for various montmorillonite–MA complexes of approximately monomolecular coverage for ions of groups IA and IIA, for which the electrostatic contribution to bonding with MA molecules is the dominant one. In this case the value of the electrostatic ion–dipole interaction energy Φ_p can be assumed to give a reasonably accurate estimate of the strength of the ion-dipole interaction in a dyad. We calculate Φ_p by:

$$\Phi_p = \mu_0 Q / r_0^2 \tag{3}$$

where μ_0 is the dipole moment of the organic molecule, Q is the charge of the ion, and r_0 is the interaction distance, that is, the distance between the center of the dipole and the center of the ion.[6]

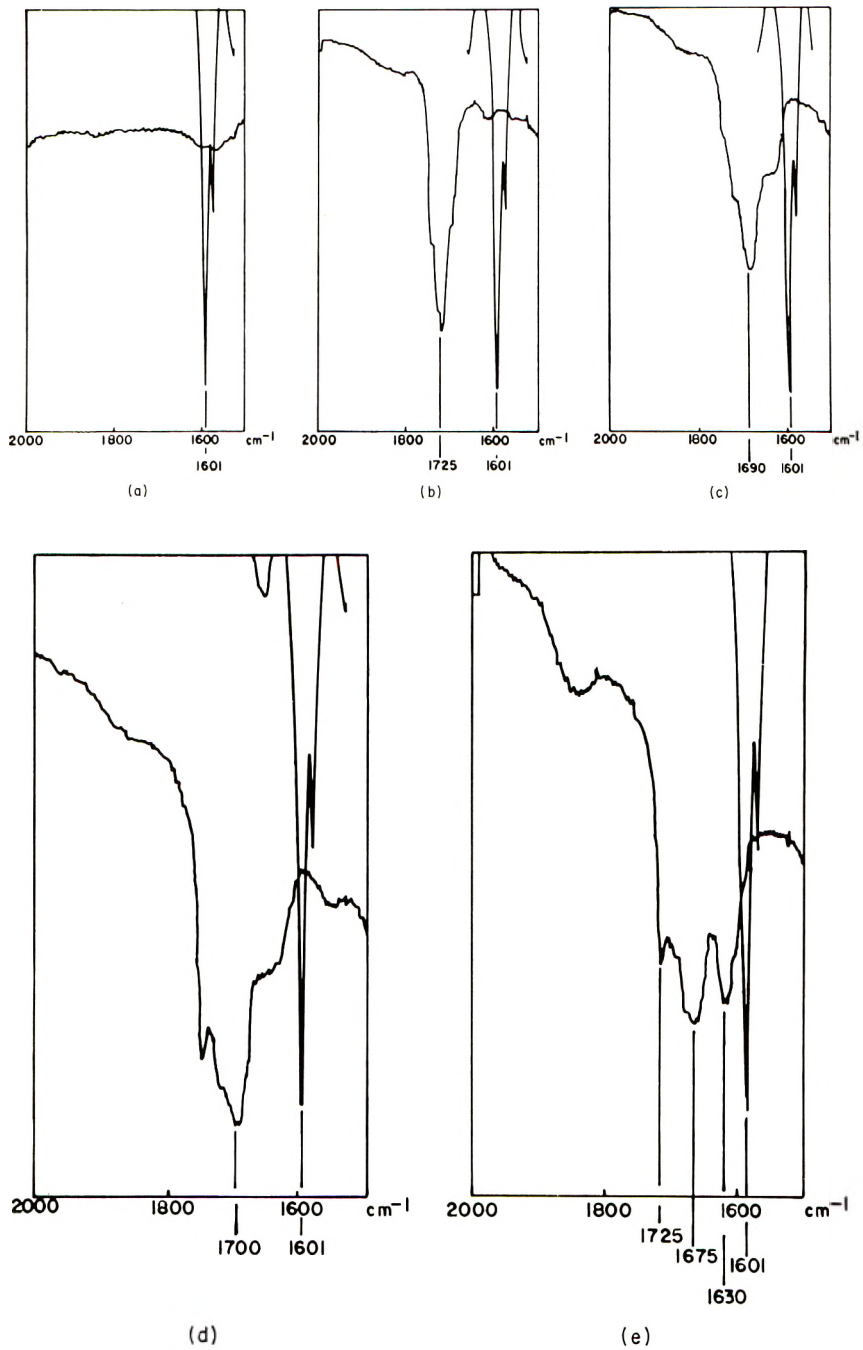

Fig. 3. Infrared spectra in the vicinity of the C=O stretching frequency: (*a*) Zn^{2+} montmorillonite; (*b*) Cs^{+} montmorillonite-methyl acetate complex; (*c*) Ca^{2+} montmorillonite-methyl acetate complex; (*d*) Zn^{2+} montmorillonite-methyl acetate complex; (*e*) Zn^{2+} montmorillonite-MMA complex.

TABLE I
Shift of the Carbonyl-Stretching Frequency and Calculated Values of the Electrostatic Interaction Energy Montmorillonite–MA Complexes for Ions of Groups IA and IIA

Ion	r_0, Å	Φ_p, kcal/mole	$\Delta\bar{\nu}$, cm^{-1}
Li^+	3.38	13.2	40
Na^+	3.65	11.1	35
K^+	4.03	9.1	20
NH_4^+	4.13	8.5	50
Cs^+	4.37	7.4	17
Mg^{2+}	3.36	26.0	56
Ca^{2+}	3.67	22.0	55
Ba^{2+}	4.04	17.7	47

We know from x-ray evidence[7,8] that the aliphatic polar molecule is oriented with its dipole parallel to the surface of the lamella. If we assume that the center of the ion tends to be coaxial with the dipole of the organic molecule and that the ion and carbonyl oxygen are in contact, the interaction distance can be readily estimated. The orientation of an electrostatically complexed dyad is illustrated in Figure 4*a* for an ion of radius 1.0 Å. Figure 4*b* shows an ion of the same radius complexing two monomer molecules through coordination bonds with the carbonyl groups. It is apparent that in both cases the two monomer molecules can only join internally in an isotactic sequence. The constrained molecules lie in the plane parallel to the surface of the lamella. In the former case, the distance between the two reacting double bonds is some 5 Å, in the latter, about 3.5 Å. For polymerization in the solid state, Hirshfeld and Schmidt have postulated that the maximum distance between reactive centers is approximately 4 Å, if the activation process does not alter the dimensions of the monomer molecule.[9] At first glance, it might seem that the reactive centers in an electrostatically bound dyad are too far apart to allow polymerization. Actually, the molecules of the dyad are brought together more closely than in the simplified model illustrated in Figure 4*a* for three reasons: (a) the molecules have some mobility in two dimensions;[5,7] (b) some ions are preferentially located inside the hexagonal cavities of the array of oxygen atoms populating the surface of the lamellae, and the molecules can thus be brought in close contact; (c) some of the bonds may not be entirely electrostatic and a compromise between the two cases of Figure 4 is possible.

In Figure 5, $\Delta\bar{\nu}$, the experimental infrared shift, is plotted versus the calculated electrostatic interaction potential Φ_p for ions of groups IA and IIA. It is possible to see that with the exception of ammonium, a linear relationship between $\Delta\bar{\nu}$ and Φ_p exists. Ammonium montmorillonite behaves unusually in two respects; the infrared spectrum of the complex and the isotactic content of the polymer. If $\Delta\bar{\nu}$, rather than Φ_p, is used to estimate the ion–dipole interaction, the behavior of ammonium montmorillonite ceases to be exceptional.

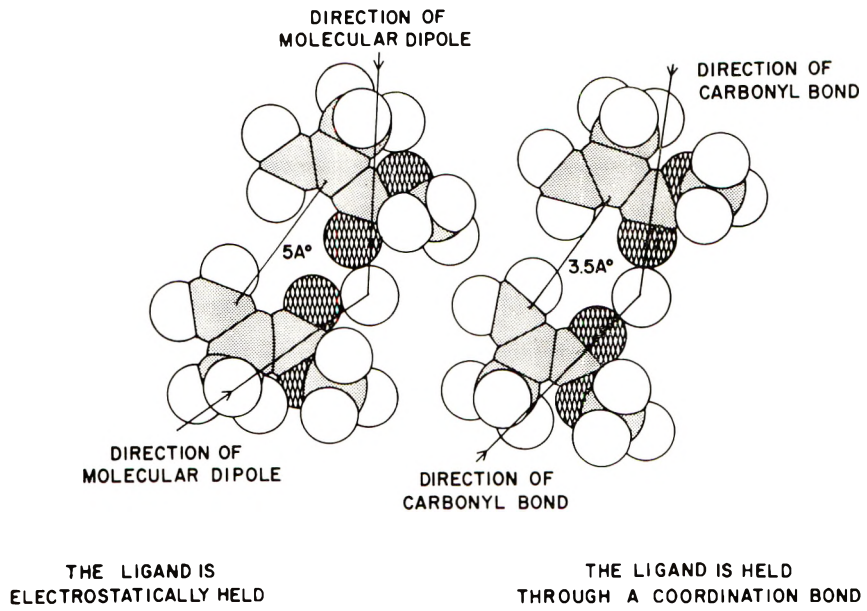

Fig. 4. An isotactic dyad of MMA around an exchangeable ion.

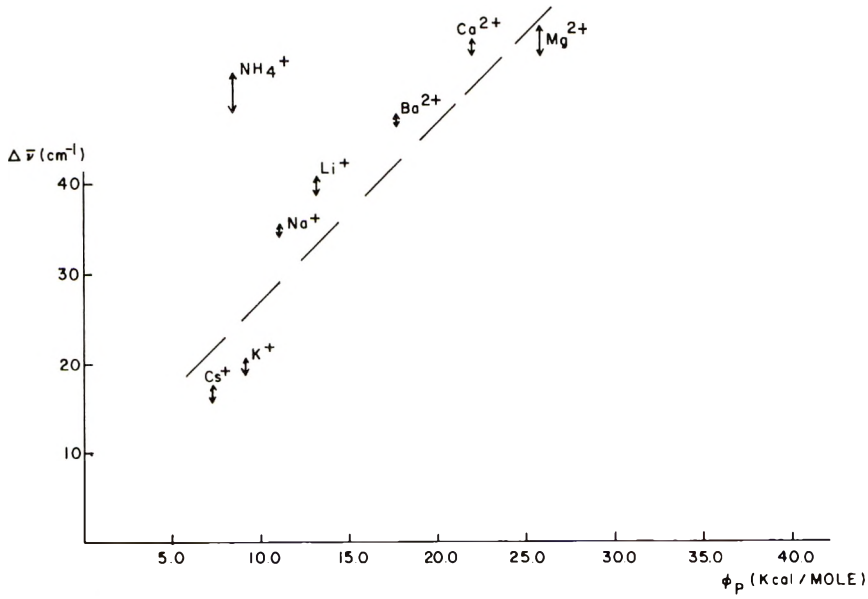

Fig. 5. $\Delta\bar{\nu}$ vs. the calculated value of the electrostatic interaction potential Φ_p (in kcal/mole) for MA.

For ions such as Cu^{2+}, Zn^{2+}, or Al^{3+}, which complex the monomer molecules through coordination bonds, the value of $\Delta\bar{\nu}$ ives an easily measurable qualitative estimation of the strength of the interaction.

Table II gives P_i, P_s, and P_h (the percentage of heterotactic triads), the mean length of closed isotactic sequences μ_I, and the persistence ratio[10] ρ for

TABLE II
Stereostructure of Insertion PMMA for Different Exchangeable ions

Ion	$\Delta\bar{\nu}$, cm^{-1}	P_i, %	P_s, %	P_h, %	μ_1[a]	ρ[a]	Method of preparation[b]
Cs^+	17	31.8	21.1	47.1	2.29	1.13	A
K^+	20	29.9	28.8	41.3	2.45	1.21	B
Na^+	35	38.8	15.6	45.6	2.76	1.04	A
Li^+	40	30.4	23.6	46.0	2.32	1.08	A
NH_4^+	47	38.0	23.9	38.1	3.13	1.26	A
Ba^{2+}	47	34.9	19.7	45.4	2.54	1.07	A
Mg^{2+}	56	41.9	14.6	43.5	2.92	1.06	A
Ca^{2+}	55	48.3	10.1	41.6	3.32	1.02	A
Ni^{2+}	47	39.3	16.5	44.2	2.78	1.07	B
Zn^{2+}	47	39.9	14.9	45.2	2.76	1.04	B
Al^{3+}	57	46.2	13.2	40.6	3.27	1.10	B

[a] Calculated according to Coleman and Fox.[10]

[b] Methods of preparation: method A, complex prepared via adsorption from vapor phase at 30°C, polymerized with γ-rays at 25°C; method B, complex prepared via adsorption from vapor phase at 70°C, polymerized with AIBN at 70°C or 90°C.

polymers obtained from various homoionic complexes. The stereosequence distribution is independent of degree of conversion.[2,5] This suggests that polymerization proceeds homogeneously throughout the complex and lends validity to our assumption that monads and dyads add to the growing chain at the same rate.[2]

It is apparent that P_i increases with increasing value of $\Delta\bar{\nu}$ while the persistence ratio remains essentially the same regardless of the nature of the ion and of the method of preparation of the polymer.

In Figure 6, P_i is plotted versus $\Delta\bar{\nu}$ to show that the percentage of isotactic triads increases with increasing strength of the ion–monomer interaction. The trend is unmistakable, and the experimental values of P_i and P_s reach, within the limits of error, the values calculated from eqs. (1) and (2), thus confirming the validity of the model outlined above.

The persistence ratio is remarkably independent of the nature of the ion, and its value shows that the polymer consists of short stereosequences, as expected for a combination of placements of isotactic dyads and free monads. The percentage of isotactic dyads appears to depend only on the strength of the ion–dipole interaction (as qualitatively measured by the value of $\Delta\bar{\nu}$) and not on the coordination number of the ion or on the nature of the interaction (electrostatic or coordination bonds). It is interesting to note that the degree of conversion and the overall polymerization kinetics depend strongly on the nature of the ion–monomer bond and that with Cu^{2+} and Ti^{4+} polymerization was inhibited.[5]

The line drawn through the scatter of points in Figure 6 does not mean that a quantitative relationship between P_i and $\Delta\bar{\nu}$ was found to exist. The complexity of the system makes the establishment of such a relation

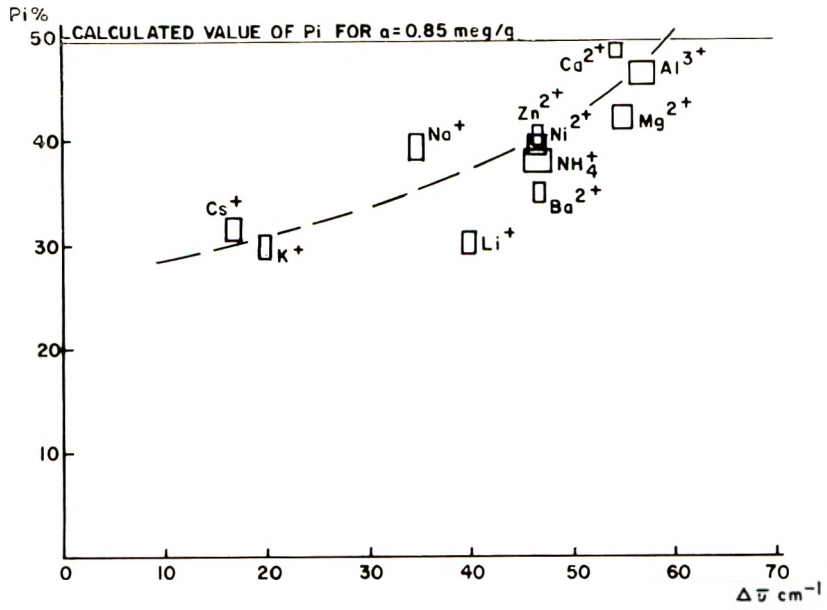

Fig. 6. P_i vs. $\Delta\bar{\nu}$.

extremely difficult. The error on the measurement of $\Delta\bar{\nu}$, approximately represented on Figure 6, is mainly due to the width of the carbonyl peak of the complex. The values of P_i given here were uncorrected for fluctuations in coverage of the mineral surface. Such fluctuations never exceeded 3–4% and were found to introduce an error in P_i of less than 2%.[2] The best results were usually obtained when complex formation and polymerization were carried out at roughly the same temperature so as to leave the complex undisturbed. The values of P_i reported here were mostly obtained when complex formation and polymerization were either close to room temperature or 70°C. A few of the values of P_i represent polymerization of complexes far removed from their equilibrium conditions (complex formation at 70°C and polymerization at 90°C). When the monomer-montmorillonite complex is stable at 90°C, the values of P_i obtained by polymerization at this temperature are consistent with the values of P_i obtained by polymerization at room temperature and at 70°C. This confirms our previous observation with Na montmorillonite,[2] namely that above room temperatures, tacticity is very little temperature-dependent within the range of stability of the complex.

The isotactic content of polymers prepared from complexes with Li^+ montmorillonite is significantly below the general trend regardless of the method of preparation. This illustrates one of the uncertainties which are inherent to the nature of the system: the dependence of the value of P_i on the geometry of distribution of the exchangeable cations within and around the elementary lamellae of the montmorillonite. Small ions have a tendency to diffuse toward the negative substitution sites within the lattice and

this decreases the number of ions available for association with the monomer molecules. Furthermore, small ions are often strongly hydrated and lose their hydration later with considerable reluctance. It is necessary to heat such minerals to produce partial or total dehydration, and this in turn accelerates the diffusion of such ions and decreases the number of ions available for solvation. Lithium montmorillonite is an outstanding example of such a phenomenon, which can also be exhibited by other strongly hydrated ions.

Quantitative discussion of the influence of the nature of the ion is further hampered by the complex nature of the interactions between the cation and MMA molecule. The electrostatic dipole–ion interaction is only one of the ligand forces involved and care must be exercised in comparing cations with dissimilar electronic structures, but it is clear that the percentage of isotactic triads increases with increasing strength of the ion-monomer interaction in agreement with our polymerization model.[2] To our knowledge, this is the only example of a predominantly isotactic PMMA obtained by free-radical polymerization in which the population of isotactic triads can be varied as will between 15 and 50%.

The financial support of Owens-Illinois Technical Center is gratefully acknowledged.

References

1. A. Blumstein, R. Blumstein, and T. H. Vanderspurt, *J. Colloid Sci.*, **31**, 237 (1969).
2. A. Blumstein, S. L. Malhotra, and A. C. Watterson, *J. Polym. Sci., A-2*, **8**, 1599 (1970).
3. C. W. Pyun and T. G. Fox, *J. Polym. Sci., A-2*, **9**, 615 (1971).
4. F. A. Bovey, and G. V. D. Tiers, *J. Polym. Sci.*, **44**, 173 (1960).
5. S. L. Malhotra, K. Parikh, and A. Blumstein, *J. Colloid Surface Sci.*, in press.
6. K. K. Bissada W. D. Johns, and F. S. Cheng, *Clay Miner.*, **7**, 155 (1967).
7. D. M. C. McEwan, *Trans. Faraday Soc.*, **44**, 349 (1948).
8. A. Blumstein, *J. Polym. Sci., A*, **3**, 2653 (1965).
9. F. L. Hirshfeld and G. M. J. Schmidt, *J. Polym. Sci. A*, **2**, 2181 (1964).
10. B. D. Coleman and T. G. Fox, *J. Polym. Sci. A*, **1**, 3183 (1963).

Received January 4, 1971
Revised March 5, 1971

JOURNAL OF POLYMER SCIENCE: PART A-2 VOL. 9, 1693–1702 (1971)

Glass Transition in Nylons

GERALD A. GORDON, *Corporate Research and Development Department, Continental Can Company, Chicago, Illinois 60620*

Synopsis

Differential thermal analysis (DTA) of some commercial nylons has disclosed some anomalous phenomena with respect to the glass transition, generally considered to occur at 40–50°C. On the first heat cycle the transition occurs normally. On cooling, however, no corresponding transition occurs, and on an immediate rerun the transition has disappeared. If another DTA thermogram is made after a few hours, the transition begins to reappear, but at a temperature lower by a few degrees. After about five days rest, the transition is again normal in size and temperature. On annealing at 75°C, the 43°C transition is pushed up to about 92°C. On resting after annealing, transitions appear at both 40 and 92°C. These phenomena are explained in terms of the slow formation of a hydrogen-bonded network in the amorphous regions of the polymer. It is the disruption of this network that is normally considered to be the glass transition in nylons. The network is slow in re-forming because of problems involved in matching up potential hydrogen-bonding sites, which are, of course, distributed at intervals along the polymer chain. The temperature at which the network is disrupted is apparently dependent not so much on the ratio of bonding to nonbonding sites, as on the temperature at which it was formed.

Introduction

It is widely accepted that the glass transition temperatures T_g of various nylons lie in the neighborhood of 40–50°C.[1–4] There have been reports, however, based on penetrometer studies[5] and crystallization kinetics considerations,[6] suggesting that the glass transition in these materials actually occurs at a much lower temperature, pehaps as low as −65°C. Boyer, in a review of thermal transitions in polymers,[7] attempts to reconcile these conflicting viewpoints by suggesting that the nylons are an unusual case "because of the alternation of the nonpolar hydrocarbon segments ... and the very polar amide linkages." He accepts the transition at about 50°C as satisfying most of the criteria for T_g and suggests that the anomalous crystallization kinetics data result from "in-chain motion of subgroups."

We report here the results of our differential thermal analysis (DTA) studies on some commercial nylons which indicate the unusual nature of the 40–50°C transition in the nylons and suggest an explanation for this behavior.

Procedure

The materials used in this study were all commercial extrusion or general-purpose grade nylons. The nylon 11 was from Belding Chemical Industries, the nylon 6 was from The Allied Chemical Company, both the nylon 66 and the nylon 610 were from E. I. du Pont de Nemours & Company, and the nylon 12 was from Emser Werke.

The instrument used for the DTA work was a DuPont Model 900 differential thermal analyzer, with a low-temperature cell. Sample size was generally about 15 mg. The heating rate was 10°C/min, and the most sensitive scale available (0.1°C/in) was used on the ΔT axis. All runs were made in a flowing, dry nitrogen atmosphere and with a carborundum reference (240 grit). The samples were prepared by melting about 15 mg of polymer in the bottom of a 4 mm diameter "macrotube" whereupon the thermocouple bead was embedded in the bottom center of the sample. This technique of sample preparation was used because fused samples gave more reproducible thermograms than did unfused samples, because of better thermal contact. Thermograms made with unfused, unheated samples (film and pellets, as received) indicate that the procedure does not introduce artifacts with respect to the phenomenon under discussion here.

The infrared spectra were made on a Perkin-Elmer 421 grating spectrophotometer run in the regular scanning mode. The sample was prepared by dissolving nylon 6 film in C5 Fluoroalcohol (technical grade, E.I. duPont de Nemours & Company) and then casting a film on an NaCl block. The solvent was removed by heating under a heat lamp. Comparison of the nylon spectra with the fluoroalcohol spectrum indicated that all of the solvent had been removed before the nylon spectra were made.

All materials used for DTA measurements were dried in a vacuum oven at 80°C for 24 hr in pellet form prior to cutting and packing. Before the initial run (5 to 10 days after packing) and between all the following runs, except where wet samples were desired, the samples were kept in a desiccator over anhydrous calcium sulfate. Annealed samples were heated in a vacuum oven at 75°C for 24 hr.

In interpreting the thermograms a choice had to be made between the minimum in the curve and the break from the baseline as the determinant of the transition point. A first-order transition is generally defined by the maximum or minimum point in the thermogram, while a second-order transition is generally considered to occur at the point where the curve breaks from the baseline. Since, as discussed below, the phenomenon presented here is considered to be a second-order transition, the transition points were read at the temperature of the break from the baseline. The intercept of the straight lines, as indicated in the figures, shows the method used for determining this point.

Results

Figures 1 and 2 show DTA thermograms at high sensitivity for nylon 11 in the temperature range of −20°C to +120°C. The transition data are

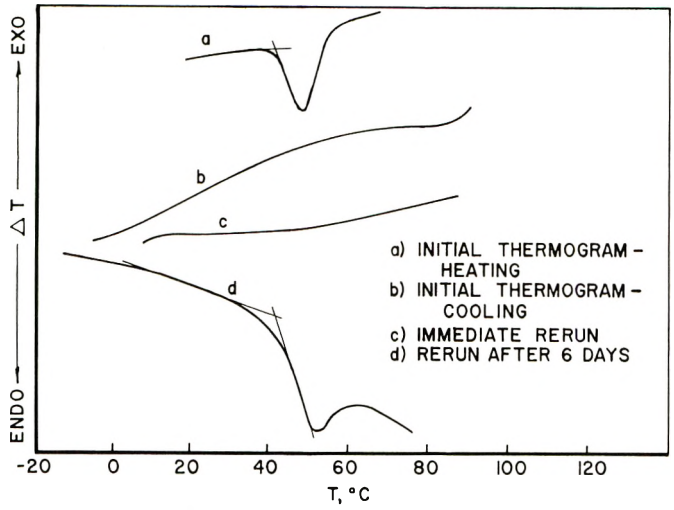

Fig. 1. Glass transition behavior in nylon 11.

tabulated in Table I. In Figure 1, curve *a* is the initial heating curve, curve *b* is the corresponding cooling curve, curve *c* is the heating curve for an immediate rerun of the same sample, and curve *d* is another rerun taken 6 days later. The transition in question is the one that appears at about 43°C on curves *a* and *d*. The point of interest is that there is no corresponding transition on either curve *b* or *c*.

TABLE I
Transitions in Nylon 11

Thermal history	T_g, °C	T_m, °C
Initial thermogram	43	189
Immediate rerun	—	189
Rerun after 5 hr	33	—
Rerun after 24 hr	40	—
Rerun after 6 days	43	—

Figure 2 shows a series of thermograms for the same sample of nylon 11 run varying periods of time after the last previous thermogram. It can be seen that while the transition does not appear in the immediate rerun (curve *b*), after 5 hr (curve *c*) it has started to come back, though at a lower temperature. After 24 hr (curve *d*) the transition is more pronounced, and at a temperature intermediate between those of curves *a* and *c*, and after 6 days (curve *e*) the transition is practically identical with that on the initial thermogram (curve *a*).

Figure 3 shows the initial thermogram for a series of nylons: 6, 66, 610, 11, and 12. The transition data are collected in Table II. In each case the transition apparent at 40–50°C does not appear in an immediate rerun of

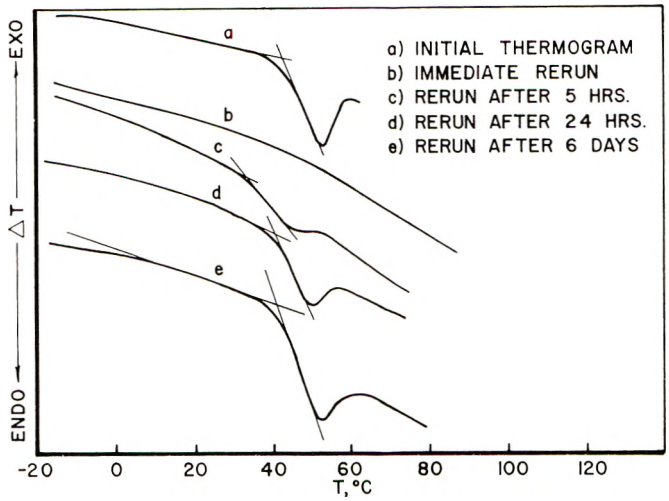

Fig. 2. Time dependence of glass transition of nylon 11.

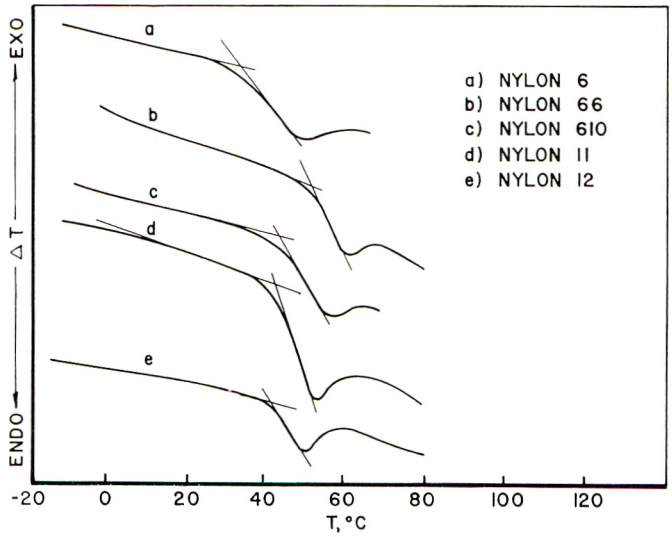

Fig. 3. Glass transition in various nylons.

the thermogram, but does reappear when the polymer is allowed to rest at room temperature for about 5 days. In all cases, melting and other behavior are normal. Table II also shows the number of methylene groups between potential hydrogen bonding sites on the polymer chain.

Figure 4 shows the effect of annealing on the transitions in question in nylon 11. If, after packing, a sample is annealed at 75°C for 24 hr and a thermogram taken immediately (curve *a*) no transition appears at 43°C, but a transition does appear at 92°C. If, on the other hand, the sample is allowed to rest at room temperature in a desiccator for 3 days after anneal-

TABLE II
Transitions in Various Polyamides

Material	Methylene groups between H-bond sites	T_g, °C			T_m, °C
		Initial	Rerun	After 5 day	
Nylon 11	10	43	—	43	189
Nylon 6	5	40	—	36	219
Nylon 66	6, 4	52	—	52	260
Nylon 610	6, 8	40	—	44	220
Nylon 12	11	42	—	42	178

ing (curve *b*), transitions occur at both 40 and 92°C. That the annealing process is the critical factor here is shown by the fact that a resting period before annealing has no effect on this phenomenon (curve *c*).

Figure 5 shows four infrared absorption spectra for the same sample of nylon 6 in the region of 3000–4000 cm^{-1}. Curve *a* was made immediately after the sample was prepared by casting onto a salt block from fluoro-alcohol solution. Curve *b* was made after the sample had been held for one week in a desiccator at room temperature. Curve *c* was made after the sample was heated in a circulating air oven at 80°C for 15 min and allowed to cool to room temperature during another 15 min, and curve *d* was made after the sample was held for a week at room temperature in the desiccator. The absorption peaks near 3060, 3200, and 3300 cm^{-1} for intramolecularly and intermolecularly hydrogen-bonded NH,[8] do not appear to show any significant differences among the four spectra. In the region between 3400 and 3500 cm^{-1}, however, where unbonded NH absorbs,[8] there is a small, but significant absorption in curves *a* and *c* as compared to curves *b* and *d*. This effect, though small, suggests that delayed formation of hydrogen bonds may have taken place, with the elimination of absorptions caused by unbonded NH groups. (A broad absorption in this region has also been attributed to the presence of water,[9] but it is felt that this is not the case in this instance because of the precautions taken to keep the sample dry.) The number of bonds formed is apparently so small, compared with the number of bonds already present, that there is no significant change in the absorptions caused by bonded NH, but there are enough unbonded NH groups eliminated that the disappearance of the absorption near 3400 cm^{-1} is clear.

In all of the experiments described above, care was taken to assure that the polymer was dry. To determine the effect of water on the phenomenon, the nylon 11 sample was placed in a 100% humidity atmosphere at room temperature for 3 days, and then run as before. Under these conditions the sample picked up about 1.4% of water. The only difference noted in these thermograms from those described above is that the transition temperature is reduced by about 5°C for the wet samples.

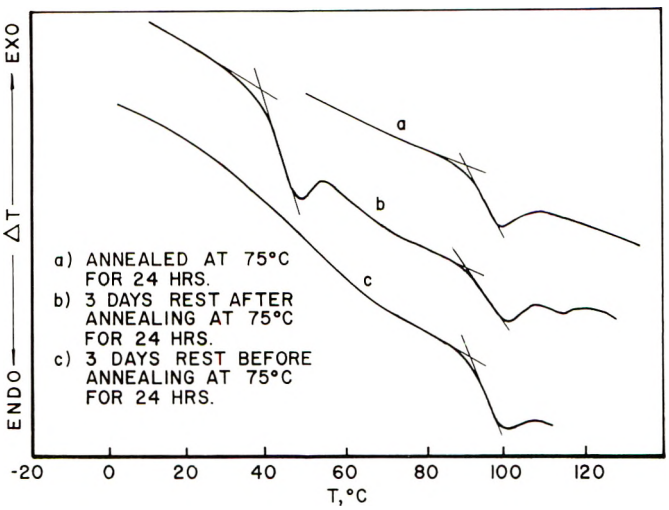

Fig. 4. Effect of annealing on nylon 11 transitions.

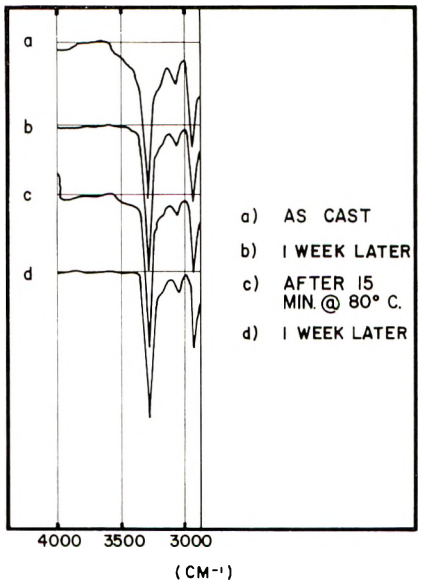

Fig. 5. Infrared spectra of nylon 6.

Discussion

The data cited above illustrate some of the unusual features of the 40–50°C thermal transition, generally considered the glass transition in nylons. The most striking of these features are the absence of any indication of a transition on the cooling portion of the DTA thermogram (Fig. 1*b*), the time-dependent behavior for reappearance of the transition (Fig. 2), the shift of the transition to higher temperatures on annealing

(Fig. 4), and the disappearance of absorptions for unbonded NH from the infrared spectrum after heating for 15 min at 80°C (Fig. 5).

The glass transition is commonly defined as being "caused by the onset of motion of chain segments in the amorphous region of the polymer."[2b] We would like to suggest here that this definition is not sufficent to explain the 40–50°C transition in nylons. If it were, there would be no reason to expect that the transition should not be freely reversible as the temperature level is cycled about T_g. Such is the case, for example, with polystyrene (Fig. 6), where the glass transition appears on the initial heating curve, on the cooling curve, (curve *a* and *b*, respectively), and also on an immediate rerun (not shown). Polystyrene, of course, has a much stiffer and bulkier chain than any of the nylons considered here, but even so, there is little hysteresis apparent in the location of the glass transition temperature when heating and cooling curves are compared. Likewise, the long delay necessary for the reappearance of the transition, as shown in Figure 2, and the temperature shift on annealing (Fig. 4) are difficult to explain on the basis of the definition cited above. These phenomena are more characteristic of first-order transitions. Thus, they might be explained on the basis of supercooling and crystallization rate factors. But Wilhoit and Dole,[10] using calorimetric methods, have shown that there is no latent heat of transition in the neighborhood of 47°C, at least for nylon 66. Therefore, the phenomenon in question cannot be a first-order transition.

In order to further elucidate this problem, let us look more closely at the nature of the first- and second-order transitions in polymers. A first-order transition, a melting transition, for example, is a change in the conformation of the polymer chains involving a latent heat. In the case of the melting transition the crystalline substance absorbs heat in the process of stripping off or removing chains from the ordered regions of the crystal matrix. This energy transfer appears in the DTA thermograms as a minimum in the curve, its sharpness depending on the narrowness of the melting range.

A second-order transition, on the other hand, indicates a change in the mode by which energy is accepted by the amorphous regions of the polymer

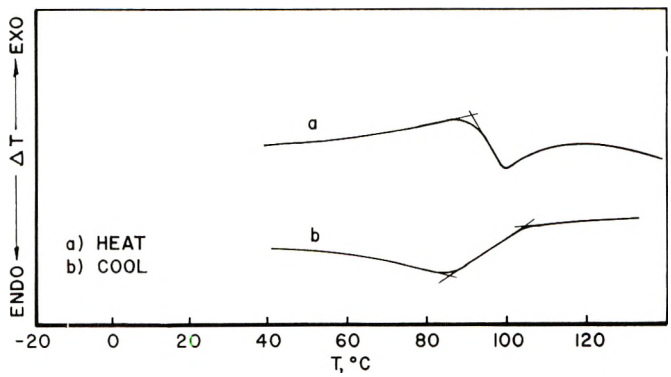

Fig. 6. Polystyrene glass transition.

molecule. Thus, this kind of transition does not involve a latent heat, but only a change in the heat capacity of the material. It appears on the DTA thermogram as a step-change in the position of the pen on the ΔT-axis, but with no change in the slope of the DTA base line.

Woodward and co-workers[11,12] have suggested that the principal amorphous transition in nylons (which they found by dynamic mechanical measurements at about 77°C, but which corresponds to the transition under discussion here) is caused by the breaking of hydrogen bonds in the amorphous regions of the polymer. We would like to suggest that at temperatures below the transition temperature these bonds form a three-dimensional network, but without the ordering required for crystallization. While the hydrocarbon chain segments between the hydrogen bonds can start rotating at a very low temperature, perhaps as low as −120°C,[7,11] this network is stable at considerably higher temperatures. The hydrogen bonds act like crosslinks to restrict the scale of molecular motion to the distance between bond sites. When the bonds break, at higher temperatures, motions on a larger scale, capable of accepting more energy, become possible. Because of the lack of long-range order there need be no latent heat effect associated with the formation or destruction of this network. Since there are steric problems in the mechanical rearrangements necessary for the formation of the hydrogen bonds, however, it is to be expected that there would be a time lag for re-formation of the network at lower temperatures. [The infrared spectra (Fig. 5) substantiate this expectation.] These rearrangements would not have to be as extensive, however, as those required for crystallization. It is the disruption of this network, providing an additional mode of energy absorption, which appears in the DTA thermogram as the glass transition. Because the slow-forming network is disrupted during the heating portion of the thermogram, there is no sign of it during the cooling portion or during an immediate rerun, and an infrared spectrum taken at this time shows an absorption in the region assigned to unbonded NH. After some time, the network re-forms, but in the early stages, before it has reached its equilibrium state, the transition indicated by DTA is small and shifted to lower temperatures. As the network becomes more complex, the DTA indication becomes stronger and shifts back to higher temperatures, and the infrared spectrum indicates that the absorption in the region assigned to unbonded NH is no longer present.

While the term "glass transition" would seem to be something of a misnomer for this phenomenon, because the physical state at lower temperatures is not very glasslike, the transition does meet several of the criteria proposed by Boyer for T_g,[7] and therefore it will be accepted as such here.

The effect of annealing can be accounted for in this concept if it is understood that the nature of the network will be affected by the temperature at which it forms (just as in crystallization of polymers, the melting point is a function of the crystallization or annealing temperature). Once the network has formed at the annealing temperature, it is relatively stable and

does not break down rapidly at any lower temperature. But since at room temperature the hydrocarbon segments of the polymer chains are still mobile, and therefore the hydrogen bonds are in dynamic equilibrium, another, superimposed network forms when the polymer rests at that temperature. In this way the appearance of two transitions in the thermogram of a nylon which has been annealed and then allowed to rest at room temperature before testing (Fig. 4*b*) can be explained.

The effect of water on this phenomenon appears to be that of a plasticizer or lubricant. It water is present while the thermogram is being run, the transition appears a few degrees below its temperature for a dry sample. This seems to be the case whether the moisture is introduced upon cooling from a previous run or after the sample has had a few days to rest.

One further set of facts which can be interpreted to support the hypothesis is indicated by the data of Table II. In this table it is noted that the number of methylene groups between potential hydrogen bonding sites on the polymers in question varies from 4 to 11. With such variation the observed uniformity of transition temperature seems strange. However, this factor can be accounted for by the proposed mechanism if it is realized that the existence of the transition is dependent not on the flexibility of the network (i.e., the distance between hydrogen-bonding sites) but on the existence and disruption of hydrogen bonds at points throughout the amorphous regions of the polymer. The configuration of these bonds, and thus the observed transition temperature, is determined mainly by the temperature at which the bonds are formed.

Conclusions

We have described here some unusual aspects of the glass transition in nylons which we believe to be related to the alternation of nonpolar chain segments with strongly hydrogen-bonding groups along the polymer chain. This unusual behavior can be explained in terms of a postulated network built up of hydrogen bonds in the amorphous regions of the polymer, which, however is not so highly ordered as to have a latent heat associated with its formation or disruption. Since the hydrogen bonding sites occur only at intervals along the chain, there are steric factors which hinder the formation of the network, which explains the long times necessary for the appearance of the experimentally observable transition.

The author wishes to thank Mr. John D. Matlack for the DTA results, Mr. Russell J. Hansen for the infrared results, and Mr. Matlack, Mr. Alfred P. Metzger, and Dr. Joseph D. Benigni for helpful discussions during the preparation of this paper.

References

1. W. A. Lee and G. J. Knight, in *Polymer Handbook*, J. Brandrup, and E. H. Immergut, Eds., Interscience, New York, 1966, p. III-74.

2. B. Ke, in *Newer Methods of Polymer Characterization*, B. Ke, Ed., Interscience, New York, 1964, (a) pp. 354, 394; (b) p. 393.

3. D. W. McCall and E. W. Anderson, *J. Chem. Phys.*, **32**, 237 (1960); quoted by R. F. Boyer, *Rubber Chem. Technol.*, **36**, 1368 (1963).

4. R. F. Boyer and R. S. Spencer, *J. Appl. Phys.*, **15**, 398 (1944).

5. F. Rybnikar, *J. Polym. Sci.*, **28**, 633 (1958).

6. A. H. Willbourn, *Trans. Faraday Soc.*, **54**, 717 (1958); quoted by R. F. Boyer, *Rubber Chem. Technol.*, **36**, 1400 (1963).

7. R. F. Boyer, *Rubber Chem. Technol.*, **36**, 1303 (1963).

8. L. J. Bellamy, *The Infra-red Spectra of Complex Molecules*, Wiley, New York, 1958, pp. 205, 224–227.

9. I. Abu-Isa, *J. Polym. Sci. A-1*, **9**, 199 (1971).

10. R. C. Wilhoit and M. Dole, *J. Phys. Chem.*, **57**, 14 (1953).

11. A. E. Woodward, J. M. Crissman, and J. A. Sauer, *J. Polym. Sci.*, **44**, 23 (1960).

12. J. A. Sauer and A. E. Woodward, *Revs. Mod. Phys.*, **32**, 88 (1960).

Received October 14, 1970
Revised April 15, 1971

JOURNAL OF POLYMER SCIENCE: PART A-2 VOL. 9, 1703–1717 (1971)

Experimental Determination of the Relationships Among Various Measures of Fluid Elasticity

ROBERT A. STRATTON* and ALLAN F. BUTCHER,
Mobil Chemical Company, Edison, New Jersey 08817

Synopsis

The viscoelastic properties of a 4% solution of monodisperse polystyrene (molecular weight 394,000) in Aroclor 1260 were determined by the following techniques: creep recovery, stress relaxation upon cessation of steady flow, dynamic measurements, and normal stress difference and shear stress measurements in steady flow. All measurements were carried out with cone and plate geometry in a Weissenberg rheogoniometer. The modification of this instrument to perform creep and creep recovery experiments by use of an air-bearing suspension and an air-turbine drive is described. A broad range of shear rates and frequencies encompassing both linear and nonlinear behavior was employed. The elastic behavior is described in terms of the recoverable shear strain s or the steady-state compliance J_e°. The first three techniques gave identical results for J_e° in the range of linear viscoelasticity for which it is defined. The normal stress difference measurements confirmed Lodge's relation $s = (P_{11} - P_{22})/2\sigma_{21}$. Reasons for previous experimental disagreement with this result are discussed.

INTRODUCTION

For more than a decade a controversy has been in progress concerning the relation between the first normal-stress difference $P_{11} - P_{22}$ and other measures of polymer elasticity. In 1956 Lodge[1] proposed his theory of elastic liquids, which predicted the following relation between the ultimate constrained shear recovery (or total recoverable shear strain) s, the first normal stress difference, and the shear stress σ_{21}

$$s = (P_{11} - P_{22})/2\sigma_{21} \tag{1}$$

The following year Philippoff, Gaskins, and Brodnyan[2] presented experimental support for the so-called "solid theory" of Weissenberg[3] and Mooney[4] which predicts

$$s = (P_{11} - P_{22})/\sigma_{21} \tag{2}$$

The difference, by a factor of two, between eqs. (1) and (2) has been the focal point for the ensuing controversy.

Subsequently, the theory of viscoelasticity for a second-order fluid of Coleman and Markovitz[5] and a number of constitutive equations[6] have all

* Present address: The Institute of Paper Chemistry, Appleton, Wisconsin 54911.

obtained the result given by eq. (1). On the experimental side, Philippoff and collaborators[2,7,8] have apparently confirmed eq. (2), while Benbow and Howells[9] find agreement between their results and eq. (1). These investigators have directly compared normal stress and "recoil" (creep recovery) measurements.

In addition, relationships between other measures of a fluid's elasticity have been sought. The second-order theory[5] suggests

$$\lim_{\omega \to 0} (2G''/\omega^2) = \lim_{\dot{\gamma} \to 0} [(P_{11} - P_{22})/\dot{\gamma}^2] \tag{3}$$

where G'' is the real component of the complex modulus measured at circular frequency ω and $\dot{\gamma}$ is the shear rate. Equation (3) may also be obtained by combination of Lodge's result, eq. (1), the definition from the phenomenological theory of linear viscoelasticity of s in terms of the steady-state compliance J_e°,

$$s = J_e^\circ \sigma_{21} \tag{4}$$

and the definition of J_e° from the latter theory in terms of dynamic quantities

$$J_e^\circ = \lim_{\omega \to 0} (G''/\omega^2\eta^2) \tag{5}$$

where η is the steady-flow viscosity. Plots of $2G''$ against ω and $P_{11}-P_{22}$ against $\dot{\gamma}$ have been found[10,11] to superpose at $\omega = \dot{\gamma}$ in the linear (Newtonian) and slightly nonlinear regions of flow.

Stress relaxation upon cessation of steady flow (SRUCSF) affords[12] another measure of s:

$$s = \dot{\gamma} \int_0^\infty \sigma_{21}(t)dt/\sigma_{21}(0) \tag{6}$$

Here $\dot{\gamma}$ and $\sigma_{21}(0)$ are the shear rate and stress during steady flow, respectively, and $\sigma_{21}(t)$ is the relaxing stress after cessation of flow. Values of s obtained by this method[12] are in good agreement with those from total creep recovery. Equation (6) is strictly valid only in the region of linear viscoelasticity.

Upon equating angular frequency and shear rate in the region of constant steady-flow viscosity η equal to constant dynamic viscosity η' the following relations may be derived:

$$\begin{aligned} s &= J_e^\circ \sigma_{21} \\ &= J_e^\circ \dot{\gamma} \eta \\ &= J_e^\circ \omega \eta' \\ &= J_e^\circ G'' \\ &= \left(\lim_{\omega \to 0} J' \right) G'' \\ &= \left(\lim_{\omega \to 0} \frac{G'}{G'^2 + G''^2} \right) G'' \end{aligned}$$

where J' and G'' are the storage compliance and loss modulus, respectively. As $\omega \to 0$, $G'' \gg G'$

$$s = G'/G'' = \cot \delta \tag{7}$$

where δ is the mechanical loss angle. Thus, in the region of low frequency where $G'' \gg G'$ and $\eta' = \eta$, the recoverable shear strain may be calculated from the loss angle in a dynamic experiment. Equation (7) follows directly from eqs. (4) and (5), but the intermediate steps have been presented to show the relation of the approximations to the final result. Obviously, this equation can only hold in a limited domain within the region of linear viscoelasticity.

Philippoff has argued theoretically[13,14] that the loss angle δ between the stress and the strain in a dynamic experiment at a circular frequency ω should be identical to twice the extinction angle χ measured in a flow birefringence experiment at a shear rate $\dot{\gamma}$ equal to ω. He also showed[13] this identity experimentally by plotting 2 cot δ and 2 cot 2χ at $\omega = \dot{\gamma}$ and achieving superposition.

Finally, Philippoff and collaborators[2,7,8,15] have verified the expression

$$P_{11} - P_{22})/\sigma_{21} = 2 \cot 2\chi \tag{8}$$

for a number of polymer systems in the non-Newtonian range of viscoelastic behavior.

In the present paper we seek to compare the values of s as calculated by eqs. (1), (2), (4), (6), and (7) by creep recovery, stress relaxation upon cessation of steady flow, steady flow, and dynamic measurements on the same sample and with the same instrument. Hopefully, this will provide a conclusive test of the two theories and will also point up inconsistencies, if any, in the theory of linear viscoelasticity, eqs. (4), (6), and (7).

MATERIALS AND METHODS

As was pointed out in the Introduction, many of the mathematical relations presented hold only in the range of linear viscoelasticity and some only in the region of constant dynamic viscosity of where $G'' \gg G'$. To compare the results of different experimental techniques, the measurements must be made in or close to the linear region. This requirement, which has not always been appreciated by previous investigators, implies measurements made at very low shear rates and stresses. The results are low levels of elasticity with consequent difficulty in attaining adequate accuracy in their determination. The situation can be improved in two ways: (1) by use of a highly viscous solvent, the absolute magnitude of the stresses can be raised to a moderate level and the relaxation times can be increased, thereby increasing the degree of elasticity; (2) by proper choice of the polymer–solvent system, one can assure linear behavior over at least a portion of the experimentally accessible range of shear rates and frequencies. The second step requires a recognition of those factors which contribute to nonlinear viscoelastic behavior. The most important of these are polymolecularity,

entanglement coupling, and high molecular weight. It is well known[16,17] that samples with narrow molecular weight distribution retain constant steady flow and dynamic viscosities to higher shear rates and frequencies than those with greater polydispersity. It has been postulated[18] that the presence of entanglements is the major source of non-Newtonian behavior in polymers of high molecular weight. Entanglement coupling can be avoided by using a polymer solution with $\phi_2 M < M_c$, where M is the molecular weight, ϕ_2 is volume fraction of polymer, and M_c is the critical breakpoint in the log η–log M plot of its undiluted homologs. The factor of molecular weight presents contradictory features. On the one hand, the Rouse theory predicts[19] an increase in elasticity with increasing molecular weight.

$$J_e^\circ = 0.4\, M/cRT \tag{9}$$

which is desirable, while on the other the onset of non-Newtonian flow is predicted[20,21] to occur at lower shear rates as molecular weight increases. It is evident that some compromise must be made.

In keeping with the above observations, an anionically polymerized polystyrene of moderate molecular weight was dissolved in a viscous solvent to produce a dilute solution. The polymer was a commercial sample, sample 3a, prepared by Pressure Chemical Company, Pittsburgh, Pennsylvania with a weight-average molecular weight of 394,000 measured[22] by light scattering in cyclohexane at 50°C. The weight average/number average ratio is reported by the manufacturer to be 1.06.

The solvent, Aroclor 1260 (a mixture of chlorinated diphenyls), was kindly furnished by Mr. R. W. Ehrhardt of Monsanto Chemical Company. Its viscosity was determined at 35°C with the Weissenberg rheogoniometer and was 1480 P. The density measured by pycnometer was 1.618 g/ml at 25°C; the thermal expansion coefficient was 8.2×10^{-4} deg^{-1}.

A 4% solution of the polystyrene in the solvent was made up by weight. Dissolution was achieved by slow stirring at 90°C. Concentrations at 35°C of 0.0628 g/ml (6.00 vol-%) were calculated from the densities of the polymer and solvent, assuming additivity of volumes. From the latter result the product $\phi_2 M$ was 23,600, somewhat less than the M_c for polystyrene[23] of 33,000. Hence, there should be no effect of entanglement coupling on the measurements reported here.

The Weissenberg rheogoniometer (WRG) was used for all the experiments. Measurements were made at 35, 45, or 58°C to obtain the best accuracy from the particular experiment. Shear rates and shear stresses were measured during all experiments and were used to reduce all data to a reference temperature of 35°C. Reduction of σ_{21}, $P_{11} - P_{22}$, G', and G'' was achieved by multiplication by the factor $T_0\rho_0/T\rho$, where ρ and ρ_0 are the solution densities at the absolute temperature of measurement T and at T_0 = 308°K and is signified as usual by the subscript p. Shear rates and frequencies were multiplied by the shift factor a_T obtained from the steady flow viscosities.

$$a_T = \eta T_0\rho_0/\eta_0 T\rho$$

where η and η_0 are the Newtonian viscosities at the temperature of measurement T and the reference temperature T_0. The viscosities at 35, 45, and 58°C of the solution were 7.95×10^4, 6.0×10^3, and 4.40×10^2 P, respectively. Temperatures were controlled to ±0.1°C.

All measurements except the creep recoveries were made using a cone and plate of 7.50 cm diameter with a 1° 32.5′ cone angle. Because of the limited range of torques available, the creep recoveries were made by use of a cone and plate of 2.50 cm diameter and cone angle 3° 49′, so that larger stresses in the same range as the other experiments could be produced. Several recalibrated torsion bars were used as needed to provide maximum accuracy at the different temperatures.

Normal stress measurements by the total thrust method were carried out as previously described.[7] Fluid inertia effects were entirely negligible at the shear rates employed. It is to be noted that there are essentially two relaxation times of the instrument–sample system in addition to those of the sample itself. The first is due to the lag in the servo response system and can be made fairly small (but not zero) by judicious adjustment of the sensitivity of the servo amplifier. Because of this lag the cone and plate tend to (and indeed, for the servo system to operate, must) separate slightly before the servo system can apply the balancing force equal to the normal thrust. During the separation there is a macroscopic flow of sample radially inward, and this material must be returned to its initial radial position to achieve steady-state conditions. The relaxation time for this flow is determined by the stiffness of the normal force spring and the viscosity of the fluid and may be of the order of minutes for a moderately viscous liquid. The steady-state normal stress will not be attained until a number of these relaxation times have occurred; the situation deteriorates further by the tendency of the system to oscillate slowly about the steady state value as a result of the coupling between the normal force spring-viscous sample–servo system. The upshot of this discussion is that great patience must be exercised to obtain real steady-state normal thrusts. Further, the time-dependent normal stress behavior of the sample can probably not be separated from the time dependence of the response of the sample–instrument system in a transient or dynamic oscillatory experiment using the current techniques with the WRG.

The measurement of stress relaxation upon cessation of steady flow has been described elsewhere.[12] The integral in eq. (6) was obtained by using an integrating digital voltmeter. The critical time[12,24] for the instrument-sample response, $t_c = \eta/kb$, where η is the steady flow viscosity, k is the torsion bar constant, and b is the form factor, was much shorter than the viscoelastic response of the sample and could be neglected. Measurements made with torsion bars of different stiffnesses gave essentially the same results.

Dynamic measurements were made over a frequency range from 0.02 to 1.2 Hz. A Birnboim ultralow frequency phasemeter[25] as modified for use with the WRG by O'Reilly[26] was constructed (Noel J. Mackisoc, Willingboro, New Jersey) and was used to measure the phase angle and amplitude

ratio. The instrument was further modified by using infinitely variable gain preamplifiers to present constant peak voltages of 10 volts to the trigger circuits, thereby increasing the precision. In practice the amplitudes of the stress and strain were read directly from the transducer meters with $\pm 1\%$ reproducibility. Comparison of these with the amplitude ratios determined with the phasemeter showed no error at these low frequencies when using the visual method. Measurements made with the stress and strain inputs to the twin filter networks in the normal hookup and then with the inputs reversed were averaged to eliminate any phase angle difference between the two filters.[26,27] The differences found were very small at these low frequencies. Phase angles measured with the phasemeter were generally reproducible to within 0.1° or better. The components of the complex modulus $G^* = G' + iG''$ were calculated by using the usual formulas[28] including corrections for movement of the plate. Fluid inertia corrections[29] were negligible for these low frequencies.

The WRG was modified to permit constant stress (creep) and creep recovery measurements. The disposition of the various components is shown diagramatically in Figure 1. Everything in the box enclosed by dashed lines is part of the normal set-up of the WRG. The torsion bar has been removed and replaced by a unit consisting of a rotary variable differential transformer (RVDT), air bearing, and air turbine all supported by a bracket (not shown). The upper air bearing (Lifetime components, Inc., No. IC-2036-C-20), which provides both radial and axial thrust, supports the plate and all moving parts above it. Rotational motion is sensed by the RVDT (Schaevitz Engineering, No. R-17BSL) which has a linear range of ±5° and was furnished without bearings to ensure zero friction. The transducer rotor is centered within its coils by the air bearing. The driving torque is provided by a regulated jet of air impinging on the vanes of a centrifugal fan (Ripley Co., Model UK 2000 without the motor). A

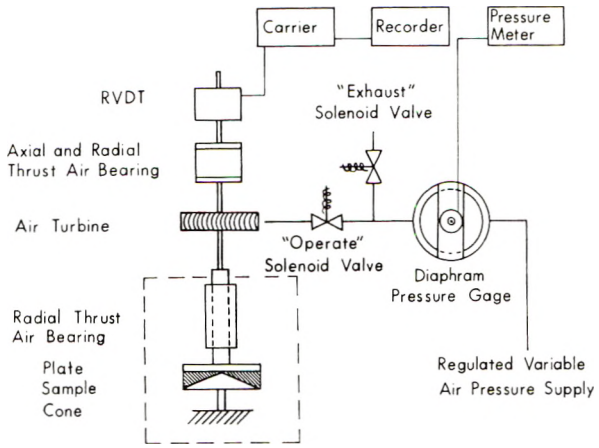

Fig. 1. Schematic representation of modification of the Weissenberg rheogoniometer for creep and recovery measurements.

housing (not shown) around the vanes prevented stray air currents from disturbing the system. Because the shaft and couplings between the two air-bearings are not perfectly true, there is a preferred orientation of the upper assembly which adds a residual torque. In practice, the electrical zero of the transducer is adjusted to be as close as possible to the mechanical zero to minimize this residual torque. During creep the residual torque is negligible compared to the driving torque, but during creep recovery it makes itself manifest as a slow drift after recovery is finished. Extrapolation of this linear drift with time back to the initiation of creep recovery provides a recoverable shear strain corrected for the drift.

The means of achieving a controlled jet of air is shown in the right-hand side of Figure 1. The laboratory compressed-air supply at about 100 psi is led through a surge tank and air filter to a pair of regulators (Conoflow Corp., Model H-10XT-H) which permit fine control of the pressure in the ranges from 0 to 5 and from 5 to 30 psi. Steady flows at all pressures of interest are possible with this system. To measure pressure $\ll 1$ psi, a diaphragm-type gage with transducer sensor was designed and constructed. This consisted of a short steel cup, 4 in. in diameter, closed with a 0.025-in. thick beryllium copper diaphragm. The core of a linear variable differential transformer (Boutlon-Paul Aircraft Ltd., Wolverhampton, England, Type F.51/T/M) was attached to the center of the diaphragm and the coils of the transducer were suspended above. The output of the LVDT was monitored on a Boulton-Paul Aircraft Ltd. transducer meter, type EP597. Deflections at the center of the diaphragm of less than 10 μin. could be sensed. The usual range of operation was from 0.2 to 47 mils; individual readings of deflection could be measured to $\pm 1\%$. The gage was calibrated in terms of shear stress applied to the sample in the viscometer rather than air pressure in the following manner. A sample of NBS standard oil OB was installed in the WRG and subjected to a range of torques by the air turbine. From the measured shear rates and known viscosity (238.2 P at 25°C), the corresponding shear stresses were calculated. A calibration plot of shear stress against gage deflection was then prepared and used for subsequent measurements. A range of shear stresses from 3×10^1 to 2×10^4 and from 1×10^0 to 7×10^2 dyne/cm^2 was possible by use of the 2.5- and 7.5-cm cone-and-plate assemblies, respectively. The lower limit is set by the necessity that the driving torque be much greater than that due to the preferred mechanical orientation and presumably could be lowered by using more accurately machined components. The upper limit is set by the available line pressure.

To allow an essentially instantaneous application and removal of torque, a set of two solenoid valves (Automatic Switch Co., No. 826226) was placed between the transducer gage and the jet. These were wired through a relay so that as one valve was opened the other was simultaneously closed. The "exhaust" valve in the open state was used to set the desired air pressure (stress level), the relay was then actuated, and the pressure was applied to the turbine via the "operate" valve.

The output of the RVDT used as the rotational deformation sensor was demodulated and amplified by a Schaevitz Engineering carrier system, Type CAS 2500, and then fed to a recorder (E. H. Sargent and Co., Model SR). A sensitivity of better than 4×10^{-4} strain units or in terms of angular deflection of 1.6×10^{-3} degrees was possible. The RVDT was calibrated by turning the cone–sample–plate–transducer system through a known angle with the conventional drive mechanism of the WRG with no driving air pressure on the turbine. The RVDT–carrier–recorder system was perfectly linear over the operating range within the readability of the recorder chart.

The advantages of the present system are the ease with which it may be converted from the conventional viscometer to a creep apparatus and back again, the wide range of stresses possible, the sensitivity of response, and the simplicity of operation. The use of the RVDT as a sensor also permits the creep apparatus to be used as a conventional (constant shear-stress) rotational viscometer. A similar concept, involving the use of an air bearing suspension and air turbine drive with a concentric cylinder viscometer, has been recently described.[30,31]

Creep recovery measurements were carried out after subjecting the sample to a total creep strain at least ten times the magnitude of the recoverable shear strain at a given shear stress. Values of s from duplicate measurements generally agreed to within $\pm 2\%$. The effect of a finite moment of inertia of the rotor was visible only at the highest shear rates for this solution. This could be observed by adding a disc of known moment of inertia approximately equal to that of the rotor alone to the top of the RVDT and noting the decrease in s produced thereby. This amounted to 2–5% for shear stresses greater than 10^3 dyne/cm^2. The correction was not applied to the measurements presented here.

RESULTS

Dynamic mechanical measurements made at 45 and 58°C and reduced to 35°C are shown in Figure 2. Here the contribution of the solvent $\omega\eta_s$ has been subtracted from the measured G'' to give the polymer contribution to the loss modulus. The data have been fitted in the limiting low-frequency region to the curves predicted by the Rouse theory. Deviations from theory at the higher frequencies are probably due to the effects of hydrodynamic interaction and excluded volume,[17,32,33] but their consideration is outside the scope of the present work. From the limiting low-frequency data for G'_p with slope 2 in Figure 2, the steady-state compliance has been calculated according to eq. (5)[34] and is listed in Table I.

Three determinations of P_{11}–P_{22} as a function of shear rate were made at about 58°C and are shown reduced to 35°C in Figure 3. The data (not the Rouse theoretical curve) for the storage modulus from Figure 2 plotted here as $2G'_p$ are shown as a smooth curve. The solid line identifies the terminal region with slope 2. The plot provides further evidence for the conclusion[10,11] that $2G'$ and P_{11}–P_{22} are equivalent at $\omega = \dot{\gamma}$ in and near the region

TABLE I
Steady-State Compliance from Various Experiments

Method of Measurement	$J_e^\circ \times 10^4$, cm²/dyne
Dynamic	1.52
SRUCSF	1.60
Creep recovery	1.58

of terminal slope 2. Although the present normal stress data do not reach the terminal region, there appears to be no tendency for a deviation from the $2G'$ data as the shear rate is decreased.

Measurements of SRUCSF were made at 45°C, and the results calculated according to eq. (6) are shown reduced to 35°C in Figure 4. From the straight line drawn with unit slope in this plot the steady-state compliance was calculated[12] from eq. (4) and is listed in Table I.

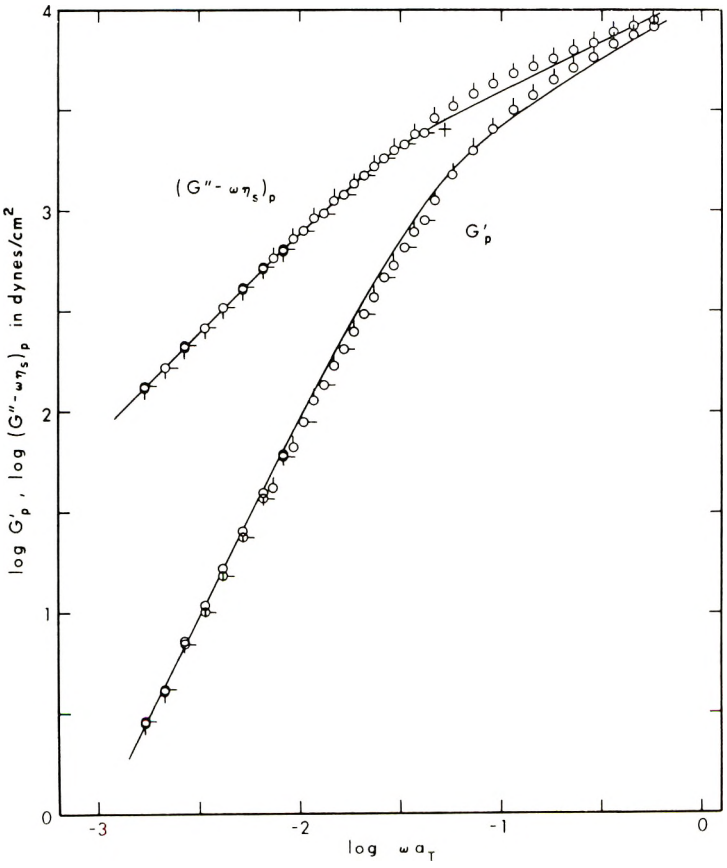

Fig. 2. Logarithmic plots of G'_p and $(G''-\omega\eta_s)_p$ against ωa_T for 4% polystyrene, M = 394,000 in Aroclor 1260, reduced to 35°C: (○) measured at 45°C; (○, ♀) measured at 58°C. Curves represent Rouse theory with origin of dimensionless plot at cross.

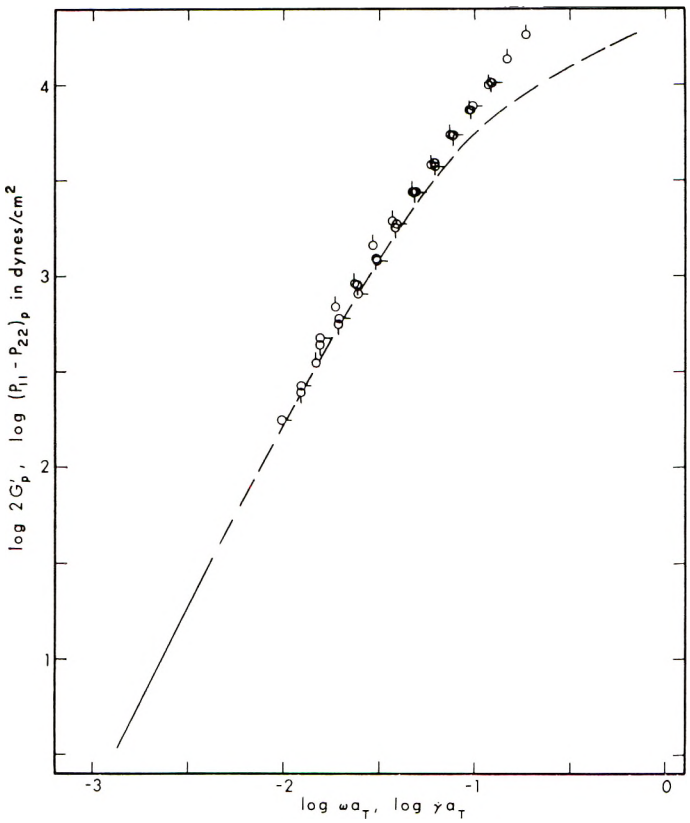

Fig. 3. Logarithmic plot of $(P_{11}-P_{22})_p$ against $\dot{\gamma}a_T$, reduced to 35°C; replicate measurements at 58°C indicated by different pip positions. Curve represents data of Fig. 2 plotted as $2G'_p$ against ωa_T; solid line indicates region with slope 2.

Three determinations of s from creep recovery as a function of shear stress were made at 35°C by using the modified WRG. The results are plotted logarithmically as s against reduced shear stress. A straight line with unit slope drawn through the data permits calculation of J_e° from eq. (4); the value is listed in Table I. The steady-state compliance is constant to shear stresses of at least 4000 dynes/cm^2 as shown by both the recoil and SRUCSF results. Deviations from linearity at the highest shear stresses in the creep recovery measurements can probably be completely accounted for by the moment-of-inertia effect mentioned previously.

Also shown in Figure 4 is a logarithmic plot of reduced shear rate against reduced shear stress. The straight line drawn with unit slope serves to define the region of constant viscosity. It is seen that J_e° remains constant even in the non-Newtonian region for this (nonentangled) system.

DISCUSSION

Theory of Linear Viscoelasticity

The three experiments in the range of linear viscoelasticity permit a test of the phenomenological theory. This is most simply done by comparing

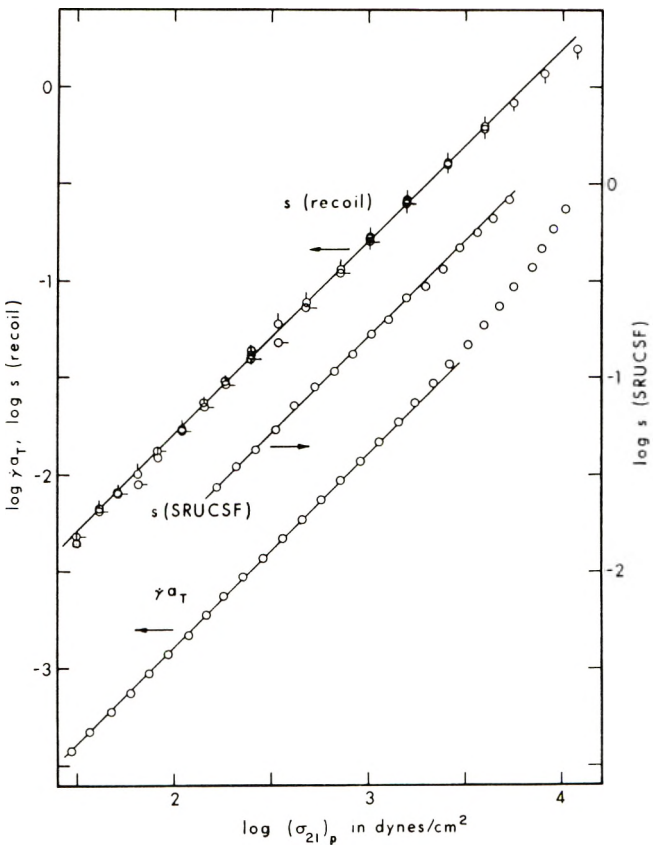

Fig. 4. Logarithmic plot of s from recoil, s from SRUCSF, and γa_T against shear stress reduced to 35°C; replicate measurements of s from recoil at 35°C indicated by different pip positions. Lines are drawn with unit slope.

the magnitude of J_e° as calculated from the results of the three distinct methods. The agreement shown in Table I is gratifying and represents the first critical test of the theory in the terminal zone of the relaxation spectrum.

Comparison with Rouse Theory

The quantity $cRTJ_e^\circ/M$ was calculated from the data and compared to the Rouse value 0.40 [eq. (9)]. The larger result 0.64 is probably the consequence of a small degree of molecular weight heterogeneity.[19] Similar results for the terminal relaxation time τ_1 are obtained from the fit of the dynamic data to the Rouse curves in Fig. 2. Here the abscissa value of the cross denotes the position of $\omega\tau_1 = 1$ for the theoretical curves. From this value τ_1 of the solution is 19.0 sec. This may be compared with the theoretical value from $\tau_1 = 6\eta M/\pi^2 cRT$ of 11.8 sec. Again polydispersity probably accounts for the difference.

Elastic Solid versus Elastic Liquid Theories

All the data are plotted logarithmically in Figure 5 as s calculated from eqs. (1), (4), (6), and (7) against reduced shear rate or frequency. In the range of low shear rate (frequency), the data coincide as predicted by the theory of linear viscoelasticity. At moderate shear rates (frequencies) the dynamic and normal stress data depart from the unit slope behavior characteristic of the recoil and SRUCSF measurements. At still higher rates (frequencies), the normal stress and dynamic data diverge from one another. The departure of the creep recovery and SRUCSF data from linearity at the highest shear rates is a result of the onset of non-Newtonian viscosity in this range, and, as noted previously, not a decrease in J_e°. Unfortunately, the lowest value for the quantity $(P_{11}-P_{22})/2\sigma_{21}$ is at $\log \dot{\gamma}a_T = -2.01$, outside the terminal region. It is not possible to make a categorical statement concerning this quantity in the region where $P_{11}-P_{22}$ varies as $\dot{\gamma}^2$. However, on the basis of the good agreement between the dynamic and normal stress results in the present and earlier[10,11] work as predicted by theory [eq. (3)], as the terminal region is approached, it appears extremely likely that the prediction of eq. (1) is fulfilled. If the "solid theory" were to hold, the data from the normal stress difference measurements would

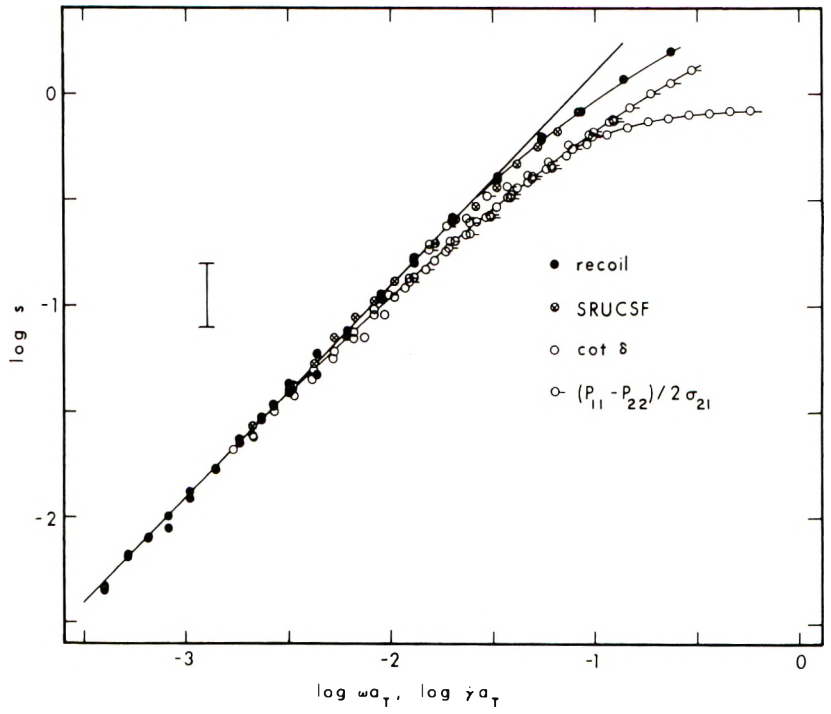

Fig. 5. Logarithmic plot of s from the indicated experiments against frequency or shear rate reduced to 35°C. Bold straight line drawn with unit slope. Vertical bar represents factor of 2.

have to be shifted up by a factor of two, which magnitude is shown by the vertical bar in Figure 5. The data thus plotted obviously would not converge toward that from recoil and SRUCSF. Furthermore, eq. (3) will not then hold unless the dynamic measurements are also multiplied by two. In this event, the J_e° calculated from the dynamic measurements will be twice as large as that from the creep recovery and SRUCSF determinations and will, moreover, violate eq. (7) from the theory of linear viscoelasticity. Since these results would be rather unpalatable, it must be concluded that eq. (2) is invalid.

Philippoff has argued[13] that $s = 2 \cot \delta$. This expression is at variance with the prediction of the theory of linear viscoelasticity [eq. (7)] and with the experimental results (Fig. 5 and Table I) and is no longer tenable. The present results do not contradict his findings $2 \cot \delta = 2 \cot 2\chi$ and $(P_{11}-P_{22})/\sigma_{21} = 2 \cot 2\chi$. They do require a reinterpretation of the relation of these to s in line with eqs. (1) and (7).

It is of interest to attempt to calculate J_e° from the normal stress results. A relationship is predicted by the second-order fluid theory[5] and is implicit in the elastic liquid theory[1]

$$(P_{11}-P_{22})/2\sigma_{21}^2 = J_e^\circ \tag{9}$$

However, if the data are plotted as the left-hand side of eq. (9) against shear stress, as shown in Figure 6, the ordinate is not of constant magnitude equal to J_e°. At the highest shear stresses the function does appear to be reaching a constant value of about two-thirds of J_e°, but this is in the non-Newtonian region outside the range of validity of the theory. As the shear stress is decreased below 3000 dyne/cm^2, the ordinate increases and at the

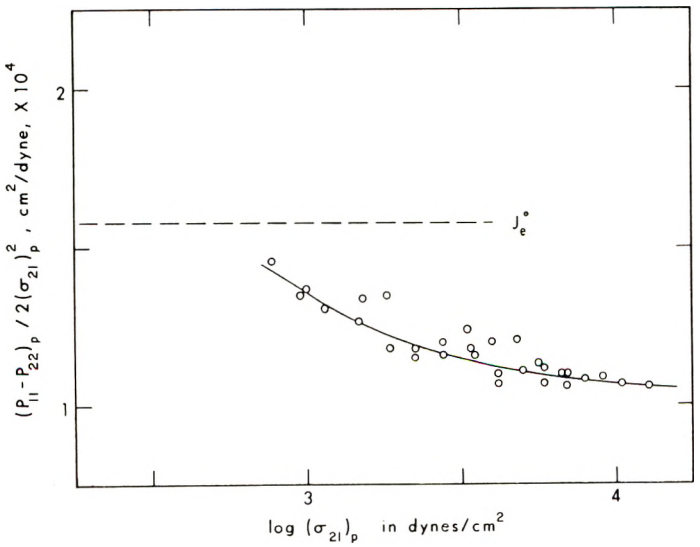

Fig. 6. Plot of $(P_{11}-P_{22})_p/2(\sigma_{21})_p^2$ against logarithm of the shear stress. Horizontal line is the value of J_e° over the indicated range from creep recovery measurements.

lowest accessible shear stresses appears to be approaching J_e° asymptotically. The nonconstancy of the ordinate undoubtedly is a consequence of the fact that $P_{11}-P_{22}$ does not vary as $\dot{\gamma}^2$ in this region as required by theory.[5] At a shear stress of 1300 dyne/cm^2, where the viscosity is still Newtonian, the ordinate has decreased to 1.3×10^{-4} cm^2/dyne, in contrast to the creep recovery and SRUCSF data which provide constant J_e° as noted previously to a shear stress of at least 4000 dynes/cm^2. Evidently, the normal stress data in the region where $P_{11}-P_{22}$ varies as less than the square of the shear rate contain different information from data of the other two experiments at the same shear rates. This further implies that the recoverable shear strain s can be calculated from normal stress data according to eq. (1) only in the region of proportionality of $P_{11}-P_{22}$ to $\dot{\gamma}^2$; outside this region the values of s calculated will be too small.

Comparison of Earlier Experimental Evidence with Theory

As mentioned previously, a great deal of evidence has been reported in the literature in support of eq. (2). In the light of the present findings, this presents an apparent paradox. To clarify the dilemma, the restrictions on the theories and, therefore, on the rheological behavior of the samples will be reiterated. The realm of linear viscoelastic behavior including Newtonian viscosity is by definition required for application of eqs. (4), (5), (6), and (7). In addition the prediction of constant viscosity by the second-order fluid and elastic liquid theories suggests that they, too, apply only in the Newtonian regime. No experiment to date has compared normal stress and creep recovery data in the range where $P_{11}-P_{22}$ is proportional to $\dot{\gamma}^2$. The tests, including the present work, have consisted of extrapolation of the normal stress data to the limiting low-shear-rate behavior. The extrapolations of previous work were made more uncertain by the extremely nonlinear behavior of the systems caused mainly by polydispersity and entanglement coupling. In the present experiments the approach has been to minimize these effects with the hope of a shorter extrapolation.

CONCLUSIONS

It is concluded that the prediction of eq. (1) is borne out experimentally as the limiting case at low shear rates and stresses. The connection between s and $P_{11}-P_{22}$ at higher shear rates and the physical significance, if any, of the quantity $(P_{11}-P_{22})/2\sigma_{21}$ under these conditions remain open questions.

The authors would like to thank Dr. W. Philippoff for introducing them to the problem of the factor of two and for many enlightening discussions. They also wish to thank Professors Robert B. Bird, John D. Ferry, and Donald J. Plazek for helpful comments and discussions. The careful machining of the components of the creep apparatus and the diaphragm gage was carried out by Mr. Ray Kadash.

References

1. A. S. Lodge, *Trans. Faraday Soc.*, **52**, 120 (1956).
2. W. Philippoff, F. H. Gaskins, and J. G. Brodnyan, *J. Appl. Phys.*, **28**, 1118 (1957).
3. K. Weissenberg, *Proceedings, First International Congress on Rheology*, North-Holland, Amsterdam, 1949.
4. M. Mooney, *J. Colloid Sci.*, **6**, 96 (1951).
5. B. D. Coleman and H. Markovitz, *J. Appl. Phys.*, **35**, 1 (1964).
6. D. C. Bogue and J. O. Doughty, *Ind. Eng. Chem. Fund.*, **5**, 243 (1966).
7. W. Philippoff and R. A. Stratton, *Trans. Soc. Rheol.*, **10**:**2**, 467 (1966).
8. W. Philippoff and R. A. Stratton, *Proceedings, Fifth International Congress on Rheology*, Vol. 4, University Park Press, Baltimore, 1971.
9. J. J. Benbow and E. R. Howells, *Polymer*, **2**, 429 (1961).
10. K. Osaki, M. Tamura, T. Kotaka, and M. Kurata, *J. Phys. Chem.*, **69**, 3642 (1965).
11. J. M. O'Reilly and W. M. Prest, *Trans. Soc. Rheol.*, in press.
12. R. A. Stratton, in preparation.
13. W. Philippoff, *J. Appl. Phys.*, **36**, 3033 (1965).
14. W. Philippoff, *Trans. Soc. Rheol.*, **12**:**1**, 85 (1968).
15. W. Philippoff, *J. Appl. Phys.*, **27**, 984 (1956).
16. R. S. Porter and J. F. Johnson, *Trans. Soc. Rheol.*, **7**, 241 (1963).
17. J. E. Frederick, N. W. Tschoegl, and J. D. Ferry, *J. Phys. Chem.*, **68**, 1974 (1964).
18. W. W. Graessley, *J. Chem. Phys.*, **43**, 2696 (1965).
19. J. D. Ferry, M. L. Williams, and D. M. Stern, *J. Phys. Chem.*, **58**, 987 (1954).
20. F. Bueche, *J. Chem. Phys.*, **22**, 1570 (1954).
21. A. Peterlin and M. Copic, *J. Appl. Phys.*, **27**, 434 (1956).
22. L. A. Papazian, unpublished measurements.
23. V. R. Allen and T. G Fox, *J. Chem. Phys.*, **41**, 337 (1964).
24. F. W. Schremp, J. D. Ferry, and W. W. Evans, *J. Appl. Phys.*, **22**, 711 (1951).
25. M. H. Birnboim, *Bull. Am. Phys. Soc.*, **8**, 270 (1963); U.S. Pat. 3,286,176 (Nov. 15, 1966).
26. J. M. O'Reilly, private communication.
27. K. Bogie and J. Harris, *Rheol. Acta*, **5**, 212 (1966).
28. K. Weissenberg, *The Testing of Materials by Means of the Rheogoniometer*, Sangamo Controls, Ltd., 1964.
29. K. Walters and R. A. Kemp, *Deformation and Flow of High Polymer Systems*, Macmillan, New York, 1967, p. 211.
30. S. S. Davis, J. J. Deer, and B. Warburton, *J. Sci. Instr.*, **1**, 933 (1968).
31. S. S. Davis, *J. Sci. Instr.*, **2**, 102 (1969).
32. N. W. Tschoegl, *J. Chem. Phys.*, **39**, 149 (1963).
33. N. W. Tschoegl, *J. Chem. Phys.*, **40**, 473 (1964).
34. L. A. Holmes, K. Ninomiya, and J. D. Ferry, *J. Phys. Chem.*, **70**, 2714 (1966).

Received January 21, 1971

NOTES

Spin-Lattice Relaxation from Endgroups in Atactic Polystyrenes

Introduction

In a recent paper on nuclear magnetic spin-lattice relaxation in atactic polystyrenes, Connor[1] has observed that the relaxation times T_1 in the range below 200°K increase with increasing molecular weight. This low-temperature relaxation process was associated with the *n*-butyl endgroup of the polymer, though no clear relation between endgroup concentration (molecular weight) and T_1 was apparent. Connor also discussed two theoretical models for the dependence of T_1 on molecular weight which are both at variance with experimental observations we have made on branched and linear polyethylenes.[2] In this note we propose to reinvestigate the experimental dependence of the low-temperature relaxation rates on molecular weight and consider models of endgroup motion and spin diffusion to account for the observed results.

Experimental

The three atactic polystyrenes of intermediate molecular weight (PS 1–3 in Table I) were anionically polymerized in this laboratory with *n*-butyl lithium as the initiator. These polymers have the structure I

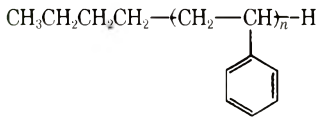

I

with one *n*-butyl endgroup per molecule. The molecular weights were determined by osmometry and viscometry on solutions in toluene. The high molecular weight sample (PS 4) was obtained from Utopia Instrument Co. The nature of the extremely dilute endgroups in this specimen is unknown, but is of no consequence in these experiments as will be seen below. This sample had been characterized by the manufacturer and was used without further purification. From the molecular weights recorded in Table I it is seen that all the polystyrenes are essentially monodisperse.

TABLE I
Molecular Weights and Relaxation Rates of Atactic Polystyrene Samples

Sample	$\bar{M}_n$	$\bar{M}_v$	N_m	$(1/T_1)_{max}$, sec^{-1}	Background, sec^{-1}	$(1/T_1)_{corr}$, sec^{-1}
PS 1	17,900	19,700	2.17×10^{-3}	0.202	0.060	$0.14 \pm .01$
PS 2	41,500	44,100	7.73×10^{-4}	0.125	0.070	$0.05 \pm .01$
PS 3	67,400	69,200	5.79×10^{-4}	0.095	0.065	$0.03 \pm .01$
PS 4	780,000	860,000	$<5 \times 10^{-5}$	—	~0.085	—

To insure the removal of any residual solvent which might affect the NMR results, the polymer samples were dried in a vacuum oven at 135°C for 48 hrs. They were then degassed under high vacuum (10^{-6} torr) for 18 hr before being sealed in sample tubes under 0.5 atm helium. The spin-lattice relaxation times were measured with conventional pulsed NMR apparatus[3] operating at 38 MHz. No evidence was observed for nonexponential or multiple decays, and all relaxation times were perfectly reversible with respect to temperature.

Results and Discussion

The temperature dependence of the spin-lattice relaxation times of the polystyrene samples between 100°K and room temperature is shown in Figure 1. The semilogarithmic format of $1/T_1$ versus reciprocal temperature is used to facilitate the separation of relaxation mechanisms. Throughout this work, the quantity $1/T_1$ will be referred to as to the relaxation rate; the maximum value of $1/T_1$, corresponding to the depth of a T_1 minimum, will be called the relaxation intensity or relaxation strength. The increase in $1/T_1$ at the highest temperatures in Figure 1 results from the onset of the β and α processes with a possible contribution from the γ relaxation as suggested by Connor;[1] these effects will not concern us further. The focus of this work is the molecular weight dependent relaxation peak centered around 143°K. Two effects are apparent in this region: both the relaxation strength and low-temperature slope of the 143°K peak decrease with increasing molecular weight. In fact the points for the sample of highest molecular weight, which have been omitted for the sake of clarity, show no maximum whatever.

It is apparent from both the low-temperature slopes and the behavior of the high molecular weight sample that there is an essentially temperature-independent relaxation mechanism superimposed on the molecular weight dependent relaxation at low temperatures. The origin of this "background" relaxation is uncertain, but it should be noted that most polymers exhibit virtually temperature-independent relaxation times on the order of tens of seconds at low temperatures where large-scale molecular motion has ceased.[4,5] This effect is generally attributed to relaxation associated with residual paramagnetic impurities, which need be present in concentrations of less than one part in 10^6 to account for observed results.[4,5] As the magnitude of this background relaxation can vary from sample to sample, we have adopted the following separation procedure to

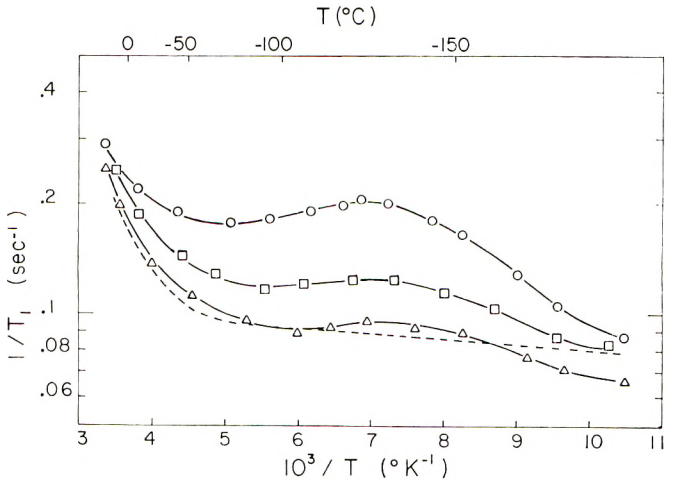

Fig. 1. Temperature dependence of the spin-lattice relaxation in atactic polystyrenes: (○) $\bar{M}_n$ = 17,900; (□) $\bar{M}_n$ = 41,500; (△) $\bar{M}_n$ = 67,400; (- -) $\bar{M}_n$ = 780,000.

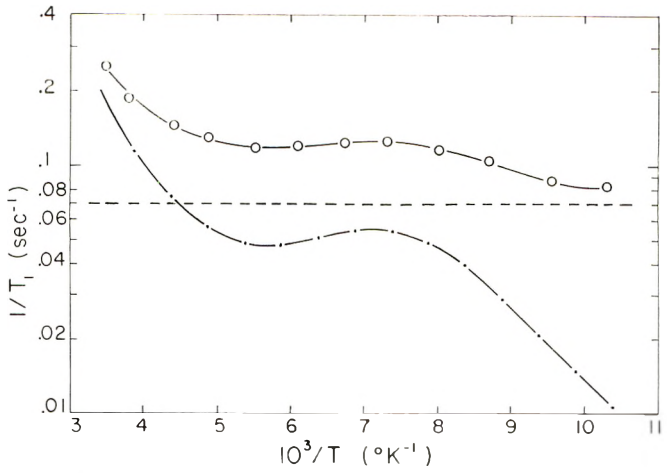

Fig. 2. Separation procedure used to extract $(1/T_1)_{corr}$ illustrated for sample PS 2 ($\bar{M}_n$ = 41,500). With the background relaxation (- -) adjusted to 0.07 sec^{-1}, the remaining relaxation curve (—·—) has a low temperature slope corresponding to 1.3 kcal/mole.

evaluate the molecular weight dependent relaxation strength. The low temperature slope of Connor's sample of lowest molecular weight ($\bar{M}_n \approx 1200$) is the least susceptible to this background interference and corresponds to an apparent activation energy of 1.3 kcal/mole. To anticipate the arguments to follow, this slope corresponds exactly to that observed for the low-temperature (methyl) relaxation in branched polyethylene,[3] which lends credence to this figure. The height of the background relaxation was therefore adjusted so as to give a low-temperature slope of 1.3 kcal/mole for the remaining temperature dependent relaxation rate. This procedure is illustrated in Figure 2. The maximum uncertainty inherent in this separation, arising from a possible temperature dependence of the background or an error in the chosen reference slope, is ± 0.01 sec^{-1}. This is indicated in Table I and in Figure 3.

It is well established that reorientation of methyl protons about the C_3 axis gives rise to spin-lattice relaxation time minima in the region of 150°K.[2,6,7] This has lead us to the conclusion that the motion of a portion of the *n*-butyl endgroups suggested by Connor[1] as the origin of the molecular weight dependent relaxation in polystyrene is indeed the reorientation of the methyl group at the end of the polymer chain. To examine this model more closely, we have plotted in Figure 3 the corrected relaxation strengths $(1/T_1)_{corr}$ against the fraction of methyl protons X_m for the polystyrenes used in this study; also included are points from Connor's data* which have been corrected for background relaxation as described above and adjusted to 38 MHz. It can be seen that the agreement between the two sets of data is excellent. Along the top of Figure 3 are indicated the number-average molecular weights, which are inversely proportional to X_m in this range.

To determine the experimental dependence of the relaxation strength on endgroup concentration, we performed a least-squares fit of the data and obtained

$$\log [(1/T_1)_{corr})] = 1.03 \log X_m + \log 69$$

* Two of the polystyrenes from Pressure Chemical Company used by Connor had been incorrectly characterized. The sample designated PS 900 has a number-average molecular weight $\bar{M}_n$ = 1200 and PS 4800 has $\bar{M}_n$ = 3750; the correct values were used in calculating X_m for Figure 3. We are indebted to Dr. J. V. Dawkins of Imperial Chemical Industries, Ltd. for informing us of the correct molecular weights.

indicated by the line in Figure 3. The standard deviation from this expression is 0.08, corresponding to ±20% in linear units of $1/T_1$. The most significant feature of this relation is the slope of 1.03, which indicates that the observed relaxation intensity is an essentially linear function of the fraction of methyl protons in the sample. This is to be contrasted with the results of Connor, who found a slope of 0.57 from a comparable analysis. This discrepancy is believed to result from the slightly different separation procedures employed and from the error in the molecular weights. It should be noted that we have neglected the data for Connor's sample of $\bar{M}_n$ = 498,000, as the weak relaxation effect in this material is very susceptible to interference from residual solvents, etc.

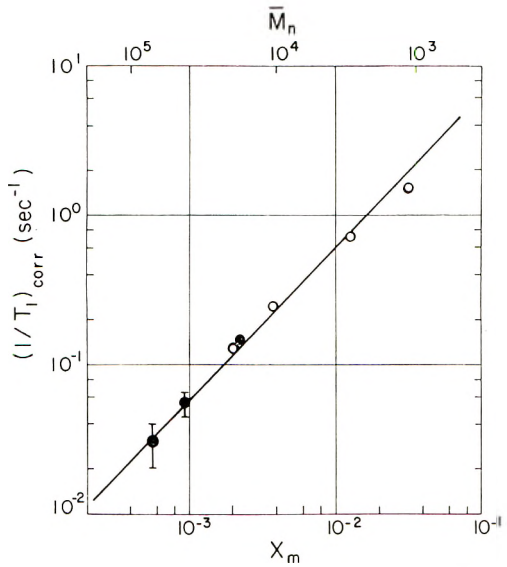

Fig. 3. Dependence of the corrected relaxation strength $(1/T_1)_{corr}$ on the fraction of methyl protons X_m (●) for atactic polystyrene; also included are (○) the data of Connor[1] adjusted to 38 MHz.

The absolute values of the relaxation strengths can be used to check the assertion made above that the terminal methyl protons are responsible for the (corrected) T_1 values. Assuming that the slope in Fig. 3 is equal to unity, one can write

$$1/T_1 = X_m/T_1^m \tag{1}$$

If the proportionality constant $1/T_1^m$ is the relaxation rate of the methyl protons, this expression is identical to that derived assuming fast spin diffusion to the methyl relaxation sites.[6,8] The value of $1/T_1^m$ obtained from the present experiments is 60 sec^{-1}, which is somewhat larger than both the 45 sec^{-1} calculated for methyl protons at 38 MHz and the 40–45 sec^{-1} observed in polyethylenes and paraffins.[2] The origin of this inconsistency is not understood, but perhaps it lies in systematic errors in either the determination of methyl group concentrations or the separation procedure. It is also possible that the methyl protons experience additional dipolar interactions in amorphous polystyrene, or even that the larger —CH_2CH_3 group is responsible for the spin-lattice relaxation; these latter explanations are considered unlikely.

In the preceding paragraphs we have demonstrated that the relaxation strength is proportional to $\bar{M}_n^{-1}$ rather than $\bar{M}_n^{-1/3}$ or $\bar{M}_n^{-2/3}$ as was derived by Connor. This discrepancy can be explained in the following manner. Douglass and Jones[9] have considered the relaxation of paraffin protons coupled by one-dimensional spin diffusion to methyl protons at the chain ends. Their results may be written as

$$1/T_1 \propto X_m \propto L^{-1} \quad \text{(fast diffusion limit)} \tag{2}$$

$$1/T_1 \propto L^{-2} \quad \text{(slow diffusion limit)}. \tag{3}$$

In eq. (2) the reciprocal of the chain length L simply expresses the dependence of the relaxation rate on the concentration of methyl protons. Note that this expression is equivalent to eq. (1). In the slow-diffusion limit, however, the chain length L in eq. (3) represents the path length over which the excess spin energy must diffuse before encountering a relaxation site. Connor has erroneously substituted a three-dimensional path length R for L in eqs. (2) and (3), and by further substitution of $\bar{M}_n \propto R^3$ he obtained the $-1/3$ and $-2/3$ power dependence of $1/T_1$ on molecular weight. The substitution of R for the concentration factor L in eq. (1) is clearly unjustified. It should also be noted that eq. (3) applies only to one-dimensional cases such as paraffin chains, in which the magnetization at a specific site is determined by one relaxation center. For the three-dimensional case, the effects of many relaxation centers are felt at a particular site and lead to the expression[10]

$$1/T_1 \propto R^{-3} \tag{4}$$

for the relaxation resulting from paramagnetic impurities. The same arguments should apply to the relaxation arising from nuclear dipole–dipole interactions, and again lead to

$$1/T_1 \propto R^{-3} \propto \bar{M}_n^{-1} \tag{5}$$

when the relaxation centers at the ends of the polymeric chains are dispersed randomly throughout the sample.

From the molecular weight (or methyl proton concentration) dependence of the relaxation strength it is apparent that no distinction can be made between the fast and slow spin diffusion limits in the case of three-dimensional diffusion; in both limits the relaxation intensity is proportional to X_m or $\bar{M}_n^{-1}$. For the present example of relaxation arising from the motion of terminal methyl protons in atactic polystyrenes, the reasonable agreement between the observed relaxation rates and those calculated for the fast-diffusion or endgroup limited case supports this particular model; if the slow diffusion limit is assumed, the calculated relaxation times are an order of magnitude too short.[8,11] A more rigorous distinction between the two cases can best be made by experimental investigation of the frequency dependence of the relaxation rates as has been discussed by Haeberlen.[12]

In conclusion, it can be stated that the spin-lattice relaxation arising from terminal methyl protons can be used to rather accurately determine number average molecular weights up to certain limits which appear to depend primarily on the magnitude of extraneous "background" relaxation effects. This relaxation strength has been shown in this note and in previous publications[2,6] to be a linear function of methyl concentration over a range of three decades for various substances. Although the T_1 technique is reasonably rapid (some 2 hr is needed for a low-temperature sweep) and requires only ca. 0.1 g of material, this method is not generally recommended for the determination of $\bar{M}_n$; the somewhat stringent requirements for successful application of this technique have been outlined previously.[13] It is suggested, however, that observation of methyl group relaxation intensities could fruitfully be applied to $\bar{M}_n$ determinations in otherwise intractable substances (e.g., high-temperature polymers[13]), as well as evaluation of branching frequency and residual concentrations of solvents containing methyl groups.

The author gratefully acknowledge the financial support of the Camille and Henry Dreyfus Foundation. Mr. Joel Williams generously supplied the polystyrene samples.

References

1. T. M. Connor, *J. Polym. Sci. A-2*, **8**, 191 (1970).
2. B. Crist and A. Peterlin, *J. Macromol. Sci.*, **B4**, 791 (1970).
3. B. Crist and A. Peterlin, *J. Polym. Sci. A-2*, **7**, 1165 (1969).
4. N. J. Trappenier, C. J. Gerritsma, and P. H. Oosting, *Physica*, **30**, 997 (1964).
5. J. C. Powles and B. I. Hunt, *Physics Letters*, **14**, 202 (1965).
6. J. E. Anderson and W. P. Slichter, *J. Phys. Chem.*, **69**, 3099 (1965).
7. Y. Tanabe, J. Hirose, K. Okano, and Y. Wada, *Polym. J.*, **1**, 107 (1970).
8. U. Haeberlen, *Polymer*, **9**, 50 (1968).
9. D. C. Douglass and G. P. Jones, *J. Chem. Phys.*, **45**, 956 (1966).
10. A. Abraham, *Principles of Nuclear Magnetism*, Oxford Univ. Press, London, 1961, p. 379 ff.
11. T. M. Connor, *Polymer*, **7**, 426 (1966).
12. U. Haeberlen, *Kolloid-Z. Z. Polym.*, **225**, 15 (1968).
13. R. Liepins, B. Crist, and H. G. Olf, *J. Polym. Sci. A-1*, **8**, 2049 (1970).

Buckley Crist, Jr.

Camille Dreyfus Laboratory
Research Triangle Institute
Research Triangle Park, North Carolina 27709

Received October 15, 1970
Revised January 11, 1971

Diffusion of Radioactively Tagged D-*Fructose Through Swollen Crosslinked Poly(β-hydroxymethyl Methacrylate) Solutions*

One method of gauging local molecular mobility in a concentrated or undiluted polymer system is based on the diffusion of a small molecule (typically somewhat larger than the monomer unit of the polymer) in trace amounts through the system.[1-3] The translational friction coefficient of the diffusing molecule, ζ_1, is obtained as kT/D, where k is Boltzmann's constant, T the absolute temperature, and D the diffusion constant. Measurements in a variety of rubbery polymers with radioactively tagged penetrant molecules[1-3] have shown that ζ_1 is approximately proportional to ζ_0, the translational friction coefficient per monomer unit of the polymer itself, as derived from the time or frequency dependence of viscoelastic properties in the transition zone by a modification of the theory of Rouse. In fact, for *n*-hexadecane or 1,1-diphenylethane as penetrant, ζ_1 is closely similar to ζ_0 in magnitude when comparison is made for a number of rubbery polymers. Also, for at least one system (polyisobutylene diluted with *n*-hexadecane), the effects of diluent in diminishing ζ_1 and ζ_0 were found to be closely similar.[1,4]

In some other cases, however, especially when the polymer is not far above its glass transition temperature, ζ_1 has been found to be smaller than ζ_0 by several orders of magnitude.[1]

Poly(β-hydroxyethyl methacrylate) is a quite different kind of polymer from those previously investigated in view of its polarity, the probability of contributions of hydrogen bonding to its mechanical properties, and its miscibility with polar diluents such as water and diethylene glycol.[5] In a previous study,[6] ζ_0 was determined from transition-zone dynamic viscoelastic measurements for gels of poly(β-hydroxyethyl methacrylate) polymerized and crosslinked in the absence of diluent and subsequently swollen in diethylene glycol to volume fractions of polymer (v_2) between 0.17 and 0.61. The present study was undertaken to determine the concentration dependence of ζ_1 from diffusion of a radioactively tagged small molecule over a similar range of v_2. For this purpose, D-fructose was chosen. It is soluble in the diluent and moreover is of some interest in connection with biomedical applications of this polymer[7] in which dissolved molecules such as the hydrodynamically equivalent glucose may diffuse through gels swollen in aqueous biological fluids.

The crosslinked polymers were the samples identified elsewhere[6,8] as A1 and A2; they were prepared with 0.0855 and 0.136 $\times 10^{-4}$ mole crosslinking agent/cc (ethylene glycol dimethacrylate), and their equilibrium swellings in ethylene glycol have been reported[8] as $v_2 = 0.134$ and 0.157, respectively. Samples were swollen in water, cut to size, dried, and then swollen in diethylene glycol to different degrees as described previously.[8] (One portion of sample A1 was swollen to $v_2 = 0.112$, representing a somewhat higher degree of maximum swelling than previously reported.) The D-fructose tagged with ^{14}C was purchased from International Chemical Corporation in diethylene glycol solution at an activity level of 5 mCi/g of solution (concentration approximately 0.5%). The diffusion experiments were performed by the thin smear method of Moore and Ferry[1] taking into account contributions to measured activity from below the sample surface.[2] The temperature was between 24.97 and 25.05°C except for one measurement at 25.20°C. Further details are given elsewhere.[9]

Diffusion coefficients and friction coefficients calculated from them are listed in Table I, and log ζ_1 is plotted against v_2 in Figure 1. It is evident that the friction coefficient for D-fructose is not affected by the degree of crosslinking in this range and varies by about a factor of 30 over the concentration range covered. The concentration dependence can be described quite well by the free-volume equation of Fujita,[3,6] with $\beta'/B_d = 0.15$ and $f_0/B_d = 0.10$ corresponding to a reference concentration of $v_2 = 0.508$. Here f_0 is the fractional free volume f at the reference concentration, β' is $-df/dv_2$, and B_d is a dimensionless parameter, not far from unity, which can be regarded as related to the

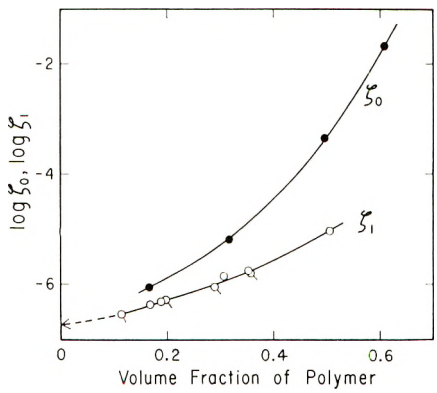

Fig. 1. Log ζ_0 and log ζ_1 plotted against v_2 for samples A1 (tagged circles) and A2 (circles without tags). Arrow on ordinate axis corresponds to glucose in pure solvent (value in water corrected to viscosity of diethylene glycol).

open volume required for motion of a diffusing penetrant molecule relative to the volume of a polymer segment involved in a unit jump process.

It is now of interest to compare with the concentration dependence of ζ_0 as derived from viscoelastic measurements. The values of ζ_0 plotted in Figure 1 are those quoted for sample A2 in reference 6 except for $v_2 = 0.168$, which has been extrapolated in a different manner; instead of the empirical linear extrapolation of Figure 7 of that publication, the Fujita equation [eq. (3) of reference 6] was used to obtain log $\zeta_0 = -6.06$. Evidently ζ_0 and ζ_1 are similar in magnitude in highly swollen gels, but ζ_0 increases much more rapidly with increasing polymer concentration than does ζ_1.

The free-volume analysis of Fujita applied to the concentration dependence of ζ_0 yields[6] $\beta'/B = 0.10$, $f_0/B = 0.06$ at $v_2 = 0.508$. Here B is related to the open volume required for motion of a segment (tacitly assumed to be unity in reference 6). The differences between these and the diffusion parameters can be interpreted by concluding that B is substantially larger than B_0; that is, the mobility mechanism is more efficient for translation of fructose than for translation of polymer segments. The divergence in Figure 1 is reminiscent of diffusion data in poly(vinyl acetate) and poly(*n*-hexyl methacrylate),[11] where, at temperatures only 30 to 40°C above T_g, ζ_1 for a moderately sized penetrant is considerably smaller than ζ_0. In our system, T_g is about -10°C for $v_2 = 0.6$. Whether proximity to T_g is the primary cause of the divergence is uncertain, however.

TABLE I
Diffusion Coefficients (cm²/sec) and Friction Coefficients (dyne-sec/cm)

Sample	v_2	log D	log ζ_1
A1	0.112	−6.862	−6.53
	0.194	−7.105	−6.29
	0.290	−7.319	−6.07
	0.358	−7.594	−5.80
A2	0.169	−7.015	−6.37
	0.189	−7.072	−6.32
	0.307	−7.465	−5.93
	0.352	−7.617	−5.77
	0.508	−8.37	−5.02

Finally, the diffusion coefficient of D-fructose in highly swollen gels may be compared with that of its isomer glucose in the pure solvent. For glucose in water at 25°, $D = 6.73 \times 10^{-6}$ cm²/sec.[11] Corrected to the viscosity of diethylene glycol, about 0.30 poise at 25°,[12] assuming D to be inversely proportional to η, $\log D = -6.70$ and $\log \zeta_1 = -6.69$. This point is included in Figure 1. At a polymer concentration of $v_2 = 0.2$, the diffusion coefficient is reduced by about a factor of 2 from its value in the pure solvent.

References

1. R. S. Moore and J. D. Ferry, *J. Phys. Chem.*, **66**, 2699 (1962).
2. S. P. Chen and J. D. Ferry, *Macromolecules*, **1**, 270 (1968).
3. C. P. Wong, J. L. Schrag, and J. D. Ferry, *J. Polym. Sci. A-2*, **8**, 991 (1970).
4. J. R. Richards, K. Ninomiya and J. D. Ferry, *J. Phys. Chem.*, **67**, 323 (1963).
5. O. Wichterle and D. Lim, *Nature*, **185**, 117 (1960).
6. J. Janáček and J. D. Ferry, *Macromolecules*, **2**, 370 (1969).
7. Abstracts, *Hydrophilic Gels in Medicine*, Czechoslovak Academy of Sciences, Prague, 1969.
8. J. Janáček and J. D. Ferry, *Rheol. Acta*, **9**, 208 (1970).
9. C. P. Wong, Ph.D. Thesis, University of Wisconsin, 1970.
10. J. D. Ferry, *Viscoelastic Properties of Polymers*, 2nd ed., Wiley, New York, 1970, p. 372.
11. L. G. Longsworth, *J. Amer. Chem. Soc.*, **75**, 5705 (1953).
12. A. K. Doolittle, *The Technology of Solvents and Plasticizers*, Wiley, New York, 1954.

Chiu-Ping Wong
John L. Schrag
John D. Ferry

Department of Chemistry
University of Wisconsin
Madison, Wisconsin 53706

Received March 15, 1971

The *Journal of Polymer Science* publishes results of fundamental research in all areas of high polymer chemistry and physics. The *Journal* is selective in accepting contributions on the basis of merit and originality. It is not intended as a repository for unevaluated data. Preference is given to contributions that offer new or more comprehensive concepts, interpretations, experimental approaches, and results. Part A-1 *Polymer Chemistry* is devoted to studies in general polymer chemistry and physical organic chemistry. Contributions in physics and physical chemistry appear in Part A-2 *Polymer Physics*. Contributions may be submitted as full-length papers or as "Notes." Notes are ordinarily to be considered as complete publications of limited scope.

Three copies of every manuscript are required. They may be submitted directly to the editor: For Part A-1, to C. G. Overberger, Department of Chemistry, University of Michigan, Ann Arbor, Michigan 48104; and for Part A-2, to T. G Fox, Mellon Institute, Pittsburgh, Pennsylvania 15213. Three copies of a short but comprehensive synopsis are required with every paper; no synopsis is needed for notes. Books for review may also be sent to the appropriate editor. Alternatively, manuscripts may be submitted through the Editorial Office, c/o H. Mark, Polytechnic Institute of Brooklyn, 333 Jay Street, Brooklyn, New York 11201. All other correspondence is to be addressed to Periodicals Division, Interscience Publishers, a Division of John Wiley & Sons, Inc., 605 Third Avenue, New York, New York 10016.

Detailed instructions on preparation of manuscripts are given frequently in Parts A-1 and A-2 and may also be obtained from the publisher.